AD-A244 898

FINAL TECHNICAL REPORT

15 July 90 — 14 Jan 91

MOLECULAR OPTICS

Nonlinear Optical Processes in
Organic and Polymeric Crystals and Films

DTIC
ELECTE
JAN 1 9 1992
S D
D

PART I

Principal Investigator   Prof. A.F. Garito

Program Manager   Dr. Charles Lee

92-01060

92 1 10 046

92 1 10 048

REPORT DOCUMENTATION PAGE

1. AGENCY USE ONLY (Leave blank)	2. REPORT DATE	3. REPORT TYPE AND DATES COVERED
	November 1991	Final Report 7/15/88 – 7/14/91

4. TITLE AND SUBTITLE	5. FUNDING NUMBERS
Molecular Optics: Nonlinear Optical Processes in Organic and Polymeric Crystals and Films	61102F 2303/A3 61101E 4989/08

6. AUTHOR(S)

A. F. Garito

7. PERFORMING ORGANIZATION NAME(S) AND ADDRESS(ES)	8. PERFORMING ORGANIZATION REPORT NUMBER
University of Pennsylvania Department of Physics Philadelphia, PA 19104	

9. SPONSORING MONITORING AGENCY NAME(S) AND ADDRESS(ES)	10. SPONSORING MONITORING AGENCY REPORT NUMBER
AFOSR/NC Bolling AFB, DC 20332-6448	F49620-88-C-0127

11. SUPPLEMENTARY NOTES

12a. DISTRIBUTION AVAILABILITY STATEMENT	12b. DISTRIBUTION CODE
Approved for public release; distribution is unlimited	

13. ABSTRACT (Maximum 200 words)

See Back

14. SUBJECT TERMS			15. NUMBER OF PAGES
			520
			16. PRICE CODE

17. SECURITY CLASSIFICATION OF REPORT	18. SECURITY CLASSIFICATION OF THIS PAGE	19. SECURITY CLASSIFICATION OF ABSTRACT	20. LIMITATION OF ABSTRACT
UNCLASSIFIED	UNCLASSIFIED	UNCLASSIFIED	SAR

Optical bistability is a quantum optical realization of a first order phase transition far from equilibrium. A nonlinear optical material contained in an optical cavity driven resonantly by an external coherent optical field undergoes a first order phase transition to a new nonequilibrium stationary state of broken symmetry. Resonant and nonresonant nonlinear optical response of pi-electron excitations in conjugated electronic structure provides the nonlinearity essential to the onset of bistability. Electronic correlation effects in reduced dimensions are responsible for nonresonant nonlinear optical responses. Saturable absorption studies of glassy polymer films consisting of quasi-two dimensional conjugated disc-like structure of silicon naph-thalocyanine demonstrate that on-resonance the system behaves as an optical Bloch system with an intensity dependent refractive index of 1×10^{-10} cm^2/kW. Based on the results of these studies, electronic absorptive optical bistability is observed on a nanosecond time scale in a nonlinear Fabry-Perot interferometer employing the saturable absorbing silicon naphthalocyanine film as the nonlinear optical medium.

FINAL TECHNICAL REPORT

15 July 90 - 14 Jan 91

TITLE: Molecular Optics: Nonlinear Optical Processes in
         Organic and Polymeric Crystals and Films

PRINCIPAL INVESTIGATOR: Prof. A. F. Garito   (215) 898-5810

PROGRAM MANAGER: Dr. Charles Lee   (202) 767-4960

ARPA ORDER: 4989   PROGRAM CODE: 8D10

CONTRACTOR: University of Pennsylvania

EFFECTIVE DATE: 15 July 88   EXPIRATION DATE: 14 July 91

CONTRACT NUMBER: F49620-88-C-0127   AMOUNT: $1,739,465

Accesion For		
NTIS CRA&I	☑	
DTIC TAB	☐	
Unannounced	☐	
Justification		
By		
Distribution /		
Availability Codes		
Dist	Avail and/or Special	
A-1		

PART I
RESONANT NONLINEAR OPTICAL PROCESSES
IN LOWER DIMENSIONAL ELECTRONIC SYSTEMS

ABSTRACT

RESONANT NONLINEAR OPTICAL PROCESSES
IN LOWER DIMENSIONAL ELECTRONIC SYSTEMS

Optical bistability is a quantum optical realization of a first order phase transition far from equilibrium. A nonlinear optical material contained in an optical cavity driven resonantly by an external coherent optical field undergoes a first order phase transition to a new nonequilbrium stationary state of broken symmetry. Resonant and nonresonant nonlinear optical response of π-electron excitations in conjugated electronic structure provides the nonlinearity essential to the onset of bistability. Electronic correlation effects in reduced dimensions are responsible for nonresonant nonlinear optical responses. Saturable absorption studies of glassy polymer films consisting of quasi-two dimensional conjugated disc-like structure of silicon naphthalocyanine demonstrate that on-resonance the system behaves as an optical Bloch system with an intensity dependent refractive index of 1×10^{-4} cm^2/kW. Based on the results of these studies, electronic absorptive optical bistability is obeserved on a nanosecond time scale in a nonlinear Fabry-Perot interferometer employing the saturable absorbing silicon naphthalocyanine film as the nonlinear optical medium.

.

TABLE of CONTENTS

Chapter 4. Optical Excitations in Random Glass Media:

Chapter 5. Nonlinear Optical Excitations: Saturable Absorption 155

Chapter 6. Absorptive Optical Bistability 216

LIST of TABLES

LIST of FIGURES

Chapter 2

Chapter 6

CHAPTER 1

INTRODUCTION

Nonequilibrium systems may exhibit instabilities that are analogous to phase transitions in thermodynamic equilibrium systems. Thus, when an open system is driven far from equilibrium by an external source, it may change either continuously, or discontinuously, from an initial disordered state of independent atomic motion to a macroscopic ordered state of cooperative motion. This instability occurs only in the presence of nonlinear interactions between the atoms and the external field. A major physical realization of such instability phenomena is bistable transmission in a nonlinear optical system where an external coherent optical field resonantly drives a nonlinear optical material contained in an optical cavity to new nonequilibrium stationary states of broken symmetry.

Optical bistability can be generally understood as quantum optical analog of a first order phase transition of a thermodynamic equilibrium system, and the two dimensional Ising spin system in an external magnetic field has an almost identical formal analogy to optical bistability. According to the mean field theory of a ferromagnetism, the Ginzburg-Landau potential $F(\phi)$ is given by

$$F(\phi) = -H\phi + \frac{(kT - J\gamma)}{2}\phi^2 + \frac{kT}{12}\phi^4 + \dots \qquad (1.1.1)$$

where H is the external magnetic field, ϕ is the magnetization (order parameter), J is coupling constant, and γ the number of nearest neighbors. The state equation for a ferromagnet in an external field is determined by minimizing the potential $F(\phi)$.

$$H = k(T - T_c)\phi + \frac{kT}{3}\phi^3 \qquad (1.1.2)$$

with $T_c = J\gamma/k$. Below T_c, a first order phase transition takes place, and the magnetization (order parameter) shows hysteresis behavior upon increase and decrease of the exeternal field.

1

Certain nonlinear optical systems in Fabry-Perot cavity configurations may exhibit a similar phase transition when resonantly driven by a coherent optical field from a disordered fluorescent state to a macroscopic ordered, coherent state. The output field intensity transmitted through the system shows hysteresis behavior upon change of the incident light intensity. A quantum optical instability, however, is not a phase transition in a thermodynamic equilibrium system in which a Gibbs ensemble can be introduced and a thermodynamic potential can be defined. Instead, optical bistability is one example of a phase transition that occurs far from equilibrium, where a nonlinear interaction between the system and external field is essential to the onset of the instability. This can be illustrated by the nonlinear optical response of an optical Bloch system to a coherent optical field, where the Bloch susceptibility, $\chi(\omega)$, is expressed as

$$\chi(\omega) = (\frac{\alpha_0 c}{4\pi\omega})(\frac{\Delta + i}{1 + \Delta^2 + I/I_s})$$ (1.1.3)

where $\Delta = (\omega - \omega_a)T_2$, the difference between the optical frequency and atomic resonance frequency. As appears in the denominator, the dipole moment induced in an optical Bloch system is a nonlinear function of the incident light intensity. In contrast to a thermodynamic equilibrium phase transition, the absence in a nonequilibrium system of a thermodynamic potential, such as a free energy, makes it difficult to describe a phase transition far from equilibrium. In a quantum optical system such as the optical Bloch system, however, a generalized Ginzburg-Landau potential can be defined through a Fokker-Planck equation which is equivalent to a Maxwell-Bloch equation describing a resonant nonlinear optical process in the Bloch system contained in a Fabry-Perot cavity. In steady state, a bistable transmission in a nonlinear optical system can be described by a generalized Ginzburg-Landau potential, $F(x)$.

$$F(x) = \frac{2}{q}\{\frac{1}{2}(x - y)^2 + C\ln(1 + x^2)\}$$ (1.1.4)

where the transmitted output optical field amplitude x is the order parameter, the incident coherent optical field amplitude y is the external field, C is the cooperativity

2

of the nonlinear optical system, in analogy to temperature in an equilibrium system, and q is a measure of stochastic force destroying the macroscopic long range order of microscopic optical dipole moments. The corresponding state equation is then

$$y = x + \frac{2Cx}{1 + x^2} \qquad (1.1.5)$$

For a nonlinear optical system with a large enough cooperativity, which is analogous to an Ising spin system at a temperature below T_c, the transmitted output field amplitude x (order parameter) can be either in a low transmittance state or in a high transmittance state for a given incident light intensity depending on whether the incident light field intensity y (external field) is increased or decreased.

The first experimental observation of optical bistability was made in sodium vapor in a Fabry-Perot cavity.[1][2] Since then, optical bistabilty studies have flourished to become one of the main subjects of study in nonlinear optics. Bistable behavior has been experimentally observed in various forms of materials that include atomic gases, semiconductors, Kerr liquids, and liquid crystals. Each material system provides a special condition or regime of bistability. Many theoretical studies are currently focused on the connection with nonlinear dynamics, and optical bistability is providing superior experimetal realizations of theoretical modeling for nonlinear instabilities such as bifurcation and chaos.

The major studies of this report are experimental and theoretical studies of optical bistability phenomena mediated by a resonant third order optical response function of random glassy polymer films. These studies have led to the discovery of the important case of absorptive optical bistability occurring through the nonlinear electronic excitations in a random solid medium. The medium consists of quasi-two dimensional conjugated discs randomly distributed in a glassy matrix. The report is thus organized as follows.

3

Chapters 2 and 3 combine to describe a quantum optical phase transition. In Chapter 2, a thermodynamic phase transition in both equilibrium and nonequilibrium states is reviewed. In a linear nonequilibrium system, no phase transition can take place according to the minimum entropy production theorem. When a thermodynamic force acting on a nonequilibrium system is increased, a nonlinear response of the system to a thermodynamic force should be accounted for, and a nonlinear interaction gives rise to a phase transtion, causing the system assume a new, ordered, symmetry broken state. A detailed description of nonequilibrium phase transitions is presented in Sec.2.1.

In Sec.2.2, this understanding is applied to a nonlinear optical system, and optical bistability is discussed in analogy to a two-dimensional Ising spin system. Maxwell-Bloch equations describing the resonant nonlinear interaction between an optical Bloch system and coherent optical field are introduced. In adiabatic following, where the microscopic atomic dipole field follows a macroscopic optical field (order parameter), the Maxwell-Bloch equations can be reduced to a single Langevin equation for the macroscopic optical field (order parameter) and the incident coherent optical field (external field). When the stochastic force is assumed to be white noise, the Langevin equation can be reformulated into a Fokker-Planck equation for the probability distribution function of the order parameter for the given external field. In a stationary state, the generalized Ginzburg-Landau potential can be introduced to describe a phase transition far from equilibrium. A cooperative parameter, C, is found to be equivalent to the temperature in a thermodynamic equilibrium system. For C larger than 4, a phase transition is allowed, resulting in bistable transmission behavior upon increase and decrease of the external coherent optical field.

In Chapter 3, a microscopic many-electron description of third order optical susceptibilities of conjugated organic structures is reviewed for one dimensional chain and extended to two dimensional cyclic chain structure. In a nonresonant

4

regime, a quantum mechanical perturbative expansion of the response function is allowed, leading to an analytical expression for the microscopic nonlinear optical susceptibility. Virtual excitations of highly correlated π-electrons are found to be responsible for unusually large nonlinear optical responses. For a cyclic chain structure, it is found that the isotropic, averaged value of the third order suscpetibility is much smaller than the corresponding linear chain, simply because of the reduction in the effective length for π-electron motion. The discussion then turns to a resonant nonlinear optical processes in Sec.3.4-7. In a resonant process, a real population of excited state occurs, and the change in population of the ground and excited states is actually a nonlinear optical response which can be described by a Bloch susceptibility. The Bloch equation of motion is derived, and transient processes of optical Bloch systems are reviewed. In steady state, a simple Bloch susceptibility can be defined, which leads to an intensity dependent refractive index n_2. In quasi-two dimensional conjugated structures, we demonstrate that resonant π-electron optical excitations exhibit exceptionally large value of n_2.

In Chapter 4, we first present the results of experimental and theoretical studies of the linear optical excitations of random glassy polymers. After a linear absorption spectrum is described in Sec.4.1, a study of an optical line broadening is presented based on irreversible statistical mechanics. Line broadening in a solid comes from the interaction of an optical site with phonons. The microscopic line broadening mechanism is manifested in the characteristic temperature dependence of the homogeneous linewidth. In order to obtain an analytic expression for a homogeneous linewidth, a general line shape theory is discussed in terms of projection operator formalism, in Sec.4.2-3. With a specific stochastic process, the characteristic line shape is obtained; for example, in a Markoffian process, a Lorentzian line shape results. When the short memory approximation is taken as in Sec.4.4, the memory function which is directly related to the line shape can be expanded in the interaction Hamiltonian between an optical site and the phonons. In later

5

sections, a specific example of line broadening is presented. First, the temperature dependence of the homogeneous line width is calculated for an optical site in a crystalline field in order to show that in a random glassy medium, the line broadening mechanism is quite different from the crystal case. Low excitation energy TLS's (two level system) are distributed in the random medium and are responsible for the characteristic physical properties of glassy systems such as a glass or polymer matrix. The TLS model is described in Sec.4.6, and an analysis of the temperature dependence of the linewidth for optical sites in a random glassy medium is presented in Sec.4.7.

Chapter 5 addresses the major subject of nonlinear optical excitations in random glassy polymers. First, the results of numerical simulation studies of dynamical transmission in a saturable absorber are presented in Sec.5.2. Then intersystem crossing between electronic states in conjugated organic structures is discussed. Spin-orbit coupling is responsible for the intersystem crossing between singlet and triplet manifolds, and the strength of intersystem crossing depends on the atomic number of key atoms in our molecular structure. Experimental results for glassy polymer films of the silicon- naphthalocyanine (SINC) disc-like structure are presented and discussed in Sec.5.4-5. Saturable absorption experiments are perfomed on three different forms of samples (pure SINC thin film, SINC solid solution thin film, and SINC liquid solution) at various laser pulse widths. In the short pulse regimes of picoseconds and nanoseconds, a gas Raman cell was utilized to generate a coherent light near sample linear absorption peak, while an acousto- optical modulator processesed CW dye laser was employed in the long pulse regime (microseconds to seconds). The measured saturation threshold powers for thin films at different pulse widths are found to agree with the theoretical predictions from the dynamical transmission calculations. From the measured threshold power for saturation, the intensity dependent refractive index n_2 was obtained. The experimental observation of the same saturation behavior of a pure SINC film and a SINC solid solution

film at picosecond time scales lead to the important conclusion that the on-site π- electron excitations of individual molecule sites are responsible for the resonant nonlinear optical response of SINC thin films. The dispersion of saturable absorption was also measured throughout the inhomogeneous, site-broadened, Gaussian absorption band, and was analyzed by Kramers-Kronig relations to obtain the real part of the nonlinear optical susceptibility.

In Chapter 6 after a standard Fabry-Perot interferometer is briefly described, steady state optical bistability in the dispersive and absorptive regimes is discussed in Sec.6.2-3 based on the general analytical expression of the transmission function of a nonlinear Fabry-Perot cavity containing an optical Bloch system. Transient behavior of optical bistability is briefly described in connection with nonlinear dynamical studies. In Sec.6.5, the optical bistability experiments perfomed on SINC thin films are presented. In the optical bistability experiment, a single longitudinal mode of a laser pulse was essential to directly observe a hysteresis behavior of the transmitted light intensity that results from the nonlinear electronic excitations in SINC thin films. A Ti:sapphire laser was found to be ideal for this purpose, and is described in Sec.6.5.1. The observed absorptive optical bistability at nanosecond time scales is discussed based on the physical model for optical excitations in a random glassy medium introduced in Chapter 4. Also presented are results in the long pulse regime for thermal effects. In the long laser pulse regime, a local heating of the thin film sample is responsible for the observed dispersive bistability, which is completely different from the short nanosecond pulse, electronic behavior.

Chapter 7 is the concluding chapter. Appendix contains detailed mathematical formalisms appearing in the text.

7

References: Chapter 1

[1] Gibbs, H.M., McCall, S.L., and Venkatesan, T.N., Phys. Rev. Lett. **36**, 1135 (1976)

[2] For a general reference, see, for example, Gibbs, H.M., *Optical Bistability - Controlling Light with Light*, Academic, New York (1985)

CHAPTER 2

NONEQUILIBRIUM PHASE TRANSITION: OPTICAL BISTABILITY

Optical bistability (O.B.)[1]-[4] is a third order nonlinear optical process due to changes in the intensity dependent refractive index of a nonlinear optical material contained inside a Fabry-Perot (F-P) cavity. A F-P interferometer with a cavity spacing tuned to the incident light frequency becomes detuned when the light intensity inside the cavity is increased because the change in the refractive index causes an additional phase change in the propagation of optical wave. The transmission of the nonlinear F-P is a highly nonlinear function of the input light intensity with the actual functional form depending on several important parameters such as the initial cavity phase setting, the atomic detuning, and the temporal response of the nonlinear optical medium.

O.B. has been one of the main subjects of study in nonlinear optics in recent years. Szoeke et al.[5] and Seidal[6] were the first to propose that a saturable absorber inside a F-P cavity(Figure 2.1) can exhibit an O.B. behavior. The first observation of bistability was made in sodium vapor in 1976.[7] Sodium vapor has well-known sharp atomic transitions called D-lines (D_1; 589.6 nm, D_2; 589.0 nm), and when a single longitudinal mode of a CW dye laser is tuned near resonance of these lines, the sodium vapor can be treated as an effective two-level system exhibiting a nonlinear optical response. The transmitted power through the nonlinear F-P containing the sodium vapor showed bistable behavior upon the increase and the decrease of the incident power. Because the maximum bistable effect was observed with the initial cavity detuning set to a nonzero value, it is attributed to the dispersive effect of the nonlinear susceptibility, and is thereby refered to as dispersive bistability. The search for nonlinear optical materials related to the optical bistability lead to the study of various forms of materials including ruby crystal, [8] liquid crystals, [9]-[15] semiconductors, [16][17] multiple quantum well structures (MQW) (Figure

2.2), [18]-[25] Kerr liquids, [26]-[29] and liquid solutions of organic dyes. [30]-[32]

Immediatly after the suggestion of utilizing the standard nonlinear F-P configuration for O.B., different configurations were explored. One is the hybrid, or electrooptical O.B., [33]-[35] where the feedback of the light intensity into the nonlinear optical material is provided through an electrooptical crystal rather than through F-P mirrors (Figure 2.3). Another proposed configuration is a thin film of nonlinear optical material (Figure 2.4). [36]-[41] When the incident angle is set at the critical angle for total internal reflection, a change in the refractive index takes place for the high intensity, and the critical angle changes accordingly, destroying total internal reflection.[36] Upon decrease of the incident light intensity, multiple reflections between the nonlinear optical thin film boundaries provide a feedback mechanism, resulting in hysteresis behavior. In this thesis, we restrict our discussion to the standard nonlinear F-P cavity configuration.

Multistability and hysteresis behavior of physical systems are well-known in statical physics of phase transitions, and they are general features of the first-order phase transition. One simple example is the well-known case of Van-der-Waals gas. Below the critical temperature for the first-order phase transiton, the molar density is a bistable fuction of the pressure between p_1 and p_2 (Figure 2.5), and the metastable state such as supercooling can be observed easily in the experiment. Quite strikingly, O.B. also can be understood in terms of the nonequilibrium first-order phase transition, which will be discussed in Sec.2.1.

The nonlinear optical response of the optical Bloch system inside a F-P interferometer is discussed in Sec.2.2 by showing the solution to the Maxwell-Bloch equation and the transmission function characteristic of bistable behavior. The bistable behavior is most clearly described by a generalized Ginzburg-Landau potential which can be introduced through a Fokker-Planck equation, equivalent to the Maxwell-Bloch equation in an adiabatic following approximation. A physical condition for the realization of optical bistability is also examined.

10

2.1 Optical Bistability as a Nonequilibrium First Order Phase Transition

In this section, we discuss the analogy between quantum optical processes and thermodynamic phase transitions. In optical processes, we can make distinction between spectroscopy and quantum optics, the difference between them lying in the fact that in spectroscopy the optical properties of an individual molecule are studied independent of the other nearby molecules, while in quantum optics there is a characteristic cooperative effect coming from the coherent dipole radiation of many molecules mediated through an intense, coherent, monochromatic optical field. These quantum optical effects, which include laser threshold, superfluorescence, parametric or Raman-Stokes oscillators, and O.B., belong to a stationary nonequilibrium state with a broken symmetry, and there exists a close formal analogy with thermodynamic equilibrium phase transtions.[42]

First, we briefly review equilibrium thermodynamic phase transitions.[43]−[44] The second law of thermodynamics states that an isolated closed system at thermodynamic equilibrium will be in a state of maximum entropy. The system in nonequilibrium evolves to the maximum entropy state in time.

$$dS \geq 0 \tag{2.1.1}$$

The maximum entropy state means that the system is in its most disordered state, and, hence, we cannot expect any macroscopic ordering or coherence for an isolated system. When a system is allowed to exchange energy with a heat reservoir, the closed system at equilibrium has a minimum Helmholtz free energy F,

$$F = U - TS \tag{2.1.2}$$

and the probability that the system is at an energy between E and $E + dE$ is given by the canonical distribution.

$$P \propto g(E) \exp(-\frac{E}{kT}) \tag{2.1.2}$$

11

where $g(E)$ is the density of states. The canonical distribution in equilibrium corresponds to the maximum entropy state under the restriction that the temperature is kept constant through energy exchange with the heat reservoir. That is, for a closed system in equilibrium,

$$dS_{equilibrium \ closed \ system} = 0 \qquad (2.1.3)$$

or equivalently,

$$dS = -\frac{1}{T} dF|_{T,V} = 0 \qquad (2.1.5)$$

Even if the system reaches the maximum entropy state in equilibrium, we find that there is a possibility of realizing a macroscopic ordering or coherence in the system in a canonical distribution when the temperature is lowered. The canonical distribution states that as the temperature is decreased, the energy levels with lower energy has a larger probability to be occupied than the energy levels with higher energy, suggesting that the system will be in a less disordered state because a fewer number of the energy levels are occupied. If we look at the free energy F, we find that the contribution of the entropy term in the free energy decreases as temperature is decreased, which permits a phase transition from a disordered state (where the entropy term is dominant) to an ordered state (where the internal energy, or the interaction between the molecules comprising a thermodymanic macroscopic system, is dominant). From these considerations, we find that a phase transition in a thermodynamic equilibrium comes from a competition between the intermolecular interactions and the entropy. In another words, the emergence and maintenance of a macroscopic ordering, or coherence, in a closed system at equilibrium is a result of the cooperative effect of intermolecular interactions winning over the disorder favored by the maximum entropy. From this consideration, we can draw some important conclusions that a closed system with an infinite entropy cannot undergo a phase transition at finite temperature as long as the intermolecular interaction is short range (this corresponds to a one-dimensional Ising spin system), and a

12

system having no intermolecular interactions cannot undergo a phase transition because cooperative effects between molecules are absent (this coresponds to an ideal gas).

One of the best known examples of an equilibrium thermodynamic phase transition is the Ising model for a spin system where the spins can be either up $N_\uparrow$ or down $N_\downarrow$ and the interaction between spins are restricted to nearest neighbors. When an Ising system is placed in an external magnetic field H, the Hamiltonian for the ferromagnetic system is

$$E = -J \sum_{n.n} S_i S_j - H \sum_i S_i \tag{2.1.6}$$

where $J > 0$ is the coupling constant between spins. In the mean field approximation (in fact, this corresponds to the zeroth approximation,) the expectation value of an individual spin is replaced by the average value of the spins. With the average value of the spin defined as the order parameter ϕ of the system,

$$\phi = \frac{N_\uparrow - N_\downarrow}{N} = \frac{1}{N} \sum S_i \tag{2.1.7}$$

the internal energy E coming from the nearest neighbor interaction is

$$E = -J \frac{N\gamma}{2} \phi^2 - NH\phi \tag{2.1.8}$$

where N is the total number of spins, and γ is the number of nearest neighbor spins for a given spin. The entropy of the system can be accounted for just from a simple combinatorics.

$$S = k \ln \frac{N!}{\{\frac{N}{2}(1 + \phi)\}!\{\frac{N}{2}(1 - \phi)\}!} \tag{2.1.9}$$

Substituting the internal energy and the entropy into the free energy and expanding F in the order parameter ϕ up to fourth order, we get the free energy, F, as follows.

$$\frac{F}{N} = -\frac{J\gamma}{2}\phi^2 - H\phi + kT\{\frac{(1+\phi)}{2}\ln(1+\phi) + \frac{(1-\phi)}{2}\ln(1-\phi) - \ln 2\}$$

$$= -H\phi + \frac{(kT - J\gamma)}{2}\phi^2 + \frac{kT}{12}\phi^4 + \ldots \tag{2.1.10}$$

13

The expression for the free energy shows that there is a competition between the internal interaction energy (cooperative effect) and the entropy (maximum disorder). As will be discussed later, the coefficient for the term which is second order in the order parameter ϕ determines the transition behavior of the system, and in this case, the critical temperature is simply the product of the coupling constant, J, and the number of the nearest neighbors, γ. We see that for strong coupling or a large number of nearest neighbors, the critical temperature is high, which means that large cooperative effects between the spins increase the critical temperature. It is well known that the mean field approximation is quite misleading in the one-dimensional Ising spin system since an exact calculation shows that no phase transition occurs in the one-dimensional Ising system, where only nearest neighbor, or a short range interaction is assumed to exist. The one-dimensional Ising spin system is exactly soluble by transfer matrix method, and no spontaneous magnetization occurs in the 1-D Ising spin system except at $T=0$. In the mean field approximation, however, the existence of a long range interaction is assumed in the beginning when an order parameter is introduced, thereby predicting a phase transition at a finite temperature, and the mean field approximation gets better as the dimensionality increases. In a physical system with the spatial dimension larger than one, the local statistical fluctuation of spin alignment becomes uncritical in determining the macroscopic thermodynamic order parameter, simply because, in the thermodynamic limit, the number of spins involved in the fluctuation becomes negligible compared to the total number of spins.

According to classical Landau theory of phase transitions, the macroscopic state of a physical system is described by an order parameter ϕ, and the equilibrium value of ϕ is determined through minimizing the Landau-Ginzburg potential F, or equivalently maximizing the probability distribution function f below and above the critical temperature T_c. The probability distribution function f is defined as

$$f(\phi, T) = N \exp(-F(\phi, T)/kT). \qquad (2.1.11)$$

14

The generally accepted (until the development of modern theory of critical phenomena initiated by Kadanoff[45] and Wilson[46]) assumption is that the free energy F is analytic function of the order parameter ϕ, and hence, can be expanded in terms of ϕ near the phase transition temperature, yielding

$$F(\phi, T) = F(0, T) + \frac{\alpha(T)}{2}\phi^2 + \frac{\gamma(T)}{3}\phi^3 + \frac{\beta(T)}{4}\phi^4 + \ldots \qquad (2.1.12)$$

For an equilibrium stable system, β is always positive, while γ vanishes for a second-order phase transition, and is non-zero for a first-order phase transition. Since the order parameter ϕ corresponding to the minimum of F changes as the sign of α changes, the transition point is determined by the equation $\alpha(T) = 0$, and, near this point, $\alpha(T)$ can be expanded as an integral power of $T - T_c$.

$$\alpha(T) \propto (T - T_c) \qquad (2.1.13)$$

As shown, for example, in the case of a second order phase transition in Figure(2.6), the free energy curve flattens as T approaches T_c continuously, leading to a bifurcation and breaking of inversion symmetry of the system below T_c. For T just above T_c, the flattening of the free energy curve means that the susceptibility χ_T of the system diverges,

$$\frac{1}{\chi_T} = \frac{\partial^2 F}{\partial \phi^2}|_T \to 0 \qquad (2.1.14)$$

resulting in a critical slowing down. That is, when a small external field is applied to the system, a macroscopic large scale fluctuation takes place in the order parameter, and the system cannot return quickly back to the equilibrium state. As shown earlier, the well-known example of a second order phase transition is the spontaneous magnetization of an Ising spin system, or the paramagnetic to the ferromagnetic phase transition. When the mean field approximation is adopted and the average value of the spin magnetization is assumed as the order parameter, the free energy has the Landau-Ginzburg potential form.

15

In a first order phase transition ($\gamma \neq 0$), the order parameter changes abruptly as the temperature is lowered below the critical temperature, and the entropy, or equivalently the first derivative of free energy, is discontinuous(Figure 2.7). There are abundant examples of first order phase transitions in equilibrium statistical mechanics. The best-known example, of course, is the gas-liquid phase transition. When the order parameter is plotted against temperature and the path of the order parameter is studied as a function of temperature, it is easily seen that a hysteresis behavior occurs between temperature and free energy as shown in Figure(2.8). For a fixed temperature below $T_c(\alpha < 0)$, there exists a hysteresis relation for another set of parameters; that is, between the order parameter and the parameter describing the external force, for example, pressure for the gas-liquid phase transition.(Figure(2.5))

It is well-established that the properties of a phase transition change when a thermodynamic system is subject to an external field whose action depends on the value of the order parameter ϕ. The application of an external field is accounted for by introducing the perturbation Hamitonian into the free energy. In general, the perturbation Hamiltonian is linear in the value of the order parameter, and because a linear term is present, the system undergoes a first order phase transition when the temperature is lowered. However, the apprearance of a linear term in the free energy means that ϕ is nonzero for any magnitude of the field, however weak, for all temperatures. Thus, the symmetry of the system is always broken as long as the external field is present, and the difference between the two phases for $T > T_c$ and $T < T_c$ disappears. Consequently, there is no discrete phase transition and the first order phase transition is smoothed out. In our discussion, we shall see that, most remarkably, the case of a ferromagnetic system in an external magnetic field has an almost identical formal analogy with O.B..[60][61]

We recall that according to the mean field theory of a ferromagnetism, the probability density $f(\phi)$ of the magnetization ϕ for a ferromagnet placed in an

16

external magnetic field H is the canonical distribution.

$$f(\phi) = N \exp(-F(\phi)/kT). \qquad (2.1.15)$$

where the Landau-Ginzburg potential $F(\phi)$ is given by

$$F(\phi) = -H\phi + \frac{\alpha}{2}\phi^2 + \frac{\beta}{4}\phi^4 \qquad (2.1.16)$$

and is plotted in Figure 2.9. The ensemble average of the magnetization is defined as the expectation value of ϕ with respect to the probability density $f(\phi)$.

$$\langle\phi\rangle = \int \phi f(\phi) d\phi \qquad (2.1.17)$$

In the classical theory of phase transitions, the average value of the order parameter is assumed to be identical to the most probable value of the order parameter which corresponds to the minimum of the Landau-Ginzburg potential. Therefore, the state equation for a ferromagnet in an external field is determined by putting the derivative of the potential with respect to the order parameter equal to zero,

$$\frac{\partial}{\partial\langle\phi\rangle} F(\langle\phi\rangle) = 0 \qquad (2.1.18)$$

From Eq.(2.1.16) the state equation is then simply

$$H = \alpha\langle\phi\rangle + \beta\langle\phi\rangle^3 \qquad (2.1.19)$$

or,

$$H = k(T - T_c)\langle\phi\rangle + \frac{kT}{3}\langle\phi\rangle^3 \qquad (2.1.20)$$

with $T_c = J\gamma/k$. Above T_c, $\alpha > 0$, the system exhibits paramagnetism, and there exists only one value of $\langle\phi\rangle$ for a given H. That is, the order parameter is mapped to the external field one-to-one. Below T_c, $\alpha < 0$, a first order phase transition takes place, and the order parameter shows hysteresis behaviour upon increase and decrease of the exeternal field. See Figure (2.10).

17

Similar symmetry changing phase transitions are observed in systems far from thermal equilibrium.[47]−[55] In a system in contact with more than one heat reservoir each having a different temperature, the reservoirs impose external forces and energy fluxes on the system, preventing it from reaching a thermal equilibrium state. In such systems, a macroscopic structural change takes place toward a lower symmetry state, such as, spatial anisotropy, when all of the states belonging to a high symmetry (for example, homogeneity and isotropy) become unstable.

In order to understand the phase transition mechanism in a system far from thermal equilibrium, we shall recall a few key thermodynamic properties of a nonequilibrium system. In a nonequilibrium closed system, the entropy change is not zero, and the system changes to the maximum entropy state in time through the exchange of energy with the heat reservoir. The system is said to be undergoing an irreversible process because the entropy of the system keeps on increasing; that is,

$$dS_{nonequil. \; closed \; system \; single \; res.} > 0 \qquad (2.1.21)$$

The nonequilibrium state is unstable in the sense that the system cannot remain in nonequilibrium indefinitely. When the system is perturbed by a thermodynamic fluctuation, it reestablishes the thermodynamic equilibrium.

Now suppose that we have a system in thermal contact with more than one heat reservoir, each having a different temperature. The heat reservoirs keep the system from reaching thermal equilibrium, and there occurs an energy flow through the system from one heat reservoir with a high temperature to another heat reservoir with a lower temperature. The heat reservoirs exert a generalized thermodynamic force, X_k, on the system, called an affinity, giving rise to a corresponding flux, J_k. For example, when only energy flow is allowed, the temperature difference between two heat reservoirs is the thermodynamic force, and the energy flow is the corresponding flux. In some cases, we can consider a system where matter flow as well as energy flow is allowed, and the affinity and the flux are defined

18

accordingly. The flux flow through the system causes a change in the entropy of the system. Equivalently, it can be said that in time t, the entropy is produced inside the system through a dissipating process.

$$P = \frac{\partial_i S}{\partial t} = \int dV \sum J_k X_k \qquad (2.1.22)$$

In contrast to a closed system in thermal contact with only one heat reservoir, a system in thermal contact with more than one heat reservoir is always in nonequilibrium, and the macroscopic state of the system is strongly affected by the energy and/or matter flow. The total entropy change in the system comes from both the entropy flow into the system and the increase of the entropy inside the system through a dissipative irreversible process; that is,

$$dS_{nonequil. \ closed \ system, \ many \ reser.} = d_e S + d_i S \qquad (2.1.23)$$

where $d_e S$ is the entropy flow into the system, and $d_i S$ is the entropy produced inside the system. The total entropy change in time can be written as

$$\begin{aligned} \frac{\partial S}{\partial t} &= \frac{\partial_e S}{\partial t} + \frac{\partial_i S}{\partial t} \\ &= -\int_{surface} d\vec{\Sigma} \bullet \vec{J_s} + \int dV \sum J_k X_k \end{aligned} \qquad (2.1.24)$$

where $\vec{J_s}$ is the entropy current into the system from the heat reservoirs, X_k is the affinity, and J_k is the flux corresponding to the given affinity. The entropy change through an irreversible process from inside, $d_i S$, is greater than zero because the system itself is in nonequilibrium. A system is said to be at a steady state if the thermodynamic state variables do not evolve in time. This means that in steady state, the total entropy change dS is zero, or from Eq.(2.1.23)

$$d_e S = -d_i S < 0 \qquad (2.1.25)$$

We find that in order to maintain a n.oneqilibrium steady state, it is necessary to have a continuous, negative entropy flow into the system that is equal to the value of the internal entropy production inside the system.

Now we discuss the thermodynamic stability of a nonequilibrium steady state. A system with an affinity much smaller than the thermal energy is called a linear system. When only energy flow is allowed between the system and a heat reservoir, this corresponds to the case that the temperature gradient is much smaller than the average temperature. In such systems, the flux can be approximated to be linearly proportional to the affinity. For example, the heat conduction in a linear system is given by

$$J_z = -\kappa \nabla_z T = \kappa T^2 \nabla(\frac{1}{T}) \tag{2.1.26}$$

For a linear system, from Onsager's reciprocity theorem and the linearity, it can be shown that the entropy production from inside the system is minimum when in a steady state. This is called the 'minimum entropy production' theorem. It implys that the system prepared not in steady state evolves toward the steady state by producing entropy at a rate always larger than the entropy production rate for the final steady state. In another words, the production rate is largest in the beginning, and *gets smaller as the system approaches the steady state.* As shown in Figure(2.11), when the entropy production from inside the system is plotted in time, it approaches to the minimum entropy production rate corresponding to the steady state value. If we recall the role of a thermodynamic potential the minimization of which determining a macroscopic state of a thermodynamic system, the entropy production rate, $P = \partial_i S / \partial t$, can be viewed as an appropriate thermodynamic potential in determining the stability of a linear system. Say the system has a disordered configuration $\{q_0\}$ in a steady state, and then perturbed by a small linear fluctuation to a new configuration $\{q\}$. The entropy production, $P(\{q\})$, corresponding to $\{q\}$ is always larger than $P(\{q_0\})$, and the system reestablishes the steady state by minimizing the entropy production P (Refer to Figure(2.12)). That is, the steady state with the maximum entropy ($dS = 0$) and with the minimum entropy production from inside ($P = \partial_i S / \partial t = minimum$) is stable against any linear thermodyanmic perturbation that pulls the system from steady state, because

20

the entropy production is always large enough to return the system back to the steady state. This means that a disordered state cannot evolve to an ordered state as long as the system deviates from equilibrium only through fluctuations or random perturbations. Morover, in a system obeying linear laws, a spontanoeus emergence of order in the form of spatial or temporal patterns differing qualitatively from equilibrium behavior cannot take place.

However, in a nonlinear system, where the affinity is on the order of or larger than the thermal energy, the minimum entropy production theorem does not hold in general. Therefore, a systematic change of one of the thermodynamic parameters or the increase of the affinity (for example, the increase of a temperature gradient) might force the system to find another steady state with a new configuration. This means that the steady state which is stable in a linear regime becomes unstable in a nonlinear regime, and evolves in time toward a new stable state which possesses different thermodynamic values. This new stable state becomes a steady state, and exhibits completely new macroscopic behavior. In many of cases, the nonlinearity works to provide a positive feedback to the system, allowing a macroscopically ordered state as a steady state. Therefore, it is possible to have a nonequilibrium phase transition from a disordered to an ordered state. The fundamental difference from an equilibrium phase transition is that the nonequilibrium system should be kept far from thermal equilibrium by energy flow through the system in order to maintain the macroscopic ordering achieved by a phase transition. The actual evolution pattern to a new stable state is different from one physical system to another physical system, depending on the interaction Hamiltonian. The stability has been studied in nonlinear dynamics, and even an apparently simple nonlinear system shows a whole variety of instabilities. The nonequilibrium phase transition behavior can be understood by reducing the problem to a nonlinear dynamics problem.

Hydrodynamics, chemical reactions, and laser threshold are only a few ex-

21

amples of physical systems where a symmetry breaking phase transition takes place when the system is maintained far from equilibrium. Thus, a fluid layer in gravity heated from below develops a regular convection pattern called the Benard instability. This formation of a pattern in the fluid is in fact a symmetry breaking phase transition from a homogeneous, isotropic state to a well-formed, anisotropic state. The fluid is an open system where there is an energy flow from the bottom hot plate to the top air. The convection pattern persists as long as the temperature difference is maintained, allowing an energy flow across the boundaries of the fluid.

Another example can be found in a chemically reacting system which is closed to mass flow but open to energy flow across its boundary. The chemical reaction between N_2O_4 and NO_2 under illumination is known to show multiple stationary states of NO_2 concentration. When an equilibrium mixture of NO_2 and N_2O_4 is irradiated with visible light, the light is absorbed only by NO_2 and most of the absorbed light ultimately convert into heat. The increase in temperature accelerates the production of NO_2, resulting in an increased light absorption, and, hence an increased temperature, which in turn produces even more NO_2. As long as the incident light intensity is strong enough, the mixture of NO_2 and N_2O_4 undergoes a phase transition to the pure NO_2.

As these examples illustrate, we can expect a symmetry broken ordered state in system far from equilibrium. The emergence of order and coherence extending over scales much larger than the characteristic scales of the individual molecules in a system far from equilibrium reminds us of the order-disorder phase transition in thermal equilibrium. Similar to the equilibrium phase transition, the cooperative effects between molecules (the detailed form of the cooperativity depending on the intercation Hamiltonian of the system) inside an open system is the single most important fact in giving a macroscopic, long range order. Even if these two phase transitions share a formal similarity, there is a fundamental difference in the origin for the phase transition. The origin of the thermal equilibrium phase transition

22

can be traced back to the competition between the interaction energy and the entropy, these two comprising the free energy of a closed system. In contrast, a structural phase transition in an open system far from equilibrium originates from nonlinear interactions inherent in the Hamiltonian of the system, and the ordered phase can be maintained only in the presence of energy and/or matter flow through the sytem. The stability and the origin of bifurcation in nonequilibrium system have been studied in nonlinear dynamics, and it has been found that a nonlinear interaction term in the Hamiltonian is responsible for the onset of instability. The nonlinear source can be easily identified once a suitable microscopic description of the system is obtained. In hydrodynamics, a term of the from $\vec{v} \bullet \vec{\nabla} \vec{v}$ in the fluid velocity $\vec{v}$ appearing in the Navier-Stokes equation is the nonlinear source, while in the $NO_2 - N_2O_4$ chemical reaction, a temperature dependent nonlinear reaction rate constant k gives rise to the instability

The last example is the case of laser threshold which is directly relevant to the overall discussion. In laser threshold, a stimulated scattering process occurs between two mirrors of F-P cavity, [56]−[59] and laser threshold is an important example of second order phase transition of a stationary nonequilibrium system. As illustrated in Figure(2.13), the electric field amplitude E is taken as the order parameter that describes the macroscopic state of the system, and λ is the optical pumping intensity which determines the inversion population. For very weak optical pumping, the system may be considered as being in a nonequilibrium state with a finite relaxation time fluctuating from thermal equilibrium, and the order parameter is zero. With increased pumping, the nonlinear interaction of light with matter leads to the onset of instability. Critical slowing down takes place, and the system cannot be appoximated to be near thermal equilibrium any more. Instead, the system is understood to be near a stationary nonequilibrium state as indicated by the infinite relaxation time. For $\lambda > \lambda_c$ where λ_c is a threshold pumping intensity, a new branch of states is found to be stable with a non-zero order parameter

23

and a finite relaxation time. The two different branches of state have different symmetries, which is the phase of the electric field amplitude in this case. For the zero amplitude branch, the phase of each microscopic dipole is random, and there exists a complete phase angle rotation invariance. This phase symmetry is broken on the finite amplitude branch, and the broken symmetry implies the existence of long range order in space and time. In other words, the microscopic dipoles with random phase were undergoing spontaneous emission process in the zero amplitude branch, and above threshold pumping, the microscopic dipole moments are strongly correlated through stimulated emission leading to an ordered coherent emission. The random phase of individual dipoles is then slaved by the non-zero order parameter, or the resultant laser light, to possess an arbitrary but fixed phase.

For this quantum optical phase transition to take place, there is a critical number density of the molecules similar to the critical temperature in the thermodynamic phase transitons. In laser threshold, for example, the electric field can be taken as an order parameter and the population inversion as the temperature, and above the critical population inversion the system composed of the photons and the molecules undergoes a second-order phase transtion breaking the spatial symmetry, i.e., from the disordered phase to the ordered phase. The nonequilibrium phase transition, however, is not in thermal equilibrium, and energy is constantly flowing through the system. The system is an open system with respect to the number of photons present. But there does exist a concept corresponding to thermal equilibrium. For example, in laser threshold, there exists a photon flux equilibrium. In fact, in all quantum optical processes, flux equilibrium is achieved rather than thermal equilibrium, and a generalized free energy can be defined. The minimization of the generalized free energy for a given number density of the optical sites determines the macroscopic state of the system. Optical bistability can be understood in the exactly same way. The state equation describing the nonlinear Fabry-Perot interferometer has a close formal analogy with to the state equation for a ferromagnet

in an external magnetic field. O.B. is a quantum optical analogue of the first-order phase transition, having a well-defined generalized Landau-Ginzburg potential. The incident laser intensity corresponds to the external magnetic field, the output light intensity to the order parameter (magnetization), and the cooperative parameter to the temperature.[60](Table 2.1)

A complete description of a nonequilibrium phase transition requires the introduction of the Langevin equation for the order parameter and the corresponding Fokker-Plank equation describing the time evolution of the probability distribution function of the order parameter. A Markovian process is commonly assumed. The stationary solution of the Fokker-Planck equation[62][63] is directly obtainable, and the generalized Landau-Ginzburg potential can be defined.

Here we briefly review for illustration the Langevin equation and obtain the corresponding Fokker-Planck equation by using the simple physical example of a Brownian particle. When a large particle is immersed in a viscous fluid, the particle is subject to a continuous, random bombardment from the incessant thermal motion of the fluid molecules. The thermodynamic system is defined as the Brownian particle plus the viscous liquid. The system is isolated from its surrounding. The Brownian particle is in simple thermal contact with a single large heat reservoir which is the viscous liquid. In thermal equilibrium, a probability distribution of velocity of the Brownian particle is a canonical distribution. But here we are interested in the nonequilibrium state of the Brownian particle where the dissipation of kinetic energy of the Brwonian particle and the collision of the Brownian particle with the viscous liquid should be considered explicitly. The nonequilibrium microscopic processes are best described by stochastic theory. For example, the equation of motion of the Brownian particle is given by Langevin equation,

$$\frac{dv}{dt} = -\gamma v + F(t) \qquad (2.1.27)$$

where v corresponds to the velocity of the particle, $-\gamma v$ is the frictional force linearly proportional to v with γ the dissipation rate, and $F(t)$, called a Langevin force,

describes the random, fluctuating forces acting on the Brownian particle. In order to properly take into account the random fluctuations of the Langevin force $F(t)$, a themodynamic ensemble of the system is introduced. In the thermodynamic ensemble, the Langevin force varies from system to system, and only the ensemble averages of the force are known. The macroscopic behavior of the Brownian particle can be described only in terms of these ensemble average values of the stochastic Langevin forces which are assumed to be time-correlated in a specific way depending on the actual form of the stochastic prcesses. The ensemble average of $F(t)$ should vanish

$$\langle F(t) \rangle = 0 \tag{2.1.28}$$

because the average velocity $\langle v \rangle$ of the Brownian particle decays exponentially. In most cases, the collision of the particle with the fluid molecules takes place in a very short time compared to the relaxation of the velocity acquired from the collision. Two successive Langevin forces acting separately in a time longer than the collision time are independent, and under this condition, the ensemble average of the Langevin forces is zero. When the collision is assumed to be instantaneous, or, equivalently, the correlation time of the Langevin forces are zero, the Langevin force is said to be delta-function correlated; that is,

$$\langle F(t)F(t') \rangle = Q\delta(t - t') \tag{2.1.39}$$

Q is the magnitude of the auto-correlation of the Langevin force, and is a measure of the noise strength. A delta-function correlated Langevin force is called white noise because the spectral distribution obtained from Fourier transformation of a delta-function is constant, independent of frequency. When the spectral distribution has a frequency dependence, it is called colored-noise, one typical example being a Gaussian-correlation. •

$$\langle F(t)F(t') \rangle = \frac{Q}{\tau} \exp\{-|t - t'|/\tau\} \tag{2.1.30}$$

26

For colored-noise, the general solution of the Langevin equation is obtainable by numerical methods. Keeping our discussion simple, we will consider the case of white-noise and recall the physical implications of the time-correlation of the Langevin forces.

The Langevin equation Eq.(2.1.37) for a Brownian particle is linear because the frictional force on the particle is linear in v and the magnitude of delta-correlation is independent of v. In the case of a linear Langevin equation, the analytical solution of $v(t)$ is

$$v(t) = v_0 \exp(-\gamma t) + \int_0^t F(t') \exp\{-\gamma(t - t')\} dt'. \qquad (2.1.31)$$

Most of the physical properties of the Brownian particle can be obtained from Eq.(2.1.29) and Eq.(2.1.31). For example, the mean kinetic energy of the Brownian particle can be immediately derived

$$E = \frac{m}{2} \langle v(t)^2 \rangle = \frac{m}{2} \int_0^t \int_0^t \langle F(t_1)F(t_2) \rangle \exp(-2\gamma t) \exp(\gamma t_1 \gamma t_2) dt_1 dt_2$$

$$= \frac{mQ}{4\gamma}(1 - \exp(-2\gamma t)) \qquad (2.1.32)$$

After a time much longer than the inverse of the dissipation rate ($t >> 1/\gamma$), the Brownian particle will be in a thermal equilibrium with the fluid molecules, and the kinetic energy of the Brownian particle is $3kT/2$ from the equipartition theorem,

$$E = \frac{m}{2} \langle v^2 \rangle = \frac{mQ}{4\gamma} = \frac{3}{2}kT \qquad (2.1.33)$$

or

$$Q = \frac{6\gamma kT}{m} \qquad (2.1.34)$$

This shows that the magnitude of the noise is related to the friction, which is the simplest example of the fluctuation-dissipation theorem. Furthermore the time-correlation of the Langevin force has been identified with other macroscopic quantities, the dissipation rate, γ, and the temperatue of the heat reservoir, T. In

27

principle, the noise strength Q can be derived rigorously from the equation of motion for all microscopic variables. Here, however, we have resorted to the physical argument through the equipartition theorem to find the physical implications for Q.

Now we consider the diffusion of the Brownian particle. The diffusion is defined as the mean displacement of the Brownian particle as a result of the stochastic collisions with the fluid molecules, and can be viewed as a macroscopic physical manifestation of the microscopic stochastic processes. Once the velocity correlation is known, the diffusion of the Brownian particle in time is directly obtained by integration.

$$\langle (x(t) - x_0)^2 \rangle = \langle [\int_0^t v(t_1)dt_1]^2 \rangle = \int_0^t \int_0^t \langle v(t_1)v(t_2) \rangle dt_1 dt_2$$
$$= \frac{Q}{\gamma^2} t = 2Dt \tag{2.1.35}$$

where the velocity correlation is approximated as

$$\langle v(t_1)v(t_2) \rangle \approx \frac{1}{\gamma^2} \langle F(t_1)F(t_2) \rangle = \frac{Q}{\gamma^2} \delta(t_1 - t_2) \tag{2.1.36}$$

which corresponds to neglecting the transient velocity change because we are interested in the diffusion in thermal equilibrium. From Eq.(2.1.34) and Eq.(2.1.35) we get the well-known Einstein relation.

$$D = \frac{Q}{2\gamma^2} = \frac{3kT}{m\gamma} \tag{2.1.37}$$

The important conclusion is that the diffusion of a Brwonian particle inside a viscous fluid is related to the correlation of the Langevin forces, or in other words, the process of diffusion is nothing but a random walk at a molecular level.

In general, the Langevin equation is nonlinear, and the analytical form of the ensemble average of the velocity is not easily available. The general Langevin equation with white-noise is expressed by the relation

$$\frac{dx}{dt} = K(x) + F(t) \tag{2.1.38}$$

$$\langle F(t) \rangle = 0, \quad \langle F(t)F(t') \rangle = Q(x)\delta(t - t') \qquad (2.1.39)$$

where now x is a general variable. The ensemble average of the variable x is difficult to obtain for a general nonlinear Langevin equation just because the analytic solution is not known except for a trivial case. Rather than trying to obtain the rigorous solution of the Langevin equation, we find a differntial equation for the probability density, or the probability distribution function, $f(x, t)$, of finding the variable x in the interval $(x, x + dx)$ at time t. In principle, once the probability distribution function is known, the ensemble average can be obtained immediately just by integration. Then the question comes down to whether the Langevin equation can be reduced to an equation for the probability density in a simple way. Fortunately, for the case of white noise, it is known that the Langevin equation can be reformulated to a differential equation for the probability density, called the Fokker-Planck equation first derived to describe Brownian motion. Furthermore, as will be seen later, the reformulation of the Langevin equation by the Fokker-Planck equation is important in providing a thermodynamic potential concept that is very useful in studying a nonequilibrium phase transiton. The thermodynamic potential concept, which is even applicable to a system far from equilibrium, allows us to make an analogy between the nonequilibrium phase transition and the equilibrium phase transition.

In the case of delta-correlated white noise, which is a Markovian process, the derivation of the Fokker-Planck equation is rather simple. The Fokker-Planck equation corresponding to the general Langevin equation Eq.(2.1.38) is

$$\frac{\partial f(x, t)}{\partial t} = -\frac{\partial}{\partial x}K(x)f(x, t) + \frac{1}{2}\frac{\partial^2}{\partial x^2}Q(x)f(x, t) \qquad (2.1.40)$$

which is an equation of motion for the probability distribution function $f(x, t)$. Here K is refered to as the 'drift' term, and Q the 'diffusion' term. The Fokker-Planck equation can be expressed as a continuity equation for the probability.

$$\frac{\partial f}{\partial t} = -\frac{\partial}{\partial x}(Kf - \frac{1}{2}\frac{\partial}{\partial x}Qf) = -\frac{\partial}{\partial x}j(x, t) \qquad (2.1.41)$$

where $j(x, t)$ is the probability current. Thus, the change of the probability density $f(x, t)$ in time is equal to the negative of the divergence of the probability current $j(x, t)$. When the drift term is absent ($K=0$), Eq.(2.1.40) is a diffusion equation, and for constant Q, the time dependent solution is

$$f(x, t) = \frac{1}{\sqrt{2\pi Q t}} \exp\{-\frac{(x - x_0)^2}{2Q t}\} \tag{2.1.42}$$

Without a 'drift' term K, the probability density $f(x, t)$ gets broadened in time, which eventually becomes flat. In a real physical system, the drift term is manifested as a restoring force which keeps the probability density from spreading out temporally while the diffusion term appears as a stochastic force which makes the probability density broaden in time. One standard way to reduce the time-dependent Fokker-Planck equation to a time-independent equation is to change the equation into an eigenvalue equation. The time dependent part can be separated by assuming the following product function

$$f(x, t) = e^{\lambda t} \Psi(x) \tag{2.1.43}$$

The spatial part Fokker-Planck equation becomes

$$\lambda \Psi(x) = -\frac{\partial}{\partial x} K(x) \Psi(x) + \frac{1}{2} \frac{\partial^2}{\partial x^2} C(x) \Psi(x) \tag{2.1.44}$$

Once the eigenvalues of Eq.(2.1.44) are obtained, the probability density $f(x, t)$ is expressed as a linear combination of the linearly independent solutions.

$$f(x, t) = \sum_{m=0}^{\infty} e^{\lambda_m t} \Psi_m(x) \tag{2.1.45}$$

The stationary solution corresponds to $\lambda_0 = 0$. There are various ways to solve the time dependent Fokker-Planck equation, but the nonlinear differential equation itself causes a lot of difficulty in obtaining an analytic solution. Even the one dimensional problem cannot be solved without using a numerical method. In the

30

steady state ($t \to \infty$), the two competing terms balance out, and there is no temporal change in the probability density $f(x,t)$ exhibiting a stationary behavior. The stationary (steady state) solution is quite simple. Neglecting the time derivative in Eq.(2.1.41), the stationary probability $f(x)$ is simply

$$f(x) = \frac{N}{Q(x)} \exp(2 \int \frac{K(x)}{Q(x)} dx) = \frac{N}{Q(x)} \exp(-F(x)) \qquad (2.1.46)$$

$F(x)$ introduced in Eq.(2.1.46) is the generalized Landau-Ginzburg potential for a stationary state, which is an important concept for understanding the physical behavior of the system. Let's look at the Brownian particle one more time to understand the physical implication of the Landau-Ginzburg potential. For the Brownian particle, the stationary solution is

$$F(v) = -2 \int \frac{K(v)}{Q(v)} dv = \frac{2}{Q} \int \gamma v \, dv = \frac{2}{Q} \frac{\gamma v^2}{2} = \frac{mv^2}{2kT} \qquad (2.1.47)$$

and the probability density is given as

$$f(v) = N \exp(-F(v)) = \sqrt{\frac{m}{2\pi kT}} \exp(-\frac{mv^2}{2kT}) \qquad (2.1.48)$$

The ensemble average of the kinetic energy is then simply given by

$$\frac{m}{2} \langle v^2 \rangle = -\frac{\partial}{\partial \beta} \ln \int_{-\infty}^{\infty} f(v) dv = \frac{1}{2} kT \qquad (2.1.49)$$

We find that the probability density follows the Maxwell distribution, the standard deviation determined by the temperature, or the magnitude of stochastic force. Now let's look at the potential, Eq.(2.1.47). The potential is of a parabolic form, and the stationary state can be visualized by considering a point particle in the parabolic potential well. The thermal fluctuations (more precisely the stochastic Langevin force) from the fluid molecules keep pushing up the point particle along the potential well (note a large Q means a flatter parabola), and the frictional force (or the drift term) attract the point particle down to the minimum position of

31

the potential well (note a large frictional force correspond to a sharper parabola.). We note that a small Q corresponds to a deep potential well, or a sharp peak in the probability density $f(x)$, implying the stationary state is well-defined. A Brownian particle has been chosen to elucidate the idea behind the Fokker-Planck equation. The Brownian particle was in the thermal equilibrium with the viscous fluid, and the diffusion was found to be linearly proportional to the temperature of the heat reservoir. However, the application of the Fokker-Planck equation is not restricted to systems near thermal equilibrium. For an open system far from thermal equilibrium, once the Langevin equation describing the time dependence of the order parameter is identified from an equation of motion for the relevant nonequilibrium physical system, we can build the Fokker-Planck equation with an appropriate delta-correlated stochastic force. This then allows a definition of the generalized Landau-Ginzburg potential in the stationary state. By examining the Landau-Ginzburg potential, the phase transition behavior of the nonequilibrium state can be studied.

2.2 Bloch Saturable Absorber System inside a Fabry-Perot Cavity

With this background, let's consider a system composed of resonant atoms in an F-P cavity. The F-P cavity contains N two-level Bloch type atoms with the transition frequency ω_a. The mirror spacing of the F-P cavity can be varied. For a given mirror spacing, the cavity mode ω_c is determined simply by the standing wave condition. We now send in a coherent laser light of optical frequency ω, that is in complete resonance with the atomic transition frequency ω_a. The cavity mode ω_c is tuned to the incident laser frequency ω, which corresponds to the setting of the F-P cavity at the maximum transmission peak. Thus,

$$\omega = \omega_c = \omega_a$$

This corresponds to the condition for purely absorptive O.B.. The interaction of a Bloch system with an electromagnetic field is described by a Bloch equation as will

be discussed in Chapter 3. When the incident light frequency is resonant with the atomic frequency, the Bloch equation Eq.(3.5.26-28) reduces to

$$\dot{v} = \frac{\mu}{\hbar}\varepsilon w - \gamma_{\perp} w \qquad (2.2.1)$$

$$\dot{w} = -\frac{\mu}{\hbar}\varepsilon v - \gamma_{\|}(w - w_{eq}) \qquad (2.2.2)$$

Now we need an equation of motion for the electromagnetic field, which is, of course, the Maxwell equation. The wave equation is

$$\left(\frac{\partial^2}{\partial z^2} - \frac{1}{c^2}\frac{\partial^2}{\partial t^2}\right)\bar{E}(z,t) = \frac{4\pi}{c^2}\frac{\partial^2}{\partial t^2}\bar{P}(z,t) \qquad (2.2.3)$$

Since the rotational wave approximation (RWA) was used in deriving the Bloch equation (Refer to Chapter 3, Sec.3.5), a rapidly changing part of the electric field and the polarization field does not affect the atoms appreciably, and the reaction of the atoms back on the electric field is slow. The slowly varying envelope approximation (SVEA) for the fields is, thus, satisfied. Setting

$$\bar{E}(z,t) = E(z,t)\exp i(kz - \omega t), \quad \bar{P}(z,t) = P(z,t)\exp i(kz - \omega t) \qquad (2.2.5)$$

we find a linear wave equation in SVEA neglecting the second order derivatives as follows.

$$\frac{\partial E}{\partial t} + c\frac{\partial E}{\partial z} = i2\pi\omega P \qquad (2.2.6)$$

The polarization of the Bloch system is given as (see Eq.(3.7.1))

$$P = \frac{N}{V}\mu(u - iv) = -i\frac{\mu}{V}Nv \qquad (2.2.7)$$

for perfect tuning of the laser frequency with the atomic transition frequency ($\omega = \omega_a$). The macroscopic parameters are redefined as,

$$S = -\frac{Nv}{2}, \quad \Delta = \frac{1}{2}(N_1 - N_2) = -\frac{Nw}{2} \qquad (2.2.8)$$

33

where S is related to the macroscopic dipole moment, and Δ is half of the population difference between the ground state (N_1) and the excited state (N_2). The Maxwell-Bloch equations Eq.(2.2.1) (2.2.2) (2.2.6) reduce to a set of coupled Langevin equations Eq.(2.2.9)-(2.2.11) when the spatial average is taken for the electromagnetic field. (See Appendix A1 for a derivation of Maxwell-Bloch equation in the second quantization formalism)

$$\dot{E} = -gS - \kappa(E - E_i/\sqrt{T}) + F_E(t) \qquad (2.2.9)$$

$$\dot{S} = \frac{\mu}{\hbar}E\Delta - \gamma_\perp S + F_S(t) \qquad (2.2.10)$$

$$\dot{\Delta} = -\frac{\mu}{\hbar}ES - \gamma_\parallel(\Delta - \frac{N}{2}) + F_\Delta(t) \qquad (2.2.11)$$

where

$$\kappa = \frac{c(1-R)}{L}, \quad g = \frac{4\pi\omega}{V}\mu \qquad (2.2.12)$$

κ is the cavity damping constant, or the life time of photons inside the F-P cavity, and g is the dipole coupling constant between the atoms and the electric fields in the cavity modes. F_E, F_S, and F_Δ are the fluctuations responsible for the diffusion constant.[68][69] The Maxwell-Bloch equations can be reduced to the Langevin equation for the optical field E in the good cavity limit ($\kappa << \gamma_\perp, \gamma_\parallel$) where the adiabatic following of the atoms to the electric field can be assumed, in which case the time derivatives in Eq.(2.2.10) (2.2.11) can be ignored because the temporal change of the microscopic dipole moments is slaved by the macroscopic Maxwell optical field (order parameter). More explicitly, substituting Eq.(2.2.11) into Eq.(2.2.10) in the adiabatic following assumption gives

$$S = \frac{\mu}{\hbar\gamma_\perp}E\Delta$$
$$= \frac{\mu}{\hbar\gamma_\perp}E(\frac{N}{2} - \frac{\mu}{\hbar\gamma_\parallel}ES) \qquad (2.2.13)$$

or

$$S = \frac{\frac{\mu}{\hbar\gamma_\perp}\frac{N}{2}E}{1 + (\frac{1}{\sqrt{\gamma_\perp\gamma_\parallel}}\frac{\mu}{\hbar}E)^2} \qquad (2.2.14)$$

34

Substituting Eq.(2.2.14) into Eq.(2.2.9) yields the Langevin equation for the electric field.

$$\frac{1}{\kappa}\dot{E} = E_i/\sqrt{T} - E - \frac{2\frac{\mu g N}{2\hbar\kappa}\frac{1}{2\gamma_\perp}E}{1 + (\frac{1}{\sqrt{\gamma_\perp\gamma_\parallel}}\frac{\mu}{\hbar}E)^2} + F_E(t) \tag{2.2.15}$$

Introducing the Rabi frequencies (see Chapter 3 Sec 3.5)

$$\Omega_t = \frac{\mu}{\hbar}E = \frac{1}{\sqrt{T}}\frac{\mu E_t}{\hbar}, \quad \Omega_i = \frac{1}{\sqrt{T}}\frac{\mu E_i}{\hbar} \tag{2.2.16}$$

and defining the scaled amplitudes x and y for the transmitted and the incident fields, and the scaled time τ,

$$x = \frac{\Omega_t}{\sqrt{\gamma_\perp\gamma_\parallel}}, \quad y = \frac{\Omega_i}{\sqrt{\gamma_\perp\gamma_\parallel}}, \quad \tau = \kappa t \tag{2.2.17}$$

Eq.(2.2.15) reduces to a simple form

$$\frac{dx}{d\tau} = y - x - \frac{2Cx}{1+x^2} + F(t) \tag{2.2.18}$$

where

$$C = \frac{\gamma_R}{2\gamma_\perp} = \frac{1}{2}\frac{4\pi\omega\mu^2}{\hbar c}\frac{N}{V}T_2\frac{L}{1-R} = \frac{\alpha_0 L}{2(1-R)} \tag{2.2.29}$$

$$\gamma_R = \frac{\mu g N}{2\hbar\kappa} = \frac{2\pi\omega\mu^2 N}{\hbar\kappa V} \tag{2.2.20}$$

C is called the cooperative parameter, and is the ratio of the superfluorescent decay rate(γ_R) to the spontaneous decay rate, or a measure of the cooperative effect of atoms relative to a non-cooperative individual atomic effect. As will be seen below, the cooperative parameter C plays a role analogous to the critical temperature in the thermodynamic equilibrium phase transition. Note that the stochastic Langevin forces is rescaled.

$$F(t) = \frac{1}{\kappa\sqrt{\gamma_\perp\gamma_\parallel}}\frac{\mu}{\hbar}F_E(t) \tag{2.2.21}$$

In the stationary state, Eq.(2.2.18) reduces to the state equation for the system.

$$y = x + \frac{2Cx}{1+x^2} \tag{2.2.22}$$

35

The state equation can be solved in an analytical form, and there exists one real root for the output field amplitude x which is the order parameter for the system, for a given input field amplitude y for $C < 4$. But for $C > 4$, there are three real roots of x for a given y exhibiting a bistable behavior. A comparison of the state equation for O.B. to that for 2-D Ising spin system (Eq.(2.1.20)) shows a one-to-one correspondence of the thermodynamic variables clearly. The input electromagnetic field amplitude y corresponds to the external magnetic field H, the output electromagnetic field amplitude x to the total magnetization $\langle \phi \rangle$, and the cooperativity C to the temperature T.

In order to understand (i) the phase transition behavior, (ii) the temporal change of the order parameter x upon the change of the external field y, and (iii) the effects of fluctuations, we need to find the Fokker-Planck equation. The magnitude of the stochastic Langevin force can be found from the Heisenberg equation of motion of the microscopic variable. There are many sources for the fluctuations, for example, the fluctuation in the external field amplitude itself, or the fluctuation in the polarization of the electric fields. But the most dominant contribution to the noise is from the decay of the photons either in the coherence through the spontaneous radiation and the homogeneous broadening or in the numbers through a cavity leaking (i.e. a finite life time of photons inside F-P cavity). The quantum statistical analysis of O.B. identifies the corresponding thermodynamic parameters$(T_c, \alpha, \beta, \ldots)$ in terms of the optical parameters of the atoms and cavity.[64]−[69] The Fokker-Plank equation corresponding to Eq.(2.2.18) is

$$\frac{\partial f}{\partial \tau} = -\frac{\partial}{\partial x} K(x) f + \frac{1}{2} \frac{\partial^2}{\partial x^2} Q(x) f \qquad (2.2.23)$$

with

$$K(x) = y - x - \frac{2Cx}{1 + x^2} \qquad (2.2.24)$$

$$Q(x) = q \left(\frac{x}{1 + x^2} \right)^2 \qquad (2.2.25)$$

36

$$q = \frac{C}{N_s} = 2(\frac{2\pi\hbar\omega}{V})^2 \frac{\mu^4 N}{\kappa\gamma_\perp^2 \gamma_\parallel} \tag{2.2.26}$$

$$N_s = \frac{\gamma_\perp \gamma_\parallel V}{8\pi\hbar\omega\mu^2} \tag{2.2.27}$$

where N_s is the saturation photon density appearing in the quantum mechanical description of superfluorescence.[70][71] The stationary solution of the Fokker-Planck equation (2.2.23) is straightforward leading to

$$\begin{aligned}
f(x) &= N\exp(2\int \frac{K(x)}{Q(x)}dx) \\
&\approx N\exp(\frac{2}{q}\int K(x)dx) \\
&= N\exp(-\frac{2V(x)}{q}) \tag{2.2.28}
\end{aligned}$$

where q is assumed to be small, and the generalized Landau-Ginzburg potential $F(x)$ is

$$F(x) = \frac{2V(x)}{q} = \frac{2}{q}\{\frac{1}{2}(x-y)^2 + C\ln(1+x^2)\} \tag{2.2.29}$$

with

$$V(x) = -\int K(x)dx = \frac{1}{2}(x-y)^2 + C\ln(1+x^2) \tag{2.2.30}$$

In Figure(2.14-17), we plotted the above potential $F(x)$ as a function of the order parameter x, which is the output field amplitude, for various values of cooperative parameter C in a fixed input field amplitude y. It is evident that the first order phase transition occurs at $C = 4$, and there exist a hysteresis relation between the output and the input field amplitudes only for

$$C = \frac{\alpha_0 L}{2(1-R)} > 4. \tag{2.2.31}$$

Let's look at the plot for $C = 20$ (Figure 2.17). At a low input amplitude, the output amplitude (order parameter x) is near zero, say x_1, and as the input intensity is increased, a new local minimum of the potential $F(x)$ starts to appear at another positive value of order parameter, say x_2, greater than the original value x_1. For

a large enough input amplitude, the potential $F(x)$ at this new value of order parameter, x_2, becomes the global minimum, but the system still assumes the order parameter x_1 corresponding to the local minimum, because the potential barrier is high enough to prevent the system leaking through to the global minimum x_2. Once the input amplitude exceeds threshold value corresponding to the disappearance of the local minimum with the order parameter value x_1, the nonlinear Fabry-Perot switches over to a high transmission state having a new order parameter x_2, and stays there. When the above process is reversed, that is, as the input amplitude is decreased, the potential $F(x)$ shows a similar behavior upon the change of the input intensity. But this time the role of x_1 and x_2 is reversed because the system is already in a state with the order parameter value x_2, that is, in a highly transmittant state. As the input amplitude is kept being decreased, the potential $F(x)$ at the order parameter value x_1 starts to become a local minimum and evolves to the global minimum, but the system is still in a highly transmittant state untill the local minimum at x_2 disappears. Therefore the nonlinear Fabry-Perot can assume two different macroscopic states (low transmittant x_1 and high transmittant x_2) depending on the history of the preparation of the given input amplitude.

When the output field amplitude is plotted as a function of the input field amplitude from the state equation Eq.(2.2.22), it is easy to see that for C less than or equal to 4, the output field amplitude is a nonlinear function of the input field amplitude as can be seen from the stationary state equation Eq.(2.2.22), but still they are mapped by one-to-one without any bistability.

References: Chapter 2

[1] Gibbs, H.M., *Optical Bistability - Controlling Light with Light*, Academic, New York (1985)

[2] Bowden, C.M., Ciftan, M., and Robl, H.R., eds. *Optical Bistability*, Plenum, New York (1981)

[3] Bowden, C.M., Gibbs, H.M., and McCalls, S.L., eds. *Optical Bistability II*, Plenum, New York (1983)

[4] Gibbs, H.M., Peyghambarian, N., Mandel, P., and Smith, S.D., *Optical Bistability III*, Springer, Berlin (1986)

[5] Szoeke, A, Daneu, V., Goldhar, J., and Kurnit, N.A., Appl. Phys. Lett. **15**, 376 (1969)

[6] Seidal, H. U.S. Patent No.3610731 (1969)

[7] Gibbs, H.M., McCall, S.L., and Venkatesan, T.N., Phys. Rev. Lett. **36**, 1135 (1976)

[8] Venkatesan, T.N. and McCall, S.L., Appl. Phys. Lett. **30**, 282 (1977)

[9] Khoo, I.C., Appl. Phys. Lett. **41**, 909 (1982)

[10] Khoo, I.C., Hou, J.Y., Normandin, R., and So, V.C.Y., Phys. Rev. **A27**, 3251 (1983)

[11] Khoo, I.C., Normandin, R., and So, V.C.Y., J. Opt. Soc. Am. **72**, 1761 (1982)

[12] Khoo, I.C., Normandin, R., and So, V.C.Y., J. Appl. Phys. **53**, 7599 (1982)

[13] Khoo, I.C., Yan, P.Y., Lin, T.H., Shepard, S., and Hou, J.Y., Phys. Rev. **A29**, 2756 (1984)

[14] Khoo, I.C., Shepard, S., and Zhuang, S.L., Appl. Phys. **B28**, 141 (1982)

[15] Khoo, I.C., Yan, P.Y., Lin, T.H., Shepard, S., and Hou, J.Y., J. Opt. Soc. Am. **B1**, 477 (1984)

[16] Gibbs, H.M., McCall, S.L., Venkatesan, T.N.C., Gossard, A.C., Passner, A., and Wiegmann, W., Appl. Phys. Lett. **35**, 451 (1979)

[17] Venkatesan, T., Lemaire, P.j., Wikens, B., Soto, L., Gossard, A.C., Wiegmann, W., Jewell, J.L., Gibbs, H.M., and Tarng, S.S., Opt. Lett. **9**, 297 (1984)

[18] Miller, D.A.B., Smith, S.D., and Johnston, A., Appl. Phys. Lett. **35**, 658 (1979)

[19] Miller, D.A.B., Smith, S.D., and Seaton, C.T., IEEE J. Quantum Electron. **QE-17**, 312 (1981)

[20] Miller, D.A.B., Smith, S.D., and Wherrett, B.S., Opt. Commun. **35**, 221 (1980)

[21] Miller, D.A.B., Chemla, D.S., Eilenberger, D.J.,Smith, P.W., Gossard, A.C., and Wiegmann, W., Appl. Phys. Lett.**42**, 925 (1983)

[22] Miller, D.A.B., Chemla, D.S., Smith, P.W., Gossard, A.C., and Wiegmann, W., Opt. Lett. **8**, 477 (1983)

[23] Gibbs, H.M., Tarng, S.S., Jewell, J.L., Weinberger, D.A., Tai, K., Gossard, A.C., McCall, S.L., Passner, A., and Wiegmann, W., Appl. Phys. Lett. **41**, 221 (1982)

[24] Venkatessan, T.N.C. and McCall, S.L., Appl. Phys. Lett. **32**, 156 (1978)

[25] Miller, D.A.B., Smith, S.D., and Johnston, A., Appl. Phys. Lett. **35**, 658 (1979)

[26] Bischofberger, T. and Shen, Y.R., Appl. Phys. Lett. **32**, 156 (1978)

[27] Bischofberger, T. and Shen, Y.R., J. Opt. Soc. Am. **68**, 642 (1978)

[28] Bischofberger, T. and Shen, Y.R., Opt. Lett. **4**, 40 (1979)

[29] Bischofberger, T. and Shen, Y.R., Phys. Rev..A**19**, 1169 (1979)

[30] Zhu, Z.-F., and Garmire, E., IEEE J. Quantum Electron. **QE-19**, 1495 (1983)

[31] Zhu, Z.-F., and Garmire, E., *Conference on Lasers and Electro-Optics, Technical Digest* (1983)

[32] Zhu, Z.-F., and Garmire, E., Opt.,Commun. **46**, 61 (1983)

[33] Smith, P.W., and Turner, E.H., J. Opt. Soc. Am. **67**, 250 (1977)

[34] Smith, P.W., and Turner, E.H., Appl. Phys. Lett. **30**, 280 (1977)

[35] Smith, P.W., and Turner, E.H., IEEE J. Quantum Electron. **QE-13**, 42 (1977)

[36] Kaplan, A.E., Sov. Phys. JETP **45**, 896 (1977)

[37] Chen, W., and Mills, D.L., Phys. Rev. **B35**, 524 (1987)

[38] Leung, K.M., J. Opt. Soc. Am. **B5**, 571 (1988)

[39] Trutsch , and Lederer, F., J. Opt. Soc. Am. **B5**, 2530 (1988)

[40] Basharov, A.M., Zh. Eksp. Theor. Fiz. **94**(9), 12 (1988)

[41] Perchel, T. and Dannberg, P., J. Opt. Soc. Am. **B5**, 29 (1988)

[42] Bonifacio, R. and Lugiato, L.A., In *Pattern Formation by Dynamic Systems and Pattern Recognition*, ed. H. Haken, Springer-Verlag, Berlin (1979)

[43] Callen, H.B., *Thermodynamics and An Introduction to Thermostatistics*, 2nd ed. Wiley,New York (1985)

[44] Landau, L.D. and Lifshitz, E.M., *Statistical Physics*, Part 1, 3rd ed. Pergamon, Oxford (1978)

[45] Kadanoff, L.P., Physics(N.Y.) **2**, 263 (1966)

[46] Wilson, K.G., Phys. Rev. **B4**, 3174, 3184 (1971)

[47] Haken, H., Rev. Mod. Phy. **47**, 67 (1975)

[48] Haken, H., *Synergetics, An Introduction*, 3rd ed. Springer-Verlag, Berlin (1985)

[49] Koch, S.W., *Dynamics of First-Order Phase Transition in Equilibrium and Nonequilibrium Systems* Vol.27 of Lecture Notes in Physics, Springer-Verlag, Berlin (1985)

[50] Pippard, A.B., *Response and Stability*, Cambridge, New York (1985)

[51] Sattinger, D., *Topics in Stability and Bifurcation* Vol.309 of Lecture Notes in Mathematics, Springer-Verlag, Berlin (1973)

[52] Garrido, L. ed. *Systems Far from Equilibrium* Vol.132 of Lecture Notes in Physics, Springer-Verlag, Berlin (1980)

[53] Nicolis, G. and Prigogine, I., *Self-Organization in Non-Eqilibrium Systems: From Dissipative Structures to Order Through Fluctuations* Wiley, New York (1977)

[54] Glansdorf, P. and Prigogine, I., *Thermodynamics of Structure, Stability and*

Fluctuations Wiley, New York (1971)

[55] Velardo, M.G. ed. *Nonequilibrium Cooperative Phenomena in Physics and Related Fields* (NATO ASI Series), Plenum, New York (1984)

[56] Graham, R. In *Springer Tracts in Modern Physics*, Vol. 66, Springer-Verlag, Berlin (1973)

[57] Graham, R. and Haken, H., Z. Physik **237**, 31 (1970)

[58] Graham, R. and Haken, H., Z. Physik **213**, 420 (1968)

[59] DeGiorgio, V. and Scully, M.O., Phys. Rev. A2, 1170 (1970)

[60] Bonifacio, R. and Lugiato, L.A., Opt. Commun. **19**, 172 (1976)

[61] Wills, C.R., Opt. Commun. **23**, 151 (1977)

[62] Fokker, A.D., Ann. Physik. **43**, 810 (1914)

[63] Planck, M. Sitzber. Preuss. Akad. Wiss. p.324 (1917)

[64] Bonifacio, R. and Lugiato, L.A., Phys. Rev. Lett. **40**, 1023 (1978)

[65] Bonifacio, R. and Lugiato, L.A., Phys. Rev. A18, 1129 (1978)

[66] Bonifacio, R., Gronchi, M, and Lugiato, L.A., Phys. Rev. A18, 2266 (1978)

[67] Graham, R. and Schenzle, A., Phys. Rev. A23, 1302 (1981)

[68] Schenzle, A. and Brand, H., Opt. Commun. **27**, 485 (1978)

[69] Agarawal, G.S., Narducci, L.M., Gilmore, R., and Feng, D. H., Phys. Rev. Lett. **18**, 620 (1978)

[70] Bonifacio, R. and Lugiato, L.A., Phys. Rev. A11, 1507 (1975)

[71] Bonifacio, R. and Lugiato, L.A., Phys. Rev. A12, 587 (1975)

[72] Orenstein, M., Katriel, J., and Speiser, S., Phys. Rev. A35, 1192 (1987)

[73] Orenstein, M., Katriel, J., and Speiser, S., Phys. Rev. A35, 2175 (1987)

[74] Speiser, S., and Chisena, F.L., SPIE vol. 824, 144 (1987)

[75] McCall, S.L., Phys. Rev. A9, 1515 (1974)

[76] Felber, F.S. and Marburger, J.H., Appl. Phys. Lett. **28**, 731 (1976)

[77] Marburger, J.H. and Felber, F.S., Phys. Rev. A17, 335 (1978)

[78] Agarawal, G.P. and Carmichael H.J., Phys. Rev. A19, 2074 (1979)

[79] Lugiato, L.A., In *Progress in Physics*, ed. E. Wolf, Vol. XXI. North-Holland, Amsterdam (1985)

[80] Born, M. and Wolf, E., *Principles of Optics*, Pergamon, New York, (1970)

[81] Hernandez, G., *Fabry-Perot interferometers*, Cambrige University, New York, (1986)

[82] Schenzle, A. and Brand, H., Opt. Commun. **31**, 401 (1979)

[83] Farina, J.D., Narducci, L.M., Yuan, J.M., and Lugiato, L.A., Opt. Eng. **19**, 469 (1980)

[84] Lugiato, L.A., Farina, J.D., and Narducci, L.M., Phys. Rev. **A22**, 253 (1980)

[85] Mandel, P. and Erneux, T., Opt. Commun. **44**, 55 (1982)

[86] Stoker, J.J, *Nonlinear Vibrations*, Interscience, New York (1950)

[87] Bray, A.J. and McKane, A.J., Phys. Rev. Lett. **62**, 493 (1989)

[88] Tsironis, G.P. and Grigolini, P., Phys. Rev. Lett. **61**, 7 (1989)

[89] Jung, P. and Hanggi, P, Phys. Rev. Lett. **61**, 11 (1989)

[90] Guckenheimer, J. and Holmes, P., *Nonlinear Oscillations, Dynamical Systems, and Bifurcations of Vector Fields*, Vol. 42 of Applied Mathematical Sciences, Springer, Berlin (1983)

Figure Captions: Chapter 2

Figure 2.1; Nonlinear Fabry-Perot for Optical Bistability

Figure 2.2; Multiple Quantum Structures

Figure 2.3; Hybrid Optical Bistability

Figure 2.4; Optical Bistability in a Nonlinear Optical Thin Film

Figure 2.5; Phase Diagram for Liquid-Gas

Figure 2.6; Landau-Ginzburg Potential $F(\phi, T)$ for a Second Order Phase Transition

Figure 2.7; Landau-Ginzburg Potential $F(\phi, T)$ for a First Order Phase Transition

Figure 2.8; Hysteresis Behavior of Order Parameter as a Function of Negative Temperature

Figure 2.9; Landau-Ginzburg Potential $F(\phi, T)$ in the Presence of an External Field

Figure 2.10; Hysteresis Behavior of Order Parameter as a Function of the External Field

Figure 2.11; Entropy Production Rate at a Steady State

Figure 2.12; Entropy Production Rate as a Thermodynamic Potential

Figure 2.13; Critical Slowing Down near Phase Transition

Figure 2.14; Landau-Ginzburg Potential for Optical Bistability (C=3) with Various Input Amplitudes (3, 6, 9, 12, ..., 30)

Figure 2.15; Landau-Ginzburg Potential for Optical Bistability (C=5) with Various Input Amplitudes (3, 6, 9, 12, ..., 30)

Figure 2.16; Landau-Ginzburg Potential for Optical Bistability (C=10) with Various Input Amplitudes (3, 6, 9, 12, ..., 30)

Figure 2.17; Landau-Ginzburg Potential for Optical Bistability (C=20) with Various Input Amplitudes (3, 6, 9, 12, ..., 30)

•

44
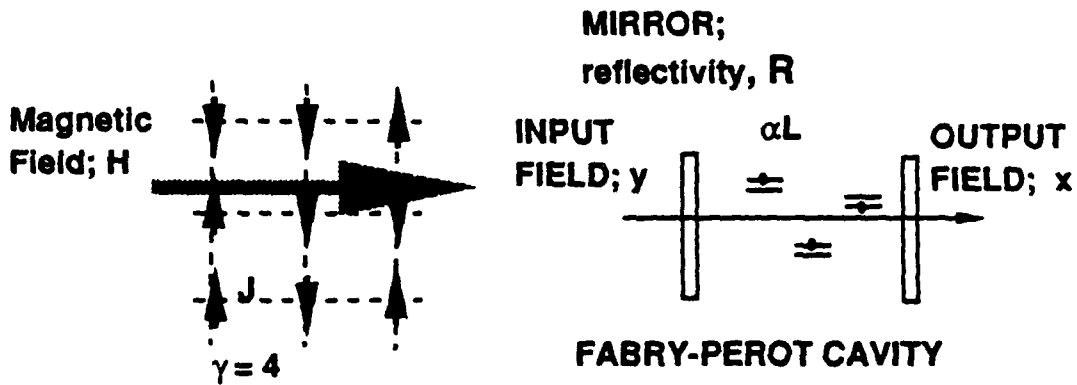
Phase Transitions

	SPIN SYSTEM	OPTICAL BISTABILITY
SYSTEM	THERMAL EQUILIBRIUM	FAR FROM EQUILIBRIUM
EXTERNAL FIELD	MAGNETIC FIELD, H	INPUT FIELD, y
ORDER PARAMETER	$(N_{up} - N_{down})/N$	OUTPUT FIELD AMPLITUDE, x
PHASE TRANSITION PARAMETER	Temperature, T $T < Tc=J/y$	Cooperativity, C $C=\alpha L/2(1-R) > 4$
STOCHASTIC FORCE	Thermal Energy	Spontaneous Decay, q

Table 2.1

45

Nonlinear Fabry-Perot for Optical Bistability

Figure 2.1

Multiple Quantum Well Structures

GaAs AlGaAs

Figure 2.2

47
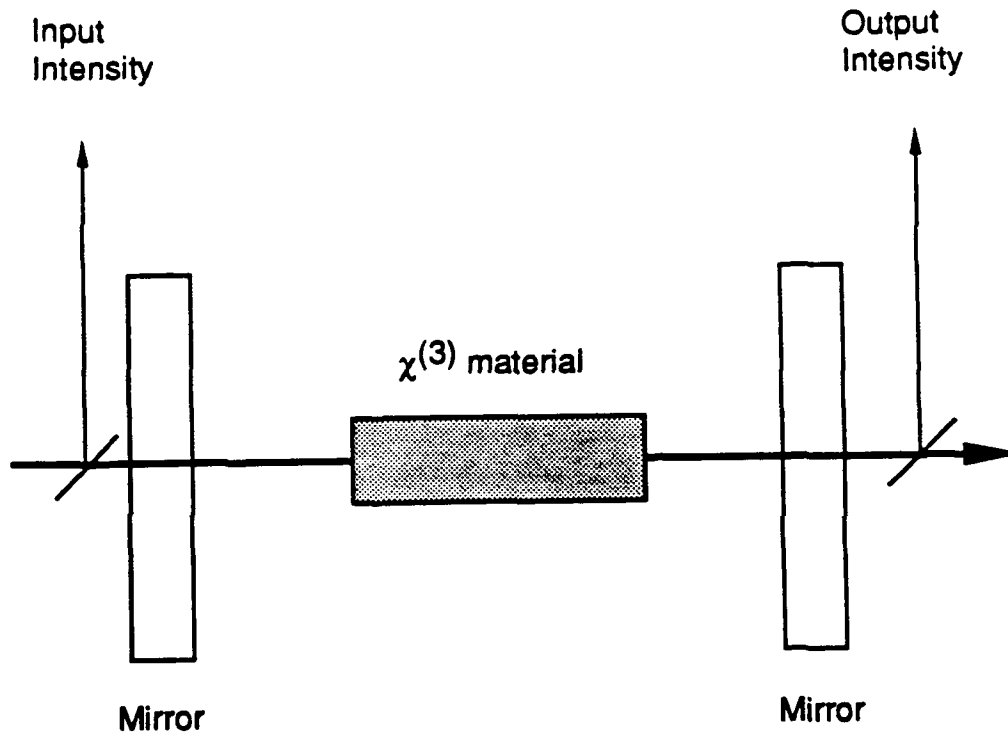
Hybrid Optical Bistability
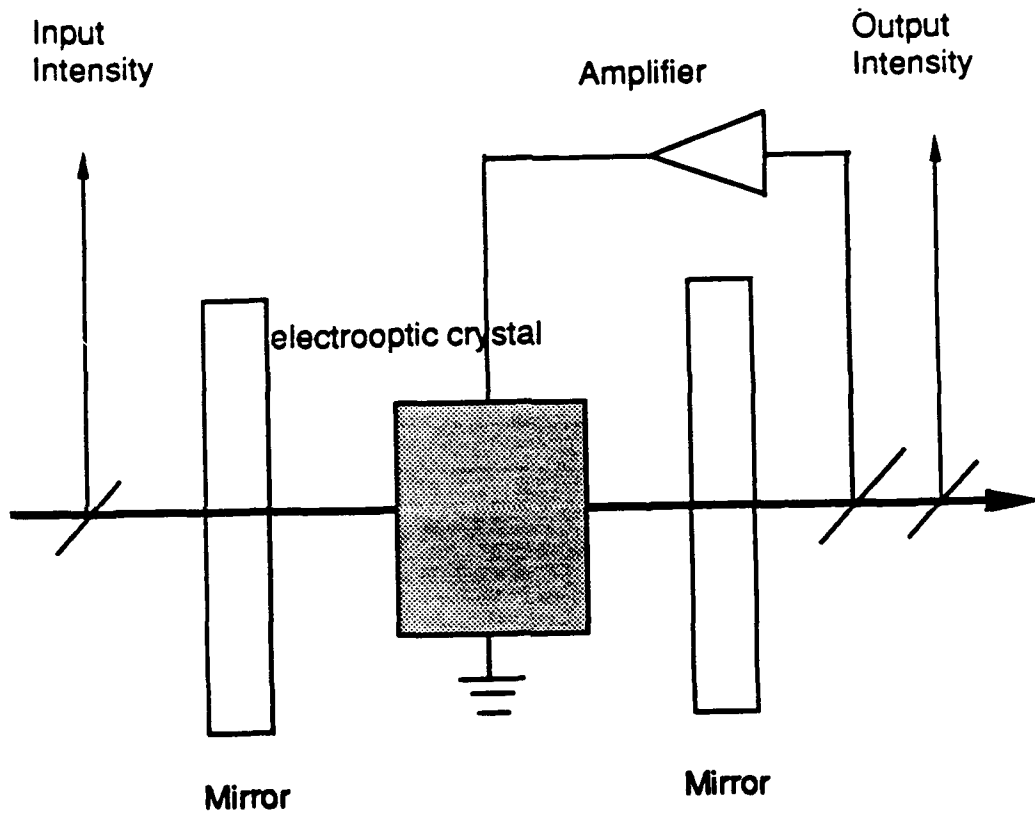
Figure 2.3

Optical Bistability in a Nonlinear Optical Thin Film

Input
Intensity

Output
Intensity

nonlinear optical
thin film
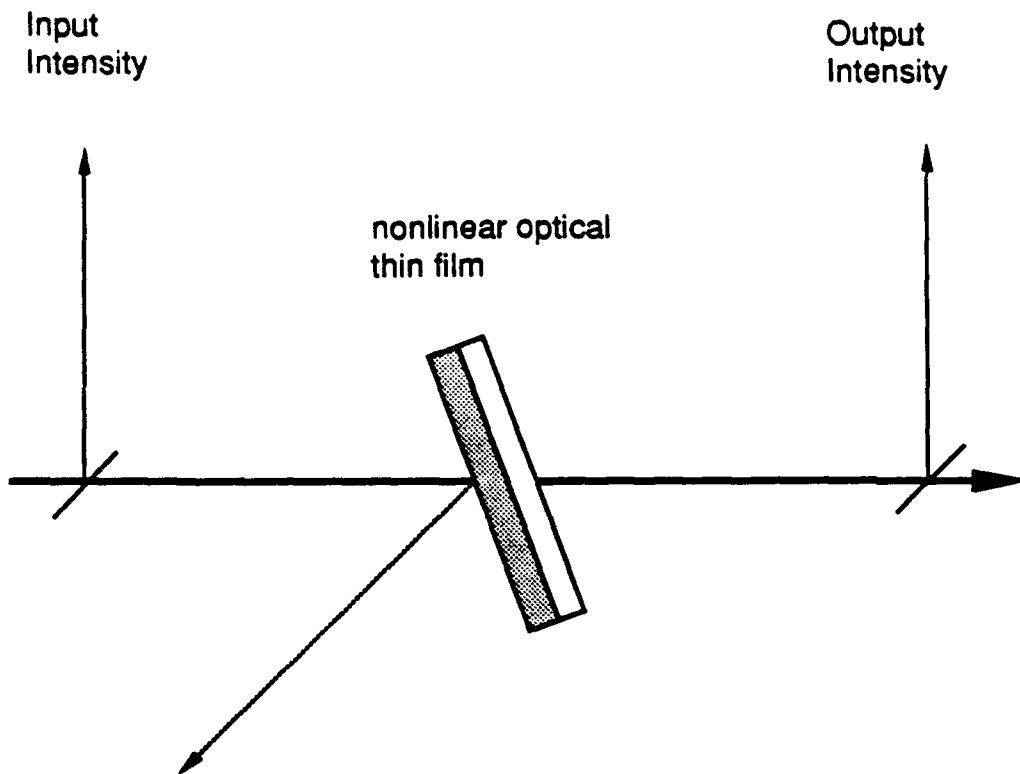
Figure 2.4

Phase Diagram for Liquid-Gas
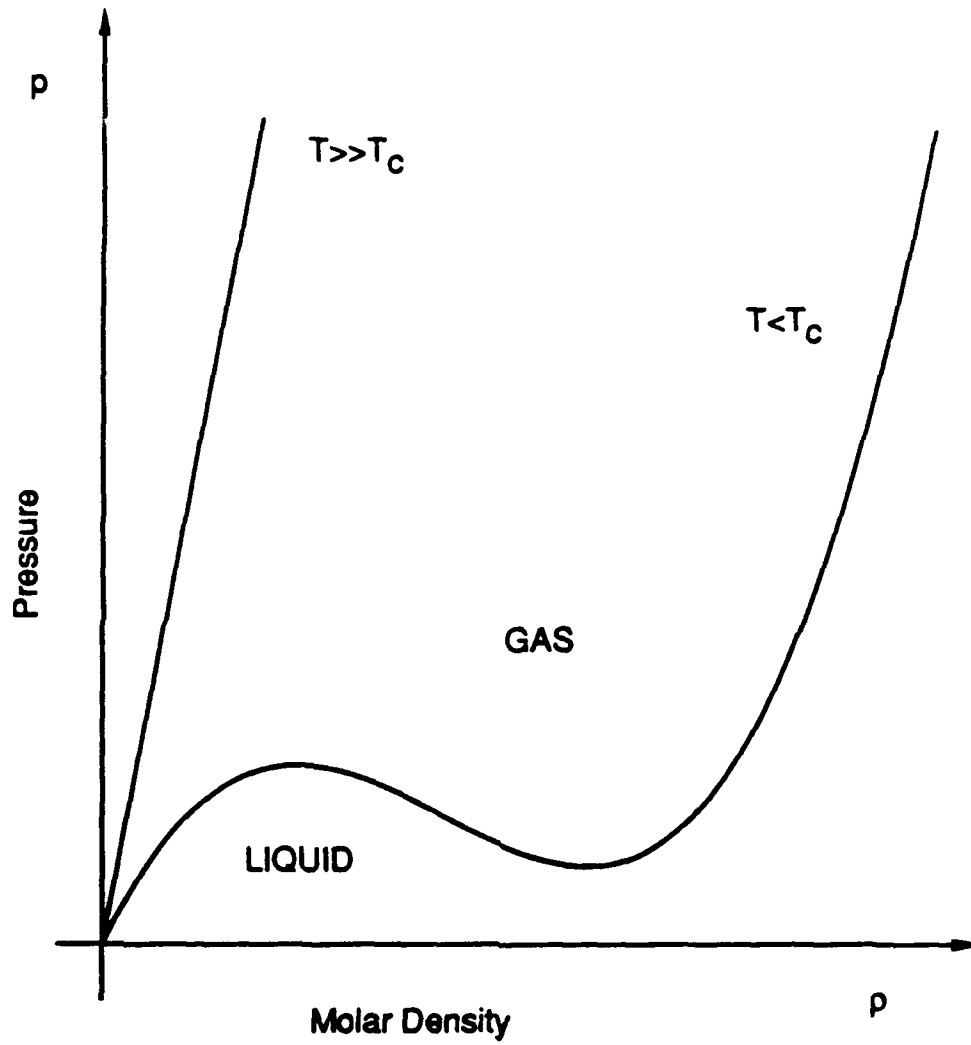
Figure 2.5

**Landau-Ginzberg Potential F(ϕ,T)
for a second order phase transition
($T_3 > T_2 > T_1$)**

T_3

T_2

T_1

$F(\phi,T)$

ϕ

Figure 2.6

**Landau-Ginzberg Potential F(φ,T)
for a first order phase transition
(T₃ > T₂ > T₁)**

Figure 2.7

Hysteresis Behavior of Order Parameter as a Function of Negative Temperature
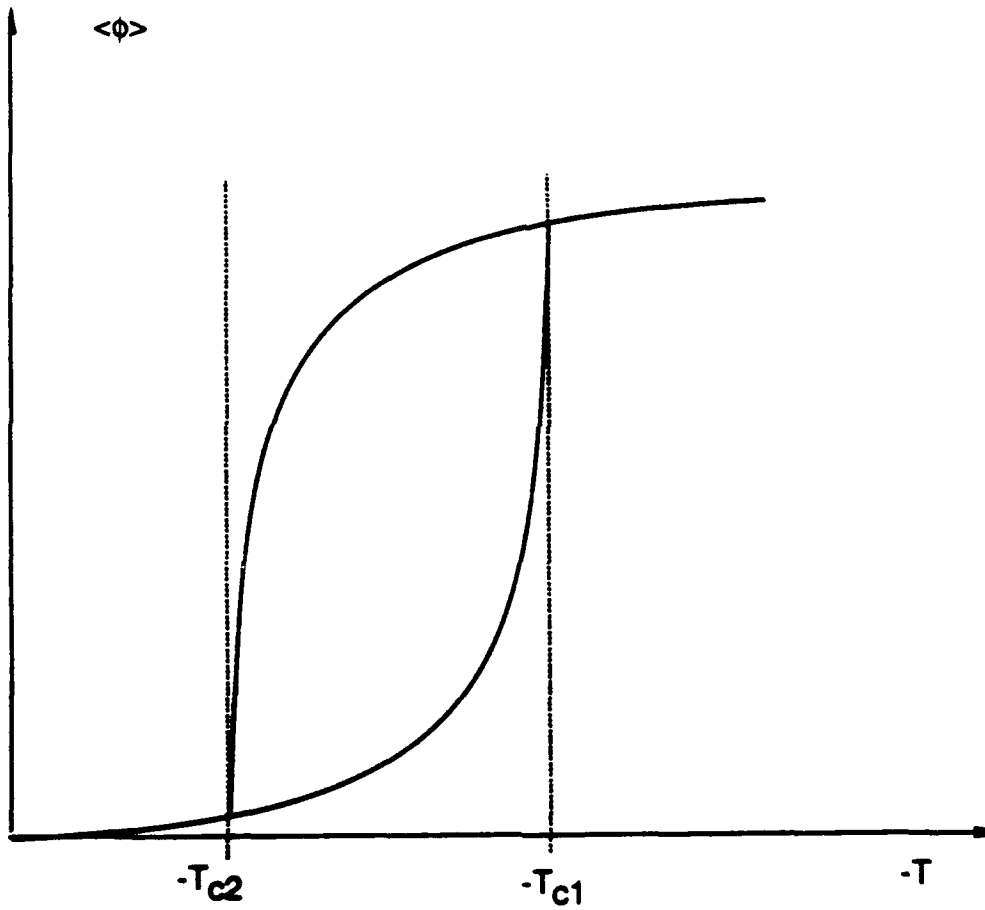
Figure 2.8

**Landau-Ginzberg Potential F(φ,T)
in the presence of an external field
(T < T$_c$)**
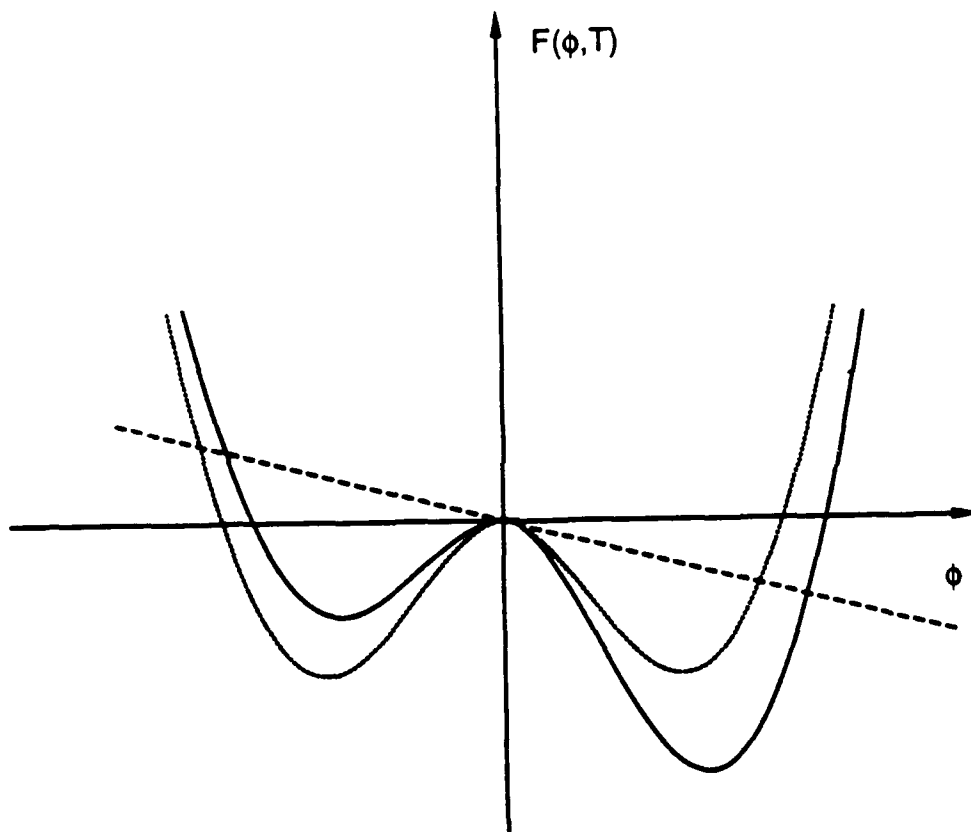
Figure 2.9

**Hysteresis Behavior of Order Parameter as
a Function of the External Field**
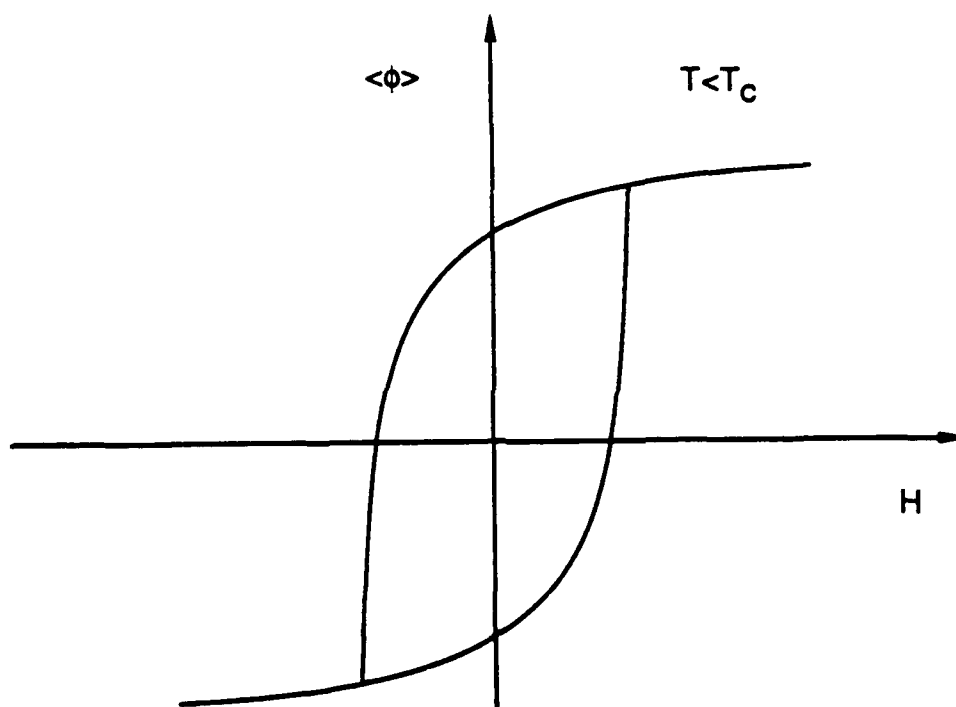
Figure 2.10

Entropy Production Rate at a Steady State

$P = d_i S/dt$

; Entropy Production Rate
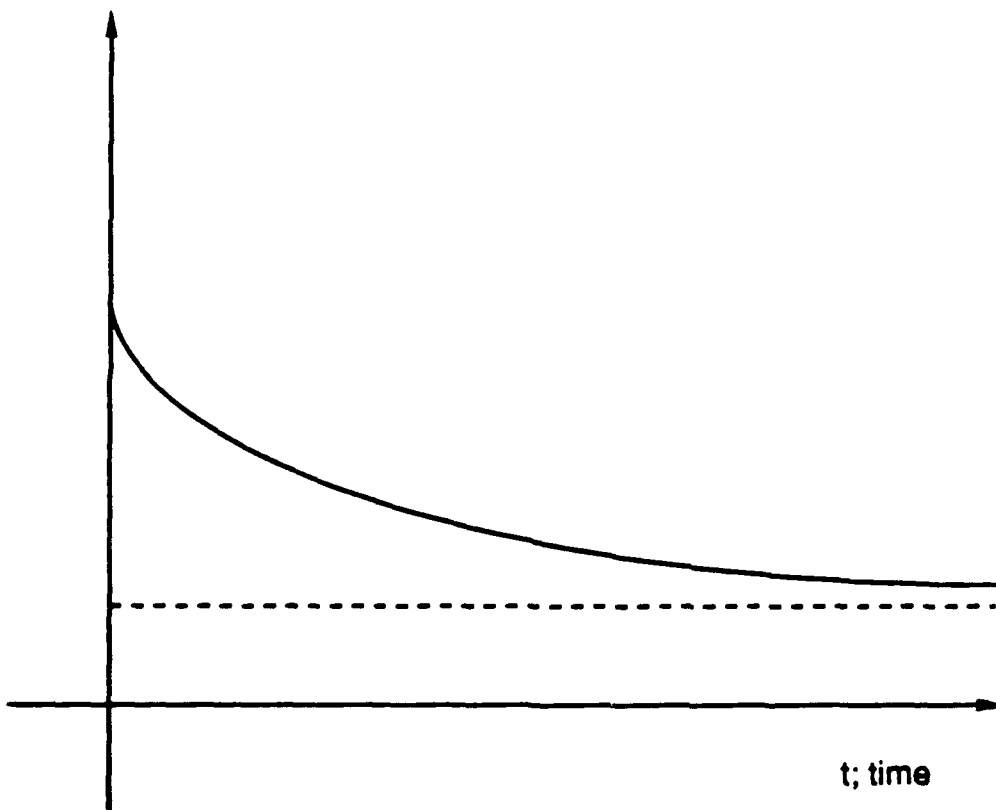
Figure 2.11

**Entropy Production Rate
as a Thermodynamic Potential**

$P(\{q\}) = d_i S/dt$
; Entropy Production Rate
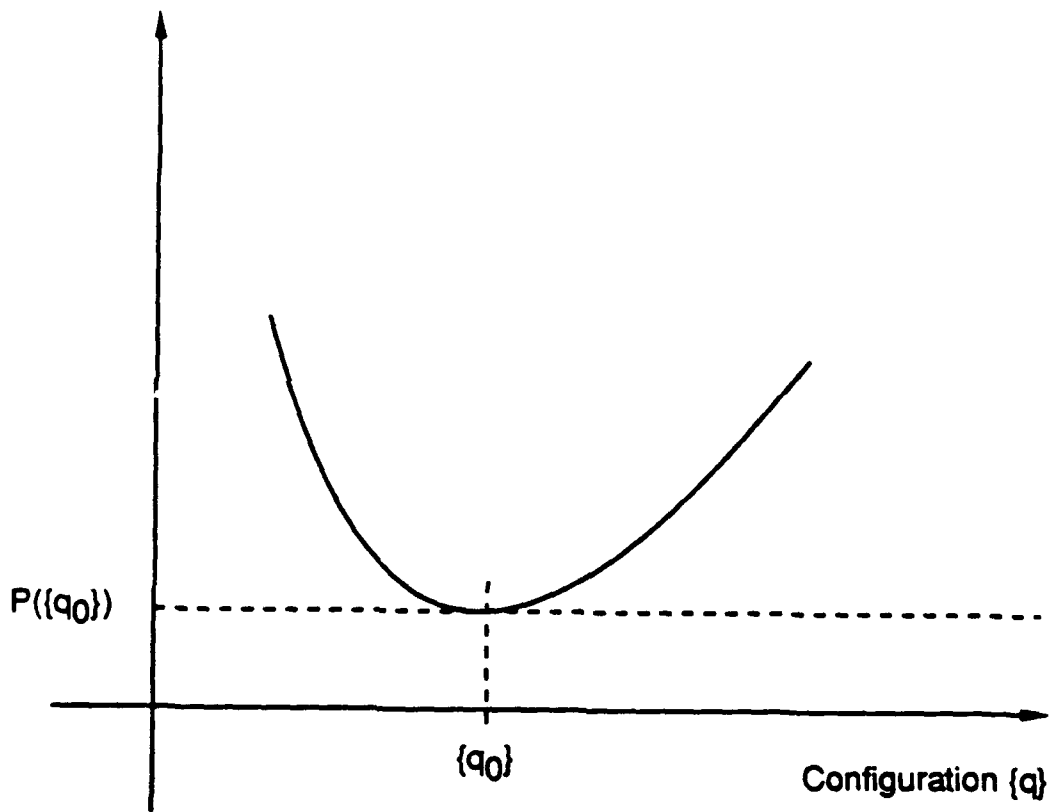
Figure 2.12

**Critical Slowing Down
near Phase Transition**

Order Parameter

Relaxation Time
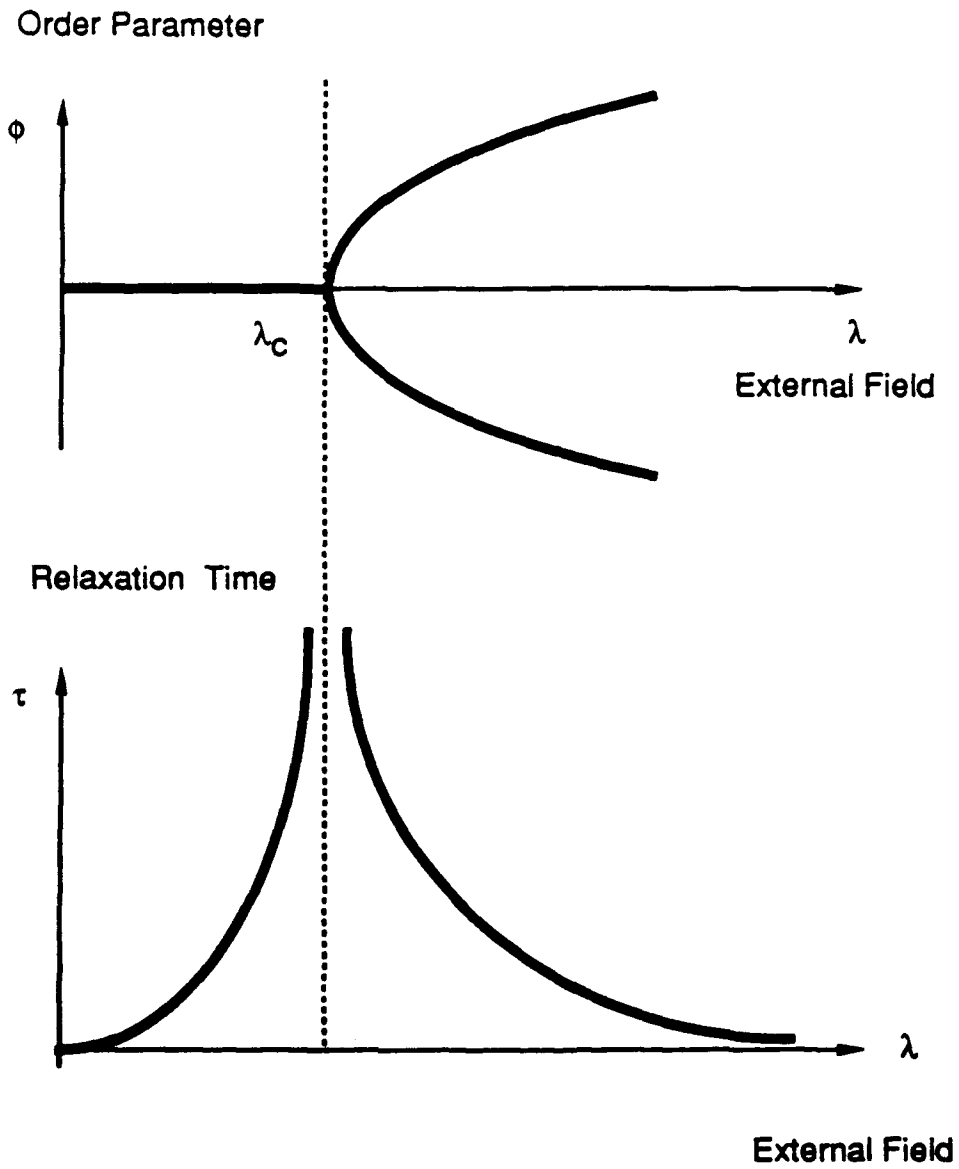
Figure 2.13

Landau-Ginzburg Potential for Optical Bistability (C=3)
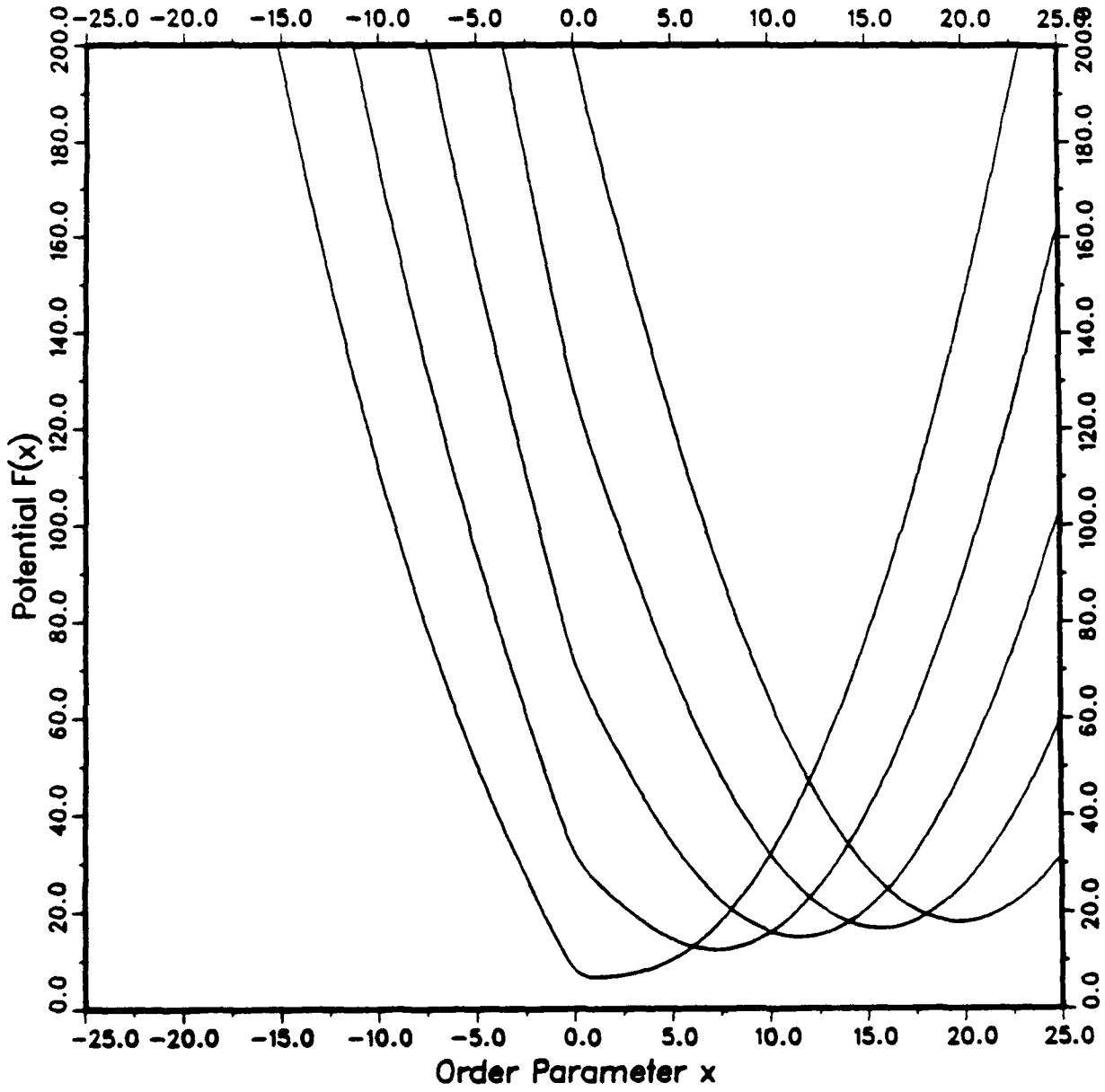
Figure 2.14

Landau-Ginzburg Potential for Optical Bistability (C=5)
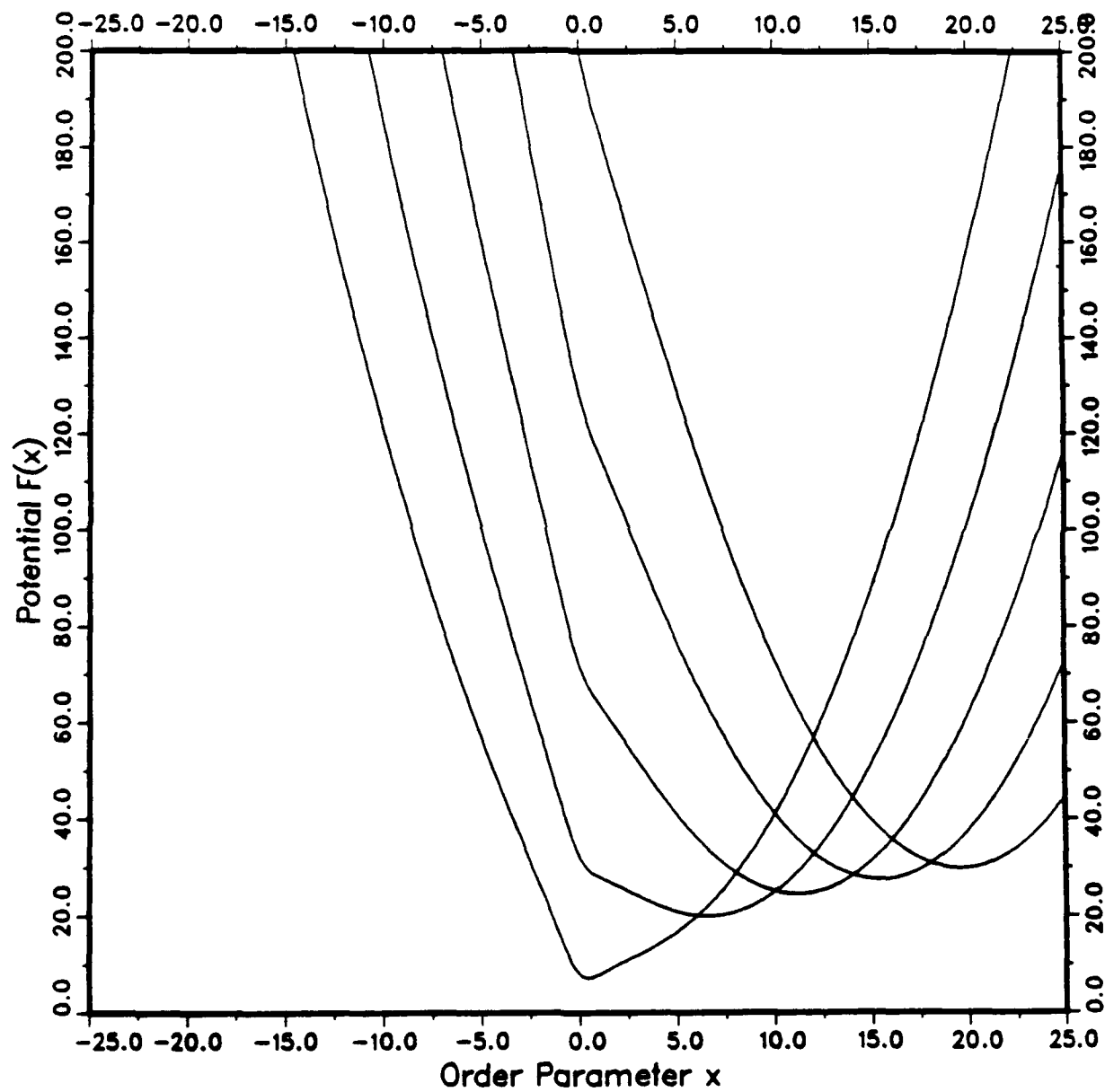
Figure 2.15

Landau-Ginzburg Potential for Optical Bistability (C=10)
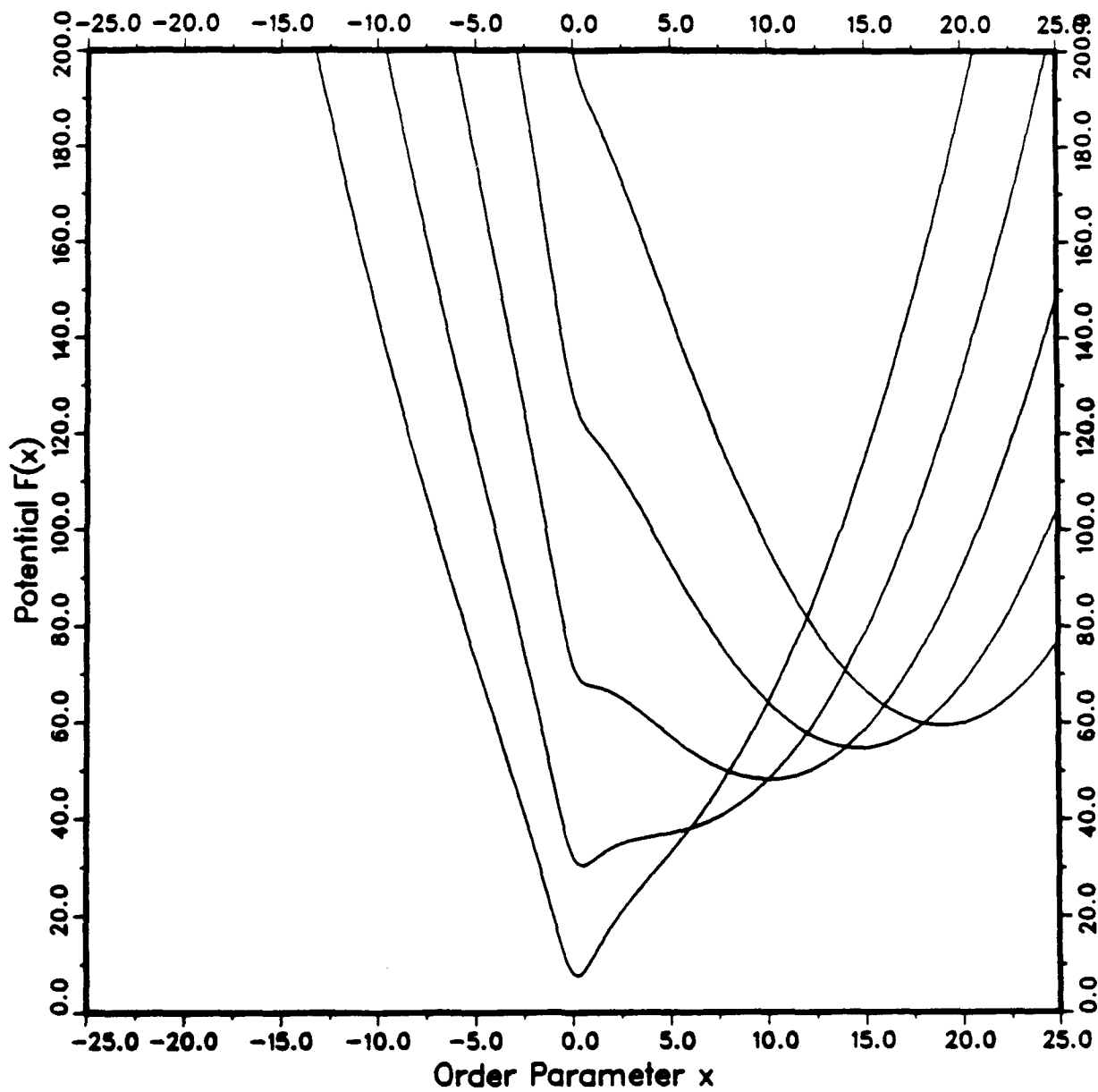
Figure 2.16

Landau-Ginzburg Potential for Optical Bistability (C=20)
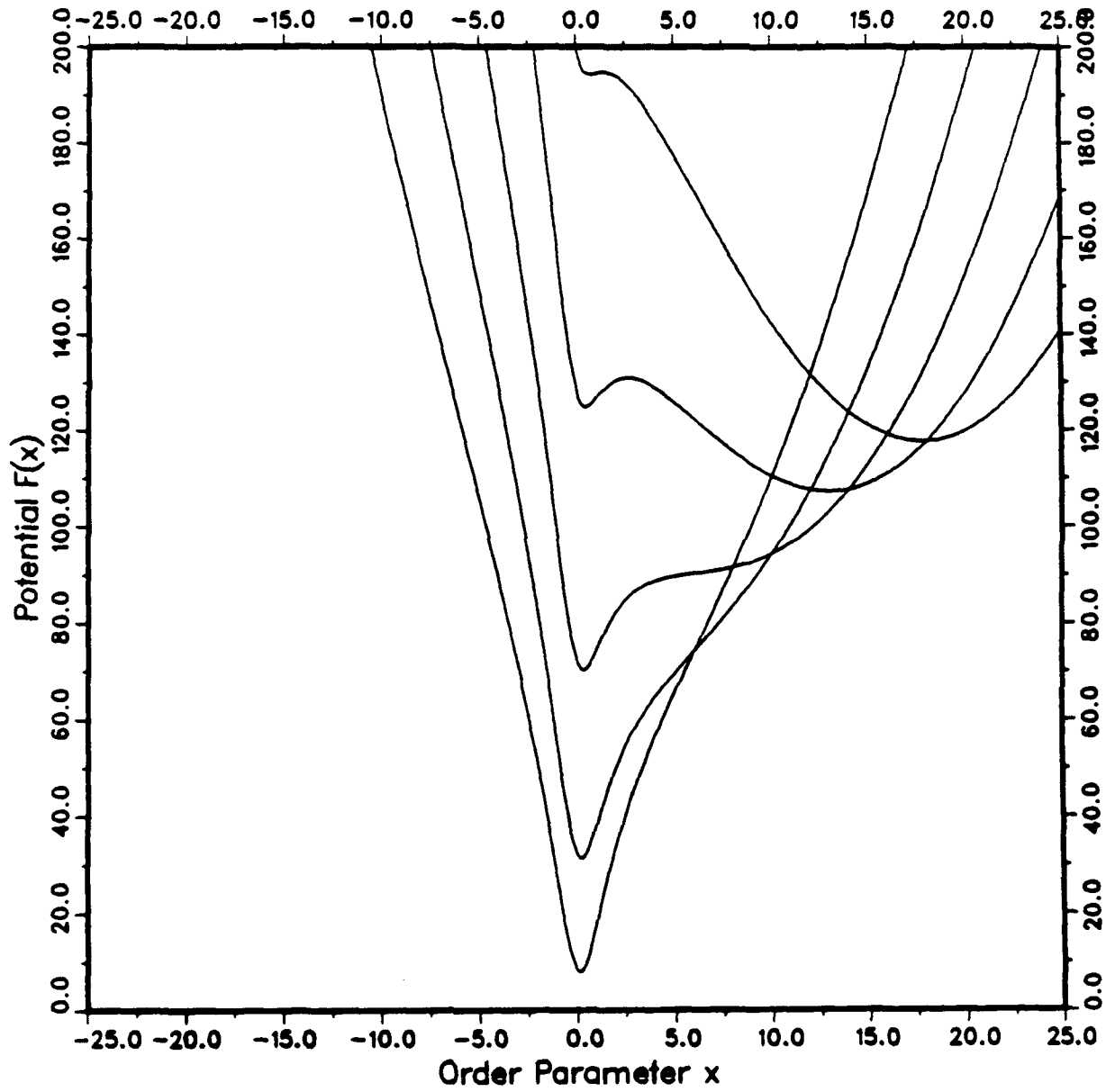
Figure 2.17

CHAPTER 3

NONLINEAR OPTICAL PROCESSES: RESONANT AND NONRESONANT

Conjugated π-electron organic and polymer structures are now well known [1]–[6] to exhibit exceptionally large nonresonant second order $\chi_{ijk}^{(2)}(-\omega_3;\omega_1,\omega_2)$, and third order $\chi_{ijkl}^{(3)}(-\omega_4;\omega_1,\omega_2,\omega_3)$ nonlinear optical susceptibilities, and their microscopic origin and mechanisms can be successfully described by quantum field theory of many electron systems in one and two dimensions. In this description, as the spatial dimensionality of the many-electron system is effectively lowered, the motion among the many electrons becomes highly correlated.[7] Electron correlation plays a major role in determining $\chi_{ijk}^{(2)}(-\omega_3;\omega_1,\omega_2)$ and $\chi_{ijkl}^{(3)}(-\omega_4;\omega_1,\omega_2,\omega_3)$ in conjugated π-electron systems, and its effect cannot be neglected in properly accounting for the nonlinear optical properties of conjugated structures.[5][6]

In Sec.3.1 a direct summation method in calculating $\chi_{ijkl}^{(3)}(-\omega_4;\omega_1,\omega_2,\omega_3)$ from the transition moments of electronic transitions and the energy states in a molecule will be presented. A linear conjugated hydrocarbon chain structure is chosen as a simple system to study the importance of the electron- correlations in the third order nonlinear optical properites, which is discussed in Sec.3.2. In Sec.3.3, the theoretical analysis is extended to a quasi-two dimensional conjugated structure, and one model system is cyclic octa-tetraene (COT). The theoretical calculation of third harmonic generation dispersion for COT is presented, and compared with the linear chain case.

In Sec.3.4-7, a resonant nonlinear optical response is presented in terms of Bloch susceptibility.

3.1 Microscopic Description of Second Order Hyperpolarizability

The macroscopic nonlinear optical properties of organic molecular and polymer structures in condensed states are best described starting from the individual

responses of isolated molecular, or polymer chain, units. In the lattice gas approximation, if the nonlinear susceptibility of an isolated molecule is known, then $\chi_{ijk}^{(2)}(-\omega_3;\omega_1,\omega_2)$ or $\chi_{ijkl}^{(3)}(-\omega_4;\omega_1,\omega_2,\omega_3)$ of the macroscopic ensemble of molecules is determined by the orientational distribution function of the independent units. Local field factors must also be included to account for the effect of the dielectric environment on the electric field strength at the molecular site. The macroscopic frequency-dependent second and third order susceptibilities $\chi_{ijk}^{(2)}(-\omega_3;\omega_1,\omega_2)$ and $\chi_{ijkl}^{(3)}(-\omega_4;\omega_1,\omega_2,\omega_3)$ can then be expressed in terms of the molecular susceptibilities $\beta_{ijk}(-\omega_3;\omega_1,\omega_2)$ and $\gamma_{ijkl}(-\omega_4;\omega_1,\omega_2,\omega_3)$ as

$$\chi_{ijk}^{(2)}(-\omega_3;\omega_1,\omega_2) = N_u \sum_{s=1}^{c} R_{im'}^s R_{jn'}^s R_{ko'}^s f_{m'i'}^{\omega_3} \beta_{i'j'k'}^s(-\omega_3;\omega_1,\omega_2) f_{j'n'}^{\omega_1} f_{k'o'}^{\omega_2} \quad (3.1.1)$$

and

$$\chi_{ijkl}^{(3)}(-\omega_4;\omega_1,\omega_2,\omega_3) = N_u \sum_{s=1}^{c} R_{im'}^s R_{jn'}^s R_{ko'}^s R_{lp'}^s f_{m'i'}^{\omega_4}$$
$$\times \gamma_{i'j'k'l'}^s(-\omega_4;\omega_1,\omega_2,\omega_3) f_{j'n'}^{\omega_1} f_{k'o'}^{\omega_2} f_{l'p'}^{\omega_3} \quad (3.1.2)$$

where N_u is the number of unit cells per unit volume, the summation is over all molecules in the unit cell, R is a rotation matrix describing the orientation of each molecule in the unit cell, and f is the frequency dependent local field factor. The description of the macroscopic nonlinear optical response is thus reduced to an understanding of the microscopic second and third order susceptibilities $\beta_{ijk}(-\omega_3;\omega_1,\omega_2)$ and $\gamma_{ijkl}(-\omega_4;\omega_1,\omega_2,\omega_3)$ and knowledge of the orientational distribution of the molecular units in the condensed phase. As special cases, isotropic gases and liquids reduce Eqs. (3.1.1) and (3.1.2) to simpler forms. For example, for an isotropic ensemble

$$\chi_{1111}^{(3)}(-\omega_4;\omega_1,\omega_2,\omega_3) = N f^{\omega_4} f^{\omega_1} f^{\omega_2} f^{\omega_3} \gamma_g(-\omega_4;\omega_1,\omega_2,\omega_3) \quad (3.1.3)$$

where N is the number density of molecules and γ_g is the isotropically averaged susceptibility defined by

$$\gamma_g = \frac{1}{5}[\sum_i \gamma_{iiii} + \frac{1}{3}\sum_{i\neq j}(\gamma_{iijj} + \gamma_{ijij} + \gamma_{ijji})] \quad (3.1.4)$$

64

where the indices i and j represent the Cartesian coordinates x, y, and z. The above formalism is strictly appropriate only for gases such that the mean intermolecular distance is large enough for the interaction between molecules to be negligible. The fact that the intramolecular interaction energy is much stronger than the intermolecular interaction energy in organic molecular crystals, liquids, solutions, and polymer thin films means that the starting point for understanding the macroscopic nonlinear optical properties of these various condensed phases lies in an accurate description of the microscopic response from an isolated molecular unit.

The general theoretical expression for the components of the microscopic third order susceptibility tensor $\gamma_{ijkl}(-\omega_4;\omega_1,\omega_2,\omega_3)$ is derived from time dependent, quantum electrodynamic perturbation theory. In order to avoid secular divergences that would occur when any subset of the input frequencies sums to zero, the Bogoliubov- Mitropolsky method of averages [8][9] is employed. Owing to dispersive effects, $\gamma_{ijkl}(-\omega_4;\omega_1,\omega_2,\omega_3)$ is dependent on the input and output frequencies involved for each of the various possible nonlinear optical phenomena. For the particular case of third harmonic generation, for example, one obtains

$$\gamma_{ijkl}(-3\omega;\omega,\omega,\omega) = \frac{1}{3!}\left(\frac{e^4}{4\hbar^3}\right)\Bigg[$$

$$\sideset{}{'}\sum_{n_1,n_2,n_3} \Big(\frac{P_{jkl}[r^i_{gn_3}\bar{r}^j_{n_3n_2}\bar{r}^k_{n_2n_1}r^l_{n_1g}]}{(\omega_{n_3g}-3\omega)(\omega_{n_2g}-2\omega)(\omega_{n_1g}-\omega)} + \frac{P_{jkl}[r^j_{gn_3}\bar{r}^i_{n_3n_2}\bar{r}^k_{n_2n_1}r^l_{n_1g}]}{(\omega_{n_3g}+\omega)(\omega_{n_2g}-2\omega)(\omega_{n_1g}-\omega)}$$

$$+\frac{P_{jkl}[r^j_{gn_3}\bar{r}^k_{n_3n_2}\bar{r}^i_{n_2n_1}r^l_{n_1g}]}{(\omega_{n_3g}+\omega)(\omega_{n_2g}+2\omega)(\omega_{n_1g}-\omega)} + \frac{P_{jkl}[r^j_{gn_3}\bar{r}^k_{n_3n_2}\bar{r}^l_{n_2n_1}r^i_{n_1g}]}{(\omega_{n_3g}+\omega)(\omega_{n_2g}+2\omega)(\omega_{n_1g}+3\omega)}\Big)$$

$$-\sideset{}{'}\sum_{n_1n_2} \Big(\frac{P_{jkl}[r^i_{gn_2}r^j_{n_2g}r^k_{gn_1}r^l_{n_1g}]}{(\omega_{n_2g}-3\omega)(\omega_{n_2g}-\omega)(\omega_{n_1g}-\omega)} + \frac{P_{jkl}[r^j_{gn_2}r^i_{n_2g}r^k_{gn_1}r^l_{n_1g}]}{(\omega_{n_2g}-\omega)(\omega_{n_1g}+\omega)(\omega_{n_1g}-\omega)}$$

$$+\frac{P_{jkl}[r^j_{gn_2}r^k_{n_2g}r^i_{gn_1}r^l_{n_1g}]}{(\omega_{n_2g}+3\omega)(\omega_{n_2g}+\omega)(\omega_{n_1g}+\omega)} + \frac{P_{jkl}[r^j_{gn_2}r^k_{n_2g}r^l_{gn_1}r^i_{n_1g}]}{(\omega_{n_2g}+\omega)(\omega_{n_1g}-\omega)(\omega_{n_1g}+\omega)}\Big)\Bigg]$$

$$\tag{3.1.5}$$

where $r^i_{n_1n_2}$ is the matrix element $\langle n_1|r^i|n_2\rangle$ with $\bar{r}^i_{n_1n_2} = r^i_{n_1n_2} - r^i_{gg}$, $\hbar\omega$ is the excitation energy of state n, the prime on the summations indicates the ground

state is omitted, and P_{jkl} denotes the sum over all permutations of those three indices. We will be concerned here with the case where all of the optical frequencies are above the molecular vibrational and rotational modes but below the electronic excitation energies so that the nonlinear optical response is strictly electronic in origin. In addition, for conjugated organic structures, γ is dominated by the delocalized π-electron contributions which in general have both larger transition dipole moments and lower transition energies than the σ- electron excitations. Thus, with an accurate description of both the excitation energies and transition moments of the π- electron manifold, one can calculate the frequency dependence of each of the different third order nonlinear optical processes using expressions such as Eq.(3.1.5).

The theoretical method employed to achieve proper description of the π-electron manifold of conjugated organic molecular structures for calculation of $\gamma_{ijkl}(-\omega_4; \omega_1, \omega_2, \omega_3)$ consists of a multiply - excited configuration interaction calculation (SCF-MO-SDCI) performed on a molecular orbital basis obtained through self- consistent field theory in the rigid lattice CNDO/S approximation.

For a general discussion of symmertic properties of macroscopic nonlinear optical susceptibilities, refer to Appendix A2.

3.2 Conjugated Linear Chains

We briefly review here the origin of the microscopic third order susceptibility $\gamma_{ijkl}(-\omega_4; \omega_1, \omega_2, \omega_3)$ in prototype conjugated linear chains. In particular, we consider the linear polyenes which are hydrocarbon chains in which each carbon site is covalently bonded to a hydrogen and its two nearest neighbor carbons. The remaining valence electron of each carbon atom contributes to a delocalized, strongly correlated π-electron distribution along the carbon chain. The ground state of this system is a spin-singlet, broken-symmetry state in which the carbon lattice possesses a single-bond/double-bond alternation.

Because the polyenes are members of the C_{2h} symmetry group, all of the

π-electron states must possess either A_g or B_u symmetry. Within the centrosymmetric C_{2h} group, these two symmetries are of opposite parity leading to optical dipole selection rules. The ground state is always ^1A_g, and therefore the ^1B_u states are one-photon allowed transitions observable in the linear absorption spectrum. The excited ^1A_g states, on the other hand, are one-photon forbidden and are consequently known as two-photon states. Experimental and theoretical studies of one-photon and two-photon resonant processes in finite polyenes have shown that below the first optically allowed, dominant 1^1B_u state is located a strongly electron correlated two-photon 2^1A_g state.[10]−[13] The symmetries, energies, and relevant transition dipole moments of the ten lowest calculated excited states of trans- OT are listed in Table (3.1). The columns $\mu^z_{n,g}$ and $\mu^z_{n,1B}$ refer to the z- components of the transition dipole moment of each state with the ground state and with the 1^1B_u state, respectively. The optical selection rules are observed in the vanishing transition moments $\mu^z_{n,g}$ for all the ^1A_g states and $\mu^z_{n,1B}$ for all the ^1B_u states. It is also seen that the 1^1B_u state has by far the largest $\mu^z_{n,g}$ and the 6^1A_g state has the largest $\mu^z_{n,1B}$. As a result, these two are the primary contributors to γ_{zzzz} as will be described below.

It is instructive to consider the individual terms in the sum over states perturbation expansion. Based on Eq.(3.1.5) and the symmetry selection rules described above, it is evident that the π-electron states in a third order process must be connected in the series $g \rightarrow^1 B_u \rightarrow^1 A_g \rightarrow^1 B_u \rightarrow g$. For centrosymmetric structures, third order processes necessarily involve virtual transitions to both one-photon and two-photon states. For trans-OT, there are (153) terms involved in the summations of Eq.(3.1.5). However, two of these terms are an order of magnitude larger than all the others and constitute 70% of γ_{zzzz}. The remaining terms to a large extent cancel one another resulting in a much smaller net contribution. In both of the dominant terms, the only ^1B_u state involved is the dominant low-lying one-photon 1^1B_u π-electron excited state. In addition to its low excitation energy, this state

is important because its 7.8 D transition dipole moment with the ground state is more than three times larger than any other ground state transition moment. One of the two major terms comes from the double sum of Eq.(3.1.5) with both of the intermediate states being the 1^1B_u. In the case of the double sum, the middle intermediate state is always the ground state. This term makes a negative contribution to γ_{zzzz} below resonance, since both the numerator and denominator are positive but the double sum has an overall negative contribution. The other major term is from the triple sum with the 6^1A_g state as the middle intermediate. This state, calculated at 7.2 eV, has a large transition moment with 1^1B_u of 13.2 D. This term makes a positive contribution to γ_{zzzz} and is larger than the first leading to an overall positive value for γ_{zzzz}. Importantly, the 6^1A_g consists of 60% double-excited configurations indicating it is highly correlated. SCI calculations obtain a negative value for γ_{zzzz} because they do not adequately describe this state and therefore omit its large contribution.

The transition density matrix $\rho_{n,n\prime}$ is defined through the expression

$$\langle \mu_{n,n\prime} \rangle = -e \int \vec{r} \rho_{n,n\prime}(\vec{r}) d\vec{r} \tag{3.2.1}$$

with

$$\rho_{n,n\prime}(\vec{r}_1) = \int \Psi_n^*(\vec{r}_1, \vec{r}_2, \cdots, \vec{r}_M) \Psi_{n\prime}(\vec{r}_1, \vec{r}_2, \cdots, \vec{r}_M) d\vec{r}_2 \cdots d\vec{r}_M \tag{3.2.2}$$

where M is the number of valence electrons included in the molecular wavefunction Ψ.

3.3 Conjugated Cyclic Chains

In this section, we extend the microscopic description of γ_{zzzz} for one dimension to two dimensions and consider a specific example within the class of conjugated cyclic structures known as annulenes. As a major case, we consider the planar structure of cyclo-octatetraene (COT), the cyclic analog to OT with N=8, illustrated

schematically in Figure(3.1).[6] Although the geometrically-relaxed ground state of COT is known to be a non-planar, bent structure, we will examine only the planar structure of COT in this section. The purpose is to explore the effect of dimensionality on the microscopic features of $\gamma_{ijkl}(-\omega_4; \omega_1, \omega_2, \omega_3)$. Because the inclusion of the geometrically-relaxed distortions of the physically observed COT structure unnecessarily complicates comparison of cyclic structure results with those described above for linear chains, we consider only the planar structure. Analogies and contrasts between linear and cyclic structures are clearest when the only distinction is the increase in dimensionality from one to two so that one need not be concerned with decoupling dimensionality from non-planarity effects. For linear chains, since the x-component of the transition dipole moments is much larger than the y- and z- components, the isotropically averaged susceptibility γ_g is effectively determined by the γ_{xxxx} component while all components involving transverse fields make negligible contributions. This reduces Eq.(3.1.4) to

$$\gamma_g \approx \frac{1}{5}\gamma_{xxxx} \tag{3.3.1}$$

But for cyclic structures, since the in-plane x- and y- directions are equivalent, γ_{xxxx} and γ_{yyyy} should be of equal magnitude. Furthermore, components such as γ_{xxyy} will also be significant since they involve these two directions as well. The corresponding non-negligible terms of Eq.(3.1.4) are

$$\gamma_g \approx \frac{1}{5}[\gamma_{xxxx} + \gamma_{yyyy} + \frac{1}{3}(\gamma_{xxyy} + \gamma_{xyxy} + \gamma_{xyyx} + \gamma_{yyxx} + \gamma_{yxyx} + \gamma_{yxxy})] \tag{3.3.2}$$

It seems, therefore, that one might be able to enhance γ_g by moving from linear to cyclic conjugated structures and opening pathways for new components of the γ_{ijkl} tensor to contribute. We shall demonstrate below, however, a most striking, opposite finding. We show that, because of the relevant length scales involved in the two problems, the conjugated cyclic structure will necessarily have a smaller γ_g than the corresponding conjugated linear chain with an equal number of carbon sites.

Our planar model of COT is a member of the dihedral D_{4h} symmetry group which is non-Abelian and, hence, has two-dimensional irreducible representations denoted as E classes. The allowed state symmetries for π-electron excitations are A_{1g}, A_{2g}, B_{2g}, and E_u. Of these, only states of ^1E_u symmetry are one-photon allowed excitations from the $^1A_{1g}$ ground state. The ^1E_u states are doubly degenerate with the two representations related by a $\pi/2$ rotation about the z-axis perpendicular to the molecular plane. All of the remaining symmetries listed above describe nondegenerate, two-photon states. These two-photon states can be classified into two types, i.e., symmetric and anti-symmetric, according to the symmetry property under the exchange of the electronic states in the matrix elements.[14]−[16] A typical feature of conjugated cyclic molecules, including phthalocyanines and porphyrins, is the exsistence of a relatively low frequency absorption in the visible or near ultraviolet and a higher frequency absorption deeper in the ultraviolet. This feature appears in our model COT with the weak low frequency 1^1E_u state at 4.4eV and the much stronger frequency 2^1E_u state at 6.4eV. In the case of phthalocyanine, however, it is always the low frequency band which is stronger.

In Table(3.2) we list the symmetries, energies, and relevant transition dipole moments for the nine lowest calculated excited states of COT. A total of 153 states are calculated. The third and fourth columns list the x and y-components, respectively, of the transition moment between a given state and the ground state while the column labeled $\mu^x_{n,2E}$ lists the x-component of the transition moments of the state with the two degenerate representations of the 2^1E_u state; the y-components are given in the $\mu^y_{n,2E}$ column. Although the x- and y-directions are equivalent in COT, it is seen in the table that these components of the transition moments are not always equal, and this is a direct result of the double degeneracy of the E_u states. Transition moments involving any degenerate pair of ^1E_u states with a two-photon state are clearly related by a $\pi/2$ rotation or $x \to y$, $y \to -x$. Thus, the appearance of negative signs in some of the transition moments merely reflects

70

the choice of basis and has no physical meaning. By choosing an appropriate basis for the degenerate pair, the magnitudes of the x and y components can be made equal, although this is not necessary as illustrated in Table (3.2).

The first one-photon doubly degenerate $1^1 E_u$ state has very small transition moments with the ground state and a correspondingly small oscillator strength. The $2^1 E_u$ doubly degenerate state, on the other hand, has a maximum transition moment of $4.6D$ in this $x - y$ basis and is a large oscillator strength in analogy to the $1^1 B_u$ stat of OT. Thus, the transition moments of the two-photon states with the $2^1 E_u$ state determine their importance for $\gamma_{ijkl}(-\omega_4; \omega_1, \omega_2, \omega_3)$ and are also listed in Table(3.2) for the lowest-lying states. Analysis of the various terms in the summations of Eq(3.1.5) for COT reveals much similarity to the linear chain analog. As in OT, there is one dominant term in the double summation which is due to the state with the largest oscillator strength, in this case, the $2^1 E_u$ state. The dominant contributions from the triple sum also all involve the $2^1 E_u$ state, but rather than just one term, there are several significant contributions for COT. Each one is smaller than the dominant negative term from the $2^1 E_u$ state, but together they again lead to positive values for the nonresonant tensor components γ_{ijkl}. The significant contribution from several terms involving different intermediate two-photon states is similar to what was found for the linear polyenes longer than OT.

In Figure(3.2), the transition density matrix $\rho_{n,n'}$ is shown for the ground state with the two representations of the $2^1 E_u$ state. The $\pi/2$ rotational relationship of the two representations of $2^1 E_u$ is also clear here as in Table(3.2). The charge redistribution for this transition is fairly modulated as it is for the linear chains. In the particular basis shown for the representation of the doubly degenerate $2^1 E_u$ state, the transition moments along the x and y directions are comparable as seen in the Figure(3.2). The calculated dispersion of the isotropic third order susceptibility γ_g is given in Figure(3.3). The nonresonant value is quite small compared to the linear chains. Very sharp resonances occur at 1.47 eV due to a 3ω resonance to $1^1 E_u$

and 1.60 eV due to a 2ω resonance with 2^1A_{1g}. Since both of these states have very small transition moments in Table (3.2), they only make significant contributions directly on resonance. Calculations including imaginary damping terms to account for the finite width of the electronic excitations show that these resonances become completely washed out and the dispersion remains flat in this part of the spectrum. Experimental dispersion measurements, therefore, likely would not observe significant resonant enhancement until the 3ω resonance to the 2^1E_u state which occurs at 3.16eV.

The calculated values of $\gamma_{ijkl}(-3\omega; \omega, \omega, \omega)$ for COT at the nonresonant fundamental photon energy of 0.65 eV are γ_{zzzz}=0.75 and γ_{yyyy}=0.21 $\times$ 10^{-36} esu. Because of the D_{4h} symmetry, γ_{zzzz}=γ_{yyyy}, and γ_{zzyy} is equal to all other components that involve two x- component fields and two y- component fields. This equivalence between the x and y- directions is in contrast to the linear polyene case where the γ_{zzzz} component dominates all others. Furthermore, the γ_{zzzz} component of OT (13.5×10^{-36} esu) is far larger than any of the components of COT. However, since COT has significant components in both the x and y directions, it is more reasonable to compare values of the isotropically averaged susceptibility. For COT, $\gamma_g = 0.38 \times 10^{-36}$ esu as compared to 3.4×10^{-36} esu for *trans*-OT. As in the case of comparing values for the *trans* and *cis* conformations of linear polyenes, here also we must consider the actual length scale involved in the problem.

The important length for nonlinear optical responses is the largest length over which charge can be separated due to the presence of an optical electric field. For the linear polyenes, that length is the distance along the conjugation axis separating the end carbons. For COT, the equivalent length is between two points on either end of a diameter of the ring. Additionally, since π-electron motion is constrained along the carbon lattice, the relevant length is one-half of the circumference of the molecular structure. This distance is 3.3 Å for COT. For comparison, for *trans*-HT (N=6) $\gamma_g = 0.75 \times 10^{-36}$ esu at $\hbar\omega$=0.65 eV and the end-to-end length L is 6 Å.

Thus, for these two very different structures where the relevant lengths are nearly equal, we find that the calculated values of γ_g are also comparable. In the case of cyclic structures, the length which determines the magnitude of γ_g appears to be one-half of the circumference.

3.4 Resonant $\chi^{(3)}$ Processes

According to the microscopic description of nonlinear optical processes in conjugated organic materials, highly correlated π-electrons are responsible for the unusually large nonresonant nonlinear optical response of these novel structures. In the nonresonant regime a nonlinear optical response results from virtual excitations of the π-electrons, and response function can be obtained directly from quantum electrodynamics giving the microscopic, molecular hyperpolarizabilities β_{ijk} and γ_{ijkl}. However, as the light frequency approaches one of the π-electron optical excitations, the response function is resonantly enhanced and the perturbation theory employed to describe the nonlinear optical response at off-resonant regime does not hold anymore. In the resonant optical excitations there occurs a real population of the excited state and a depletion of the ground state accordingly, which depends on the incident light intensity. Therefore the optical response function of the system depends on the light intensity, which can be viewed as a third order nonlinear optical response.

In the resonant regime, the π-electron excitation resonant with the incident light can be modeled as a two-level system. A quantum mechanical description of a two-level system with the resonant excitation is well-known, especially from nuclear magnetic resonance experiments (NMR)[17] where a permanent magnetic dipole moment driven by a coherent radiofrequency magnetic field shows a characteristic resonance behavior revealing the microscopic properties of the local environment. The same mathematical formulation developed by Bloch[18] to describe NMR is applicable to the two-level electronic system resonant with an applied field.[19][20]

73

The two physical systems directly map one for one, except for the difference in scaling of the relevant physical parameters. In NMR, for example, the wavelength of the radiofrequency is large compared with the sample size; hence, the absorption length is long and the propagation effect is negligible. In the coherent optical case, however, the optical wavelength is much smaller than the sample dimension, and coherent propagation effect takes place within the sample.

In the subsequent sections, we review the Bloch equation in a density matrix formalism and discuss coherent optical transient effects. The steady state solution of the Bloch equation is studied next, leading to the definition of the intensity dependent refractive index.

3.5 Bloch Equation; Transient Behavior

Let's consider a non-degenerate two-level system with eigenstates $|1\rangle$ and $|2\rangle$.

$$H_0|1\rangle = -\frac{1}{2}\hbar\omega_a|1\rangle \qquad (3.5.1)$$

$$H_0|2\rangle = +\frac{1}{2}\hbar\omega_a|2\rangle \qquad (3.5.2)$$

The time dependence of the wave function $\Psi(t)$ of the system interacting with the external field V can be described by expressing $\Psi(t)$ as a linear combination of $|1\rangle$ and $|2\rangle$ with the time dependent coefficients.

$$\Psi(t) = a(t)e^{i\frac{1}{2}\omega_a t}|1\rangle + b(t)e^{-i\frac{1}{2}\omega_a t}|2\rangle \qquad (3.5.3)$$

The time-dependent Schroedinger equation for the full Hamiltonian $H = H_0 + V$ leads to a pair of equations, i.e., from the orthogonality of $|1\rangle$ and $|2\rangle$,

$$i\hbar\frac{da(t)}{dt} = a(t)V_{11} + b(t)e^{-i\omega_a t}V_{12} \qquad (3.5.4)$$

$$i\hbar\frac{db(t)}{dt} = a(t)e^{i\omega_a t}V_{21} + b(t)V_{22} \qquad (3.5.5)$$

where V_{ij} are the matrix elements of V. The Eq.(3.5.4) and (3.5.5) describe the time evolution of a two-level system.

74

The time dependence of a two-level system in an external field can be described in a density matrix formalism following Feynman *et al.*,[21] which gives a simple geometrical representation of the temporal behavior of the resonance response. The density matrix ρ of a two-level system is 2×2 matrix, hence, can be written as a linear combination of the identity matrix and Pauli matrices.

$$\rho(t) = \frac{1}{2}(I + \vec{r}(t)^F \bullet \vec{\sigma}) \qquad (3.5.6)$$

where the 3-vector $\vec{r}^F$ is the linear coefficients of the Pauli matrices and is uniquely determined in terms of matrix elements of ρ. In the same way the full Hamiltonian H can be expressed as

$$H = \frac{1}{2}\hbar\vec{\Omega}^F \bullet \vec{\sigma} \qquad (3.5.7)$$

where the 3-vector $\vec{\Omega}^F$ is the linear coeffieients. The equation of motion for the density matrix ρ is

$$i\hbar\frac{d}{dt}\rho(t) = [H, \rho(t)] \qquad (3.5.8)$$

The left hand side of Eq(3.5.8) is

$$i\hbar\frac{d}{dt}\rho(t) = i\hbar\frac{d}{dt}\frac{1}{2}(I + \vec{r}(t)^F \bullet \vec{\sigma}) = i\hbar\frac{1}{2}\frac{d\vec{r}(t)^F}{dt} \bullet \vec{\sigma}, \qquad (3.5.9)$$

while the right hand side of Eq(3.5.8) is

$$\begin{aligned}
[H, \rho(t)] &= [\frac{1}{2}\hbar\vec{\Omega}^F \bullet \vec{\sigma}, \frac{1}{2}(I + \vec{r}(t) \bullet \vec{\sigma})] \\
&= \frac{1}{4}[\hbar\vec{\Omega}^F \bullet \vec{\sigma}, \vec{r}(t) \bullet \vec{\sigma}] \\
&= \frac{1}{4}((\hbar\vec{\Omega}^F \bullet \vec{\sigma})(\vec{r}(t) \bullet \vec{\sigma}) - (\vec{r}(t) \bullet \vec{\sigma})(\hbar\vec{\Omega}^F \bullet \vec{\sigma})) \\
&= \frac{1}{4}2i(\hbar\vec{\Omega}^F \times \vec{r}(t)) \bullet \vec{\sigma} \qquad (3.5.10)
\end{aligned}$$

where the following identity of Pauli matrices was used

$$(\vec{A} \bullet \vec{\sigma})(\vec{B} \bullet \vec{\sigma}) = \vec{A} \bullet \vec{B} + i(\vec{A} \times \vec{B}) \bullet \vec{\sigma}. \qquad (3.5.11)$$

Substitution of Eq.(3.5.9) and (3.5.10) into Eq.(3.5.8) transforms the equation of motion for ρ to the equation of motion for $\vec{r}^F$ in terms of $\vec{r}^F$ and $\vec{\Omega}^F$,

$$\frac{d}{dt}\vec{r}(t)^F = \vec{\Omega}^F \times \vec{r}(t)^F. \tag{3.5.12}$$

Eq.(3.5.12) describes the rotation of the 3-vector $\vec{r}^F$ around the rotational axis defined by the 3-vector $\vec{\Omega}^F$, as is well-known in the newtonian equation of motion for a rotating rigid body. The 3-vectors $\vec{r}(t)^F$ and $\vec{\Omega}^F$ are related to the matrix elements of $\rho(t)$ and V in the following way.

$$\vec{r}(t)^F = \begin{pmatrix} \rho_{12} + \rho_{21} \\ +i(\rho_{21} - \rho_{12}) \\ \rho_{22} - \rho_{11} \end{pmatrix} \tag{3.5.13}$$

$$\vec{\Omega}^F = \frac{1}{\hbar}\begin{pmatrix} H_{12} + H_{21} \\ +i(H_{21} - H_{12}) \\ H_{22} - H_{11} \end{pmatrix} = \frac{1}{\hbar}\begin{pmatrix} V_{12} + V_{21} \\ +i(V_{21} - V_{12}) \\ V_{22} - V_{11} + \hbar\omega_a \end{pmatrix} \tag{3.5.14}$$

Now we consider the interaction of the two-level system with a resonant incident light. For ıe linearly polarized light with the frequency ω,

$$\vec{E} = \hat{e}\frac{1}{2}(\varepsilon e^{-i\omega t} + \varepsilon^* e^{+i\omega t}) = Re\{\hat{e}\varepsilon e^{-i\omega t}\}, \tag{3.5.15}$$

the interaction Hamiltonian in the dipole approximation is (Refer to Appendix A3)

$$V = -\vec{\mu} \bullet \vec{E} = -\vec{\mu} \bullet \hat{e}\frac{1}{2}(\varepsilon e^{-i\omega t} + \varepsilon^* e^{+i\omega t}). \tag{3.5.16}$$

Eq.(3.5.14) becomes

$$\begin{aligned}
\vec{\Omega}^F &= (-\frac{2\mu\varepsilon}{\hbar}\cos\omega t, 0, \omega_a) \\
&= (-\kappa\varepsilon\cos\omega t, -\kappa\varepsilon\sin\omega t, 0) \\
&\quad + (-\kappa\varepsilon\cos\omega t, +\kappa\varepsilon\sin\omega t, 0) \\
&\quad + (0, 0, \omega_a) \\
&= \vec{\Omega}^{+F} + \vec{\Omega}^{-F} + \vec{\Omega}^{0F}
\end{aligned} \tag{3.5.17}$$

76

where

$$\kappa = \frac{\langle 1|\vec{\mu} \bullet \hat{e}|2 \rangle}{\hbar} = \frac{\mu}{\hbar}. \tag{3.5.18}$$

$\vec{\Omega}^F$ is composed of three vectors, $\vec{r}^F$ processing around it. $\vec{\Omega}^{+F}(\vec{\Omega}^{-F})$ is a vector with magnitude $\kappa\varepsilon$, lying on the 1-2 plane and rotating around 3-axis with angular velocity $\omega(-\omega)$, while $\vec{\Omega}^{0F}$ is a constant vector along 3-axis with magnitude ω_a. According to Eq.(3.5.12) $\vec{r}^F$ is processing around $\vec{\Omega}^F$ with angular veocity $|\vec{\Omega}^F| \approx \omega_a$ (noting $\kappa\varepsilon << \omega_a$). In the rotating wave approximation (RWA), $\vec{\Omega}^{-F}$ is ignored since $\vec{\Omega}^{-F}$ rotates with the angular frequency $\omega + \omega_a \approx 2\omega$ relative to $\vec{r}^F$, hence, this rapid oscillation averages out in time and does not give an accumulative variation in amplitude. That is, in RWA, which is equivalent to ignoring $e^{+i\omega t}$ part in Eq.(3.5.16),

$$\vec{\Omega}^F \approx \vec{\Omega}^{+F} + \vec{\Omega}^{0F} = (-\kappa\varepsilon \cos\omega t, -\kappa\varepsilon \sin\omega t, \omega_a) \tag{3.5.19}$$

As shown in Figure(3.4), $\vec{\Omega}^F$ is a 3-vector rotating with angular frequency $-\omega$ around axis 3, and we make an orthogonal transformation to the frame where $\vec{\Omega}^F$ is stationary.

$$\vec{r} = \begin{pmatrix} u \\ v \\ w \end{pmatrix} = \begin{pmatrix} \cos\omega t & \sin\omega t & 0 \\ -\sin\omega t & \cos\omega t & 0 \\ 0 & 0 & 1 \end{pmatrix} \begin{pmatrix} r_1^F \\ r_2^F \\ r_3^F \end{pmatrix} \tag{3.5.20}$$

$$\vec{\Omega} = \begin{pmatrix} \cos\omega t & \sin\omega t & 0 \\ -\sin\omega t & \cos\omega t & 0 \\ 0 & 0 & 1 \end{pmatrix} \vec{\Omega}^F$$

$$= \begin{pmatrix} \cos\omega t & \sin\omega t & 0 \\ -\sin\omega t & \cos\omega t & 0 \\ 0 & 0 & 1 \end{pmatrix} \begin{pmatrix} -\kappa\varepsilon \cos\omega t \\ -\kappa\varepsilon \sin\omega t \\ \omega_a \end{pmatrix} = \begin{pmatrix} -\kappa\varepsilon \\ 0 \\ \omega_a \end{pmatrix} \tag{3.5.21}$$

$$\frac{d}{dt}^F = \frac{d}{dt} + \vec{\omega} \times \tag{3.5.22}$$

Refer to Appendix A4 for another way to make an orthogonal transformation. In the new frame (see Figure(3.5)) the Schroedinger equation has the same form as Eq.(3.5.12),

$$\frac{d\vec{r}(t)}{dt} = \vec{\Omega} \times \vec{r} \tag{3.5.23}$$

77

with

$$\vec{\Omega} = \begin{pmatrix} -\kappa\varepsilon \\ 0 \\ \omega_a - \omega \end{pmatrix} = \begin{pmatrix} -\kappa\varepsilon \\ 0 \\ \Delta \end{pmatrix} \tag{3.5.24}$$

$$|\vec{\Omega}| = \Omega = \sqrt{(\kappa\varepsilon)^2 + \Delta^2} \tag{3.5.25}$$

Eq.(3.5.23) is the Bloch equation when the damping is ignored, essentially equivalent to the time-dependent Schroedinger equation Eq.(3.5.4) and (3.5.5). The precession frequency Ω, called Rabi frequency, depends on the light intensity as well as the detuning Δ. The Bloch equation in an explicit form is

$$\dot{u} = -\Delta v - \frac{u}{T_2} \tag{3.5.26}$$

$$\dot{v} = \Delta u + \kappa\varepsilon w - \frac{v}{T_2} \tag{3.5.27}$$

$$\dot{w} = -\kappa\varepsilon v - \frac{w - w_{eq}}{T_1} \tag{3.5.28}$$

Here the phenomenological relaxation times T_1 (longitudinal) and T_2 (transverse) are introduced to account for the population decay and the coherence decay respectively. The macroscopic coherent superposition state decays out in time either through the spontaneous emission (T_1) from the excited state ending up with the equilibrium population corresponding to w_{eq} or through the dephasing (T_2) between the microscopic dipole moments, resulting in zero polarization even for a net inversion of population during the time shorter than T_1. T_2 is the inversion of the homogeneous broadening contribution to the optical linewidth. There are various contributions to the dephasing, one main contribution coming from a spontaneous decay of the excited state itself, $1/2T_1$. More explicitly, from Eq.(3.5.3) we can find the time dependences of the polarization $p(t)$ and the polpulation $n(t)$. The polarization $p(t)$ is given as an expectation value of dipole moment.

$$p(t) = \langle 2(t)|x|1(t)\rangle = e^{-t/2T_1} b^*(t)a(t)e^{i\omega_a t}\langle 2|x|1\rangle \tag{3.5.29}$$

$$n(t) = \langle 2(t)|2(t)\rangle - \langle 1(t)|1(t)\rangle = e^{-t/T_1} b^*(t)b(t) - a^*(t)a(t) \tag{3.5.30}$$

We find that the finite lifetime of the excited state affects the lifetime of a microscopic dipole moment, setting a limit on the dephasing time. Pure depahsing, not originating from a finite lifetime of the excited state, comes from various sources depending on the microscopic line broadening mechanism. In gas, collisions with other gas atoms or molecules are mainly responsible for a dephasing, while a phonon scattering with an optical excitation is accountable for the line broadening. Sometimes, these pure dephasing rates are called T_2' to distinguish it from the inhomogeneous contributions, called T_2^*, coming from a Doppler broadening or a site broadening. The relaxation times can be calculated theoretically once the microscopic relaxation mechanism is known. The temperature dependence of the relaxation rates for a two-level system in an amorphous medium will be discussed in Chapter 4.

A rigorous solution of the Bloch equation Eq.(3.5.26)-(3.5.28) is available,[22] but here we consider a simple transient case when T_1 and T_2 are long enough or during the time the system did not relax to equilibrium. When the damping is ignored, the equation can be solved analytically. According to Eq.(3.5.24) $\vec{\Omega}$ is a 3-vector in the 1-3 plane. Now we make transformation to a coordinate where $\vec{\Omega}$ is along the 1-axis. The transformation matrix is

$$\mathbf{R}(\theta = \arctan \frac{\Delta}{-\kappa\varepsilon}) = \begin{pmatrix} \cos\theta & 0 & \sin\theta \\ 0 & 1 & 0 \\ -\sin\theta & 0 & \cos\theta \end{pmatrix}. \qquad (3.5.31)$$

The Bloch vector is affected in the same way yielding

$$\vec{r}'(t) = \mathbf{R}\vec{r}(t). \qquad (3.5.32)$$

In the new frame the Bloch equation is in the same form again as Eq.(3.5.12),

$$\frac{d\vec{r}'(t)}{dt} = \vec{\Omega}' \times \vec{r}' = \begin{pmatrix} 0 & 0 & 0 \\ 0 & 0 & \Omega \\ 0 & -\Omega & 0 \end{pmatrix} \vec{r}' \qquad (3.5.33)$$

with

$$\vec{\Omega}' = \begin{pmatrix} \Omega \\ 0 \\ 0 \end{pmatrix}. \qquad (3.5.34)$$

The solution of Eq.(3.5.33) is straightforward since $\vec{r}'$ is rotating around the 1-axis with the angular frequency Ω.

$$\vec{r}'(t) = \begin{pmatrix} u'(t) \\ v'(t) \\ w'(t) \end{pmatrix} = \Omega\vec{r}'(0) = \begin{pmatrix} 1 & 0 & 0 \\ 0 & \cos\Omega t & -\sin\Omega t \\ 0 & \sin\Omega t & \cos\Omega t \end{pmatrix} \vec{r}'(0) \qquad (3.5.35)$$

Now transforming back to $\vec{r}(t)$,

$$\vec{r}(t) = \begin{pmatrix} u(t) \\ v(t) \\ w(t) \end{pmatrix} = \mathbf{R}^{-1}\vec{r}'(t) = \mathbf{R}^{-1}\Omega\vec{r}'(0) = \mathbf{R}^{-1}\Omega\mathbf{R}\mathbf{R}^{-1}\vec{r}'(0) = \mathbf{R}^{-1}\Omega\mathbf{R}\vec{r}(0)$$

$$= \begin{pmatrix} \frac{(\kappa\varepsilon)^2 + \Delta^2\cos\Omega t}{\Omega^2} & \frac{-\Delta}{\Omega}\sin\Omega t & \frac{-\Delta\kappa\varepsilon}{\Omega^2}(1-\cos\Omega t) \\ \frac{\Delta}{\Omega}\sin\Omega t & \cos\Omega t & \frac{\kappa\varepsilon}{\Omega}\sin\Omega t \\ \frac{-\Delta\kappa\varepsilon}{\Omega^2}(1-\cos\Omega t) & \frac{-\kappa\varepsilon}{\Omega}\sin\Omega t & \frac{\Delta^2 + (\kappa\varepsilon)^2\cos\Omega t}{\Omega^2} \end{pmatrix} \begin{pmatrix} u(0) \\ v(0) \\ w(0) \end{pmatrix} \qquad (3.5.36)$$

This is called the Rabi solution[19][23] and describes the interesting transient resonant behavior of a two-level system interacting with a radiation field. Let's consider a couple of special cases of Eq.(3.5.36). First we assume that at time $t = -\infty$ the two-level system was in the ground state ($w_0 = w(0) = -1$) and in an incoherent state ($u_0 = u(0) = 0, v_0 = v(0) = 0$). If the light frequency is on resonance with the two-level system eigen frequency, i.e. $\Delta = 0$, the vector $\vec{\Omega}$ is on the 1-axis and the solution is quite simple as can be seen directly from the geometrical representation. With the given initial conditions the Bloch vector $\vec{r}(t)$ rotates around the 1-axis on the 2-3 plane, starting from the negative 3-axis. It is useful to define the area $\theta(t)$ of the incident pulse at time t,[24]

$$\theta(t) = \int_{-\infty}^{t} \kappa\varepsilon dt'. \qquad (3.5.37)$$

After the time corresponding to $\theta(t) = \pi$, a complete inversion of population occurs, the Bloch vector along the positive 3-axis. At time corresponding to 2π the two-level system restores back to the initial configuration where all the molecules are in the ground state. When a coherent optical pulse with total pulse area of 2π propagates through a Bloch system, the coupling of Maxwell equation to Bloch equation leads

80

to a self-induced-transparency, as the excitation of the two-level system by the first half (area π) of the pulse is followed by a coherent deexcitation by the second half (total area 2π) resulting in no net absorption by the absorber.[25]-[29]

In the original frame the vector $\vec{\Omega}$ is rotating with the optical frequency ω ($\sim 10^{15}$ Hz) with the Bloch vector $\vec{r}$ precessing with the Rabi frequency Ω ($\sim 10^8$ Hz on resonance for the light intensity $100 W/cm^2$ and the dipole moment 10^{-2} Debye, 1 Debye $= 10^{-18} esu\ cm$). The precession is damped out in time from the relaxations of T_1 and T_2, similar to a spinning top precessing around a fixed axis damping through the friction. For a step-function light pulse this precession shows up as an intensity modulation near the leading edge, and the decaying modulation can be observed for many cycles when the Rabi frequency is much higher than the dephasing frequency, easily achievable with a sufficiently high incident light intensity. This phenomenon is called optical nutation,[30]-[32] after the similar well-known nuclear magnetic resonance effect of transient nutation. Other interesting coherent transient effects include free induction decay[33] and photon echo,[34]-[37] the basic physical idea of which is easy to understand from the geometrical picture discussed above. Nonlinear optical process can be combined with the coherent resonant optical process to give a Raman echo or trilevel echos.[38]-[41]

3.6 Steady State Solution of Bloch equation

Now we examine the steady state solution of the Bloch equation. In steady state, the time derivative vanishes, and the solution is staightforward.

$$u = -\frac{\kappa\varepsilon T_2 \Delta T_2}{1 + \Delta^2 T_2^2 + T_1 T_2 \kappa^2 \varepsilon^2} w_{eq} \qquad (3.6.1)$$

$$v = -\frac{\kappa\varepsilon T_2}{1 + \Delta^2 T_2^2 + T_1 T_2 \kappa^2 \varepsilon^2} w_{eq} \qquad (3.6.2)$$

$$w = \frac{1 + \Delta^2 T_2^2}{1 + \Delta^2 T_2^2 + T_1 T_2 \kappa^2 \varepsilon^2} w_{eq} \qquad (3.6.3)$$

In order to get a physical understanding of the Bloch equations, let us consider a classical Lorentzian oscillator. A comparison of the classical oscillator with the quantum mechanical oscillator gives a better understanding of a Bloch equation. The equation of motion for a classical Lorentzian oscillator is

$$\frac{d^2 x}{dt^2} + 2\gamma \frac{dx}{dt} + \omega_a^2 x = \frac{e}{m} \varepsilon e^{i\omega t} \tag{3.6.4}$$

The steady state solution is

$$x = \frac{1}{\omega_a^2 - \omega^2 + i2\gamma\omega} \frac{e}{m} \varepsilon$$
$$= \left[\frac{1}{(\omega_a^2 - \omega^2)^2 + 4\gamma^2\omega^2}\right]^{\frac{1}{2}} e^{i\theta} \frac{e}{m} \varepsilon \tag{3.6.5}$$

with

$$\tan \theta = -\frac{2\gamma\omega}{\omega_a^2 - \omega^2} \tag{3.6.6}$$

Now we solve Eq.(3.6.4) by a similar method empolyed to solve a quantum mechanical two-level system. Let

$$x(t) = \big(u(t) + iv(t)\big) e^{i\omega t} \tag{3.6.7}$$

Keeping terms up to first order, which is sufficient for studying resonance behavior,

$$\dot{u} = -\Delta v - \gamma u = -\Delta v - \frac{u}{T_2} \tag{3.6.8}$$

$$\dot{v} = \Delta u - \gamma v - \frac{e}{m} \frac{\varepsilon}{2\omega} = \Delta u - \kappa\varepsilon - \frac{v}{T_2} \tag{3.6.9}$$

with

$$\kappa = \frac{e}{2m\omega}. \tag{3.6.10}$$

The steady state solution is

$$u = \frac{\kappa\varepsilon T_2 \Delta T_2}{1 + \Delta^2 T_2^2} \tag{3.6.11}$$

$$v = -\frac{\kappa\varepsilon T_2}{1 + \Delta^2 T_2^2}. \tag{3.6.12}$$

82

Comparision of Eq.(3.6.11) and (3.6.12) with Eq.(3.6.1)-(3.6.3) shows the difference between the classical Lorentzian oscillator and the quantum oscillator described by the Bloch equation. First, the term $T_1 T_2 \kappa^2 \epsilon^2$ in the denominators for the quantum oscillator comes from the coupling between v and w and there is only a phase relaxation time in the classical oscillator while there are two kinds of relaxation times in the quantum oscillator. It is obvious that in the limit $T_1 \rightarrow 0$, $w = w_{eq}$ and there is no difference between the classical and quantum oscillators. Second, if we set $w = w_{eq} = -1$, the Bloch equation Eq(3.5.26)-(3.5.28) reduces to the classical oscillator equation Eq(3.6.8)-(3.6.9), which means that the characteristic nonlinear response of the quantum oscillator comes from the real population of the upper state of the two level system.

3.7 Nolinear Optical Susceptibility; Intensity-dependent Refractive Index

In order to get the nonlinear optical susceptibility of the Bloch system to the external external field, we calculate the expectation value of the polarization.

$$
\begin{aligned}
N \langle \mu(t) \rangle &= N tr(\rho(t) \mu) = N\mu(\rho_{12}(t) + \rho_{21}(t)) \\
&= N\mu r_1^F(t) = N\mu(u \cos \omega t - v \sin \omega t) \\
&= Re\{N\mu(u - iv)e^{-i\omega t}\}
\end{aligned}
\tag{3.7.1}
$$

Introducing a complex susceptibility $\chi(\omega)$,

$$
\begin{aligned}
N \langle \mu(t) \rangle &= Re\{\chi E\} = Re\{(\chi' + i\chi'')\epsilon e^{-i\omega t}\} \\
&= (\chi' \cos \omega t + \chi'' \sin \omega t)\epsilon.
\end{aligned}
\tag{3.7.2}
$$

Comparing Eq(3.7.1) and Eq(3.7.2), the complex susceptibility χ can be expressed in terms of u and v.

$$
\chi' = N\frac{\mu}{\epsilon}u, \qquad \chi'' = -N\frac{\mu}{\epsilon}v
\tag{3.7.3}
$$

Substitution of Eq.(3.6.1)-(3.6.3) into Eq.(3.7.3) leads to the steady state suscepti-bilities χ' and χ''.

$$\chi' = -\frac{\mu^2 T_2 \delta N_0}{\hbar} \frac{\Delta T_2}{1 + \Delta^2 T_2^2 + T_1 T_2 \kappa^2 \epsilon^2} \tag{3.7.4}$$

$$\chi'' = -\frac{\mu^2 T_2 \delta N_0}{\hbar} \frac{1}{1 + \Delta^2 T_2^2 + T_1 T_2 \kappa^2 \epsilon^2} \tag{3.7.5}$$

$$\delta N = \delta N_0 \frac{1 + \Delta^2 T_2^2}{1 + \Delta^2 T_2^2 + T_1 T_2 \kappa^2 \epsilon^2} \tag{3.7.6}$$

where

$$\delta N = Nw, \qquad \delta N_0 = Nw_{eq}. \tag{3.7.7}$$

The complex susceptibility can be written in terms of the linear absorption coeffi-cient on resonance. Noting

$$\eta + i\kappa = \sqrt{\epsilon' + i\epsilon''} = \sqrt{1 + 4\pi\chi' + i4\pi\chi''} \tag{3.7.8}$$

and the following relation of the linear absorption coefficient α_0 to the imaginary part of the susceptibility

$$\alpha_0 = 2\kappa\frac{\omega}{c} = 4\pi\frac{\omega}{c}\chi''(\Delta = 0, \epsilon \to 0) = \frac{4\pi\omega}{\hbar c}NT_2\mu^2 \tag{3.7.9},$$

we get the complex susceptibility of a Bloch system in steady state from Eq.(3.7.4), (3.7.5), and (3.7.9).

$$\chi(\omega) = \left(\frac{\alpha_0 c}{4\pi\omega}\right)\left(\frac{\Delta T_2 + i}{1 + \Delta^2 T_2^2 + T_1 T_2(\frac{\mu\epsilon}{\hbar})^2}\right)$$

$$= \left(\frac{\alpha_0 c}{4\pi\omega}\right)\left(\frac{\Delta + i}{1 + \Delta^2 + I/I_s}\right) \tag{3.7.10}$$

where

$$I_s = \frac{c}{8\pi}\left(\frac{\hbar}{\mu\sqrt{T_1 T_2}}\right)^2 \tag{3.7.11}$$

and Δ is redefined as

$$\Delta = \Delta T_2 = (\omega - \omega_a)T_2. \tag{3.7.12}$$

To get the third order nonlinear susceptibility $\chi^{(3)}$ or n_2, we find the linear coefficient of the term that is linear in intensity when the Bloch susceptibility is expanded.

$$\eta = 1 + 2\pi\chi' = 1 + \left(\frac{\alpha_0\lambda}{4\pi}\right)\left(\frac{\Delta}{1+\Delta^2+I/I_s}\right) \qquad (3.7.13)$$

Now

$$n_2 = \frac{d\eta}{dI}\Big|_{I=0} = -\left(\frac{\alpha_0\lambda}{4\pi I_s}\right)\frac{\Delta}{(1+\Delta^2)^2} \qquad (3.7.14)$$

The term depending on the detuning, $\frac{\Delta}{(1+\Delta^2)^2}$, has the maximum value when Δ equals to $\frac{1}{\sqrt{3}}$. Therefore, the maximum value available for n_2 is

$$n_2 = \pm 0.026 \frac{\alpha\lambda}{I_s}. \qquad (3.7.15)$$

A remark is necessary for the physical units of the third order susceptibility. The refractive index is a dimensionless physical quantity either in cgs units or in MKS units. The intensity dependent refractive index n_2 is defined as

$$n = n_0 + n_2 I. \qquad (3.7.16)$$

The incident light intensity is the absolute value of the Poynting vector $\vec{S}$. For the linearly polarized light as denoted in Eq.(3.5.15),

$$I(esu) = |\vec{S}| = \frac{c}{4\pi}|\vec{E} \times \vec{H}| = \frac{c}{4\pi}\frac{1}{2}|\varepsilon\sqrt{\frac{\epsilon}{\mu}}\varepsilon| = \frac{c}{8\pi}n_0|\varepsilon|^2 \qquad (3.7.17)$$

$$I(MKS) = \frac{1}{2}cn_0\epsilon_0|\varepsilon|^2 \qquad (3.7.18)$$

The dielectric constant ϵ is related to the susceptibility and the refractive index in the following way.

$$\epsilon = n^2 = (n_0 + n_2 I)^2 = n_0^2 + 2n_0 n_2 I$$
$$= 1 + 4\pi\chi = 1 + 4\pi\chi^{(1)} + 4\pi\chi^{(3)}\varepsilon\varepsilon \qquad (3.7.19)$$

85

In cgs units the susbstitution of the intensity from Eq(3.7.17) into Eq.(3.7.19) leads to the following relation.

$$n_2(esu) = \frac{1}{c}\left(\frac{4\pi}{n_0}\right)^2 \chi^{(3)}(esu) \tag{3.7.20}$$

In MKS units the relation between the susceptibility and the dielectric constant is different.

$$n^2 = \frac{\epsilon}{\epsilon_0} = \frac{1}{\epsilon_0}(1 + \chi) \tag{3.7.21}$$

Taking Eq.(3.7.18) into Eq.(3.7.21) gives

$$n_2(MKS) = \frac{1}{c}\left(\frac{1}{n_0\epsilon_0}\right)\chi^{(3)}(MKS). \tag{3.7.22}$$

In a real experiment, the units of cm^2/kW is often used for n_2. Noting

$$n_2(esu)I(erg/cm^2 sec) = 10^{-10}n_2(cm^2/kW)I(kW/cm^2), \tag{3.7.23}$$

we then have

$$n_2(cm^2/kW) = 10^{10}n_2(esu) = \frac{10^{10}}{c}\left(\frac{4\pi}{n_0}\right)^2\chi^{(3)}(esu) = \frac{1}{3}\left(\frac{4\pi}{n_0}\right)^2\chi^{(3)}(esu). \tag{3.7.24}$$

For a semiconductor, n_2 in cm^2/kW has value similar to $\chi^{(3)}$ in esu units.

References: Chapter 3

[1] See, for example, *Nonlinear Optical Properties of Organic and Polymeric Materials*, Williams, D.J., ed., ACS Symp. Series, Vil. 233 (Americal Chemical Society, Washington, D.C., 1983)

[2] Lalama, S.J. and Garito, A.F., Phys. Rev. **A20**, 1179 (1979)

[3] Singer, K.D. and Garito, A.F., J. Chem. Phys. **75**, 3572 (1981)

[4] Teng, C.C. and Garito, A.F., Phys. Rev. Lett. **50**, 350 (1983); Phys. Rev. **B28**, 6766 (1983)

[5] Heflin, J.R., Wong, K.Y., Zamani-Khamiri, O., and Garito, A.F., Phys. Rev. **B38**, 1573 (1988)

[6] Wu, J.W., Heflin, J.R., Norwood, R.A., Wong, K.Y., Zamani-Khamiri, O., Garito, A.F., Kalyanaraman, P., and Sounik, J., J. Optc. Soc. Am. **B6**, 707 (1989)

[7] Solyom, J., Adv. in Phys. **28**, 201 (1979)

[8] Bogoliubov, N.N. and Mitroplosky, Y.A., *Asymptotic Methods in the Theory of Nonlinear Oscillations*, Gordon and Breach, (1961)

[9] Orr, B.J. and Ward, J.F., Mol. Phys. **20**, 513 (1971)

[10] Schulten, K., Ohmine, I., and Karplus, M., J. Chem. Phys. **64**, 4422 (1976)

[11] Schulten, K., Dinur, U., and Honig, B., J. Chem. Phys. **73**, 3927 (1980)

[12] Soos, Z.G. and Ramasesha, S., Phys. Rev. **B29**, 5410 (1984)

[13] Tavan, P. and Schulten, K., Phys. Rev. **B36**, 4337 (1987)

[14] Monson, P.R. and McClain, W.M., J. Chem. Phys. **53**, 29 (1970)

[15] McClain, W.M., J. Chem. Phys. **55**, 2789 (1971)

[16] Kuzyk, M.G., Norwood, R.A., Wu, J.W., and Garito, A.F., J. Opt. Soc. Am. **B6**, 154 (1989)

[17] Abragam, A., *The Principles of Nuclear Magnetism*, Clarendon, Oxford (1961)

[18] Bloch, F., Phys. Rev. **70**, 460 (1946)

[19] Allen, L. and Eberly, J.H., *Optical Resonance and Two-level Atoms*, Wiley, New York (1975)

[20] Steinfeld, J.I. *An Intrioduction to Modern Molecular Sepctroscopy*, 2nd ed. MIT Press, Cambridge (1984)

[21] Feynman, R.P., Vernon, F.L., Helwarth, R.W., J. Appl. Phys. **28**, 49 (1957)

[22] Torrey, H.C., Phys. Rev. **76**, 1059 (1949)

[23] Rabi, I.I., Phys. Rev. **51**, 652 (1937)

[24] McCall, S.L. and Hahn, E.L., Phys. Rev. A2, 861 (1970)

[25] McCall, S.L. and Hahn, E.L., Phys. Rev. Lett. **18**, 908 (1967)

[26] Patel, C.K.N. and Slusher, R.E., Phys. Rev. Lett. **19**, 1019 (1967)

[27] McCall, S.L. and Hahn, E.L., Phys. Rev. **183**, 457 (1969)

[28] Slusher, R.E. and Gibbs, H.M., Phys. Rev. A5, 1634 (1972)

[29] Gibbs, H.M. Phys. Rev. A8 446, (1973)

[30] Brewer, R.G. and Shoemaker, R.L., Phys. Rev. Lett. **27**, 631 (1971)

[31] Hocker, G.B. and Tang, C.L., Phys. Rev. Lett. **21**, 591 (1969)

[32] Tang, C.L. and Statz, H., Appl. Phys. Lett. **10**, 145 (1967)

[33] Brewer, R.G. and Shoemaker, R.L., Phys. Rev. A6, 2001 (1972)

[34] Kurnit, N.A., Abella, I.D., and Hartmann, S.R., Phys. Rev. Lett. **13**, 567 (1964)

[35] Patel, C.K.N. and Slusher, R.E., Phys. Rev. Lett. **20**, 1087 (1968)

[36] Becker, P.C., Fragnito, H.L., Brito Cruz, C.H., Fork, R.L., Cunningham, J.E., Henry, J.E., and Shank, C.V., Phys. Rev. Lett. **61**, 1647 (1988)

[37] Kobayashi, T., Terasaki, A., Hattori, T., and Kurokawa, K., Appl. Phys. B **47**, 107 (1988)

[38] Aihara, M. and Inaba, H., J. Phys. A **6**, 1709, 1725 (1973)

[39] Mossberg, T.W. and Hartmann, S. R., Phys. Rev. A **23**, 1271 (1981)

[40] Hu, P., Geschwind, S., and Jedju, T.M., Phys. Rev. Lett. **37**, 1357 (1976)

[41] Mossberg, Flusberg, A., Kachru, R., and Hartmann, S. R., Phys. Rev. Lett. **39**, 1523 (1977)

Figure Captions: Chapter 3

Figure 3.1; Schematic Diagram of Cyclo-Octatetraene

Figure 3.2; Density Matrix Diagram for Cyclo-Octateraene

Figure 3.3; THG Dispersion Curve for Cyclo-Octateraene

Figure 3.4; Bloch Vector in Pauli Matrix Space

Figure 3.5; Bloch Vector in a Rotating Frame

The symmetries, energies and selected transition dipole

moments of the calculated low-lying states of *trans*-octatetraene

Symmetry	Energy (eV)	$\mu_{n,g}^X$ (D)	$\mu_{n,1B}^X$ (D)
$2\,^1A_g$	4.15	0.00	2.82
$1\,^1B_u$	4.42	7.81	0.00
$2\,^1B_u$	4.79	0.86	0.00
$3\,^1A_g$	5.19	0.00	0.07
$4\,^1A_g$	6.00	0.00	2.84
$5\,^1A_g$	6.07	0.00	1.11
$3\,^1B_u$	6.47	0.01	0.00
$4\,^1B_u$	7.01	1.11	0.00
$6\,^1A_g$	7.16	0.00	13.24
$5\,^1B_u$	7.30	1.14	0.00

Table 3.1

The symmetries, energies and selected transition dipole
moments of the calculated low-lying states of *cyclo*-octatetraene

Symmetry	Energy(eV)	$\mu^x_{n,g}(D)$	$\mu^y_{n,g}(D)$	$\mu^x_{n,2E}(D)$	$\mu^y_{n,2E}(D)$
1^1A_{2g}	2.24	0.00	0.00	-1.60, 2.40	-2.40,-1.60
2^1A_{1g}	3.19	0.00	0.00	0.14, 0.09	-0.09, 0.14
1^1E_u	4.41	0.05	-0.03	0.00, 0.00	0.00, 0.00
1^1E_u	4.41	0.03	0.05	0.00, 0.00	0.00, 0.00
1^1B_{2g}	5.21	0.00	0.00	-0.33, 0.50	0.50, 0.33
1^1B_{1g}	5.94	0.00	0.00	1.03, 0.68	0.68,-1.03
2^1E_u	6.48	4.58	-3.04	0.00, 0.00	0.00, 0.00
2^1E_u	6.48	3.04	4.58	0.00, 0.00	0.00, 0.00

Table 3.2

91

Schematic Diagram of Cyclo-Octatetraene
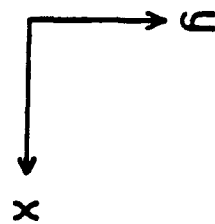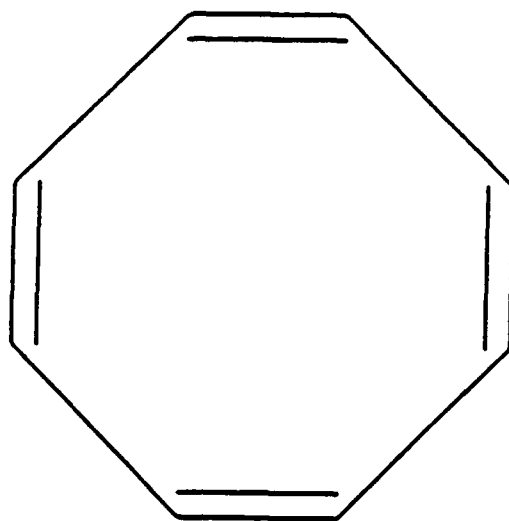
Figure 3.1

Density Matrix Diagram for Cyclo-Octatertaene
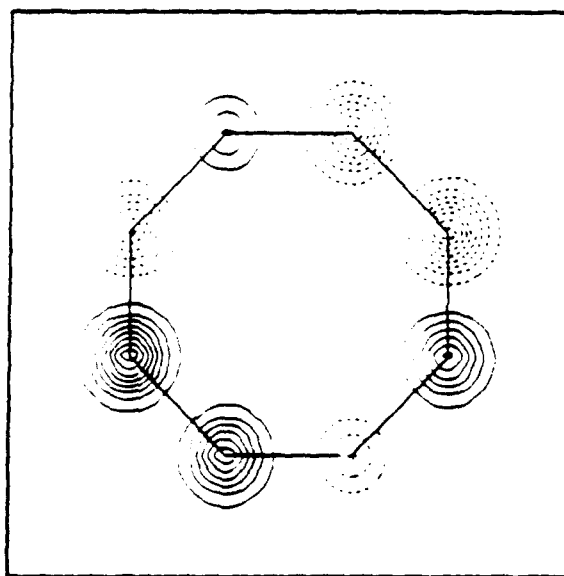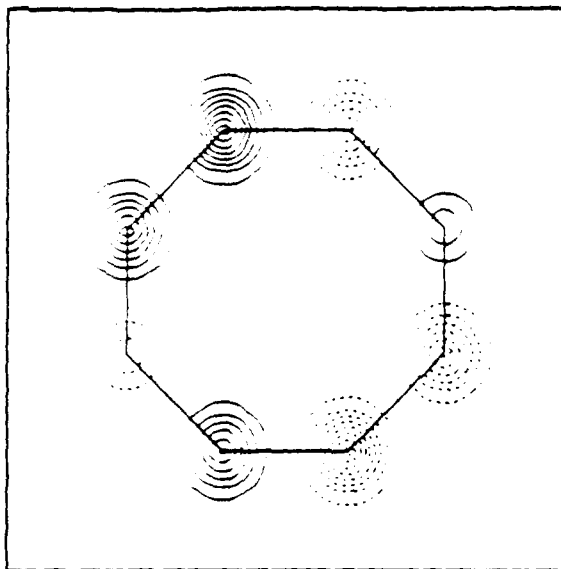
Figure 3.2

THG Dispersion Curve for Cyclo-Octatetraene

$$\gamma_g \ (-3\omega;\omega,\omega,\omega) \ (10^{-36} \text{esu})$$
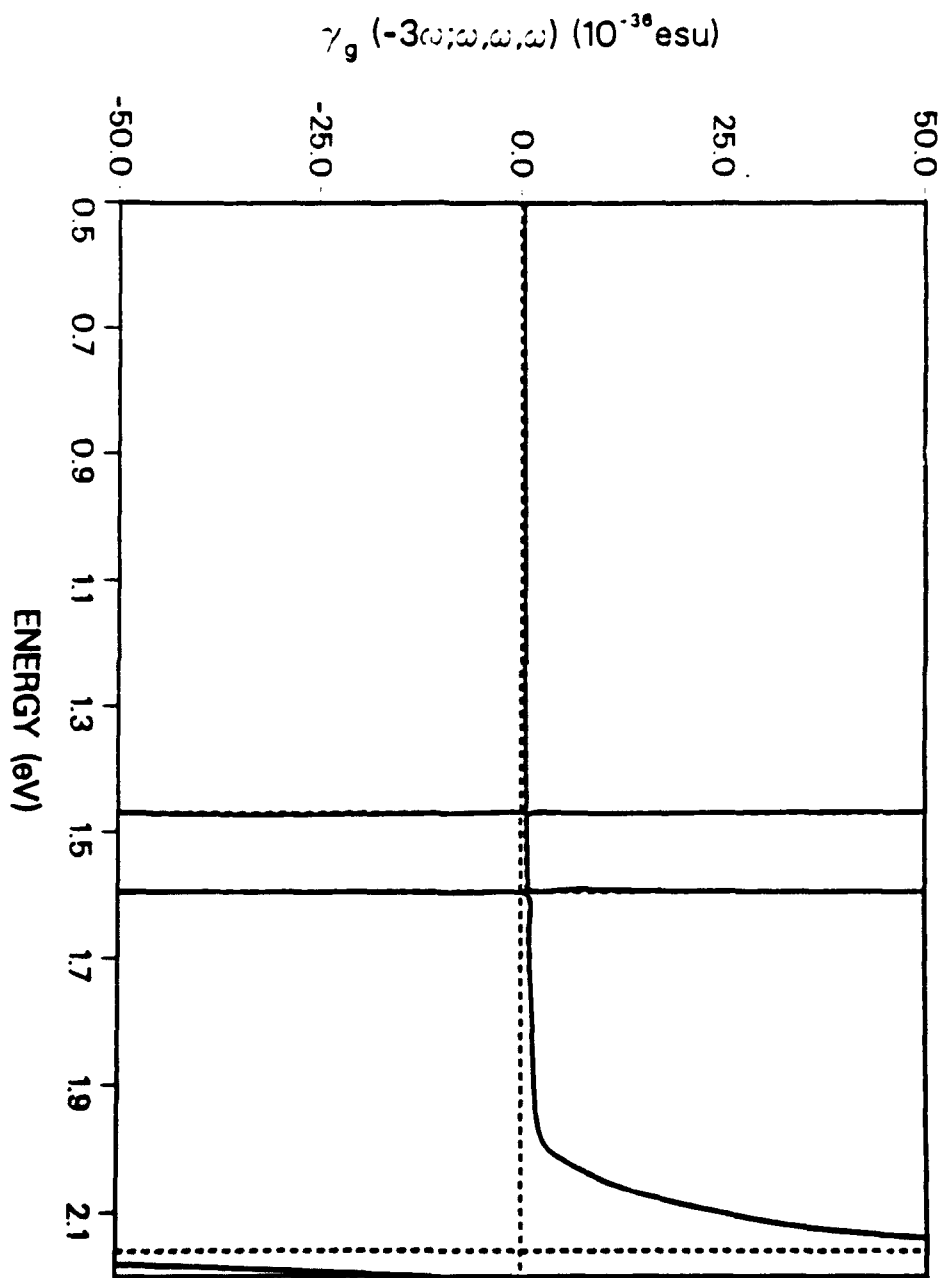
Figure 3.3

Bloch Vector in Pauli Matrix Space
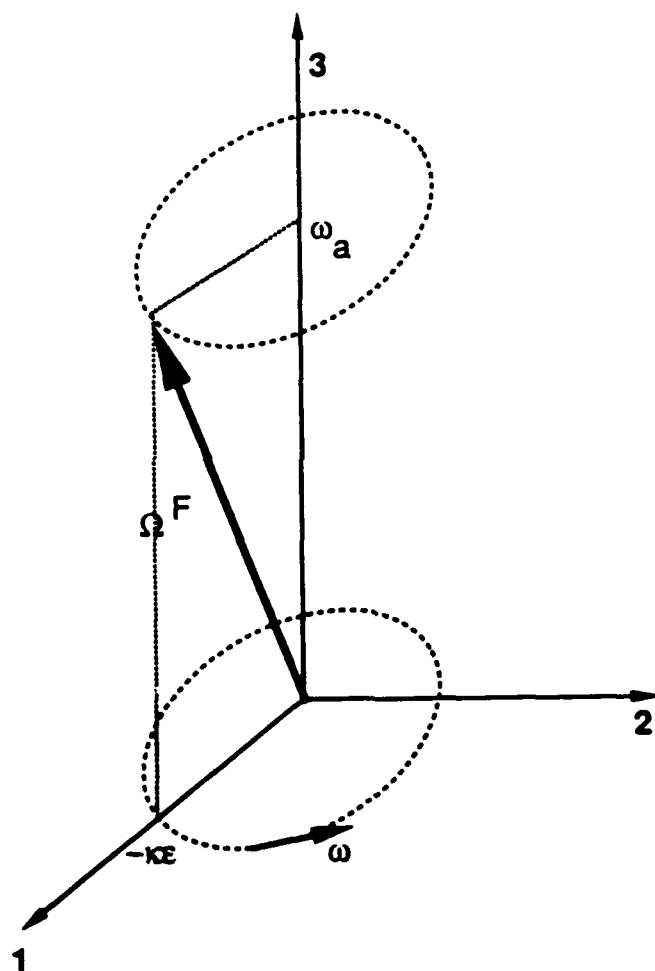
Figure 3.4

Bloch Vector in a Rotating Frame

$$\Delta = \omega_a - \omega$$

$$\Omega$$

$$-\kappa_2$$
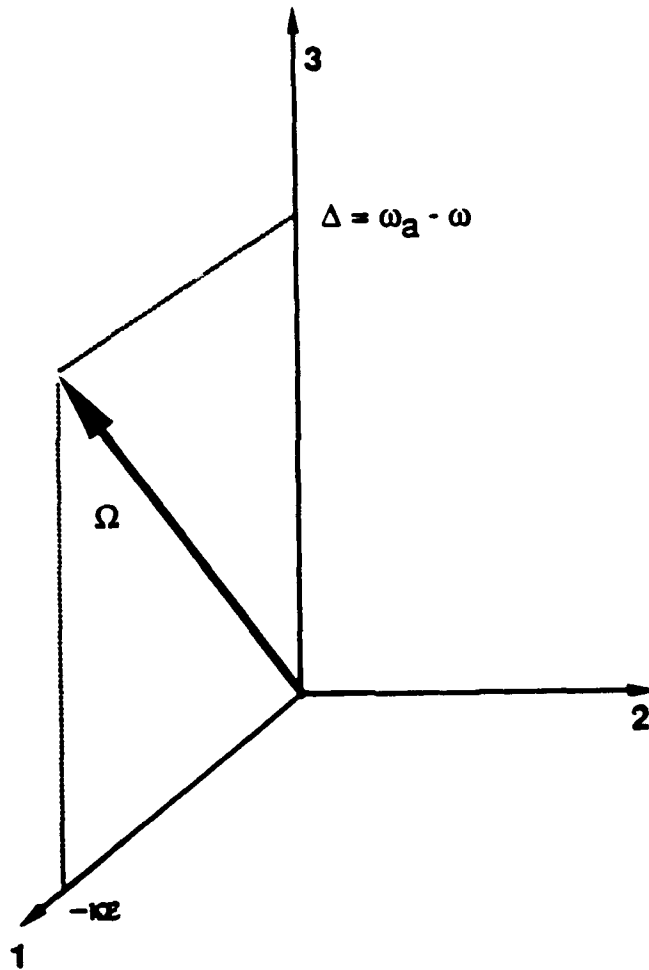
Figure 3.5

CHAPTER 4

OPTICAL EXCITATIONS IN RANDOM GLASS MEDIA:
LINEAR OPTICAL PROPERTIES

A major purpose of this study is to investigate optical instabilities in random glassy polymers resonantly driven by intense laser fields through the intensity dependent refractive index. The nonlinear optical excitations in random glass media and experimental study of the intensity dependent refractive index are presented in Chapter 5.

In this chapter, we first address the linear optical excitations of glassy polymer ultrathin film consisting of quasi-two dimensional disc-like structures randomly distributed in a glassy matrix. A major result is that the optical absorption consists of an inhomogeneous, site-broadened band of very many narrow homogeneous lines from the on-site optical excitations of the conjugated discs. A physical model for the linear optical excitations of the glassy films is presented based on theoretical description of random glass media by Anderson, Halperin, and Varma[41], which is an insightful approach focused on the microscopic mechanisms for broadening of optical excitations.

Optical linebroadening occurs when an optically active atom is disturbed by its interactions with other atoms, or excitations. In a gas, for example, the spectral line is broadened through the collisions with the other atoms in the gas, which is called 'pressure broadening'[1]-[3]. At a very low pressure, the emission spectrum of an atom has a narrow bandwidth corresponding to the excited state life time for an optical transition. As the gas pressure is increased, there occurs non-negligible collisions between the atoms which destroy the coherence of the dipole radiation. When we focus on the dipole moment of a single atom, all the other atoms in the gas can be viewed as a heat reservoir acting as a noise source giving stochastic and random collisions to the atom of interest. The collision distorts the electron wave

function for both the excited and the ground state of the atom of interest, and the distorted wave functions are not the eigen-states of the isolated atom. The dipole radiation from an excited state to the ground state of an atom with a distorted wave function is different from the dipole radiation coming from an isolated atom. When a frequency spectrum of the dipole radiation is examined, the line width appears broadened and the peak maximum shifted. Similar effects can occur in a condensed matter. Optically active ions embeded inside a crystalline lattice exhibit a different optical spectrum depending on the lattice temperature. Here the phonons in the lattice interact with the optical dipole moments of ion. The phonon bath acts as a noise source for the stochastic collisions. Without these stochastic collisions, the atom is isolated from the environment, and the spectral line width is determined by the natural radiative decay rate coming from spontaneous decay.

A physical picture of linear optical excitation of π- electrons in optical sites randomly distributed inside a polymer matrix is neccessary for the proper understanding of nonlinear optical processes in the same molecules. Quasi-two dimensional disc-like structures as the optical sites provide a number of important features and properties for sucessful studies of resonant nonlinear optical processes. Primary among these is the presence of optically intense low and high frequency bands in the visible and ultraviolet generally observed in large diverse classes. Among such classes are the well-known, large ring porphyrin and phthalocyanine structures which exhibit well-defined intense Q and Soret bands in the visible and near uv, respectively, and in addition, possess important secondary material properties such as thermal and chemical stability and ease of fabrication and processing. Free base porphyrin, for example, has long been identified as an analog of 18-annulene which possess nine double bonds, so that the microscopic description of the linear and nonlinear optical excitations for cyclic chains such as COT may be extended to these larger structures.

First, the linear optical properties of thin films of naphthalocyanine will be

described in Sec.4.1. Next, we present a formal description of a homogeneous line broadening mechanism from a view point of the linear response theory. After reviewing spontaneous decay for an isolated optical atom or molecule, a line shape function is defined in Sec.4.2. The problem of line shape change through interactions with other excitations is addressed by statistical mechanical methods. The bath, however, is not just a heat reservoir but a source of interactions which should be considered explicitly to determine the effects on the system. This is an irreversible statistical problem, where there are couple of different approaches. One approach will be a Brownian particle-like description where the stochastic forces are accounted for explicitly in the equation of motion. This approach is conceptually clear but lacks a systematic method for a higher order perturbation calculation. We adopt a projection operator method which is widely used in solving the irreversible statistical mechanical problems. Here the quantum mechanical equation of motion for the system is expanded in the interaction Hamiltonian, but the bath is assumed to be unaffected by the interactions and always in a thermal equilibrium. The projection operator technique will be presented in Sec.4.3. In Sec.4.4, the general formula for a homogeneous line width of an optical site embeded in a medium will be derived by use of projection operators. The general scheme for the derivation of homogeneous line shape will be a perturbative expansion of the transition matrix in the interaction Hamiltonian, which follows the standard procedure used to find the scattering amplitude in quantum mechanical perturbation theory.

In Sec.4.5, the formula obtained in Sec.4.4. is applied to find a homogeneous line width for an optical site in a crystalline medium where elastic phonon scattering is responsible for the line broadening. The amorphous material exhibits completely different physical behavior compared to a crystalline system. A physical model for an amorphous glassy material is presented in Sec.4.6, where a low excitation TLS (two-level-system) is introduced to explain the characteristic physical properties of an amorphous system. In Sec.4.7, the homogeneous line broadening of an optical

99

site in an amorphous medium is calculated by combining the results of Sec.4.4 and Sec.4.6. The results are discussed in connection with experimental measurements.

4.1 Linear Absorption Spectrum of SINC

A phthalocyanine (PC) molecule possesses an intense absorption peak in the visible wavelength, called a Q-band. The naphthalocyanine (NC) molecule is a derivative of the PC molecule, naphthalene attached on the sides of the central nitro-carbon conjugated ring rather than benzene. The absorption peak of NC is shifted toward IR, and the exact position of absorption peak depends on the solvents. In general, PC molecule has a very low solubility (order of 10^{-4} mole/liter), therefore, it is very difficult to prepare a thin sample with an appreciable optical density. By susbstituting a silicon atom into the middle of the two-dimensional π-electron ring of a PC molecule and attaching a polymer tail to the remaining electronic sites of silicon atom, the solubility of PC molecule can be enhanced. That is, the free volume of PC molecule can be controlled by changing the polymer tail. Our sample consists of silicon-substituted naphthalocyanine (SINC) as shown in Figure(4.1) and Figure(4.2). SINC is easily soluble in the solvent cyclohexanone (density 0.947kg/liter) and 10% weight concentration is readily available. By spin-coating the high concentrate SINC liquid solution on an optical flat, a good optical quality thin film can be readily obtained. Two kinds of thin films were made, that is, a pure dye film and a solid solution film diluted in polymethyl-methacrylate (PMMA) matrix.

In Figure(4.3) a linear absorption spectrum of a liquid solution of SINC in cyclohexanone is shown. The molar concentration was 0.5μmole/liter with optical path 1.0mm, and the Q-band peaks at 770 nm. Also seen are the phonon lines of the Q-band at 735 nm and 690 nm. We find that the zero phonon line at 770 nm is the strongest in absorption, which means that the Franck-Condon effect is much reduced in this large molecule. Figure(4.4) shows the linear absorption spectrum of

SINC pure dye film (a; solid curve) and SINC solid solution film (b; dashed curve). The optical spectrum exhibits an intense Q-band centered at near infrared (810nm (a) and 774nm (b)) with a linewidth of 0.1 eV. The films obtained by spin coating do not possess either positional or orientational long range order. Because of this random distribution of SINC molecules in the films, the excitations are strictly on-site π-electron transitions, which have a typical absorption coefficient α of 10^5 cm^{-1}. The on-site π-electron optical excitations in an isolated molecule have an intrinsic, temperature independent natural linewidth on the order of 0.1 to 1 GHz with corresponding radiative decay lifetime of 1 to 10 ns. [4]-[7]

The Q-band behaves as a Gaussian shape inhomogeneous line consisting of many narrow homogeneous lines. The large linewidth of the Q-band observed in Figure(4.4) is primarily due to inhomogeneous broadening. This site broadening in the thin film has a Gaussian shape which is a consequence of the statistical distribution of resonance frequencies of the optical centers due to a variation in local environment in the polymer matrix. Within the inhomogeneous broadened Gaussian envelope of the Q-band are a series of narrow homogeneous broadened resonances where the characteristic temperature dependence of the linewidth depends on the microscopic broadening mechanism. Each homogeneous line under the Gaussian envelope is approximated by a Lorentzian function, and the width is related to the temperature dependent population and phase relaxation rate of the excited state by Fourier transformation. The amorphous material surrounding an optical site can be considered as an ensemble of noninteracting TLS flip-flopping between two eigenstates as they emit or absorb acoustic phonons. The homogeneous line broadening in amorphous media comes from the dipole coupling of the optical sites with the TLS's, and the line width can be expressed in terms of the TLS lifetime (or flip-flopping rate), the temperature dependence of which is determined from the coupling between the TLS and the strain field manifested as acoustic phonons.

101

As discussed in Sec.4.7, temperature dependence of homogeneous linewidth in amorphous matrices is well explained in terms of TLS glass model. In this way, the line width of optical sites in the amorphous media is predicted to have $T^{1+\delta}$ ($0 < \delta \leq 1$) dependence, and the absolute magnitude can be obtained once all the physical parameters for the TLS are known. For various organic molecules in different polymeric matrices, the theoretically predicted temperature dependence of the homogeneous linewidth is in good agreement with spectral hole burning data. [8][9] According to photochemical hole burning data on porphyrins and phthalocyanines in various glasses and polymeric matrices, [10] the homogeneous linewidth of the naphthalocyanine oligomer at room temperature is estimated to be between 10 and 100 GHz. For SINC films, comparison of the homogeneous linewidth (100 GHz) with the inhomogeneous width (0.1 eV) shows that the Gaussian envelope contains on the order of ten thousand Lorentzian broadened resonances. [11][12]

Linear absorption spectrum at a various substrate temperature was measured to find out a possible thermo-chromic effect in the SINC thin film. Refer to Figures(4.5) (4.6). A SINC pure dye film was positioned inside a spectrophotometer (Hitachi Model 330) sample compartment, and a hot air is blown onto the thin film to increase the substrate temperature which was monitored by a thermocouple. Upto 75°C, the absorption spectrum does not change, but at 100°C, the peak gets higher, and the peak shifts toward a shorter wavelength. But still the linear absorption spectrum exhibits an intense Q-band. The changed spectrum did not recover back to the original spectrum, as the temperature is decreased, that is, the changed spectrum remained the same. This suggests that the polymer tail attached at the silicon atom affects the inhomogeneous broadening strongly, changing the peak absorption magnitude and position. π-electron optical excitation shown up as Q-band, however, is very stable up to the measured temperature. The thermochromatic effect is important in saturable absorption experiment on a thin film sample to identify any heating effect, which will be discussed in Chapter 5 later.

4.2 Lineshape Function

The spontaneous decay rate of an excitation is well understood in quantum electrodynamics. According to Fermi's golden rule, the transition rate from the initial state $|i\rangle$ to the final state $|f\rangle$ is given as

$$w_{i \to f} = \frac{2\pi}{\hbar} |\langle f|H_1|i\rangle|^2 \delta(E_f - E_i - \hbar\omega) \tag{4.2.1}$$

where H_1 is the dipole interaction Hamiltonian. The total transition probability per unit time is obtained by averaging over the initial states and summing over the final states

$$\Gamma(\omega) = \sum_{i,f} p_i w_{i \to f} \tag{4.2.2}$$

where p_i is the probability that the initial state $|i\rangle$ is occupied. Now we calculate the power of the emitted light of frequency between ω and $\omega + d\omega$. The emitted power is

$$dP(\omega) = \hbar\omega\Gamma(\omega)\frac{Vd^3k}{(2\pi)^3} \tag{4.2.3}$$

where $Vd^3k/(2\pi)^3$ accounts for the number of states allowed for the photons with energy $\hbar\omega$. Noting the phase space of photons and the following identity for Dirac-delta function,

$$\frac{Vd^3k}{(2\pi)^3} = \frac{Vk^2dkd\Omega}{(2\pi)^3} = \frac{V\omega^2d\omega d\Omega}{(2\pi)^3c^3} \tag{4.2.4}$$

$$\delta(x) = \frac{1}{2\pi}\int_{-\infty}^{\infty}e^{i\omega t}dt \tag{4.2.5}$$

and the normalizatoion of the electromagnetic field in second quantization (See Appendix A1),

$$\vec{E}(x,t) = -i\sum_{\lambda}\sqrt{\frac{2\pi\hbar\omega}{V}}(b_{\lambda}^{\dagger}\vec{e}_{\lambda}e^{i(\omega t-kz)} - b_{\lambda}\vec{e}_{\lambda}e^{-i(\omega t-kz)}) \tag{4.2.6}$$

the angular spectral cross section of the emitted power is

$$\frac{dP(\omega)}{d\Omega d\omega}$$

$$= \hbar\omega \sum_{i,f} p_i \frac{2\pi}{\hbar} |\langle f|H_1|i\rangle|^2 \delta(E_f - E_i - \hbar\omega) \frac{V\omega^2}{(2\pi)^3 c^3}$$

$$= \hbar\omega \sum_{i,f} p_i \frac{2\pi}{\hbar} \frac{2\pi\hbar\omega}{V} e^2 \langle i|x|f\rangle\langle f|x|i\rangle \frac{V\omega^2}{(2\pi)^3 c^3} \frac{1}{2\pi\hbar} \int_{-\infty}^{\infty} dt \exp\{i(\omega - \omega_i + \omega_f)t\}$$

$$= \hbar\omega \frac{e^2}{\hbar c} \frac{\omega^3}{2\pi c^2} \frac{1}{2\pi} \int_{-\infty}^{\infty} dt e^{i\omega t} \sum_{i,f} p_i \langle i|x|f\rangle\langle f|e^{i\omega_f t} x e^{-i\omega_i t}|i\rangle$$

$$= \hbar\omega \frac{e^2}{\hbar c} \frac{\omega^3}{2\pi c^2} \frac{1}{2\pi} \int_{-\infty}^{\infty} dt e^{i\omega t} C_{xx}(t) \qquad (4.2.7)$$

$C_{xx}(t)$ is auto-correlation function of dipole moments. The power spectrum is composed of the photon energy, the phase space factors, and a Fourier transform of the dipole auto-correlation function. [13]−[17] The lineshape function $F(\omega)$ is defined as

$$F(\omega) = \frac{1}{2\pi} \int_{-\infty}^{\infty} dt e^{i\omega t} C_{xx}(t) = Re \frac{1}{\pi} \int_0^{\infty} dt e^{i\omega t} C_{xx}(t) \qquad (4.2.8)$$

Noting that $|i\rangle$ and $|f\rangle$ are the eigen-states of the unperturbed Hamiltonian H_0, the auto-correlation function can be rewritten as follows:

$$C_{xx}(t) = \sum_{i,f} p_i \langle i|x|f\rangle\langle f|e^{iH_0 t/\hbar} x e^{-iH_0 t/\hbar}|i\rangle$$

$$= \sum_i p_i \langle i|x e^{iH_0 t/\hbar} x e^{-iH_0 t/\hbar}|i\rangle$$

$$= \sum_i p_i \langle i|x x(t)|i\rangle = Tr\{\rho_0 x x(t)\} \qquad (4.2.9)$$

where we used the Heisenberg equation motion for x, and a density matrix ρ_0 defined as

$$\rho_0 = \sum_{i,j} \rho_{ij} |i\rangle\langle j| = \sum_{i,j} p_i \delta_{ij} |i\rangle\langle j| \qquad (4.2.10)$$

has been introduced. The auto-correlation function is a quantum mechanical average value of the product of the dipole moment at time 0 and the dipole moment at

104

time t. We see that if the interaction Hamiltonian commutes with the unperturbed Hamiltonian H_0, the correlation function is independent of time, and the transition probability is zero. A time independent correlation function means that the dipole moment does not change in time and maintains coherence in time. But in the optical transition, the dipole interaction Hamiltonian does not commute with the unperturbed Hamiltonian H_0, and the dipole interaction causes a change of dipole moment in time; therefore the dipole moment is not coherent with the inital moment any longer. This incoherence shows up as a finite life time of the excited state. For a general discussion of linear response theory, see Appendix A5.

For later use, we write the correlation function in another form employing a Liouville operator L_0, or a Liouvillian.[18] The quantum mechanical equation of motion for the density matrix of a system with a Hamiltonian H_0 is given as

$$i\hbar \frac{d\rho_0(t)}{dt} = [H_0, \rho_0(t)] = L_0 \rho_0(t) \qquad (4.2.11)$$

and can be solved formally to give

$$\rho_0(t) = e^{-iH_0 t/\hbar} \rho_0(t=0) e^{+iH_0 t/\hbar} = e^{-iL_0 t/\hbar} \rho_0(t=0) \qquad (4.2.12)$$

The Liouvillian can be understood to be a superoperator acting on an operator in Hilbert space, or, in a reverse way, an operator in Hilbert space can be viewed as a vector in a Liouville space with the Liouvillian as an operator acting on the vectors. The quantum mechanical equation of motion for the density matrix in Liouville space can be interpreted as an equation describing a rotation of the density matrix 'vector' upon the application of the Liouvillian. The bases of the Liouville space can be formed from the bases of the Hilbert space,

$$|i\rangle\langle j| = |ij\rangle\rangle = \langle\langle ji| \qquad (4.2.13)$$

where we introduced the Ben-Reuven notation.[19]-[20] In Liouville space, the density matrix is a vector with components ρ_{ij}.

$$\rho = \sum_{ij} \rho_{ij} |i\rangle\langle j| = \sum_{ij} \rho_{ij} |ij\rangle\rangle = |\rho\rangle\rangle \qquad (4.2.14)$$

A quantum average of an operator in the Hilbert space is expressed as an inner product of the density matrix and the operator.

$$\langle Q \rangle_{av} = Tr\{\rho Q\} = \sum_{ij} \rho_{ij} Q_{ji} = \langle\langle \rho | Q \rangle\rangle \qquad (4.2.15)$$

With these notations, the correlation function is expressed as

$$C_{zz}(t) = Tr\{\rho_0 z z(t)\} = Tr\{\rho_0 z e^{iH_0 t/\hbar} z e^{-iH_0 t/\hbar}\}$$
$$= Tr\{z e^{-iH_0 t/\hbar}(\rho_0 z) e^{iH_0 t/\hbar}\}$$
$$= Tr\{z e^{-iL_0 t}(\rho_0 z)\} = \langle\langle z | e^{-iL_0 t}(\rho_0 z) \rangle\rangle \qquad (4.2.16)$$

Substitution of Eq.(4.2.16) into Eq.(4.2.8) yields the lineshape function $F(\omega)$ in terms of the Liouville operator.

$$F(\omega) = \frac{1}{\pi} Re \int_0^\infty dt e^{i\omega t} Tr\{z e^{-iL_0 t}(\rho_0 z)\}$$
$$= -\frac{1}{\pi} Im Tr\{z \frac{1}{\omega - L_0}(\rho_0 z)\} = -\frac{1}{\pi} Im \langle\langle z | \frac{1}{\omega - L_0}(\rho_0 z) \rangle\rangle \quad (4.2.17)$$

When the system is in thermal equilibrium with a heat reservoir, the density matrix is given by a canonical distribution.

$$\rho_0 = \frac{\exp\{-\beta H_0\}}{Tr \exp\{-\beta H_0\}} = \sum_i \frac{\exp\{-\beta E_i\}}{\sum_j \exp\{-\beta E_j\}} |i\rangle\langle i| \qquad (4.2.18)$$

4.3 Line Broadening in a Projection Operator Formalism

Now we consider a system composed of two subsystems interacting with each other. One subsystem is supposed to be much smaller than the other subsystem, and the small system is called 'system' and the large system 'bath'. The bath is in thermal equilibrium with a canonical distribution. The Hamiltonian of the entire system is

$$H = H_0^s + H_0^b + V \qquad (4.3.1)$$

106

Because of the presence of the interaction between the system and the bath, a direct product of the eigen-states of the system and the bath is not an eigen-state of the entire system. Furthermore, when the correlation function of an operator is considered in studying the response function of the system upon the application of an external field, we need the density matrix of the entire system, i.e., system plus bath, and the density matrix of the entire system is not just a direct product of the individual density matrices. Even if the exact solution form of the density matrix $\rho(t)$ for the entire system is required to describe the time evolution of the correlation function, most of the important physical properties of the sytem of interest can be obtained without complete information on the density matrix of the entire system including the bath. Usually the bath is assumed to belong to a thermal equilibrium canonical ensemble, and, hence, the density matrix of the bath is given by the canonical distribution. That is, the bath has a fixed density matrix obeying the canonical distribution, and, at the same time, is a source for an interaction with the system. This role of the bath is in accordance with the concept of a bath. The system is affected by an interaction with the bath, and the time dependence of the density matrix for the system is determined by the interaction Hamiltonian, but the effect of the interaction on the bath is ignored so that the bath is always in a thermal equilibrium.

In general, we are interested in the response function of the system rather than the entire system, which means that when we take a quantum average of a correlation function, the bath variables can be eliminated by taking a trace over the bath states. As a specific example, we consider an optical dipole moment interacting with lattice vibrations. See Figure(4.7). The entire system is composed of an optically radiating dipole moment and a phonon bath. The phonon bath is in thermal equilibrium belonging to a canonical ensemble, which means that the phonon bath follows the canonical distribution. When we are interested in the optical properties of the entire system, the optical response comes from the

optical dipole moment only, and there is no optical response from the phonon bath. However, through the interaction between the dipole moments and the phonon bath, the optical property of the system is affected by the physical properties of the phonons. These considerations allow us to define a projection operator such that the bath variable is averaged out and replaced by a value weighted with the thermal equilibrium density operator for the bath. For example, the relevant part of the density operator for the entire system is

$$\rho_1(t) = \rho^b Tr^b \rho(t) \tag{4.3.2}$$

The projected density operator is still an operator acting on the entire system, but the bath part of the density operator is explicitly given by the canonical distribution. Once the projected density operator is known, the quantum average value of an operator that pertains only to the system can be obtained by using a density matrix for the system which is defined to be

$$\rho^s(t) = Tr^b \rho_1(t) \tag{4.3.3}$$

For example, the macroscopic polarization from the entire system is given as

$$
\begin{aligned}
P(t) &= N_a Tr\{\rho(t)\mu^s\} = N_a Tr\{\rho_1(t)\mu^s\} \\
&= N_a Tr\{\rho^b Tr^b\{\rho(t)\}\mu^s\} = N_a Tr^s\{Tr^b\{\rho^b\}Tr^b\{\rho(t)\}\mu^s\} \\
&= N_a Tr^s\{Tr^b\{\rho_1(t)\}\mu^s\} = N_a Tr^s\{\rho^s(t)\mu^s\}
\end{aligned}
\tag{4.3.4}
$$

Similarly, the lineshape function $F(\omega)$ for the entire system depends on the correlation function of the dipole moments of the system. The auto-correlation function is given as a quantum average over the entire system. But the relevant operator depends on the dipole moments of the system only.

$$
\begin{aligned}
C_{zz}(t) &= Tr\{z^s e^{-iHt/\hbar}\rho z^s_. e^{iHt/\hbar}\} = Tr\{z^s e^{-iLt}\rho z^s\} \\
&= Tr\{z^s \bar{D}(t)\} = Tr\{z^s \bar{D}_1(t)\} = Tr\{z^s \rho^b Tr^b \bar{D}(t)\} \\
&= Tr^s\{z^s Tr^b\{\bar{D}_1(t)\}\} = Tr^s\{z^s \bar{D}_s(t)\}
\end{aligned}
\tag{4.3.5}
$$

108

where $\bar{D}(t)$ is an operator related to the correlation of the dipole mements, defined as

$$\bar{D}(t) = e^{-iLt}(\rho x^s) \qquad (4.3.6)$$

This can be understood as a formal solution for the time evolution of ρx^s. The projected operator for $\bar{D}(t)$ is denoted as $\bar{D}_1(t)$, and only this projected operator determines the time evolution of the correlation function of the optical dipole moments. $\bar{D}_1(t)$ is given as

$$\bar{D}_1(t) = \rho^b Tr^b \bar{D}(t) \qquad (4.3.7)$$

Now the lineshape function can be expressed in terms of the projected operator $\bar{D}_1(t)$.

$$F(\omega) = \frac{1}{\pi} Re \int_0^\infty dt e^{i\omega t} C_{zz}(t) = \frac{1}{\pi} Re \int_0^\infty dt e^{i\omega t} Tr^s \{x^s Tr^b \{\bar{D}_1(t)\}\}$$

$$= \frac{1}{\pi} Re Tr^s \{x^s Tr^b \{\int_0^\infty dt e^{i\omega t} \bar{D}_1(t)\}\} = \frac{1}{\pi} Re Tr^s \{x^s Tr^b \{D_1(\omega)\}\}$$

$$= \frac{1}{\pi} Re Tr^s \{x^s D_s(\omega)\} \qquad (4.3.8)$$

With the above examples, we find that the projector operator, which is important in the description of the interaction between the system and the bath, is the summation over the bath variable and the multiplication of the canonical distribution density matrix for the bath. The explicit form of the projection operator[21]−[23] is given as

$$P\{A\} = \rho^b Tr^b \{A\} \qquad (4.3.9)$$

with

$$\rho^b = \frac{e^{-\beta H^b}}{Tr^b e^{-\beta H^b}} \qquad (4.3.10)$$

In the Ben-Reuven's notation useful in a real calculation,

$$P = |\rho^b\rangle\rangle\langle\langle 1^b| = |\rho^b\rangle\rangle \sum_\alpha \langle\langle\alpha\alpha| \qquad (4.3.11)$$

109

It is easy to see that the projection operator defined above is indeed a projection operator, i.e., $P^2 = P$.

$$P^2\{A\} = \rho^b Tr^b\{P\{A\}\} = \rho^b Tr^b\{\frac{e^{-\beta H^b}}{Tr^b e^{-\beta H^b}} Tr^b A\}$$
$$= \rho^b Tr^b A = P\{A\} \qquad (4.3.12)$$

Furthermore we see that the projection operator defined above commutes with the unperturbed Liouvillian of the entire system.

$$PL_0 = |\rho^b\rangle\rangle\langle\langle 1^b|(L_0^s + L_0^b) = |\rho^b\rangle\rangle\langle\langle 1^b|L_0^s = L_0^s P \qquad (4.3.13)$$

and

$$L_0 P = (L_0^s + L_0^b)|\rho^b\rangle\rangle\langle\langle 1^b| = L_0^s|\rho^b\rangle\rangle\langle\langle 1^b| \qquad (4.3.14)$$

That is,

$$[P, L_0] = 0 \qquad (4.3.15)$$

Now that the projection operator is given in an explicit form, let's look at the physical properties of the projected part of an operator for the system. At $t = 0$, the system can be approximated to be independent of the bath. That is, we assume that the interaction between the system and the bath started at $t = 0$. This means that the density matrix at $t = 0$ can be approximated to be a direct product of the density matrices of the system and the bath.

$$\rho \approx \rho^s \rho^b \qquad (4.3.16)$$

Furthermore, the bath is in a thermal equilibrium with the heat reservoir, and the density matrix is given by a canonical distribution with the energy levels determined by the eigenvalues of the bath Hamiltonian.

$$L_\bullet^b \rho^b = 0 \qquad (4.3.17)$$

The fact that the initial state is in a thermal equilibrium means that the density operator is an eigen-state of the projection operator with the eigenvalue 1. That

110

is, the density operator at $t = 0$ is already assumed to be a direct product of each density operator.

$$P\rho(t = 0) \approx P\rho^s \rho^b = \rho^b Tr^b\{\rho^s \rho^b\} = \rho^s \rho^b \qquad (4.3.18)$$

or in another words

$$\rho_1(0) = \rho(0) \qquad (4.3.19)$$

It is easy to see that if the density operator satisfies the approximation in Eq.(4.3.16) the operator $\bar{D}(t)$ introduced in Eq.(4.3.6) is also an eigen state of the projection operator at $t = 0$.

$$P\bar{D}(0) = \rho^b Tr^b\{\rho x^s\} \approx \rho^b Tr^b\{\rho^s \rho^b x^s\} = \rho^b \rho^s x^s = \bar{D}(0) \qquad (4.3.20)$$

or

$$\bar{D}_1(0) = \bar{D}(0) \qquad (4.3.21)$$

Now we present a powerful perturbation method, originally developed by Zwanzig to describe an irreversible thermodynamic process. It is called a projection operator technique[24]−[25] for the reasons that will be explained later. We give a general formalism first, and then by identifying the corresponding quantities in the dipole radiation process for an optical site embedded in a medium, an explicit form for the lineshape function is obtained. Say that the total Hamiltonian of the entire system is composed of the unperturbed H_0 and the perturbation H'. The unperturbed Hamiltonian is again composed of the Hamiltonian for the system and the Hamiltonian for the bath. Let $\bar{f}(t)$ be an operator in Hilbert space, or a vector in a Liouville space. The Liouvillian is

$$L = L_0 + L' = L_0^s + L_0^b + L' \qquad (4.3.22)$$

The equation of motion for $\bar{f}(t)$ is simply given as

$$i\hbar \frac{\partial \bar{f}(t)}{\partial t} = L\bar{f}(t) \qquad (4.3.23)$$

111

Suppose that there exists a projection operator P such that

$$\bar{f}_1(t) = P\bar{f}(t), \quad \bar{f}_2(t) = (1 - P)\bar{f}(t) = Q\bar{f}(t) \qquad (4.3.24)$$

with the initial conditions

$$\bar{f}_1(0) = \bar{f}(0), \quad \bar{f}_2(0) = 0 \qquad (4.3.25)$$

Breaking up the operator $\bar{f}$ in two parts with the given initial condition can be understood in this way. When a projection operator is used, we have a 'relevant' part and an 'irrelevant' part in mind. The relevant part pertains to the system of interest, while the irrelvant part refers to the remaining part. To calculate a specified quantity of a system of interest we need information on the relevant part only. At $t = 0$ the vector $\bar{f}$ contained all the informations on the system, and as time goes by the information leaks and gets lost into the irrelevant part. Our goal is to get the time evolution of the relevant part of the operator $\bar{f}(t)$ in terms of the interaction Hamiltonian by projecting out the relevant part, or by projecting away the irrelevant part. Usually the relevant part will be the system and the irrelevant part will be the bath. If we think of the density matrix as $\bar{f}$, the projected part can be thought of as the density matrix for the system with the bath in a thermal equilibrium, and the unprojected part as the density matrix for the bath. But because of the interaction between the system and the bath, the density matrix cannot be separated as a direct product of each matrix. The time evolution of the density matrix for the system can be obtained only by projecting the relevant part of the time dependent total density matrix. Since the time dependence of the total density matix cannot be obtained without resorting to a perturbation method, the basic idea behind the projection technique is that the eqution of motion of the density matrix is written for the relevant and the irrelevant part separately, and solve for the relevant part by eliminating the irrelevant part but keeping the projection operator.

$$i\hbar \frac{\partial \bar{f}_1(t)}{\partial t} = PL\bar{f}_1(t) + PL\bar{f}_2(t) \qquad (4.3.26)$$

112

$$i\hbar \frac{\partial \bar{f}_2(t)}{\partial t} = QL\bar{f}_1(t) + QL\bar{f}_2(t) \tag{4.3.27}$$

Eq.(4.3.26) can be solved in a strightforward way, yielding

$$\bar{f}_2(t) = \exp(-iQLt/\hbar)\bar{f}_2(0) + \int_0^t dt' \exp(-iQL(t-t')/\hbar)(\frac{-iQL}{\hbar})\bar{f}_1(t')$$

$$= \int_0^t ds \exp(-iQLs/\hbar)(\frac{-iQL}{\hbar})\bar{f}_1(t-s) \tag{4.3.28}$$

where the initial condition $\bar{f}_2(0) = 0$ is used. Substituting Eq.(4.3.28) back into Eq.(4.3.26) gives the equation of motion for $\bar{f}_1$.

$$i\hbar \frac{\partial \bar{f}_1(t)}{\partial t} = PL\bar{f}_1(t) + PL \int_0^t ds \exp(-iQLs/\hbar)(\frac{-iQL}{\hbar})\bar{f}_1(t-s)$$

$$= PL\bar{f}_1(t) + \int_0^t ds \bar{K}(s)\bar{f}_1(t-s) \tag{4.3.29}$$

where $\bar{K}(s)$ is defined as

$$\bar{K}(s) = -\frac{i}{\hbar} PL \exp(-iQLs/\hbar)QL$$

$$= -\frac{i}{\hbar} PL' \exp(-iQLs/\hbar)QL' \tag{4.3.30}$$

where the assumption that the projection operator commutes with the unperturbed Liouvillian is used. In the freqency domain the relevant part of the operator f is given by a Fourier transformation.

$$\omega f_1(\omega) - i\bar{f}_1(0) = PLf_1(\omega) + K(\omega)f_1(\omega) \tag{4.3.31}$$

with

$$K(\omega) = PL' \frac{1}{\omega - QL} QL' \tag{4.3.32}$$

Now we can put the interaction Hamiltonian part into a function $M_c(\omega)$ called a memory function.

$$\omega f_1(\omega) - i\bar{f}_1(0) = P(L_0 + M_c(\omega))f_1(\omega) \tag{4.3.33}$$

113

with

$$M_c(\omega) = L' + L' \frac{1}{\omega - QL} L' \tag{4.3.34}$$

In order to understand the idea behind the memory function $M_c(\omega)$, we study Eq.(4.3.33) in a time domain. Making use of the relations in Eq.(4.3.13) and the definition of a projection operator, $P^2 = P$, the relation for the projected part of the operator $f(\omega)$ in Eq.(4.3.33) can be rewritten as

$$\omega f_1(\omega) - i\bar{f}_1(0) = (L_0^s + PM_c(\omega)P)f_1(\omega) \tag{4.3.35}$$

Noting that

$$PM_c(\omega)P = |\rho^b\rangle\rangle\langle\langle 1^b|M_c(\omega)|\rho^b\rangle\rangle\langle\langle 1^b| = |\rho^b\rangle\rangle Tr^b\{M_c(\omega)\rho^b\}\langle\langle 1^b|$$
$$= |\rho^b\rangle\rangle\langle M_c(\omega)\rangle\langle\langle 1^b| \tag{4.3.36}$$

and taking a sum over the bath states, an equation for the system part of the operator f can be obtained. Simply taking an inner product of Eq.(4.3.35) with $\langle\langle 1^b|$ yields

$$\omega f^s(\omega) - i\bar{f}^s(0) = (L_0^s + \langle M_c(\omega)\rangle)f_s(\omega) \tag{4.3.37}$$

where $\langle M_c(\omega)\rangle$ is a quantum average of memory function $M_c(\omega)$ over the bath state, that is,

$$\langle M_c(\omega)\rangle = Tr^b\{M_c(\omega)\rho^b\} = \langle\langle 1^b|M_c(\omega)|\rho^b\rangle\rangle \tag{4.3.38}$$

Solving Eq.(4.3.37) for $f^s(\omega)$ gives

$$f^s(\omega) = i\frac{1}{\omega - L_0^s - \langle M_c(\omega)\rangle}\bar{f}^s(0) \tag{4.3.39}$$

Transforming Eq.(4.3.37) back to the time domain yields the following equation of motion for the operator $f^s(t)$.

$$i\hbar\frac{\partial \bar{f}^s(t)}{\partial t} = L_0\bar{f}^s(t) + \int_0^t ds\langle \bar{M}_c(s)\rangle\bar{f}^s(t-s) \tag{4.3.40}$$

114

This is a quantum mechanical equation of motion for the operator $f^s(t)$ pertaining to the system. While the first term in the r.h.s. describes the unperturbed motion, the second term describes the effect of stochastic noises from the bath to the system, where the integration over time represents the memory effect of the bath, that is, the time evolution of an operator in the system at time t depends not only on the Hamiltonian of the system but also on the value of the operator at a previous time through an interaction with the bath. The effect of the bath at a previous time is still at work on the system. Actually the memory function itself is a time-correlation function of stochastic forces acting on the system. Short memory means that the temporal overlap of two random noises are small. In a Markovian process the stochastic forces are delta-function correlated, or

$$\langle \bar{M}_c(t - t') \rangle = -i2\pi\Lambda\delta(t - t') \qquad (4.3.41)$$

and in a frequency domain the memory function is independent of frequency,

$$\langle M_c(\omega) \rangle = -i\Lambda \qquad (4.3.42)$$

where Λ is a complex quantity. The freqency dependence of the operator $f^s(\omega)$ is simply obtained from Eq.(4.3.39).

$$f^s(\omega) = i\frac{1}{\omega - L_0^s + i\Lambda}\bar{f}^s(0) \qquad (4.3.43)$$

In a real physical problem the memory function is approximated by truncating up to the first nonvanishing order in the interaction Hamiltonian, and the dependence of the response function of the system on the bath can be seen explicitly. The memory function defined in Eq.(4.3.34) satisfies a Lippman-Schwinger type relation in a Liouville space.

$$M_c(\omega) = L' + L'\frac{1}{\omega - L_0}(1 - P)M_c(\omega) \qquad (4.3.44)$$

115

Eq.(4.3.33) with an iterative relation Eq.(4.3.44) for a memory function $M_c(\omega)$ gives the Fourier transformed relevant part of an operator in general. The Lippman-Schwinger relation allows us a perturbation expansion in the interaction Hamiltonian. In an application of the above results to a particular irreversible thermodynamic process in a real system, all we need to do is to find a proper projection operator such that the assumptions made to derive Eq.(4.3.33) are satisfied. The assumptions are the initial condition for the operator $\bar{f}$ and the commutatibility of the projection operator with the unperturbed Liouvillian.

Now going back to the lineshape function we find that the we can make an identification of $D^s(\omega)$ and $\bar{D}^s(t=0) = \rho^s x^s$ as $f^s(\omega)$ and $\bar{f}^s(t=0)$ respectively. The part of the operator $D(\omega)$ relevant to the system is obtained from Eq.(4.3.39) as

$$D^s(\omega) = i \frac{1}{\omega - L_0^s - \langle M_c(\omega)\rangle} \rho^s \rho^b x^s \qquad (4.3.45)$$

Substituting the above expression into Eq.(4.3.8) yields the line shape function $F(\omega)$ in the final form as

$$F(\omega) = -\frac{1}{\pi} Im Tr^s \{ x^s \frac{1}{\omega - L_0^s - \langle M_c(\omega)\rangle} \rho^s x^s \}$$

$$= -\frac{1}{\pi} Im \langle\langle x^s | \frac{1}{\omega - L_0^s - \langle M_c(\omega)\rangle} (\rho^s x^s) \rangle\rangle \qquad (4.3.46)$$

4.4 Perturbation Expansion in the Memory function

A comparison of Eq.(4.3.46) with the lineshape function Eq.(4.2.17) defined for an unperturbed system shows that the effect of stochastic interactions with the bath are taken into account implicitly in the memory function $\langle M_c(\omega)\rangle$. At $t = 0$ the system and the bath are viewed to be independent of each other, (Eq.(4.3.16)), and at a later time the time evolution of the dipole-dipole correlation function is described by the Heisenberg equation of motion with the full Hamiltonian including the interaction (Eq.(4.3.5)). The final form of the lineshape function (Eq.(4.3.46))

116

can be interpreted as a Fourier transform of the Heisenberg equation of motion (Eq.(4.3.5)) where the effect of the bath is put into a memory function. Now we examine how the presence of the memory function $\langle M_c(\omega) \rangle$ changes the lineshape function of the system. The trivial case is when $\langle M_c(\omega) \rangle$ vanishes. Without any interaction with the other excitations the lineshape function reduces to Eq.(4.2.17), which means that the optical linewidth is determined only by a natural radiative decay time explained in Sec.4.2.

For a nontrivial case of nonvanishing $\langle M_c(\omega) \rangle$, we need to calculate the inner product of Eq.(4.3.46) in a Liouville space.

$$
\begin{aligned}
F(\omega) &= -\frac{1}{\pi} Im \langle\langle x^s | \frac{1}{\omega - L_0^s - \langle M_c(\omega) \rangle} (\rho^s x^s) \rangle\rangle \\
&= -\frac{1}{\pi} Im \sum_{i'f',if} \langle\langle x^s | i'f' \rangle\rangle \langle\langle i'f' | \frac{1}{\omega - L_0^s - \langle M_c(\omega) \rangle} | if \rangle\rangle \langle\langle if | (\rho^s x^s) \rangle\rangle \quad (4.4.1)
\end{aligned}
$$

Since the bath states are already summed, we find that L_0^s is diagonal operator in the Liouville space of the system. In general $\langle M_c(\omega) \rangle$ is nondiagonal, and there is a probability for a crossing between the different bases of the Liouville space of the system. If the off-diagonal components of $\langle M_c(\omega) \rangle$ is much smaller than the transition energy differences, the memory function can be assumed to be diagonal. Physically this corresponds to the case where the optical transition energy levels of the system are well separated. Under this approximation, the lineshape function reduces simply to

$$
\begin{aligned}
F(\omega) &= -\frac{1}{\pi} Im \sum_{if} \langle\langle x^s | if \rangle\rangle \langle\langle if | (\rho^s x^s) \rangle\rangle \langle\langle if | \frac{1}{\omega - L_0^s - \langle M_c(\omega) \rangle} | if \rangle\rangle \\
&= -\frac{1}{\pi} Im \sum_{if} |x_{fi}^s|^2 \rho_i^s \frac{1}{\omega - \omega_{if} - \langle M_c(\omega) \rangle_{if,if}} \\
&= -\frac{1}{\pi} Im \sum_{if} |x_{fi}^s|^2 \rho_i^s \frac{1}{\omega - \omega_{if} - \delta(\omega) + i\gamma(\omega)} \\
&= \frac{1}{\pi} \sum_{if} |x_{fi}^s|^2 \rho_i^s \frac{\gamma(\omega)}{\{\omega - \omega_{if} - \delta(\omega)\}^2 + \gamma(\omega)^2} \quad (4.4.2)
\end{aligned}
$$

117

where the real and imaginary part of the memory function is separated.

$$\delta(\omega) = Re\langle M_c(\omega)\rangle_{if,if} \qquad (4.4.3)$$

$$\gamma(\omega) = -Im\langle M_c(\omega)\rangle_{if,if} \qquad (4.4.4)$$

We find an important result that the real and the imaginary part of the memory function $\langle M_c(\omega)\rangle_{if}$ correspond to the peak shift and the linewidth of the lineshape function respectively. In a Markovian process $\langle M_c(\omega)\rangle$ is independent of ω (Eq.(4.3.42)) and the lineshape function is a Lorentzian function. The Fourier transform of the lineshape function $F(\omega)$ is straightforward resulting in an exponential decay behavior, as it should.

$$F(t) \propto e^{-\gamma t} e^{-i(\omega_{if} - \delta)t} \qquad (4.4.5)$$

When a short memory approximation is made, which corresponds to a short correlation time between stochastic noises, $\langle M_c(\omega)\rangle$ is a slowly varying function near $\omega = \omega_{if}$, and in a first order approximation the incident light freqeuncy dependence of the memory function can be replaced with the atomic resonance frequency dependence.

$$\langle M_c(\omega)\rangle \approx \langle M_c(\omega_{if})\rangle \qquad (4.4.6)$$

Therefore we have a Lorentzian line shape under two assumptions. First the off-diagonal elements of the memory function is assumed to be much smaller than the transition energy differences. Second the bath is assumed to have a short memory, or the duration of each collision to the system is much shorter than the collision time between two separate collisions. These two assumptions hold in most of the interesting cases, allowing us to approxiamte a homogeneous line shape a Lorentzian. We find that the peak shift and the linewidth depend on the resonance frequency ω_{if}, but for a Markovian process where the stochastic forces are delta-function correlated the memeory function does not have frequency dependence leading to a

frequency independent peak shift and the linewidth. The lineshape function which is a macroscopic response function of a system upon an optical excitation reveals a microscopic process of the system-bath interaction, and as will be seen later, this lineshape function can be used as a probe for the charateristic physcal properties of the bath itself because the memory function contains the interaction Hamiltonian between the system and the bath and for the different baths the interactions are different imparting a characteristic optical response to the system.

Now the problem of lineshape is reduced to finding the matrix element of the memory function.

$$\delta = Re\langle\langle if|\langle M_c(\omega)\rangle_{if,if}|if\rangle\rangle \tag{4.4.7}$$

$$\gamma = -Im\langle\langle if|\langle M_c(\omega)\rangle_{if,if}|if\rangle\rangle \tag{4.4.8}$$

with

$$\langle M_c(\omega)\rangle = \langle L'\rangle + \langle L'\frac{1}{\omega - L_0}(1 - P)M_c(\omega)\rangle \tag{4.4.9}$$

The memory function can be expanded in the interaction Hamiltonian up to the first nonvanishing order, and the linewidth γ can be obtained up to the same order by calculating the matrix elements for the states involved in the optical transition. However, the calculation of the matrix elements of a memory function in a Liouville space is quite cumbersome, and it would be convenient if we could express all the relations in a Hibert space which is more familiar to us. The problem comes down to finding a relation in Hibert space equivalent to Eq.(4.4.9). Because of the projection operator $(1 - P)$, it is quite formidable to recast Eq.(4.4.9) into a Hilbert space relation. When a memory function $M(\omega)$ satisfying a Lippman-Schwinger relation is introduced (See Appendix A6), it can be shown that there exists a corresponding operator $T(\omega)$ in a Hibert space.

$$\langle M(\omega)\rangle = \langle L'\rangle + \langle L'\frac{1}{\omega - L_0}M(\omega)\rangle \tag{4.4.10}$$

119

The corresponding opertor called a transition operator satisfies the usual Lippman-Schwinger relation.

$$T(\omega) = V + V \frac{1}{\omega - H_0} T \qquad (4.4.11)$$

$M_c(\omega)$ is related to $M(\omega)$ in the following way.

$$M_c(\omega) = (1 + M(\omega)P \frac{1}{\omega - L_0^s})M(\omega) \qquad (4.4.12)$$

We find that M_c is equal to M in the lowest order approximation. Once we take the approximation of the equality of M_c to M, the lineshape is determined by δ and γ given as

$$\delta = Re\langle\langle if|\langle M(\omega)\rangle_{if,if}|if\rangle\rangle \qquad (4.4.13)$$

$$\gamma = -Im\langle\langle if|\langle M(\omega)\rangle_{if,if}|if\rangle\rangle \qquad (4.4.14)$$

After a lengthy manipulation we can express the matrix elements of $M(\omega_{if})$ in terms of the transition operator T.

$$\langle\langle if|\langle M(\omega_{if})\rangle_{if,if}|if\rangle\rangle$$
$$= \sum_\alpha \rho_\alpha^b \{\langle i\alpha|T(\omega_i + \omega_\alpha)|i\alpha\rangle - \langle f\alpha|T(\omega_f + \omega_\alpha)|f\alpha\rangle^*\}$$
$$+ 2\pi i \sum_{\alpha\alpha'} \rho_\alpha^b \langle i\alpha'|T(\omega_i + \omega_\alpha)|i\alpha\rangle\langle f\alpha'|T(\omega_f + \omega_\alpha)|f\alpha\rangle^* \delta(E_\alpha - E_\alpha') \quad (4.4.15)$$

Once we have an expression in Hilbert space it is easy to see the microscopic processes responsible for the line broadening. In order to make the microscopic processes more transparent we change Eq.(4.4.15) making use of an important property of the transition operator. In a scattering theory an S matrix is defined to describe the change in the wavefunction of the particle due to a potential well. This scattering matrix S should be unitary in order for the probability of the particle to be conservered. The transition operator, T, is defined to be the part of the scattering matrix deviating from the identity.

$$S = 1 - 2\pi i\delta(E - H_0)T \qquad (4.4.16)$$

120

The unitarity of the scattering matrix S provides an important relation for the transition operator T.

$$
\begin{aligned}
S^\dagger S &= (1 + 2\pi i \delta(E - H_0)T^\dagger)(1 - 2\pi i \delta(E - H_0)T) \\
&= 1 - 2\pi i \delta(E - H_0)(T - T^\dagger) - \{2\pi i \delta(E - H_0)\}^2 T^\dagger T \\
&= 1 \qquad\qquad\qquad\qquad\qquad\qquad\qquad\qquad\qquad (4.4.17)
\end{aligned}
$$

or,

$$
T - T^\dagger = -\{2\pi i \delta(E - H_0)\}T^\dagger T \qquad\qquad (4.4.18)
$$

The above relation is called the optical theorem in scattering theory. In terms of matrix elements the optical theorem can be rewritten as

$$
\langle i\alpha | T - T^\dagger | i\alpha \rangle = -2\pi i \sum_{i'\alpha'} |\langle i'\alpha'|T|i\alpha \rangle|^2 \delta(E_{i'\alpha'} - E_{i\alpha}) \qquad (4.4.19)
$$

With the above identity the linewidth γ is given in a final form as

$$
\begin{aligned}
\gamma &= \frac{1}{T_2} \\
&= -Im(\langle if|\langle M(\omega_{if})\rangle_{if,if}|if\rangle) \\
&= \frac{1}{2}\left(\frac{1}{T_{1i}} + \frac{1}{T_{1f}}\right) + \frac{1}{T_2^{deph}} \qquad\qquad (4.4.20)
\end{aligned}
$$

where we introduced the decay times T_{1i}, T_{1f}, and T_2^{deph}.

$$
\frac{1}{T_{1i}} = 2\pi \sum_\alpha \sum_{\alpha' i' \neq i} \rho_\alpha^b |\langle i'\alpha'|T(\omega_\alpha + \omega_i)|i\alpha \rangle|^2 \delta(E_{i'} + E_{\alpha'} - E_i - E_\alpha) \qquad (4.4.21)
$$

$$
\frac{1}{T_{1f}} = 2\pi \sum_\alpha \sum_{\alpha' f' \neq f} \rho_\alpha^b |\langle f'\alpha'|T(\omega_\alpha + \omega_f)|f\alpha \rangle|^2 \delta(E_{f'} + E_{\alpha'} - E_f - E_\alpha) \qquad (4.4.22)
$$

$$
\frac{1}{T_2^{deph}} = \pi \sum_{\alpha\alpha'} \rho_\alpha^b |\langle i\alpha'|T(\omega_i + \omega_\alpha)|i\alpha \rangle - \langle f\alpha'|T(\omega_f + \omega_\alpha)|f\alpha \rangle|^2 \delta(E_{\alpha'} - E_\alpha) \qquad (4.4.23)
$$

There are two different contributions to the coherence decay for the atomic dipole moment. T_{1i} and T_{1f} represent the loss of coherence when the atom makes an

inelastic transition out of the energy levels i and f through interactions with the bath. The population decay of the atoms in an energy eigenstate causes the loss of coherence just from the decrease of the number of the dipole moments contributing to the dipole radiation. T_2^{deph} comes from processes in which the atomic dipole moment returns to its original energy state i and f with its dephasing interrupted during interaction with the bath, and this is energetically elastic process for the system. The homogeneous line width (FWHM) from a pure dephasing process in a Lorentzian line shape is denoted as $\Delta\omega$, given as

$$\Delta\omega = 2 \times \frac{1}{T_2^{deph}} \qquad (4.4.24)$$

or,

$$\Delta\omega = \frac{2\pi}{\hbar} \sum_{p',p} \rho_p^b |\langle fp'|T(\omega_f + \omega_p)|fp\rangle - \langle ip'|T(\omega_i + \omega_p)|ip\rangle|^2 \delta(E_{p'} - E_p) \quad (4.4.25)$$

where $|f\rangle$ and $|i\rangle$ are the excited and ground states of the molecule, $|p\rangle$ and $|p'\rangle$ are the thermal bath states, ρ_p^b is the occupation probability of bath state $|p\rangle$, and T satisfies the Lippman-Schwinger equation[26]

$$T(\omega) = V + V \frac{1}{\omega - H_0} T \qquad (4.4.26)$$

This relation shows that the dephasing rate is related to the anisotropy of the transition matrix; that is, the difference between matrix elements of T in the ground state and the excited states. Once the interaction Hamiltonian V is known, $\Delta\omega$ can be obtained to the same order by perturbative expansion of the Lippman-Schwinger equation in V.

4.5 Line broadening in a crystal field

Now we apply the result for the temperature dependent optical dephasing rate to a specific physical system. The first example will be the optical site embeded in a crystalline surrounding. The periodic lattice structure of the crystal

122

can be represented as a phonon system and the interaction of the optical site with the phonons broadens the optical absorption or emission line width. At a very low temperature the line width is limited by the natural decay time, but for the increased temperature the collision of the phonons with the optical site gives a temperature dependent broadening. The Hamiltonian of an optically active molecule in a crystalline field can be written as,

$$H = H_0 + H_{12} \tag{4.5.1}$$

$$H_0 = \varepsilon_0 \Psi_0^\dagger \Psi_0 + \varepsilon_1 \Psi_1^\dagger \Psi_1 + \sum_q \hbar \omega_q (n_q + \frac{1}{2}) \tag{4.5.2}$$

$$H_{12} = \Psi_0^\dagger \Psi_0 (V_0^{(1)} \varepsilon + V_0^{(2)} \varepsilon^2) + \Psi_1^\dagger \Psi_1 (V_1^{(1)} \varepsilon + V_1^{(2)} \varepsilon^2) \tag{4.5.3}$$

where H_0 is the noninteracting Hamltonian of the molecule and the phonons; H_{12} is the interaction Hamiltonian coming from the coupling between the molecule and the strain field of the lattice, and is expanded in terms of the strain field, ε. When the Lippman-Schwinger equation (Eq.(4.4.26)) is expanded, it can be written as

$$T(\omega) = V + V \frac{1}{\omega - H_0} V + V \frac{1}{\omega - H_0} V \frac{1}{\omega - H_0} V + \cdots \tag{4.5.4}$$

Identifying the interaction Hamiltonian H_{12} with V, matrix element in Eq.(4.4.25) is

$$\langle ip' | T(\omega_i + \omega_p) | ip \rangle = \langle \Psi_0 n_q | T(\omega_0 + \omega_{n_q}) | \Psi_0 n_q \rangle \tag{4.5.5}$$

In the first order of the Lippman-Schwinger equation we have two terms contributing to the matrix element, one linear in the starin field and the other quadratic in the strain field. The interaction Hamiltonian for the ground state, for example, gives

$$\langle \Psi_0 n_q | \Psi_0^\dagger \Psi_0 (V_0^{(1)} \varepsilon + V_0^{(2)} \varepsilon^2) | \Psi_0 n_q \rangle$$
$$= \langle \Psi_0 | V_0^{(1)} | \Psi_0 \rangle \langle n_q | \varepsilon | n_q \rangle + \langle \Psi_0 | V_0^{(2)} | \Psi_0 \rangle \langle n_q | \varepsilon^2 | n_q \rangle \tag{4.5.6}$$

Using the second quantization, the strain field can be written in terms of the phonon creation and annihilation operators.

$$\varepsilon = i \sum_{q_j} \sqrt{\frac{\hbar q_j^2}{2 M \omega_{q_j}}} (a_{q_j} - a_{q_j}^\dagger) \tag{4.5.7}$$

123

$$\varepsilon^2 = i^2 \sum_{q_j, q'_j} \sqrt{\frac{\hbar q_j^2}{2M\omega_{q_j}}} \sqrt{\frac{\hbar q'^2_j}{2M\omega_{q'_j}}} (a_{q_j} - a_{q_j}^\dagger)(a_{q'_j} - a_{q'_j}^\dagger) \tag{4.5.8}$$

We find that the linear process representing a single phonon creation or annihilation does not conserve energy unless the optical states of the molecule change. That is, the term linear in the strain field vanishes for a pure dephasing process where only elastic scattering is involved. On the other hand, the interaction quadratic in the strain field gives a Raman-like contribution in the line-broadening inside a lattice. In another words, for a pure dephasing process we need to consider only a two-phonon process in the first order of the Lippman-Schwinger equation.

$$\langle \Psi_0 n_q | V_0^{(2)} \epsilon^2 | \Psi_0 n_q \rangle \tag{4.5.9}$$

Another two-phonon process can take place when the Lippman-Schwinger equation is expanded up to the second order in which case the linear strain field can appear twice and gives a contribution which is second order in ε.

$$\langle \Psi_0 n_q | V_0^{(1)} \epsilon \frac{1}{\omega - H_0} V_0^{(1)} \epsilon | \Psi_0 n_q \rangle \tag{4.5.10}$$

A linear sum of two two-phonon processes (Eq.(4.5.9) and Eq.(4.5.10)) reminds us of the photon scattering process in quantum electrodynamics, where the light scattering off atom is expressed in Kramers-Heisenberg formula.[27] In the light scattering, different regimes are classified to distinguish the characteristic scattering behavior. When the scattering is elastic and the photon energy is much smaller than the optical transition energy of the atom, it is called Rayleigh scattering. Since the phonon energy is much smaller than the optical transition energy of the molecule ($\hbar\omega << \epsilon_1 - \epsilon_0$), two-phonon scattering is in a similar regime, hence, called a Rayleigh-like process. When two matrix elements (Eq.(4.5.9) and Eq.(4.5.10)) are compared, the term coming from the second order expansion of the Lippman-Schwinger equation involves a square of coupling constant $V_0^{(1)}$, and is negligible

124

compared to the term involving $V_0^{(2)}$. That is, the first nonvanishing main contribution to the line broadening in the optical spectrum of a molecule embedded in a crystalline field can be accounted for by calculating Eq.(4.5.9) only. Substituting the strain field Eq.(4.5.8) into Eq.(4.5.9) yields the following nonvanishing terms,

$$\sum_{q'q} \langle p'|a_q^\dagger a_{q'} + a_q a_{q'}^\dagger|p\rangle$$

$$= \sum_{q'q} \Big(\sqrt{n_q+1}\sqrt{n_{q'}} \langle n_{p_1'}, n_{p_2'}, \cdots | n_{p_1}, n_{p_2}, \cdots, n_q+1, \cdots, n_{q'}-1, \cdots\rangle$$

$$+ \sqrt{n_q}\sqrt{n_{q'}+1} \langle n_{p_1'}, n_{p_2'}, \cdots | n_{p_1}, n_{p_2}, \cdots, n_q-1, \cdots, n_{q'}+1, \cdots\rangle \Big)$$

$$= 2\sum_{q'q} \sqrt{n_q+1}\sqrt{n_{q'}}\,\delta_{p'q}\,\delta_{pq'} \tag{4.5.11}$$

The above process can be represented in a space-time diagram shown in Figure(4.8). For acoustic phonons the Debye model can be adopted for the dispersion relation of phonons. Then the density of phonon states is simply given by the phase space factors. More explictly, the line width is

$$\Delta\omega$$

$$= \frac{4\pi}{\hbar} \sum_{p,p_j'} \frac{\hbar p_j^2}{2M\omega_{p_j}} \frac{\hbar p_j'^2}{2M\omega_{p_j}} \langle n_{p_j}\rangle\langle n_{p_j'}+1\rangle |\langle\Psi_1|V_1^{(2)}|\Psi_1\rangle - \langle\Psi_0|V_0^{(2)}|\Psi_0\rangle|^2 \delta(E_{p_j} - E_{p_j'})$$

$$= \frac{4\pi}{\hbar} \Big(\frac{\hbar}{2M}\Big)^2 |\langle\Psi_1|V_1^{(2)}|\Psi_1\rangle - \langle\Psi_0|V_0^{(2)}|\Psi_0\rangle|^2$$

$$\times \int d^3q \Big(\frac{q^2}{\omega_q}\Big)\langle n_q\rangle \int d^3q' \Big(\frac{q'^2}{\omega_{q'}}\Big)\langle n_{q'}+1\rangle \delta(E_{q_j} - E_{q_j'})$$

$$= \frac{4\pi}{\hbar} \Big(\frac{\hbar}{2M}\Big)^2 |\langle\Psi_1|V_1^{(2)}|\Psi_1\rangle - \langle\Psi_0|V_0^{(2)}|\Psi_0\rangle|^2$$

$$\times \int_0^{\omega_D} d\omega \Big(V\frac{4\pi}{(2\pi)^3}\frac{\omega^2}{c^3}\frac{(\omega/c)^2}{\omega}\Big)^2 \frac{1}{e^{\hbar\omega/kT}-1} \frac{e^{\hbar\omega/kT}}{e^{\hbar\omega/kT}-1}$$

$$\rightarrow T^7 \int_0^{\Theta_D/T} dx \frac{x^6 e^x}{(e^x-1)^2} \tag{4.5.12}$$

As expected, the temperature dependence of the line width is solely determined by the density of states of phonons and Bose-Einstein statistics. There are abundant

125

experimental data confirming the above theoretical results. One well-known exper-
iment is the line width measurement of ruby.[28] The spectrum of Cr^{+3} ion inside
sapphire crystal (Al_2O_3) suffers the shift and the broadening of R_1 and R_2 lines
as temperature is varied. The Debye temperature for sapphire is $760K$, and the
line width changes from $1.8 \times 10^{10} Hz$ to $4.6 \times 10^{12} Hz$ for temperatures $20K$ to
$300K$. The experimental data agree very well with Eq.(4.5.12), and it is concluded
that the Raman processes are mainly responsible for the temperature dependence
of the optical spectrum and that the inelastic scattering of phonons gives almost
zero contribution.

For optical phonons[29], the Einstein approximation can be taken because the
dispersion of the optical phonon can be neglected, and all the phonons have a single
fixed frequency ω_{op}. The line width coming from the optical phonon is simply

$$
\begin{aligned}
\Delta\omega &\propto \langle n \rangle \langle n + 1 \rangle \\
&= \frac{1}{e^{\hbar\omega_{op}/kT} - 1} \frac{e^{\hbar\omega_{op}/kT}}{e^{\hbar\omega_{op}/kT} - 1} \\
&\approx e^{-\hbar\omega_{op}/kT}
\end{aligned}
\tag{4.5.13}
$$

where the last approximation holds for a low temperature, $kT << \hbar\omega_{op}$. This
process is called the Orbach process, and has been observed for a molecule in a
molecular crystal field where localized resonance states are supposed to exist.

4.6 TLS-Glass Model for Amorphous Systems

It is well-known that the thermal properties of amorphous insulating solids
are different from their cystalline conterparts at low temperature.[30] For a periodic,
ordered lattice structures, the Debye model gives a good explanation for the specific
heat behavior. In the Debye model the phonon density state is determined simply
from the phase space volume because a linear dispersion relation is assumed. A
3-dimensional lattice, therefore, has a density of state quadratic in T leading to the

126

T^3 dependent contributions to the specific heat, while the electrons give a linear T contribution. At low temperature the electrons are below Fermi surface giving a negligible contribution to the specific heat, and the phonon contribution is dominant. The long wavelength acoustic phonons that can be thermally excited even at low temperature, are responsible for the T^3 dependence of the specific heat. We might expect that the behavior of specific heat at low temperature of amorphous, disordered system will not be much different from the Debye prediction on the grounds that the structural irregularities and random disorders in an amorphous system become less important as the phonon wavelength increases for a lowered temperature. Most remarkably, experimental measurements at low temperature show that the specific heat of a fused silica (oxide glass) has a linear temperature dependence, and is much larger than the value for a crystalline quartz. A systematic study has been performed by Zeller and Pohl[31][32] on the thermal properties of various amorphous solids, leading to the conclusion that not only oxide glass but also inorganic and organic polymer have a specific heat linear in T, that is, this anomalous thermal behavior is a universal property of amorphous, disordered random systems. Other physical properties of the amorphous systems have been studied including the thermal conductivity, the optical line width of an optical site, the acoustic attenuation, and the dielectric constant variations. As shown in Table 4.1 the temperature dependence of the important physical properties are distinctly different for amorphous and crystalline systems. Several microscopic pictures have been proposed for the amorphous system to explain the experimental observations. The most decisive experiment in determining the microscopic picture was the acoustic attenuation.[33]−[40] The experiments showed that the magnitudes of the thermal conductivity in oxide glass can be deduced from the scattering of acoustic phonons, and also that the acoustic attenuation saturates at a high intensity of acoustic wave. This implies that the Debye-like phonons do exist in oxide glass, and most importantly, are scattered by the additional resonant excitations. These low energy

excitations also participate in the heat capacity of an amorphous, disordered random system. By assuming a large number density of these low excitations with a constant density of states, Anderson *et al.*[41]−[42] explained the anomalous specific heat behavior of glass. The experimental results of acoustic studies support TLS-glass model proposed by Anderson *et al.* over some other models introduced to explain thermal behavior only.

Our main interest will be the optical line broadening mechanism of an optical site surrounded by an amorphous medium. The presence of low excitation energy TLS inside amorphous, glassy media changes the temperature dependence of the optical line width drastically from that predicted by the Debye model presented in Sec.4.5. Before we go into the line broadenig problem, we define a low excitation energy TLS system and study the interaction of TLS with a resonant acoustic phonons.[43]−[45] TLS is defined to be a two-level system with a nonvanishing tunneling probability between two eigen states. This can be pictured as a double-well potential as shown in Figure 4.9. The well-depth and the separation of two wells determine the tunneling probability represented as an off-diagonal matrix in the Hamiltonian. The noninteracting Hamiltonian of TLS can be written simply as,

$$H_0 = \frac{1}{2} \begin{pmatrix} \Delta & W \\ W & -\Delta \end{pmatrix} \qquad (4.6.1)$$

where

$$W = \hbar \omega_0 e^{-\lambda}, \qquad \lambda = \sqrt{\frac{2mV d^2}{\hbar^2}} \qquad (4.6.2)$$

where W is the tunneling frequency, λ the tunneling parameter, and Δ the energy splitting between two wells. Refer to Figure(4.9) for a schematic diagram for TLS. V is the barrier height between two wells, and $\hbar \omega_0$ is the zero point energy. As we see, W is a measure of the tunneling probability between two wells, and vanishes for a double-well with a large separation and a large depth. In order to describe an interaction with the phonons it's better to work in a new basis where the Hamiltonian

128

of TLS is diagonalized. Defining

$$\sin 2\theta = \frac{W}{\sqrt{\Delta^2 + W^2}}, \qquad \cos 2\theta = \frac{\Delta}{\sqrt{\Delta^2 + W^2}}, \qquad E = \sqrt{\Delta^2 + W^2} \qquad (4.6.3)$$

and introducing an orthogonal matrix A,

$$A = \begin{pmatrix} \cos\theta & \sin\theta \\ \sin\theta & -\cos\theta \end{pmatrix} \qquad (4.6.4)$$

the Hamiltonian and the wave function can be transformed into a diagonal form.

$$H' = AHA^{-1}, \qquad \Psi' = A\Psi \qquad (4.6.5)$$

That is,

$$H' = \frac{E}{2}\begin{pmatrix} 1 & 0 \\ 0 & -1 \end{pmatrix} = \frac{1}{2}E\sigma_z \qquad (4.6.6)$$

$$\Psi' = \begin{pmatrix} \Psi_1\cos\theta + \Psi_2\sin\theta \\ \Psi_1\sin\theta - \Psi_2\cos\theta \end{pmatrix} \qquad (4.6.7)$$

In a new basis TLS has a well-defined energy state. Now we consider the interaction of TLS with phonons. At a low temperature the amorphous system can support a long wavelength phonons which is simply an elastic wave in a continuous medium. This long wavelength elastic wave gives rise a strain field introducing a deformation in the double-well, and the deformation can be represented as an interaction between TLS and phonons. The interaction is assumed to be diagonal in the original basis of TLS without losing any generality.

$$H_{int} = \gamma\varepsilon \begin{pmatrix} 1 & 0 \\ 0 & -1 \end{pmatrix} \qquad (4.6.8)$$

In order to see the effect of phonons on TLS it is better to go to the new basis where TLS is diagonalized. Transforming the interaction Hamiltonian, H_{int}, to a new basis Ψ',

$$\begin{aligned} H'_{int} &= AH_{int}A^{-1} = \gamma\varepsilon \begin{pmatrix} \cos 2\theta & \sin 2\theta \\ \sin 2\theta & -\cos 2\theta \end{pmatrix} \\ &= \gamma\cos 2\theta \begin{pmatrix} 1 & 0 \\ 0 & -1 \end{pmatrix}\varepsilon + \gamma\sin 2\theta \begin{pmatrix} 0 & 1 \\ 1 & 0 \end{pmatrix}\varepsilon \\ &= \frac{D}{2}\sigma_z\varepsilon + \frac{B}{2}\sigma_x\varepsilon \end{aligned} \qquad (4.6.9)$$

129

where

$$\frac{D}{2} = \gamma \cos 2\theta = \gamma \frac{\Delta}{E} \tag{4.6.10}$$

$$\frac{B}{2} = \gamma \sin 2\theta = \gamma \frac{W}{E} \tag{4.6.11}$$

we find that the elastic wave in amorphous system can induce either a shift in the TLS eigen energy, E, via D (diagonal coupling) or a transition between the eigen states of TLS via B (off-diagonal coupling). Since the off-diagonal coupling allows a transition between the eigen states of TLS, TLS in the amorphous system at finite temperature keeps flip-flopping by emitting and absorbing the resonant energy phonons.[73] This resonant excitation of TLS with an acoustic wave can give all the Bloch-type resonant phenomena. In fact, the saturation in the acoutic attenuation was the clue leading to the conclusion of the existence of TLS. Similar to the photon echo in an optical Bloch system, phonon echo has been obeserved for TLS in amorphous system reconfirming the microcsopic picture.

Now we calculate the TLS relaxation rate as a function of TLS parameters and the temperature for later use. The one-phonon relaxation probability can be obtained in a straightforward way from Fermi's golden rule.

$$W(\Psi_1' \to \Psi_2') = \sum_{phonon \quad pol., \quad \alpha} \frac{2\pi}{\hbar} |\langle n_{ph} + 1\Psi_1'|H_{int}'|n_{ph}\Psi_{2'}\rangle|^2 g(E)\delta(\hbar\omega - E)$$

$$\tag{4.6.12}$$

The matrix element can be calculated using a second quantization form of a strain field. (Eq.(4.5.7))

$$\langle n_{ph} + 1\Psi_1'|\frac{B}{2}\varepsilon\sigma_x|n_{ph}\Psi_2'\rangle$$

$$= \frac{B_{\alpha\beta}}{2}\langle n_{ph} + 1|\varepsilon_{\alpha\beta}|n_{ph}\rangle\langle \Psi_1'|\sigma_x|\Psi_2'\rangle$$

$$= \frac{B}{2}\sqrt{\frac{\hbar}{2\rho\omega_{\vec{k}_\alpha}V}}k_\alpha\sqrt{n_{ph}+1} \tag{4.6.13}$$

Adopting Debye density of states for phonons, the phase factor is given as

$$\frac{V}{(2\pi)^3}4\pi k^2 dk = \frac{V}{(2\pi)^3}4\pi(\frac{\omega}{c})^2\frac{d\omega}{c} = \frac{V}{(2\pi)^3}\frac{4\pi E^2}{\hbar^3 c^3}dE \tag{4.6.14}$$

130

or, the energy densty of states $g(E)$ is

$$g(E) = \frac{V}{(2\pi)^3} \frac{4\pi E^2}{\hbar^3 c^3} \tag{4.6.15}$$

And at temperature T the Bose-Einstein statistics gives

$$n_{ph}(E) = \frac{1}{e^{E/kT} - 1} \tag{4.6.16}$$

Substituting Eq.(4.6.15) and Eq.(4.6.16) into Eq.(4.6.12) leads to the transition probability

$$
\begin{aligned}
W(\Psi_2' \rightarrow \Psi_1') &= \frac{2\pi}{\hbar}(\frac{B}{2})^2 \frac{\hbar}{2\rho\omega_{\vec{k}_\alpha}V} k_\alpha^2 (n_{ph}(E)+1) \frac{V}{(2\pi)^3} \frac{4\pi E^2}{\hbar^3 c_\alpha^3} \\
&= (\frac{B}{2})^2 \frac{E^3}{c_\alpha^5 2\pi\rho\hbar^4}(\frac{1}{e^{E/kT}-1}+1)
\end{aligned}
\tag{4.6.17}
$$

Similarly,

$$W(\Psi_1' \rightarrow \Psi_2') = (\frac{B}{2})^2 \frac{E^3}{c_\alpha^5 2\pi\rho\hbar^4}(\frac{1}{e^{E/kT}-1}) \tag{4.6.18}$$

The relaxation rate of TLS is, then, given as

$$
\begin{aligned}
\tau^{-1} &= W(\Psi_2' \rightarrow \Psi_1') + W(\Psi_1' \rightarrow \Psi_2') \\
&= \sum_\alpha (\frac{B}{2})^2 \frac{E^3}{c_\alpha^5 2\pi\rho\hbar^4} \coth(E/kT)
\end{aligned}
\tag{4.6.19}
$$

where $\alpha = l, t$ designates the phonon mode (longitudinal and transverse), c_α is the appropriate sound velocity, and ρ is the mass density of glass. We find that the relaxation rate of TLS depends on the temperature of the bulk amorphous medium, and the relaxation rate of TLS becomes larger for an increased temperature.

4.7 Line Broadening in TLS Glass media

Figure(4.10) shows a schematic diagram for two classes of line broadenings.[46] Figure(4.10.a) is called a homogeneous line broadening, while Figure(4.10.b) is

131

called an inhomogeneous line broadening. Based on our linear and nonlinear optical measurements, the linear absorption spectrum of a SINC thin fim is found to actually consist of many Lorentzian homogeneous lines under a Gaussian envelope. Similar behavior was found in independent optical hole burning and photon echo studies of related amorphous structures. The Gaussian distribution is a consequence of the statistical distribution of resonance frequencies of the optical centers due to a variation in local environment in glassy and amorphous matrices. Within the inhomogeneous broadened Gaussian envelope are a series of narrow homogeneous broadened resonances where the characteristic temperature dependence of the linewidth depends on the microscopic broadening mechanism. The linewidth of the homogeneous broadening in amorphous media[47]−[69] can be accounted for using the TLS(two level system)-glass models introduced by Anderson, Halperin, and Varma which have been fairly successful in accounting for many of the physical properties (e.g. specific heat, thermal conductivity, ultrasonic absorption) of *disordered systems such as glasses* and polymer-like matrices. The temperature dependent optical dephasing rate can be expressed directly in terms of the transition matrix,

$$\Delta\omega = \frac{2\pi}{\hbar} \sum_{p',p} W_p |\langle fp'|T(\omega_f + \omega_p)|fp\rangle - \langle ip'|T(\omega_i + \omega_p)|ip\rangle|^2 \delta(E_{p'} - E_p) \quad (4.7.1)$$

where $|f\rangle$ and $|i\rangle$ are the excited and ground states of the molecule, $|p\rangle$ and $|p'\rangle$ are the thermal bath states, W_p is the occupation probability of state $|p\rangle$, and T satisfies the Lippman-Schwinger equation

$$T(\omega) = V + V \frac{1}{\omega - H_0} T \quad (4.7.2)$$

This relation shows that the dephasing rate is related to the anisotropy of the transition matrx; that is, the difference between matrix elements of T in the ground state and the excited states. Once the interaction Hamiltonian V is known, $\Delta\omega$ can be obtained to the same order by perturbative expansion of the Lippman-Schwinger equation in V. The homogeneous line broadening of optical centers in

132

polymeric matrices is another example of a physical property where TLS-glass model is adopted for disordered system. The amorphous material surrounding an optical site can be considered as an ensemble of TLS flip-flopping between two eigenstates as they emit or absorb acoustic phonons. The Hamiltonian of the thin film on a substrate can be written as

$$H = H_0 + H_{12} + H_{23} \tag{4.7.3}$$

$$H_0 = \varepsilon_0 \Psi_0^{\dagger} \Psi_0 + \varepsilon_1 \Psi_1^{\dagger} \Psi_1 + \frac{1}{2} E \sigma^z + \sum_q \hbar \omega_q (n_q + \frac{1}{2}) \tag{4.7.4}$$

$$H_{12} = \frac{1}{2} \sum_\alpha V_0^\alpha \Psi_0^{\dagger} \Psi_0 \sigma^\alpha + \frac{1}{2} \sum_\alpha V_1^\alpha \Psi_1^{\dagger} \Psi_1 \sigma^\alpha \tag{4.7.5}$$

$$H_{23} = \frac{1}{2} \sum_\alpha f^\alpha \epsilon \sigma^\alpha \tag{4.7.6}$$

where H_0 is the noninteracting Hamiltonian of the molecule (the difference $\varepsilon_1 - \varepsilon_0$ corresponding to the Q-band absorption), the TLS, and the phonons; H_{12} is the electrostatic dipole interaction between the molecule and the TLS; and H_{23} is the interaction between the TLS and the phonons, i.e., the strain field ϵ is coupled to the TLS. With the TLS and phonons as a thermal bath, for example, we can write the phonon emission process as $|ip\rangle = |\Psi_0 \uparrow n_q\rangle$, $|ip\prime\rangle = |\Psi_0 \downarrow n_q + 1\rangle$, $|fp\rangle = |\Psi_1 \uparrow n_q\rangle$, $|fp\prime\rangle = |\Psi_1 \downarrow n_q + 1\rangle$.

When the Lippman-Schwinger equation is expanded, it can be written as

$$T(\omega) = V + V \frac{1}{\omega - H_0} V + V \frac{1}{\omega - H_0} V \frac{1}{\omega - H_0} V + \cdots \tag{4.7.7}$$

Now putting V equal to $H_{12} + H_{23}$, we get for a phonon emission process

$$\langle ip'|T(\omega_i + \omega_p)|ip\rangle$$
$$= \langle \Psi_0 \downarrow n_q + 1|T(\omega_0 + \omega_\uparrow + \omega_{n_q})|\Psi_0 \uparrow n_q\rangle \tag{4.7.8}$$

The first order terms are identical for the ground state and the excited state since only H_{23} is involved in the first order process, i.e.,

$$\langle \Psi_0 \downarrow n_q + 1|(H_{12} + H_{23})|\Psi_0 \uparrow n_q\rangle$$
$$= \langle \Psi_0 \downarrow n_q + 1|H_{23}|\Psi_0 \uparrow n_q\rangle \tag{4.7.9}$$

$$\langle \Psi_1 \downarrow n_q + 1 | (H_{12} + H_{23}) | \Psi_1 \uparrow n_q \rangle$$

$$= \langle \Psi_1 \downarrow n_q + 1 | H_{23} | \Psi_1 \uparrow n_q \rangle \qquad (4.7.10)$$

The second order terms are as follows.

$$\langle \Psi_0 \downarrow n_q + 1 | V \frac{1}{\omega_0 + \omega_\uparrow + \omega_{n_q} - H_0} V | \Psi_0 \uparrow n_q \rangle$$

$$= \langle \Psi_0 \downarrow n_q + 1 | V | \Psi_0 \uparrow n_q + 1 \rangle$$

$$\langle \Psi_0 \uparrow n_q + 1 | \frac{1}{\omega_0 + \omega_\uparrow + \omega_{n_q} - H_0} | \Psi_0 \uparrow n_q + 1 \rangle \langle \Psi_0 \uparrow n_q + 1 | V | \Psi_0 \uparrow n_q \rangle$$

$$+ \langle \Psi_0 \downarrow n_q + 1 | V | \Psi_0 \downarrow n_q \rangle \langle \Psi_0 \downarrow n_q | \frac{1}{\omega_0 + \omega_\uparrow + \omega_{n_q} - H_0} | \Psi_0 \downarrow n_q \rangle \langle \Psi_0 \downarrow n_q | V | \Psi_0 \uparrow n_q \rangle$$

$$= \langle \Psi_0 \downarrow n_q + 1 | H_{12} | \Psi_0 \uparrow n_q + 1 \rangle$$

$$\frac{1}{(\omega_0 + \omega_\uparrow + \omega_{n_q}) - (\omega_0 + \omega_\uparrow + \omega_{n_q+1})} \langle \Psi_0 \uparrow n_q + 1 | H_{23} | \Psi_0 \uparrow n_q \rangle$$

$$+ \langle \Psi_0 \downarrow n_q + 1 | H_{23} | \Psi_0 \downarrow n_q \rangle \frac{1}{(\omega_0 + \omega_\uparrow + \omega_{n_q}) - (\omega_0 + \omega_\downarrow + \omega_{n_q})} \langle \Psi_0 \downarrow n_q | H_{12} | \Psi_0 \uparrow n_q \rangle$$

$$= \frac{1}{2} V_0^- (-\frac{1}{\omega_q}) \frac{1}{2} f^z \langle n_q + 1 | \epsilon | n_q \rangle + \frac{1}{2} V_0^- \frac{1}{\omega_\uparrow - \omega_\downarrow} (-\frac{1}{2}) f^z \langle n_q + 1 | \epsilon | n_q \rangle$$

$$= \frac{1}{2} V_0^- (-\frac{1}{2}) f^z \frac{2}{\hbar \omega_q} \langle n_q + 1 | \epsilon | n_q \rangle \qquad (4.7.11)$$

The interaction Hamiltonians H_{12} and H_{23} do not commutate with each other; therefore, we have two terms in Eq.(4.7.11) with a different ordering of H_{12} and H_{23}. The second order process involving phonon emission can be represented as a diagram shown in Figure(4.11) and Figure(4.12). H_{12} is responsible for a flipping of TLS, while H_{23} is responsible for a phonon emission. In Figure(4.11) H_{23} appears first, and H_{12} comes later, and the ordering is reversed in Figure(4.12). Both terms contribute equally in the line broadening, and keeping up to the second order, we find that

$$\langle fp' | T(\omega_f + \omega_p) | fp \rangle - \langle ip' | T(\omega_i + \omega_p) | ip \rangle$$

$$= \langle \Psi_1 \downarrow n_q + 1 | T(\omega_1 + \omega_\uparrow + \omega_{n_q}) | \Psi_1 \uparrow n_q \rangle - \langle \Psi_0 \downarrow n_q + 1 | T(\omega_0 + \omega_\uparrow + \omega_{n_q}) | \Psi_0 \uparrow n_q \rangle$$

$$= \frac{1}{2} (V_1^- - V_0^-)(-\frac{1}{2}) f^z \frac{2}{\hbar \omega_q} \langle n_q + 1 | \epsilon | n_q \rangle \qquad (4.7.12)$$

134

For a phonon emission process, the occupation probability W_p for the thermal bath is simply given from the Boltzman distribution.

$$W_p = W_{\uparrow, n_q}$$
$$= \frac{\exp(-E/2kT)}{\exp(E/2kT) + \exp(-E/2kT)} = \frac{\exp(-E/2kT)}{2\cosh(E/2kT)} \tag{4.7.13}$$

where E is the difference in the eigen energies of TLS. Substituting Eq.(4.7.12) and Eq.(4.7.13) into Eq.(4.7.1), we get the homogeneous line broadening upon a resonant phonon from TLS. Since TLS in an amorphous medium has its own characteristic statistical distribution of double-well depths, widths, and transition probabilities, we need to integrate over TLS states in order to get the homogeneous linewidth. As in Eq.(4.6.8), when the interaction of TLS with the optical sites and the acoustic phonons are assumed to be diagonal in the original basis of TLS, the TLS flipping process depends on $B/2$ or W/E, while TLS non-flipping process depends on $D/2$ or Δ/E. (Refer to Eq.(4.6.9)) In the second order process involving both the optical sites and the acoustic phonons, Eq.(4.7.11) shows that H_{12} (or $V_{\pm}$) flips TLS, and H_{23} (or f^z) does not flip TLS. For a particular TLS with the zero point energy ω_0, tunneling parameter λ, and the energy splitting Δ, the coupling constants of TLS should be redefined to account for the differences in TLS. That is,

$$V_{1,0}^{\pm} = \frac{\hbar\omega_0}{E} e^{-\lambda} \bar{V}_{1,0}^{\pm} \tag{4.7.14}$$

$$f^z = \frac{\Delta}{E} \bar{f}^z \tag{4.7.15}$$

With the new coupling constants $\bar{V}$ and $\bar{f}$, the homogeneous line broadening due to an acoustic phonon emission is given by integrating over TLS states.

$$\Delta\omega^{emission} = \frac{2\pi}{\hbar} \sum_{\vec{q}_s} \int d\omega_0 d\lambda d\Delta df\, P(\omega_0, \lambda, \Delta, f)$$

$$\times \left[\frac{1}{2}\frac{\hbar\omega_0}{E} e^{-\lambda}(\bar{V}_1^- - \bar{V}_0^-)\right]^2 \left[\frac{1}{2}\frac{\Delta}{E}\bar{f}^z\right]^2 \frac{4}{(\hbar\omega_q)^2} |\langle n_q + 1|\varepsilon|n_q\rangle|^2$$

$$\times \frac{\exp(-E/2kT)}{2\cosh(E/2kT)} \delta(E - \hbar\omega_q) \tag{4.7.16}$$

135

where $P(\omega_0, \lambda, \Delta, f)$ is the probability distribution of TLS satisfyng the normalization condition.[70]-[73]

$$\int P(\omega_0, \lambda, \Delta, f) \cdot \omega_0 \, d\lambda \, d\Delta \, df = 1 \qquad (4.7.17)$$

A similar expression for the transition matrix element can be obtained for a phonon absorption process.

$$\langle fp' | T(\omega_f + \omega_p) | fp \rangle - \langle ip' | T(\omega_i + \omega_p) | ip \rangle$$
$$= \frac{1}{2}(V_1^+ - V_0^+)(-\frac{1}{2}) f^z \frac{2}{\hbar \omega_q} \langle n_q - 1 | \epsilon | n_q \rangle \qquad (4.7.18)$$

In the phonon absorption process TLS is in the lower eigen state in the beginning, having a different weight factor of the probability for the thermal bath. That is,

$$W_p = W_{\downarrow, n_q}$$
$$= \frac{\exp(+E/2kT)}{\exp(E/2kT) + \exp(-E/2kT)} = \frac{\exp(+E/2kT)}{2\cosh(E/2kT)} \qquad (4.7.19)$$

The distribution function $P(\omega_0, \lambda, \Delta, f)$ in Eq.(4.7.17) is assumed constant in the ranges of $\lambda_{min} < \lambda < \lambda_{max}$ and $0 < \Delta < \Delta_{max}$, and to vanish outside these ranges. Carrying out the λ integration for TLS, and summing over $\vec{q}$ while assuming the Debye dispersion relation, we find that

$$\Delta\omega(T) \propto T^2 \int_0^{\Theta/T} dx \frac{x e^{-x}}{1 - e^{-2x}} \qquad (4.7.20)$$

The homogeneous linewidth of an optical site in an amorphous medium shows a quadratic dependence at a low temperature, distinctly different from the T^7 dependence for a crystalline medium. The homogeneous line width of an organic molecule in a glassy matrix has been measured by optical hole burning and by photon echo experiments. [56]-[65],[73] It generally follows the power law

$$\Delta\omega(T) \propto T^{1+\delta} \quad (0 < \delta \leq 1) \qquad (4.7.21)$$

with the exact value of δ depending on the charateristics of TLS in the particular glassy matrix. In fact, by assuming a non-trivial distribution of TLS, the experimental value of $\Delta\omega(T)$ can be fit, which then allows us to understand the microscopic structure of a glassy medium responsible for the homogeneous line broadening.

136

References: Chapter 4

[1] Fano, U., Phys. Rev. **131**, 2   (1963)

[2] Baranger, M. Phys. Rev. **111**, 481, 494 (1958);**112**, 855 (1958)

[3] Redfield, A.G., Adv. Magn. Res. **1**, 1 (1968)

[4] Kosonocky, W.F. and Harrison, S.E., J. Appl. Phys. **37**, 4789 (1966)

[5] McVie, J., Sinclair, R.S., and Truscott, T.G., J. Chem. Soc. Faraday Tran. **274**, 1870 (1978)

[6] Gurinovich, G.P., Sevchenko, A.V., and Solovek, K.N., Sov. Phys. Uspkhi **6**, 67 (1963)

[7] Brannon, J.H., and Magde, D., J. Am. Chem. Soc. **102**, 62 (1980)

[8] Gutierrez, A., Castro, G., Schulte, G., and Haarer, D., in *Organic Molecular Aggregates*, P. Reineker, H. Haken, and H.C. Wolf, eds., Springer-Verlag, New York (1979)

[9] Macfarlane, R.M. and Shelby, R.M., J. Lumin. **36**, 179 (1987)

[10] Volker, S. and Macfarlane, R.M., IBM J. Res. Dev. **23**, 547 (1979)

[11] Stoneham, A.M., Rev. Mod. Phys. **41**, 82 (1969)

[12] Romagnoli, M., Moerner, W.E., Schellenberg, F.M., Levenson, M.D., and Bjorklund, G.C., J. Opt. Soc. Am. **B1**, 341 (1984)

[13] Dattagupta, S., *Relaxation Phenomena in Condensed Matter Physics*, Academic, New York (1987)

[14] Jones, K.E. and Zewail, A.H. in Springer Series in Chemical Physics, vol. 3: *Advances in Laser Chemistry*, Zewail, A.H., ed. Springer, New York (1978) p.196

[15] Jones, K.E., Zewail, A.H., and Diestler, D.J. in Springer Series in Chemical Physics, vol. 3: *Advances in Laser Chemistry*, Zewail, A.H., ed. Springer, New York (1978) p.258

[16] Burns, M.J., Liu, W.K., and Zewail, A.H. in Springer Series in Chemical Physics, vol. 3: *Spectroscopy and Excitation Dynamics of Condensed Molecular Systems*, eds. Agranovich, V.M. and Hochstrasser, R.H., North-Holland, New York

(1983) p.301; Diestler, D.J. and Zewail, A.H., J. Chem. Phys. **71**, 3103 (1979); **71**, 3113 (1979).

[17] Lovesey, S.W., *Condensed Matter Physics: Dynamic Correlations*, Benjamin, Reading, Massachusetts (1981); *Problome a N corps., Many-body physics*, edite par C. DeWitt and R. Balian, Les Houches lecture 1967, Gordon and Breach, New York (1968)

[18] Fano, U., Rev. Mod. Phys. **29**, 74 (1957); in Lectures on the Many-body Problems, vol. 2, ed. Caianiello, E.R., Academic, New York, (1964)

[19] Ben-Reuven, A. in *Advances in Chemical Physics*, Prigogine, I. and Rice, S.A., eds. Wiley, New York (1975) vol. 33

[20] Ben-Reuven, A., Phys. Rev. **A4**, 2115 (1971)

[21] Zwanzig, R., J. Chem. Phys. **33**, 1338 (1960); Phys. Rev. **124**, 983 (1961)

[22] Zwanzig, R. in Lectures in Theoretical Physcis, vol. 3, ed. Brittin, W.E., Downs, B.W., and Downs, J., Interscience, New York (1961)

[23] Kubo, R., in *Stochastic Processes in Chemical Physics* ed. Shuler, K.E., *Advances in Chemical Physics*, Prigogine, I. and Rice, S.A., eds. Wiley, New York (1969) vol. 15

[24] Grabert, H., Springer Tracts Mod. Phys. vol. 95, *Projection Operator Techniques in Nonequilibrium Statistical Mechanics*, Springer, Berlin (1982)

[25] Grigolini, P., in *Memory Function Approaches to Stochastic Problems in Condensed Matter*, ed. Evans, M.W., Grigolini, P., and Pastoriparravicini, G., *Advances in Chemical Physics*, Prigogine, I. and Rice, S.A., eds. Wiley, New York (1985) vol. 62

[26] Ziman, J.M., *Elements of Advanced Quantum Theory*, Cambridge University, Cambridge, England (1969)

[27] Sakurai, J.J., *Advanced Quantum Mechanics*, Addison-Wesley, Reading, Massachusetts (1967)

[28] McCumber, D.E. and Sturge, M.D., J. Appl. Phys. **34**, 1682 (1963)

[29] Ashcroft, N.W. and Mermin, N.D., *Solid State Physics*, Saunders College, Philadelphia, Pennsylavnia (1976)

[30] Phillips, W.A., ed. *Amorphous Solids, Low-Temperature Properties*, Topics in Current Physics, vol. 24, Springer, Berlin (1981)

[31] Zeller, R.C. and Pohl, R.O., Phys. Rev. B4, 2029 (1971)

[32] Stephens, R., Phys. Rev. B13, 852 (1976)

[33] Hunklinger, S., Arnold, W., Stein, S., Nava, R., and Dransfeld, K, Phys. Lett. A42, 253 (1972)

[34] Hunklinger, S., J. Physique C9, Suppl. C9-461 (1982)

[35] Hunklinger, S., Festkorperprobleme XVII, 1 (1977)

[36] Hunklinger, S. and Schmidt, M., Z. Phys. B- Condensed Matter, 54, 93 (1984)

[37] Doussineau, P., Matecki, M., and Schon, W., J. Physique 44, 101 (1983)

[38] Black, J., J. Physique, C 6, Suppl. C6-963 (1978)

[39] Jackle, J., Z. Phys. 257, 212 (1972)

[40] Jackle, J., Piche, L., Arnold, W., and Hunklinger, S., J. Non-Cryst. Solids 20, 365 (1976)

[41] Anderson, P.W., Halperin, B.I., and Varma, C., Philo. Mag. 25, 1 (1972)

[42] Philips, W.A., J. Low Temp. Phys. 7, 351 (1972)

[43] Sussmann, J.A., Phys. kondens. Materie, 2, 146 (1964)

[44] Sussmann, J.A., J. Phys. Chem. Solids, 28, 1643 (1967)

[45] Arnold, W., Martinon, C., and Hunklinger, S., J. Physique, C 6, Suppl. C6-961 (1978)

[46] Stoneham, A.M., Rev. Mod. Phys. 41, 82 (1969)

[47] Orlowski, T.E. and Zewail, A.H., J. Chem. Phys. 70, 1390 (1979)

[48] Jankowiak, R. and Small, G.J., J. Phys. Chem. 1986, 5612 (1986)

[49] Jankowiak, R. and Small, G.J., Chem. Phys. 118, 223 (1987)

[50] Jankowiak, R. and Small, G.J., Science 237, 618 (1987)

[51] Hayes, J.M., Stout, R., and Small, G.J., J. Chem. Phys., 74, 4266 (1981)

139

[52] Jankowiak, R. and Small, G.J., Chem. Phys. Lett. **128**, 377 (1986)

[53] Lyo, S.K. and Orbach, R., Phys. Rev. **22**, 4223 (1980)

[54] Lyo, S.K., Phys. Rev. Lett. **48**, 688 (1982)

[55] Brout, R., Phys. Rev. **107**, 664 (1957)

[56] Volker, S., Macfarlane, R.M., Genack, A.Z., and Trommsdorf, H.P., van der Waals, J.H., J. Chem. Phys. **67**, 1759 (1977)

[57] Volker, S. and Macfarlane, R., IBM J. Res. Develop. **23**, 547 (1979)

[58] Burland, D.M. and Haarer, D., IBM J. Res. Develop. **23**, 534 (1979)

[59] Reinecke, T.L., Solid State Com. **32**, 1103 (1979)

[60] Friedrich, J. and Haarer, Γ , J. Chem. Phys. **76**, 61 (1982)

[61] Friedrich, J., Wolfrum, H., and Haarer, D., J. Chem. Phys. **77**, 2309 (1982)

[62] Morawitz, H. and Reineker, Solid State Com. **42**, 609 (1982)

[63] Reineker, P. and Kassner, K., Phys. Rev. **B29**, 4546 (1984)

[64] de Bree, P. and Wiersma, A., J. Chem. Phys. **70**, 790 (1979)

[65] Molenkamp, L.W. and Wiersma, D.A., J. Chem. Phys. **83**, 1 (1985)

[66] Prasad, P.N. and Von Smith, R., J. Chem. Phys. **71**, 4646 (1979)

[67] Hess, L.A. and Prasad, P.N., J. Chem. Phys. **71**, 573 (1980)

[68] Kador, L., Schulte, G., and Haarer, D., J. Chem. Phys. **90**, 1264 (1986)

[69] Nishi, T., Arishima, K., Tabei, H., and Hiratuka, H., Japan. J. Appl. Phys. **27**, 225 (1988)

[70] Black, J.L., Halperin, B.I., Phys. Rev. **B16**, 2879 (1977)

[71] Golding, B., Graebner, J.E., Halperin, B.I., and Schutz, R.J., Phys. Rev. Lett. **30**, 223 (1976)

[72] Black, J., Phys. Rev. **B17**, 2740 (1978)

[73] Narasimhan, L.R., Pack, D.W., and Fayer, M.D., Chem. Phys. Lett. **152**, 287 (1988)

Figure Captions; Chapter 4

Figure 4.1; Schematic Diagram of the Molecular Structure of Silicon- Naphthalocyanine with a Polymer Tail

Figure 4.2; Schematic Diagram of the Molecular Structure of Silicon- Naphthalocyanine

Figure 4.3; Linear Absorption Spectrum of Liquid Solution

Figure 4.4; Linear Absorption Spectra of Thin Films; Pure Dye (solid curve) and Solid Solution (dashed curve)

Figure 4.5; Linear Absorption Spectrum of Pure Dye Thin Film at Various Temperatures (1)

Figure 4.6; Linear Absorption Spectrum of Pure Dye Thin Film at Various Temperatures (2)

Figure 4.7; Optical System in Interaction with a Thermal Bath

Figure 4.8; Phonon Scattering Process in Crystalline Media

Figure 4.9; Schematic Diagram of Two-Level-System (TLS)

Figure 4.10; Homogeneous and Inhomogeneous Broadening

Figure 4.11; Phonon Emission Process in Random Glass Media (I)

Figure 4.12; Phonon Emission Process in Random Glass Media (II)

COMPARISON between CRYSTAL and GLASS

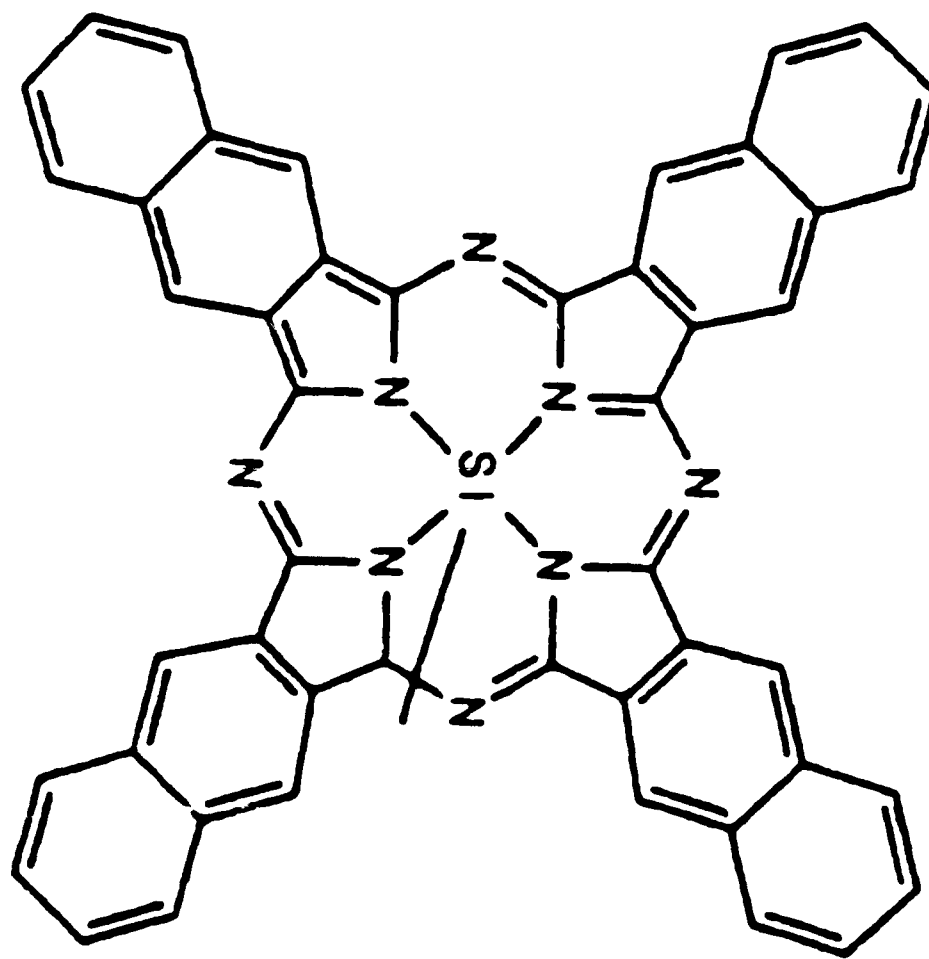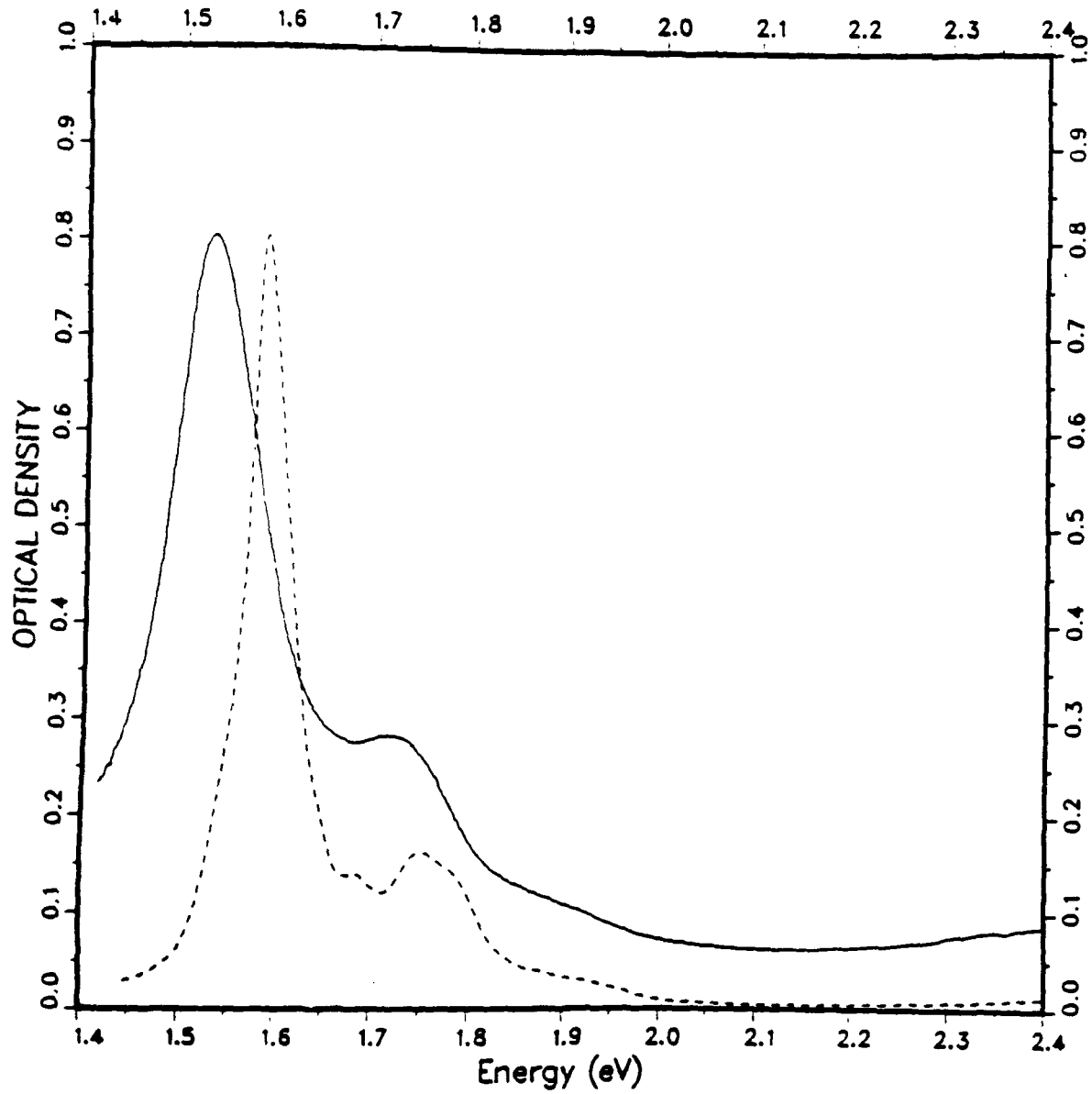| Physical Property	Crystal	Glass
Specific Heat	T^3	T
Thermal Conductivity	T^3	T^2
$\Delta\omega$	T^7	T^{1-2}
Acoustic Attenuation	No	Yes

Table 4.1

**Schematic Diagram of the Molecular Structure of
Silicon-Naphthalocyanine with a Polymer Tail**
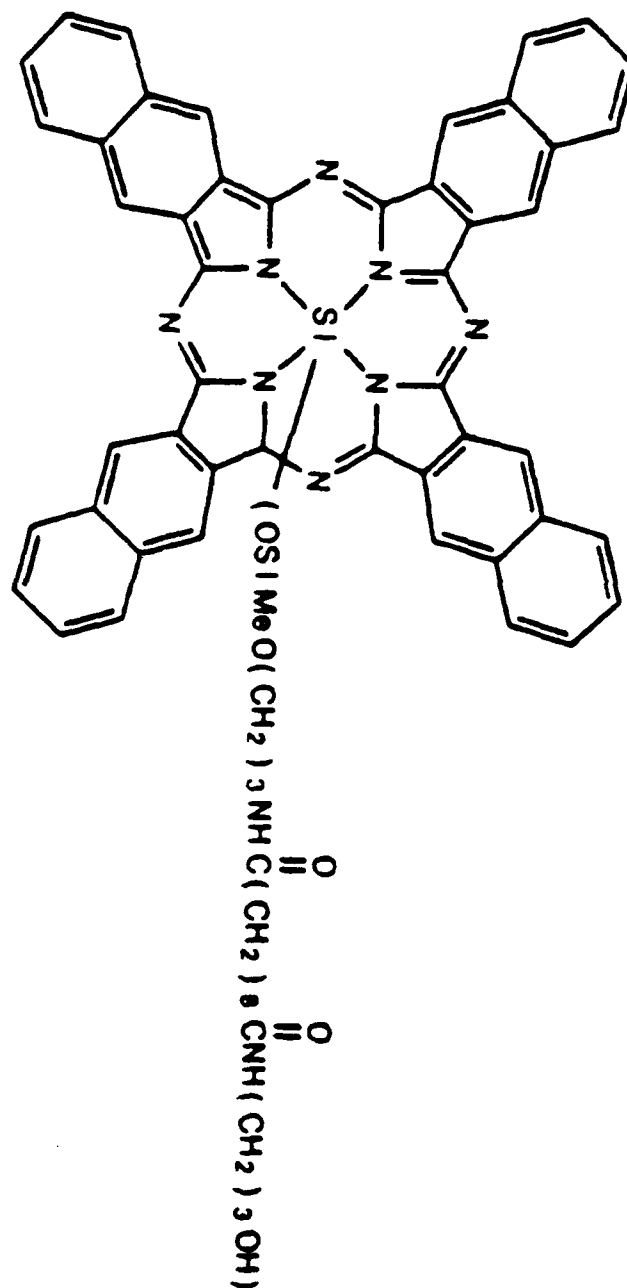
Figure 4.1

Schematic Diagram of the Molecular Structure of Silicon-Naphthalocyanine

Figure 4.2

Linear Absorption Spectrum of Liquid Solution
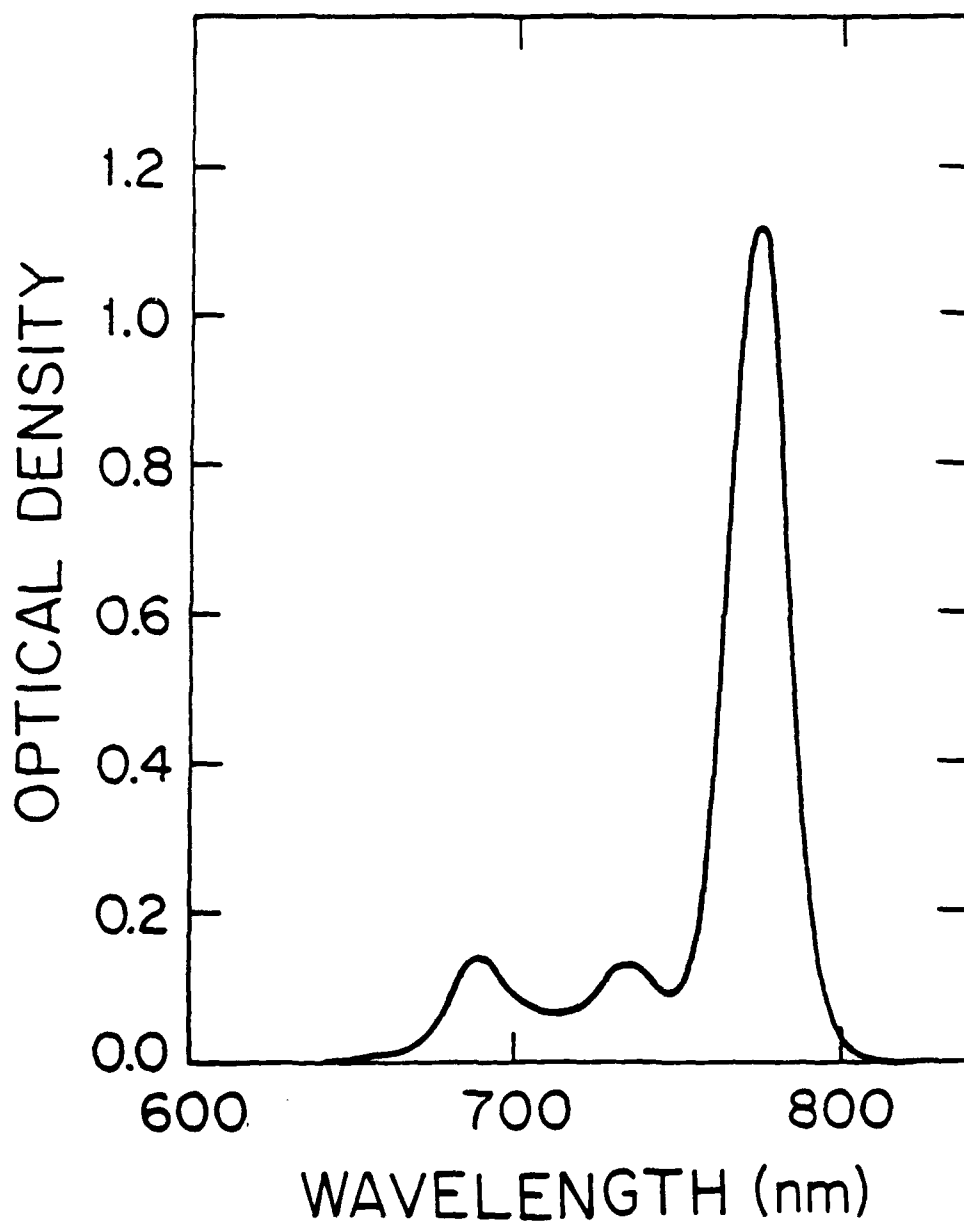
Figure 4.3

Linear Absorption Spectrum of Thin Films;
Pure Dye (solid curve) and Solid Solution (dashed curve)

Figure 4.4

146

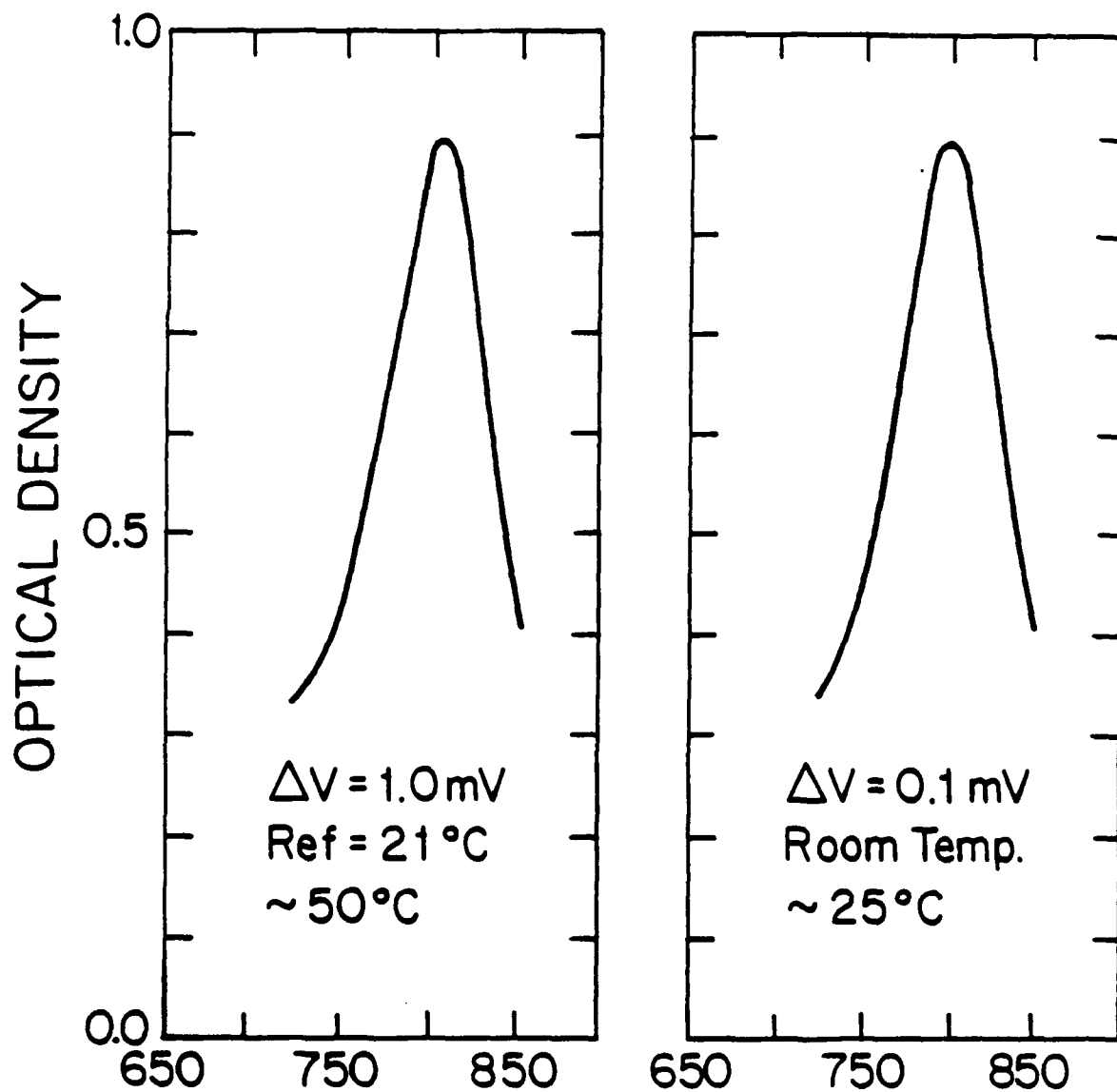**Linear Absorption Spectrum of Pure Dye Thin Films
at Various Temperatures (1)**

Figure 4.5

147

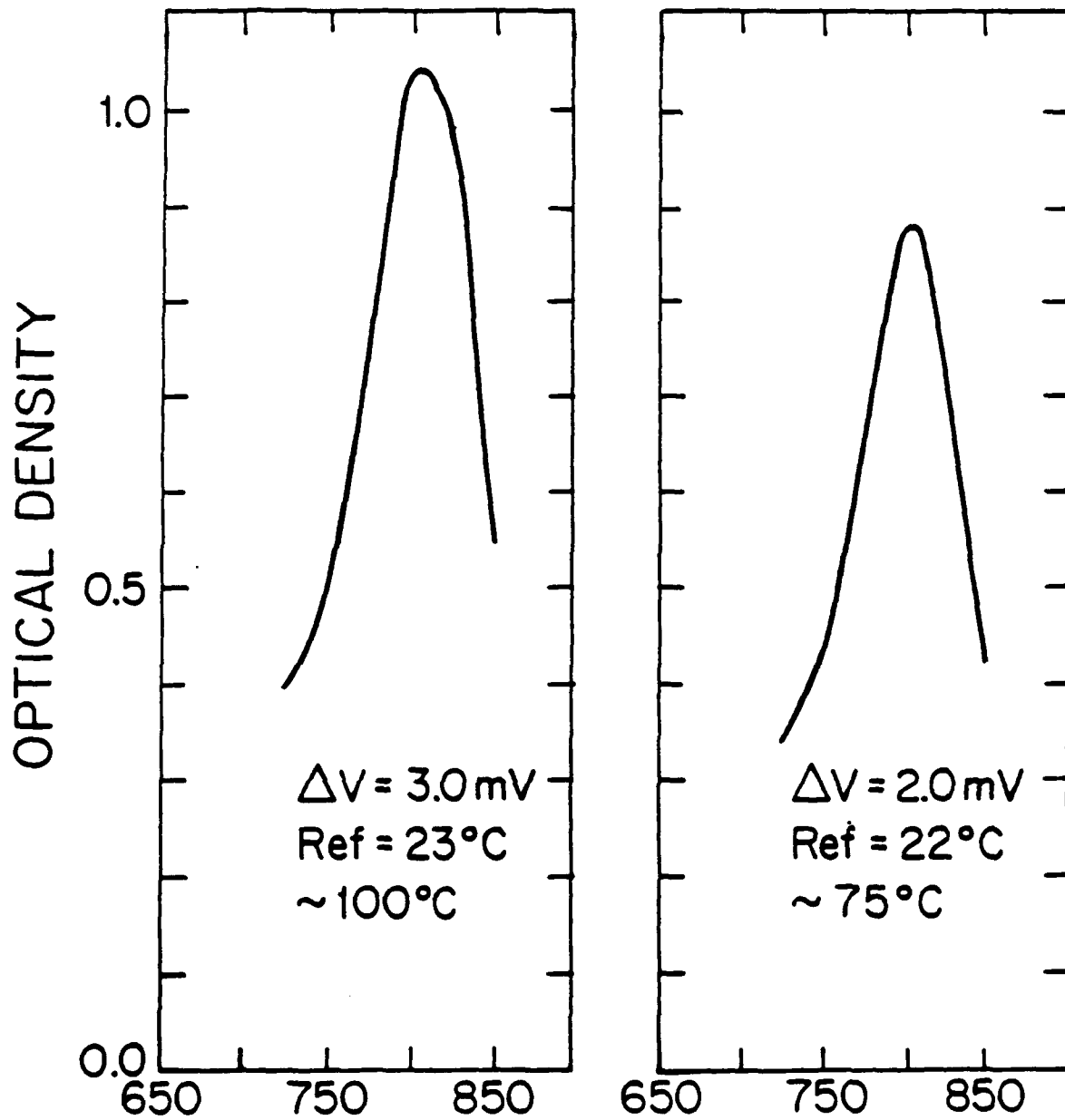**Linear Absorption Spectrum of Pure Dye Thin Films
at Various Temperatures (2)**

Figure 4.6
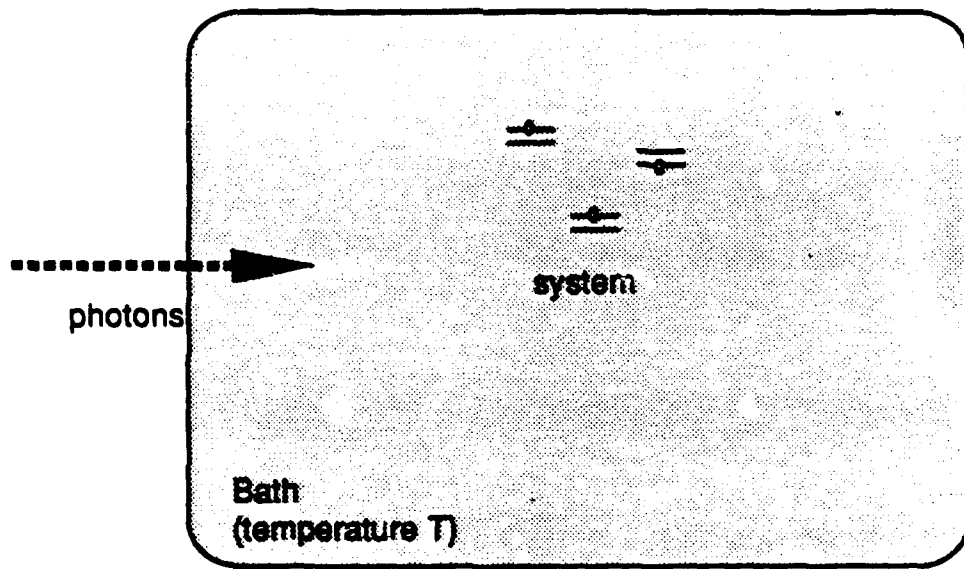
Optical System in Interaction with Bath

Figure 4.7

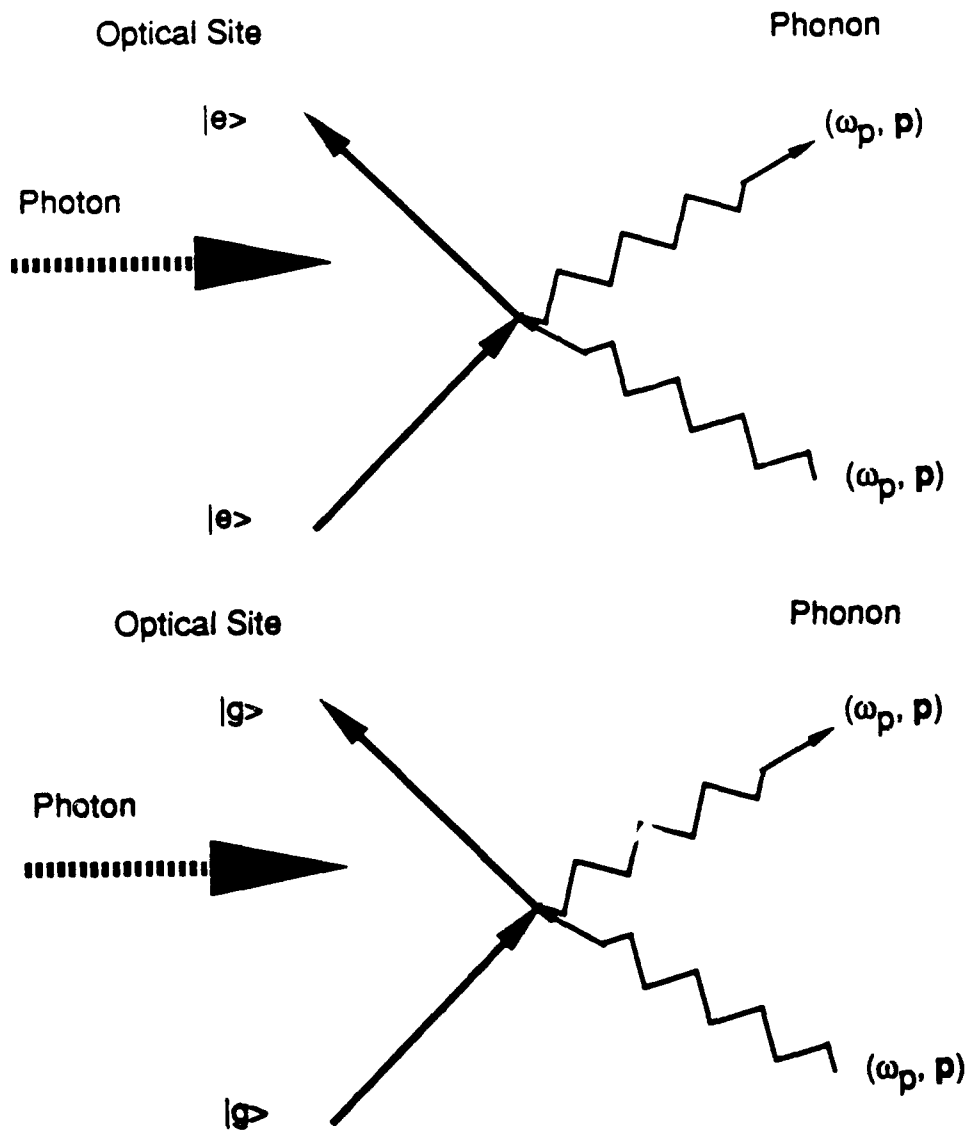**Phonon Scattering Process
in Crystalline Media**

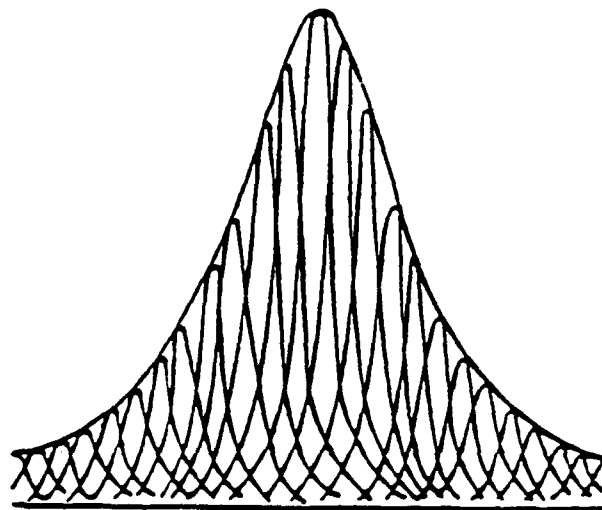Optical Site   Phonon

$|e\rangle$ $(\omega_p, \mathbf{p})$

Photon

$|e\rangle$ $(\omega_p, \mathbf{p})$

Optical Site   Phonon

$|g\rangle$ $(\omega_p, \mathbf{p})$

Photon

$|g\rangle$ $(\omega_p, \mathbf{p})$

Figure 4.8

Schematic Diagram of Two-Level-System (TLS)

Figure 4.9

Homogeneous and Inhomogeneous Broadening

(a)

(b)

Figure 4.10

Phonon Emission Process
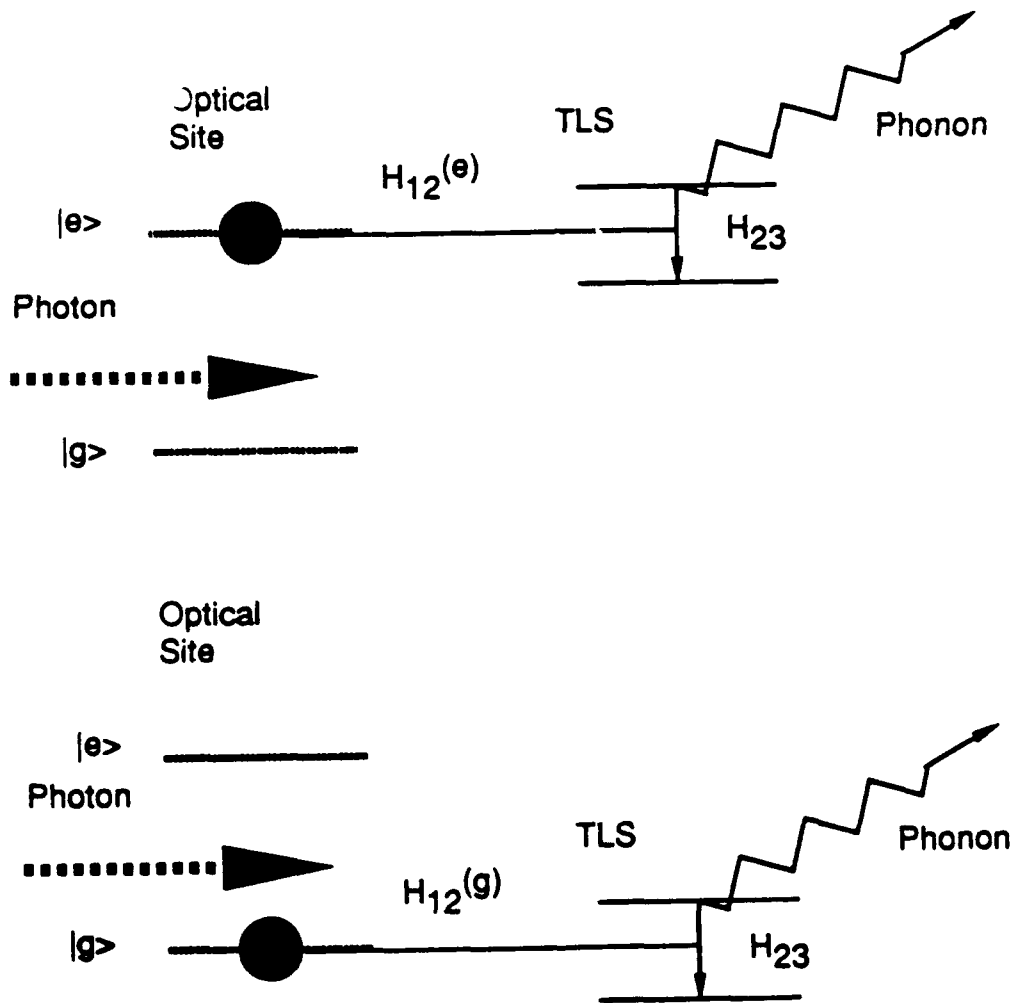## in Random Glass Media

Figure 4.11
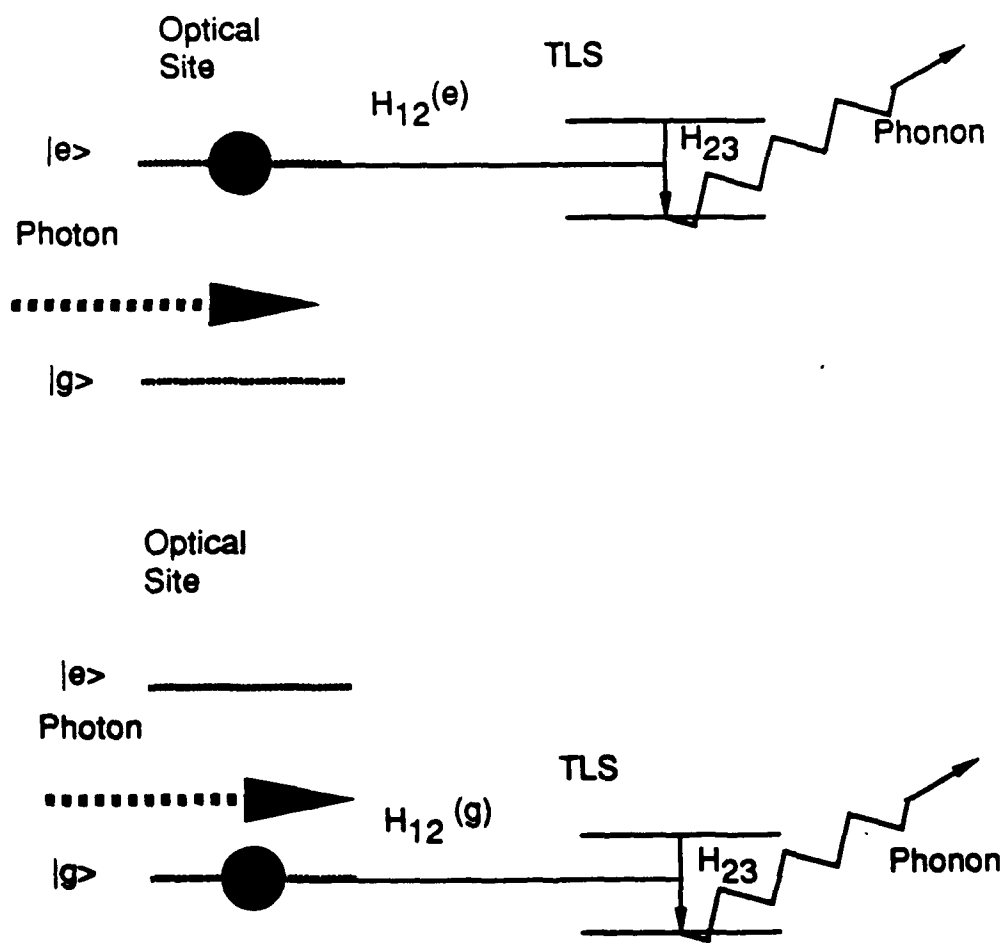
153

**Phonon Emission Process
in Random Glass Media**

Figure 4.12

CHAPTER 5

NONLINEAR OPTICAL EXCITATIONS: SATURABLE ABSORPTION

Resonant nonlinear optical processes of an electronic system such as saturable absorption can be described by a Bloch susceptibility. A Bloch-type two level system resonant with incident light shows characteristic dispersive and absorptive third order nonlinear optical responses. While the real part of the Bloch susceptibility accounts for the intensity dependent refractive index, the imaginary part is responsible for saturable absorption. The saturation threshold power is directly related to the resonant nonlinear susceptibility, n_2. The resonant n_2 has been discussed in Sec.3.7 in connection with a Bloch susceptibility introduced in Chapter 3.

After reviewing the resonant nonlinear optical susceptibility briefly in Sec.5.1, we shall discuss the dynamics of saturable absorption, in terms of a pair of rate equations, one for the number of excited state molecules, and the other for the light intensity. By introducing a normalized pulse shape function, the pair of equations can be reduced to one rate equation for the pulse shape function, which can be solved numerically. The results of our numerical calculations will be presented in Sec.5.2.

According to the dynamical transmission results, the threshold power for saturable absorption is related to the molecular absorption cross section and the radiative decay time of the excited state. In large conjugated structures, a given triplet state is quite close in energy to the corresponding singlet state, and there occurs appreciable intersystem crossing affecting the effective decay time from the first excited singlet state. The intersystem crossing rate is intimately related to spin-orbit coupling because it involves a transition between different spin manifolds. The intersystem crossing will be reviewed in Sec.5.3 leading to the important conclusion that the central atom determines the intersystem crossing rate for a two-dimensional π-electron system such as a phthalocyanine.

In Sec.5.4 we present the experimental measurements of the nonlinear optical properties of the SINC thin films. Since our main interest is the resonant behavior within the Q-band located in the near IR, different types of coherent light sources tunable in the near IR are fully described in Sec.5.4.1 along with the detection system used in the experimental measurement. In any nonlinear optics measurement, the light detectors should be carefully specified because the detector itself might behave nonlinearly. The principal results of saturable absorption experiments are presented in Sec.5.4.3. In order to fully characterize the resonant nonlinear optical excitations in the Q-band,the dispersion of saturable absorption throughout the Gaussian absorption band was measured. A Kramers-Kronig analysis is used to obtain the real part of the intensity dependent refractive index, presented in Sec.5.5.

5.1 Saturable Absorption and Resonant Nonlinear Refractive Index n_2

Saturable absorption is a resonant nonlinear optical phenomenon in which the absorption coefficient decreases for an increased incident light intensity. At a low incident light intensity, the absorption coefficient of an optical system is related to the imaginary part of the linear refractive index, which in turn is related to the linear susceptibility of the system in an electromagnetic field.[1]−[10] According to linear response theory, as shown in Chapter 4, a Lorentzian susceptibility results when a stochastic force, either an electromagnetic fluctuation manifested as a spontaneous decay, or a thermal bath responsible for a temperature dependent line shape function, is approximated to be near Markovian, or has a short memory. A Markovian stochastic force disturbs the time-correlation of dipole moments leading to a finite relaxation time. But a basic underlying assumption of linear response theory is that the interaction of the system with the external field is small, thus allowing a perturbation expansion of the response function. In quantum mechanical terms, once the interaction of the system with an external field is introduced in the

total Hamiltonian of the system, the wavefunction of the system can be divided into two parts: the unperturbed part from the system without the interaction and the perturbed part caused by the interaction. When the time evolution of the system interacting with a perturbing field is considered, the Hamiltonian operator describing a unitary transformation of the wavefunction of the system should be the total Hamiltonian, which operates on the full wavefunction.

In linear response theory, the change in temporal evolution of the wavefunction is assumed to be the sum of the product of the unperturbed Hamiltonian and the perturbed part of the wavefunction, and the product of the perturbing Hamiltonian and the unperturbed wavefunction. That is, the product of the perturbing Hamiltonian and the perturbed part of wavefunction is ignored.

$$i\hbar \frac{\partial \Psi(t)}{\partial t} = i\hbar \frac{\partial}{\partial t}(\Psi_0(t) + \delta\Psi(t))$$
$$= H\Psi(t) = (H_0 + H_a)(\Psi_0(t) + \delta\Psi(t))$$
$$= H_0\Psi_0(t) + H_0\delta\Psi(t) + H_a\Psi_0(t) + H_a\delta\Psi(t) \tag{5.1.1}$$

Or,

$$i\hbar \frac{\partial \delta\Psi(t)}{\partial t}$$
$$= H_0\delta\Psi(t) + H_a\Psi_0(t) + H_a\delta\Psi(t)$$
$$\approx H_0\delta\Psi(t) + H_a\Psi_0(t) \tag{5.1.2}$$

When the perturbing field is very intense, or the interaction of the system with the perturbing external field becomes comparable to the unperturbed Hamiltonian of the system, for example, through a resonant enhancement, the response of the system becomes large and the approximation taken in linear response theory is no longer valid. The perturbation expansion is not justified, and the optical susceptibility cannot be obtained simply from the time-correlation function of dipole moments. However, as discussed in Chapter 3, the resonant interaction of a system

157

with an intense coherent optical field can be described in terms of a Bloch equation. The Bloch susceptibility is intensity dependent, and for a light intensity above the threshold critical intensity, which is related to the population and the phase decay times, the system exhibits a characteristic nonlinear response, saturable absorption being one of them. As seen in Eq.(3.7.10), the threshold intensity is the same for the real and the imaginary part of the suscpetibility, which allows us to determine the intenisty dependent refractive index n_2. n_2 is related to the real part of the susceptibility from an experiment that measures the effect of the imaginary part of the susceptibility.

Sometimes saturable absorption is described by rate equations for the differences in the number of resonant atoms in the upper state (n_2) and the lower state (n_1).

$$\frac{dn_2}{dt} = -R(n_2 - n_1) - \frac{n_2}{T_1} \tag{5.1.3}$$

$$\frac{dn_1}{dt} = +R(n_2 - n_1) + \frac{n_2}{T_1} \tag{5.1.4}$$

By subtracting Eq.(5.1.4) from Eq.(5.1.3), we find the rate equation for the population, w,

$$\frac{dw}{dt} = -2Rw - \frac{w+1}{T_1} \tag{5.1.5}$$

It is easy to see that the above rate equation corresponds to the Bloch equation for the population when the dephasing time T_2 is assumed to be short. As can be seen in Eq.(3.5.26)-(3.5.28), for a short T_2, the polarization described by u and v in the Bloch equations assumes a steady state value of $u = 0$ and $v = \kappa \varepsilon T_2 w$ for $\Delta = 0$, yielding a self-contained equation for the population w. Comparison of Eq.(5.1.5) and Eq.(3.5.28) identifies the induced transition rate R as $\kappa^2 \varepsilon^2 T_2 / 2$. In terms of the threshold intensity, I_s, for a Bloch susceptibility introduced in Eq.(3.7.11), the rate equation Eq.(5.1.5) can be rewtitten as follows.

$$\frac{dw}{dt} = -\frac{I}{I_s}\frac{w}{T_1} - \frac{w+1}{T_1} \tag{5.1.6}$$

158

From saturable absorption measurements, we can estimate the nonlinear refractive index n_2. The nonlinear optical susceptibility $\chi(\omega)$ for a Bloch type system is given by

$$\chi(\omega) = \left(\frac{\alpha_0 c}{4\pi\omega}\right)\left(\frac{\Delta + i}{1 + \Delta^2 + I/I_s}\right) \tag{5.1.7}$$

where α_0 is the linear absorption coefficient, Δ is the atomic detuning, $(\omega - \omega_a)T_2$, and I_s is the saturation intensity. The nonlinear refractive index n_2 is the derivative of the intensity dependent refractive index n with respect to the intensity I, so for this model

$$n_2 = \frac{1}{3}\left(\frac{4\pi}{n_0}\right)^2 \chi^{(3)} = -\left(\frac{\alpha_0 \lambda}{4\pi I_s}\right)\left(\frac{\Delta}{(1 + \Delta^2)^2}\right) \tag{5.1.8}$$

The maximum n_2 occurs for an atomic detuning, $\Delta = 1/\sqrt{3}$, and the corresponding n_2 is simply $\pm 0.026\lambda\alpha/I_s$. Once the saturable absorption threshold intensity is measured, we can obtain the value of n_2 in a straightforward way.

5.2 Dynamical Transmission

The pulse duration dependence of the saturable absorption threshold intensity is well explained in terms of a two-level molecular system interacting with resonant incident light.[11]−[12]

$$\frac{\partial n(x,t)}{\partial t} = -I(x,t)\sigma\left[n(x,t) - (N_0 - n(x,t))\right] - \frac{n(x,t)}{\tau_s} \tag{5.2.1}$$

$$\frac{\partial I(x,t)}{\partial x} = -I(x,t)\sigma\left[(N_0 - n(x,t)) - n(x,t)\right] \tag{5.2.2}$$

where N_0 is the total number of molecules per unit volume, $n(x,t)$ is the number of molecules in the excited state at the depth x and time t, σ is the absorption crosssection per molecule, and τ_s is the radiative decay time of the molecular excited state.

The above two equations can be reduced to one equation for the transmission $T(x,t)$. Taking the time derivative of Eq.(5.2.2),

$$\frac{\partial^2 I}{\partial t \partial x} = -\frac{\partial I(x,t)}{\partial t}(N_0 - 2n)\sigma + 2I(x,t)\frac{\partial n}{\partial t}\sigma \tag{5.2.3}$$

159

Substituting Eq.(5.2.1) and Eq.(5.2.2) into Eq.(5.2.3) yields

$$\frac{\tau_s}{N_0\sigma}\frac{\partial^2 \ln I}{\partial t \partial x} + 2\frac{\tau_s}{N_0}\frac{\partial I}{\partial x} + \frac{1}{N_0\sigma}\frac{\partial \ln I}{\partial x} + 1 = 0 \qquad (5.2.4)$$

Integrating Eq.(5.2.4) in x, we get

$$\frac{\tau_s}{N_0\sigma}\left(\frac{\partial \ln I(x,t)}{\partial t} - \frac{\partial \ln I(0,t)}{\partial t}\right) + 2\frac{\tau_s}{N_0}(I(x,t) - I(0,t))$$

$$+ \frac{1}{N_0\sigma}(\ln I(x,t) - \ln I(0,t)) + x = 0 \qquad (5.2.5)$$

Now let the incident pulse shape $f(t)$ normalized by the intensity, i.e.

$$I(0,t) = I_0 f(t) \qquad (5.2.6)$$

As the light pulse passes through the absorbing molecule, the pulse shape experiences distortion as well as attenuation. The change in the pulse shape can be expressed by defining a transmission function $T(x,t)$ at the depth x and at time t, i.e.,

$$I(x,t) = I_0 f(t) T(x,t) \qquad (5.2.7)$$

Now the dynamic transmission can be written in terms of $T(x,t)$,

$$\frac{\partial \ln T(x,t)}{\partial t} + \frac{1}{\tau_s}\ln T(x,t) = 2\sigma I_0 f(t)(1 - T(x,t)) - \frac{N_0\sigma x}{\tau_s} \qquad (5.2.8)$$

Noting that the transmission at low intensity is given as

$$T_0 = \frac{I}{I_0} = e^{-N_0\sigma x} \qquad (5.2.9)$$

we get the final expression for the dynamical transmission.

$$\frac{\partial \ln T(x,t)}{\partial(t/\tau_s)} + \ln T(x,t) = 2\sigma\tau_s I_0 f(t)(1 - T(x,t)) + \ln T_0 \qquad (5.2.10)$$

where I_0 is the incident light intensity, T_0 is the low intensity transmission, and $f(t)$ is the incident light pulse profile. For an incident light pulse with a temporal shape of the following form (Figure 5.1),

$$f(t) = \frac{1}{2}[1 - \cos(\frac{2\pi t}{\tau_p})] \qquad (5.2.11)$$

160

a numerical solution of Eq.(5.2.10) is obtained for various incident intensities, I_0, and pulse widths, τ_p. The low intensity transmission, T_0, is taken as $10^{-0.8}$ or $e^{-1.8}$. The output temporal shape is shown for various pulse widths in Figure(5.2)-(5.12), with the intensity $\beta = I_0 \sigma \tau_s$ varying over 1000, 500, 300, 100, 50, 30, 10, 5, 3, 1, 0.5, 0.3, 0.1. Each figure corresponds to a fixed pulse width with each intensity maximum (top) and minimum (bottom).

Figure(5.13) shows the results of a numerical analysis of the dynamic transmission equation describing an interaction of a two level system with the incident resonant light for various pulse widths, where the estimated radiative lifetime of the excited state is 1 ns. We find that the threshold power for saturable absorption decreases for an increased pulse width. But this trend saturates as shown for the ratio 10 and 10^4. This can be accounted for by considering the total number of photons incident on a Bloch type system. For a light pulse with pulse width much shorter than the excited state radiative decay time, what really counts is the total number of incident photons because all the incoming photons can be stored in the excited state. In the case of a long pulse with a pulse width longer than the radiative decay time, the saturable absorption can be understood as a balanced state of absorption and emission in a steady state, and, therefore, there is not much difference between a long pulse and a very long pulse. The dynamical transmission behavior itself can be used as an indirect way to estimate the radiative decay time. Once the threshold intensities for two short pulses with different pulse widths are known, the ratio of the experimental threshold intensities can be compared with the ratio obtained from the numerical analysis result, which can be simply read off from Figure(5.13). As will be discussed in Sec.5.4.3, the estimated life time of the excited state obtained in this way is in a quite good agreement with the independent measurements of the radiative decay life time for phthalocyanine molecules.

5.3 Intersystem Crossing

When the energy of the singlet and the triplet states are degenerate, the triplet state has a lower energy than the singlet state. This, of course, is the Hund's rule, and the physical explanation is simple for a two-electron system. In the triplet state, the spin-wavefunction is symmetric and the spatial wavefunction is antisymmetric. In the relative coordinate the antisymmetry means that it has odd parity under the inversion operation, i.e., $\vec{r} \rightarrow \quad -\vec{r}$. Then the antisymmetric wavefunction has node at the origin, or the wavefunction in the relative coordinate vanishes near the origin. Equivalently, the wavefunction of each electron has the least overlap, therefore the Coulomb repulsion is smaller and the total energy is lower than the singlet state. This idea holds even for a many-electron system. In most stable molecules the ground state is singlet and the lowest excited state is triplet. (One well-known exceptional example is the oxygen molecule, which has the triplet ground state.)

The energy states of molecule can be classified by the parity symmetry. States with parity even under inversion are called g (gerade) states, while states with parity odd under inversion are called u (ungerade) states. Both the singlet state and the triplet state have a series of different spatial parities associated with them. In general the ground state is singlet with g parity (S_0). Once the molecule is excited to the first excited singlet state (S_1, this has u parity owing to the dipole selection rule), it can decay only to the singlet states with g parity through the dipole radiation since the dipole interaction has no spin flop in it. But if there is spin-orbit coupling present, this can give a first-order perturbative admixture of singlet states to the triplet state allowing the dipole transition from the singlet u state to the triplet g state.

Let's consider the spin-orbit coupling in more detail.[13]−[20] An electron with spin 1/2 has the magnetic dipole moment.

$$\vec{\mu} = -\frac{g|e|}{2mc}\vec{S} \tag{5.3.1}$$

162

where g is the gyro-magnetic constant. The interaction Hamiltonian is

$$
\begin{aligned}
H_1 &= -\,\vec{\mu} \bullet \vec{B} = -\frac{\vec{\mu}}{2} \bullet (\vec{E} \times \frac{\vec{v}}{c}) \\
&= \frac{|e|}{2mc^2}(\vec{E} \times \vec{v}) \bullet \vec{S} = \frac{|e|}{2m^2c^2}(\vec{E} \times \vec{p}) \bullet \vec{S} \\
&= \frac{1}{2m^2c^2}(|e|\vec{E} \times \vec{p}) \bullet \vec{S} = \frac{1}{2m^2c^2}(\vec{\nabla}V \times \vec{p}) \bullet \vec{S} \\
&= \frac{1}{2m^2c^2}\frac{1}{r}\frac{\partial V}{\partial r}(\vec{r} \times \vec{p}) \bullet \vec{S} = \frac{1}{2m^2c^2}\frac{1}{r}\frac{\partial V}{\partial r}\vec{L} \bullet \vec{S} \\
&= \xi \vec{L} \bullet \vec{S}
\end{aligned}
\tag{5.3.2}
$$

where the potential is assumed to be central,

$$
V = V(r) \tag{5.3.3}
$$

$$
\begin{aligned}
\vec{F} &= e\vec{E} = -|e|\vec{E} \\
&= -\,\vec{\nabla}V = -\frac{\partial V}{\partial r}\hat{r} = -\frac{\partial V}{\partial r}\frac{\vec{r}}{r}
\end{aligned}
\tag{5.3.4}
$$

and ξ is defined as

$$
\xi(r) = \frac{1}{2m^2c^2}\frac{1}{r}\frac{\partial V(r)}{\partial r} \tag{5.3.5}
$$

For a multi-electron system we have a similar interaction Hamiltonian.

$$
H_1 = \frac{1}{2m^2c^2}\sum_i\left(\frac{1}{r_i}\frac{\partial V(r_i)}{\partial r_i}\right)\vec{l}_i \bullet \vec{s}_i = \sum_i \xi(r_i)\vec{l}_i \bullet \vec{s}_i \tag{5.3.6}
$$

with

$$
\xi(r_i) = \frac{1}{2m^2c^2}\frac{1}{r_i}\frac{\partial V(r_i)}{\partial r_i} \tag{5.3.7}
$$

In order to estimate the magnitude of the spin-orbit coupling, we note that the radial wavefunction $\xi(r)$ has the form,[*]

$$
\xi(r) = \frac{Ze^2}{2m^2c^2}\frac{1}{r^3} \tag{5.3.8}
$$

163

Then the magnitude is given

$$\zeta_{nl} = \hbar^2 \langle R(r)_{nl} | \xi(r) | R(r)_{nl} \rangle = \hbar^2 \int_0^\infty R^2(r)_{nl} \xi(r) r^2 \, dr \qquad (5.3.9)$$

Noting

$$\langle R_{nl} | r^{-3} | R_{nl} \rangle = \langle r^{-3} \rangle = Z^3 a_0^{-3} (n^3(l+1)(l+\frac{1}{2})l)^{-1} \qquad (5.3.10)$$

$$\zeta_{nl} = \frac{e^2 \hbar^2}{2m^2 c^2 a_0^3} \frac{Z^4}{n^3(l+1)(l+\frac{1}{2})l} \qquad (5.3.11)$$

Therefore the magnitude of the spin-orbit coupling has Z^4 dependence, i.e.,

$$\langle H_1 \rangle_{nl} \propto \zeta_{nl} \propto Z^4 \qquad (5.3.12)$$

The coupling of the triplet state to the differnt singlet states is determined by the group properties of the angular wavefunctions. For a discussion of the selection rule in the intersystem crossing for a multi-electron system, refer to Appendix A7.

In the absence of intersystem crossing (ISC), the spin singlet states and triplet state are completely independent manifold of states where no overlap of wavefunction can occur. But a nonvanishing matrix element between singlet states and triplet states through spin-orbit coupling means that there is another decay channel for an excited singlet state. (Figure 5.14) The decay rate from S_1 to T_1 is much larger than the decay rate from T_1 to S_0, the reason being that the ground state S_0 has no life-time line broadening while S_1 and T_1 are already broadened from a finite life-time. Usually ISC between S_1 and T_1 affects the effective decay time of the excited state S_1. A large ISC corresponds to a short effective life time, and a heavy atom substituted molecule shows a dramatic change in the radiatve decay time. One well-known example is bis (4-dimethylamino-dithiobenzil) nickel (BDN) dye.[21][22] When dissolved in 1-2-dichloro-ethane, the principal optical excitation state (singlet S_1) of BDN dye has a relatively long life time, which allows BDN dye as a Q-swiching dye in Nd:YAG laser. However, in iodine-ethane solvent, ISC

164

is enhanced by a heavy atom substitution effect, resulting in a short life time of S_1 state, which allows BDN dye as a mode-locking dye as well as Q-switching dye. The phthalocyanine molecule is another example, where the central atom determines ISC rate. For a various phthalocyanines with different central atoms, refer to Table5.1. Compared to BDN dye, the heavy atom substitution effect is smaller, but still ISC allows one to control the effective radiative decay time and the saturation threshold power.

5.4 Saturable Absorption Experiments

5.4.1 Light Source and Detectors

(A) Stimulated Raman Scattering Cell

In order to study the saturable absorption property of SINC we need an intense coherent monochromatic light source. Because the absorption peak positions in the near IR, we need a tunable light source. For a pulsed laser we employed a Raman cell pumped by a picosecond or a nanosecond Nd:YAG laser. Various wavelengths available through stimulated Raman scattering from hydrogen molecules and methane molecules are listed in Table5.2. For a pure SINC film with peak maximum at 810 nm, the first anti-Stokes line 813 nm from a methane Raman cell pumped with a fundamental Nd:YAG was used, while for a solid solution and a liquid solution SINC the second Stokes line 770 nm from methane Raman cell pumped with a SHG of Nd:YAG was close to the absorption maximum. At a 300 *psi* pressure of methane gas in a 1 meter long 1 inch diameter stainless steel Raman cell with 1 inch thick fused quartz windows at both ends, the needed Raman line was easily available for 30 picosecond and 10 nanosecond Nd:YAG laser pumping. The pump beam was gradually focused in the middle of Raman cell to increase the interaction length for Raman conversion.

A mode-locked and Q-switched Quantel YAG501 picosecond laser system provides a typical pulse with energy of 30 mJ per pulse, bandwidth of 30 GHz, and pulse width 30 ps. By varying the output resonant reflector (etalon) the pulse width of YAG501 laser can be varied from 30 ps to 200 ps, and the laser bandwidth is determined by the convolution of the uncertainty principle and the intrinsic gain medium band width. With this picosecond pumping a Raman output with energy of 200 μJ per pulse with the same bandwidth and a pulse width shortened by a nonlinear Raman process by a factor of square root 2 was obtained at 813 nm, and 770 nm. The autocorrelation of the picosecond Raman output 813 nm was taken to make sure the picosecond pulse width. A nonlinear optical material transparent at doubled Raman output was used, and a simple alkaline photo-cathode PMT was used. The autocorrelation trace is shown in Figure(5.15), where one division in the horizontal scale corresponds to 30 picosecond.

For a nanosecond laser pulse, the Quanta-Ray DCR Nd:YAG laser was employed providing a Q-switched, 10 ns pulse with a typical energy of 100 mJ per pulse and bandwidth of 30 GHz. The DCR laser is designed for an unstable resonator for a maximum power out of the laser oscillator, hence, the laser intensity has a large fluctuation. The Raman conversion efficiency was lower for a nanosecond pulse giving a typical output of 20μJ at 813 nm.

The Raman line used in the experiment was singled out by an interference filter commercially available. Figure(5.16) shows the transmission spectrum of the spike filter from Ealing Optics (35-4407) at normal incidence. The peak transmission position can be continuously varied by tilting the interference filter, and for 770 nm Raman line selection we used the same filter just by tilting slightly.

770 nm and 813 nm is near IR, and human eye loses senitivity there. For the beam alignment purpose RCA CCTV camera (120 VAC, 60 HZ, TC 1500) was employed because the silicon detector inside the camera has the spectral senitivity far down near 1 μm. Sometimes a fluorescent paint (Flurescent Poster Color, 520-

166

Orange, Liquitex) on a paper can be used to find infrared light.

(B) CW Dye Laser

Although a methane Raman cell is appropriate for the saturable absorption study near absorption peak, it doesn't provide a continuously tunable wavelength for the study of the frequency dependent saturable absorption. We employed a C.W. ring dye laser for a tunable light source. Spectra-Physics 380B Ring Dye laser provided a stable monochromatic frequency between 790nm to 860 nm when LDS 821 (another name; Styryl 9) dye was used. The molecular weight of LDS 821 dye is 515.1, and the concentration of dye for Ar^+ pumping is 920 mg/liter in the solvent of 150 ml prophylene carbonate and 850 ml ethylene glycole, which correponds to 1.8×10^{-3} mole/liter. When pumped with an 8.0 Watt of Ar^+ laser, LDS 821 dye operated Ring dye laser gave nearly 200 mW output.

An acousto-optic modulator (AOM) driven by an AM-FM modulator can deflect the C.W. beam providing micosecond pulses. [23][24] Refer to Figure(5.17). The deflected laser beam after AOM crystal is upshifted or down shifted in the frequency. By AM (amplitude modulation) the intensity of the deflected light is modulated, and by FM (frequency modulation) the frequency of the laser beam is shifted by the driving frequency. Acousto-optical modulator from NRC is AOM tellurium dioxide (TeO_2) crystal (N23080) and the driver for that is model N21080-1SAS. The driving frequency is $80 \pm 5 MHz$.

In the AOM the diffracted angle depends on the acousto-optical properties of crystal, which is given as follows,

$$\theta_B = \sin^{-1} \frac{\lambda}{2n\Lambda} = \sin^{-1} \frac{\lambda f}{2nv} \approx \frac{\lambda f}{2nv} \qquad (5.4.1)$$

where $\Lambda = v/f$ is the spacing between nodes of a standing sound wave inside AOM crystal, n is the refractive index of the medium, v is the phase velocity of sound, and f is the driving sound frequency. The diffraction efficiency depends on the material parameters, and TeO_2 is found to have the largest figure of merit.

A function generator (Wavetek model 275, 12 MHz, programable arbitrary/ function generator) was used to provide a triangular wave form to the AOM driver after the negative part of triagular wave was filtered by a Shottky n^+-n diode (HP 5082-2835).

(C) Light Detectors[25]

In Figure(5.18) is shown the circuit diagram of photodiode and a schematic sketch of a diffusor box used in a saturable absorption experiment. Usually a stimulated Raman scattering output from a Raman cell has an appreciable fluctuation in the beam direction. A non-uniformity in the photo response along the photodiode surface itself can give an artifact signal shown up as a nonlinear optical response of the sample. In order to get rid of this problem, we made a diffusor box such that the laser beam does not hit the photodiode directly. Once the laser beam is scattered by the beam blocker, it bounces off the inside wall of magnesium (Mg) coated box and only a small fraction of the incident power hits the photodiode. During bouncing off the inside wall, the light beam loses its information on the original incident beam direction. With this design the fluctuation in a signal caused by the fluctuation in the beam direction was reduced dramatically, allowing an intensity measurement insensitive to the beam direction fluctuation. The signal level after a diffusor box is too low to be integrated and read in a CAMAC charge integrator. A high bandwidth preamplifier was designed to amplify the signal from the photodiode. Circuit diagram for the preamplifier is shown in Figure(5.19).

A typical PIN photodiode circuits are shown in Figure(5.20) for a negative polarity and in Figure(5.21) for a positive polarity. A silicon photo diode junction (typical active area of 0.5 mm^2) has a quantum efficiency of 70% (0.7 electron/photon) at 810 nm, which corresponds to the sensitivity of 0.7e/1.5 eV $\approx$ 0.5 A/W. The quantum efficiency can be used as a reference for the estimate in the power measurement of a laser light. For example, 1 Volt signal output at 50 Ω load

resistor with a FWHM of 1 ns corresponds to 20 mA $\div$0.5 A/W $\times$ 1 ns = 4×10^{-11} Joule. The corresponding energy density will be 4×10^{-11} Joule/0.5 mm^2 = 8×10^{-9} Joule/cm^2.

When another calibrated power meter is available such as Coherent power meter model 212, a particular photo diode can be calibrated. Given a C.W. light source such as HeNe laser, an average C.W. power can be read from a simple digital voltmeter (for example, Fluke multimeter, which has an input resistance 10 MΩ) connected to a parallel load resistor for a photo diode. For example, 1 Volt reading at Fluke meter across 1 MΩ load resistor gives a photo current of 1.0 V / 0.9 MΩ = 1.1 μA. (Note that the voltage ($\approx$ 1 V) should be much smaller than the bias voltage ($\approx$ 20 V)) At HeNe frequency, a quantum efficiency 70 % corresponds to 0.37 A/W. Therefore 1.0 V reading at a Fluke meter corresponds to 1.1 μA $\div$ 0.37 A/W $\approx$ 3 μW. Accounting for the beam size of HeNe (say 0.5 cm^2) and the photo diode active area (0.5 mm^2), the C.W. power of HeNe measured by a photo diode will be 3μW $\times$ 0.5 cm^2 $\div$ 0.5 mm^2 = 300 μW. This value can be compared with a value measured by a calibrated power meter, giving us the calibration for the power measurement at a pulsed laser experiment.

The resistor value at the bias voltage is determined by the current limit for the photodiode. For example, with a 20 V bias voltage and 10 kΩ resistor the maximum current allowed is 2 mA in CW operartion, and the maximum dissipation CW power allowed is 40 mW. For a typical 10 nsec laser pulse with a 10 Hz repetition rate, the maximum of 4 mJ/10 nsec peak power, or order of 10^3 V can appear in a 50Ω load resistor. For a very weak light with a photo current on the order of nA, a large impedence load resistor (1MΩ) is required to get an observable signal on a scope. In a short pulse experiment where time response of each pulse is monitored, the load resistor shoud be 50Ω to get rid of any ringing coming from an impedence mismatching. Some electrical dividers for 50Ω impedence cable are shown in Figure(5.22) (5.23).

In a pulsed operation of a PIN photodiode, we need a quick response of the detector. The capacitor works as a temporary battery to follow a surge in the current drawn by the photodioide upon the incident photons. The magnitude of a capacitor is chosen such that the relaxtion time for the RC circuit (load resistor 50 Ω and the capacitor connected serially to the load resistor) should be longer than the pulse width. A typical RC relaxtion time is 50 $\Omega \times 10$nF = 500 nsec, allowing the circuit shown in Figure(5.20) (5.21) good for a picosecond pulse experiment. Note that it is better to use a high-voltage rating capacitor (for example, 5nF of 0.005P, 1 kV, Z5U) to prevent the capacitance from changing upon a large current drawing for a short time, which results in ringing. It is also important to use a BNC cable along the signal path (RG 174) and to insulate photo diode and BNC connector (UG-657, or RG-58 A/U, RG-58 C/U, 50Ω cable) for signal from the housing box.

A PIN photodiode can be used with a zero bias voltage, in which case there is no dark current, allowing a high sensitivity. Once the right load resistor is used, it can measure a signal as small as the dark current. But in the absence of a bias voltage the response time is very slow, on the order of 10μsec. A no-bias-voltage configuration is ideal for monitoring a weak CW power, and the circuitary is basically the same as that of a solar cell. In fact a commercial Coherent power meter (model 212) makes use of a no-bias-voltage configuration.

When a higher gain is needed without complicating circuitary, another type of photo diode is available. An avalanche photo diode has a gain of order of 200, compared to a regular PIN photodiode which has no gain. It can be operated in either a normal linear reverse biasing mode ($V_{reverse} < V_{break\ down}(\approx 240$ V$)$) or Geiger mode ($V_{reverse} > V_{break\ down}$). A typical circuit diagram is shown in Figure(5.24). The resistor value is determined from the maximum C.W. current rating, which is 200μA typically. In a 50 Ω scope, the maximum size of signal is only 10 mV, which means it needs a voltage amplifier.

For a detection of a very weak optical signal, it is necessary to use a photo

170

multiplier tube (PMT). The quantum efficiency of a photo cathode for a PMT is much lower compared to that of a PIN photodiode. Usually it peaks near UV (400 nm), differently from photodiode. But the photocurrent is amplified with a gain of order of 10^5 at dynode stages. There are different kinds of materials for photocathodes, and the right one should be chosen depending on the individual applications. S1 photocathode[26]−[29] has a nonvanishing quantum efficiency (less than 0.1 %) even down to 1.2 μm, and is useful for an infrared applications. It is mainly composed of overlayer of Cs (cesium) on silver and oxigen. Even if Cs has the photoelectric response only up to 800nm, a surface enhancement[30] due to silver particle makes S1 photocathode sensitive down to 1.2μm. GaAs (Cs) semiconductor photocathode (for example, RCA C31034 series) has a rather broad spectral response (185 nm to 930nm), and is a popular PMT photo cathode. However, one disadvantage of a semiconductor photocathode is that the qunatum efficiency is highly sensitive to temperature changes, and a rather large dark current should be decreased by cooling the PMT housing. When a relatively large current is drawn from dynode stages, it is important to separate dynode resistors from the photocathode to prevent a temperature rise.

When a large dynamical range of light intensity is covered by a PMT, the linearity of anode current (I_p) and the divider current (I_b) should be checked carefully. In Figure(5.25) is shown a typical voltage divider circuit for a D.C. and pulsed operation of PMT. In a D.C. operation the capacitor (C_1 and C_2) should be removed. Anode ground configuration eliminates the potential difference between the external circuit and the anode, and allows the use of the load resistor as a current-to-voltage converter. I_p is the anode current, while I_b is the divider current. In a normal operation of PMT, I_p is much smaller than I_b. At the bottom of Figure(5.25) is shown a linearity curve for the ratio of anode current to divider current versus the photon flux. In a region A, it is linear, and PMT output voltage appearing across the load resistor R_L is linearly proportional to the incident light

intensity, because the anode current I_p is negligible compared to the divider current I_b. For a higer light intensity (region B), I_p increases and becomes nonnegligible compared to I_b. Hence, the voltage between the last dynode and the anode determined by the current I_b - I_p decreases, resulting in a higher H.V. distribution among the lower dynodes. This shows up as an apparent increase in the PMT gain, yielding a nonlinear current amplification. When the light intensity is further increased (region C), the voltage across the last dynode and the anode is almost zero because I_b - I_p is almost vanishing. The electron collection efficiency of the anode is saturated, and the current is lower than it should be. In order to maintain the operation in region A, the maximum practical anode current, I_p, is less than 1/20 of the divider current, I_b, where the divider current is simply determined by the magnitude of the total serial divider resistances. A typical total value of resistor is 500 kΩ at a 10 stages dynode. The corresponding divider current is 200 μA, and the maximum allowed anode current will be 10 μA. A typical maximum rating for the anode current is 1μA, still one ord $_{\text{-}}$ of magnitude below the maximum allowed current. When a higher anode current is needed, one can increase the divider current by reducing the divider resitor. But in this case care should be taken to get rid of the heat generated from the power dissipation in divider circuit, since the increased temperature increases the dark current of PMT. In a pulsed operation, a capacitor should be connected at the last couple of dynode stages to provide current surge at a short time period. A typical PMT circuit is designed for a scintillation counting detector, in which case the pulse width is order of μsec with a very low duty cycle. The maximum current that can be drawn from the capacitor is of the order of CV/100. For example, the capacitance of 0.02μF for C_1 at a 100 V last stage voltage can allow upto 0.02 μCoulomb of electrical charge.

5.4.2 Experimental Layout ‘

Saturable absorption behavior of individual π-electron optical excitations

172

within the Q-band of the thin films was investigated as a function of the pulse duration and wavelength of the incident beam. The experimental layout for saturable absorption measurement of SINC thin film is shown in Figure(5.26). Either the fundamental or the SHG line of a Nd:YAG (either nanosecond or picosecond) pumped methane Raman cell was used to produce Raman lines near absorption peak maxima (813 nm for pure dye and 770 nm for solid solution). Polarization of the pump beam was controlled by a half-wavelength wave plate to give an s-polarization configuration. In s-polarization the electric field is perpendicular to the optical plane at the pellicle beam splitters (Ealing Optics 22-8916), and no Brewster angle exists at the beam splitters, giving a much less scattering in the beam direction after reflection off the beam splitter.

A pellicle beam splitter is preferred to a glass slide beam splitter because the interference between reflections from the front and the back surfaces of a thin pellicle beam splitter (thickness of 8μm) is widely spaced. In Figure(5.27) is shown a transmission spectrum measured at a spectrophotometer. The inteference pattern is clearly visible, and the thickness of pellicle beam splitter can be readily read off from this interference pattern. One thing that we have to be careful in using the pellicle beam splitter is that it is birefringent in general, and it is necessary to orient such that the optical axis of the beam splitter is along the beam polarization.

The light intensity is varied by rotating a variable neutral density filter, and also by moving in and out of the focus of the focused beam inside a pair of positive lens. In this way a large dynamical range of light intensity could be covered. At a fixed position of beam waist, the intensity was varied by a variable neutral density filter, and the reversibility of saturable absorption was checked carefully. A CAMAC charge integrator (LeCroy 2249W ADC) with a CAMAC controller (KineticSystems 3912 Unibus Crate Controller) in a CAMAC crate (KineticSystems 1510 Power Crate Unit) was connected to a PDP-1123 microcomputer to get a digitized signal. Part of a fundamental beam was fed into a discriminator (LeCroy Model 121) to

generate a gate pulse for the charge integrator. The reference and the sample analog signal from the respective photodiode/preamplifier were integrated over the gate pulse width ($\approx$ 40 ns), and were stored in the microcomputer. The ratio was taken and plotted.

The laser power was measured by a Scientech power energy meter (model 362), and also was checked with a power meter made of 4 thermocouples (Figure(5.28))

5.4.3 Measurement and Analysis

Figure(5.29) shows the incident light intensity dependence of the absorption coefficient αL in pure dye film for 30 ps (circles, pure SINC dye; triangles, SINC solid-solution) and 10 ns (squares, pure SINC dye) pulses, respectively. The change in the absorption was reproducible through many cycles of increased and decreased incident light intensity. Data points for 10 ns are more scattered owing simply to power fluctuations in Nd:YAG pump laser. Here if the light intensity was increased more than the maximum of the data points, i.e. 30 MW/cm^2 for 30 ps pulses and 200kW/cm^2 for 10 ns pulses, an irreversible change was observed in the film, which is apparently from the mass transportation of the dye film along the substrate surface. When compared with a pure dye film, we can see that the solid solution thin film shows exactly the same saturable absorption behavior, but no irreversible change was observed upto the incident intensity of 4GW/cm^2. Saturable absorption is also studied in a liquid solution sample. Figure(5.30) shows the saturable absorption observed in a liquid solution for 30 ps pulse.

In Figures(5.29) and (5.30), the solid lines are least square fits to a Bloch-type saturable absorption

$$\alpha(I)L = \frac{\alpha_0 L}{1 + I/I_s} + \alpha_B L \qquad (5.4.2)$$

where I_s is the threshold intensity for the saturation, $\alpha_0 L$ gives the low intensity linear absorption, and $\alpha_B L$ is the unsaturable background absorption. Importantly,

174

$\alpha_B L$ was found to be zero for both films. In case of the pure dye film, the threshold intensities for saturation were 100MW/cm^2 and 440kW/cm^2 for 30ps and 10ns pulses, respectively. The threshold intensity for 10ns pulse is lower than that for 30ps pulse, but this trend saturates at or near the 10μs scale. The difference in the threshold intensities for saturation can be easily understood in the dynamical transition analysis discussed in Sec.5.2. Recalling that the saturation intensity I_s can be obtained for a given pulse width τ_p and excited state life time τ_s from a numerical simulation of the dynamical transmission equation, the ratio of saturation threshold for two given pulse widths can be used to determine the excited state radiative decay time τ_s uniquely. Using 230 as the ratio of threshold intensities at 30 psec and 10 nsec as determined from our experiment, we find the exited state life time to be 5 nsec, in good agreement with previous independent relaxation measurements on related structures, as discussed in Sec.4.1.

For the solid solution thin film, the threshold power for 30ps pulse was 100 MW/cm^2, which is the same value as that of the pure dye film. The fact that the saturable absorption behavior is identical for both pure dye and solid solution film can be accounted for by the absence of any positional, orientational and phase coherence between molecular sites in the thin film phase, and from this we can conclude that the on-site π-electron excitations of the Q-band in individual molecular sites are responsible for the large resonant nonlinear optical response. A least squares fitting for the liquid solution data gives the threshold power of 30MW/cm^2 for a 30 ps pulse, which is lower than the threshold power for thin films. There may be couple of explanations for that. First of all, the homogeneous broadening mechanism in a liquid solution sample is different from that in a thin film, and the laser light with a given bandwidth might work more efficiently for a liqiud solution. Another possibility might be that the effective radiative decay time might be longer for a liquid solution sample, reducing the threshold power for saturation. At any rate the data shows that there is a zero unsaturable background absorption in a liq-

uid solution, which reconfirms our understanding of the optical excitation in SINC molecule as an on-site π-electron excitation at the individual molecule.

Once the saturation threshold intensity is measured, the nonlinear refractive index n_2 can be obtained in a straighforward way by substituting all of the material parameters in the expression for n_2, Eq.(5.1.8). For a SINC pure dye thin fim, the linear absorption coefficient, α_0, is $\sim 10^5$ cm^{-1} at $\lambda = 810$ nm. For a C.W. saturation intensity, we can interpolate from nanosecond data as 400 kW/cm^2. From these experimetal values, we obtain a value of n_2 for the pure SINC dye film of 1×10^{-4} cm^2/kW.

5.5 Dispersion of Saturable Absorption

To fully characterize the nonlinear absorption properties of the thin film, we measured the dispersion of the Q-band saturable absorption. A tunable (790-860 nm) 10 μs pulse was obtained by chopping an Ar$^+$ pumped cw ring dye laser output (LDS 821 dye opreration) by an acousto-optic modulator. The first order of deflected light can be tailor shaped by amplitude modulating the radiofrequency acoustic wave at AOM driver. A relatively long (order of μsec) pulse was readily obtained by a function generator, and the beam was focused on the thin film sample. Refer to Figure(5.31).

The dispersion of the saturable absorption of the pure dye thin film for the fixed incident intensity 80kW/cm^2 is compared in Figure(5.32) with the linear absorption spectrum. It is clear that the change in the absorption is maximum on resonance and is decreased in moving away from the peak. The dashed lines are a least squares fit to a Gaussian envelope model for the linear absorption, and the dispersion was derived from the Kramers-Kronig relations. For a discussion of Kramers-Kronig relation, refer to Appendix A8. The dotted lines are the fitted curves for the saturable absorption and dispersion. We can see that the maximum

176

change of refractive index as obtained from Eq.(5.1.8) occurs at $\lambda = 776$ nm, and the maximum n_2 at $\lambda = 776$ nm results from a linear superposition of the refractive index change of each homogeneously broadened resonance with the inhomogeneously broadened envelope.

In conclusion, we have demonstrated that a quasi-two dimensional π-electron structure such as SINC can be designed as wide area, spin coatable nonlinear optical films and that these can be represented as a microscopic composite system of molecular optical sites in a TLS-glass random medium. The resonant nonlinear optical properties of homogeneously broadened lines contained in the inhomogeneously broadened Gaussian envelope were directly investigated by standard saturable absorption measurements. These results showed for the SINC pure dye films that saturable absorption occurs at the peak maximum of the low frequency Q-band near 810nm with essentially zero unsaturable absorption background and that on-site π-electron excitations of the Q-band in individual molecular sites are responsible for the large resonant nonlinear optical response n_2 of 1×10^{-4} cm^2/kW at 810nm.

References: Chapter 5

[1] Kosonocky, W.F. and Harrison, S.E., J. Appl. Phys. **37**, 4789 (1966)

[2] Armstrong, J.A., J. Appl. Phys. **36**, 471 (1965)

[3] Hercher, M., Chu, W., and Stockman, D., IEEE. J. Quantum Elec. **QE-4**, 954 (1968)

[4] Seldon, A.C., IEEE. J. Quantum Elec. **QE-5**, 523 (1969)

[5] Ho, Z.Z., Ju, C.Y., and Hetherington III, W.H., J. Appl. Phys. **62**, 716 (1987)

[6] Chemla, D.S., Miller, D.A.B., Smith, P.W., Gossard, A.C., and Wiegmann, W., IEEE. J. Quantum Elec. **QE-20**, 265 (1984)

[7] Lee, Y.H., Chavez-Pirson, A., Koch, S.W., Gibbs, H.M., Park, S.H., Morhange, J., Jeffery, A., Peyghambarian, N., Banyai, L., Gossard, A.C., and Wiegmann, W., Phys. Rev. Lett. **57**, 2446 (1986)

[8] Gibbs, H.M., Gossard, A.C., McCall, S.L., Passner, A., Wiegmann, W., and Venkatesanm T.N.C., Solid State Comm. **30**, 271 (1979)

[9] Knox, W.H., J. Opt. Soc. Am. **B4**, 1771 (1987)

[10] Fox, A.M., Maciel, A.C., Shorthose, M.G., and Ryan, J.F., Appl. Phys. Lett. **51**, 30 (1987)

[11] Gires, P.F. and Combaud, F., J. Physique, **26**, 325 (1965)

[12] Seldon, A.C., Brit. J. Appl. Phys. **18**, 743 (1967)

[13] McGlynn, S.P., Azumi, T., and Kinoshita, M., *Molecular Spectroscopy of the Triplet State*, Prentice-Hall, New Jersey, (1969)

[14] Steinfeld, J.I. *An Intrioduction to Modern Molecular Sepctroscopy*, 2nd ed. MIT Press, Cambridge (1984)

[15] McClure, D.S., J. Chem. Phys. **17**, 905 (1949); J. Chem. Phys. **20**, 682 (1952)

[16] Weissman, S.L., J. Chem. Phys. **18**, 905 (1950)

[17] Goodman, L. and Krishna, V.G., Rev. Mod. Phys. **35**, 541 (1963)

[18] Kearns, D., J. Chem. Phys. **36**, 1608 (1962)

[19] Robinson, G.W. and Frosch, R.P., J. Chem. Phys. **38**, 1187 (1963)

[20] Strickler, S.J. and Berg, R.A., J. Chem. Phys. **37**, 814 (1962)

[21] Drexhage, K.H. and Reynolds, G.A., Opt. Comm. **10**, 18 (1974)

[22] Magde, D., Bushaw, B.A., Windsor, M.W., Chem. Phys. Lett. **28**, 263 (1974)

[23] Yariv, A. and Yeh, P., *Optical Waves in Crystals* Wiley, New York, (1984)

[24] Adler, R., IEEE Spectrum, **4**, 42 (1967)

[25] Muller, J., Advances in Electronics and Electron Physics, **55**, 189 (1981)

[26] Chen, Q.Y. and Bates, Tr., C.W., Phys. Rev. Lett. **57**, 2737, (1986)

[27] Schmidt-Ott, A., Schurtenberger, P., and Siegmann, H.C., Phys. Rev. Lett. **45**, 184, (1980)

[28] Olpin, A.R., Phys. Rev. **36**, 251, (1930)

[29] Sommer, A.H., *Photoemissive Material*, Wiley, New York, (1968)

[30] Chang, R.K. and Furtak, T.E., ed.,

Surface Enhanced Raman Scattering, Plenum, New York, (1982)

Figure Captions; Chapter 5

Figure 5.1; Input Pulse Shape for a Numerical Analysis of Dynamical Transmission
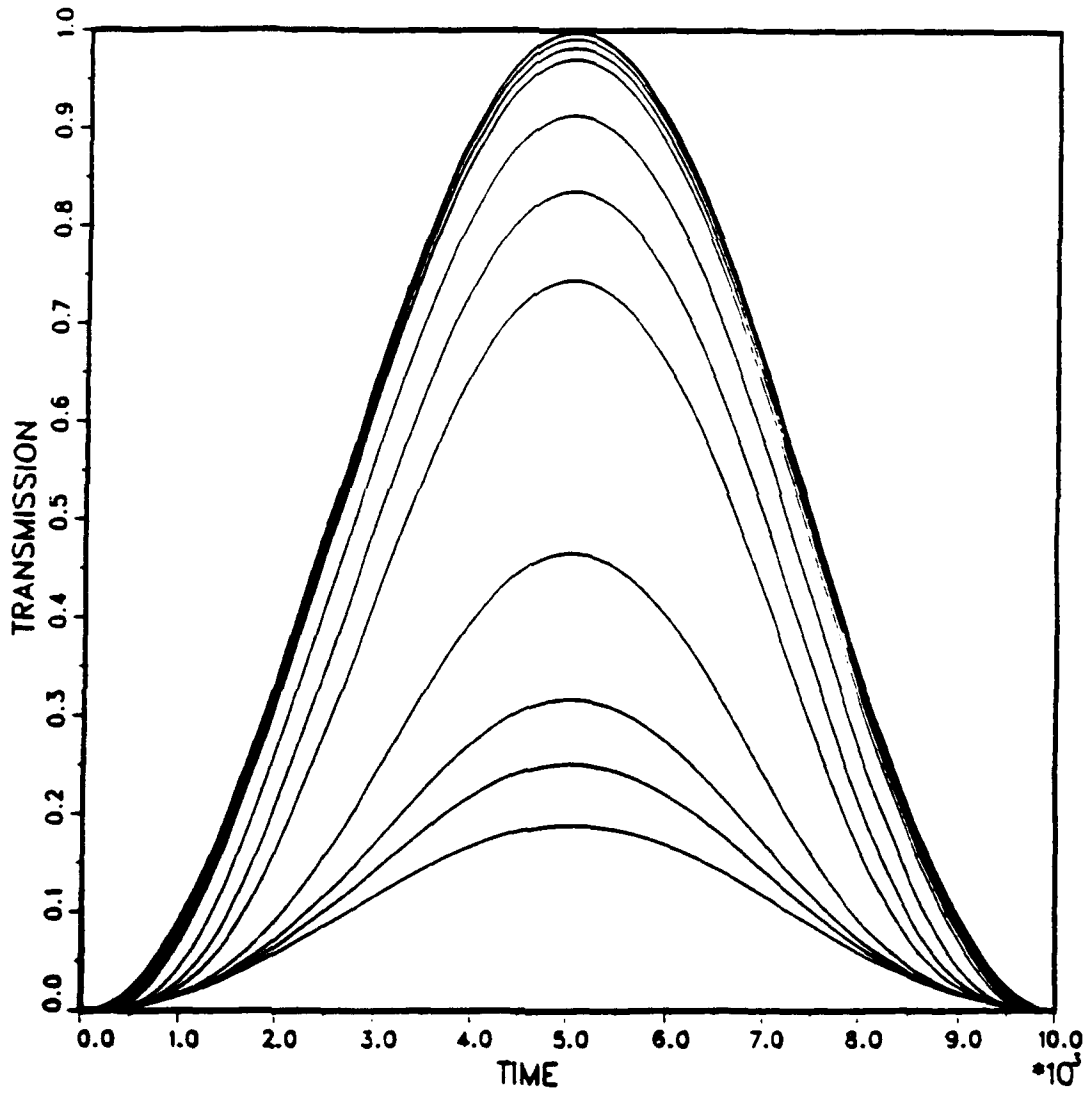
Figure 5.2; Output Pulse Shape for $r = 10^4$
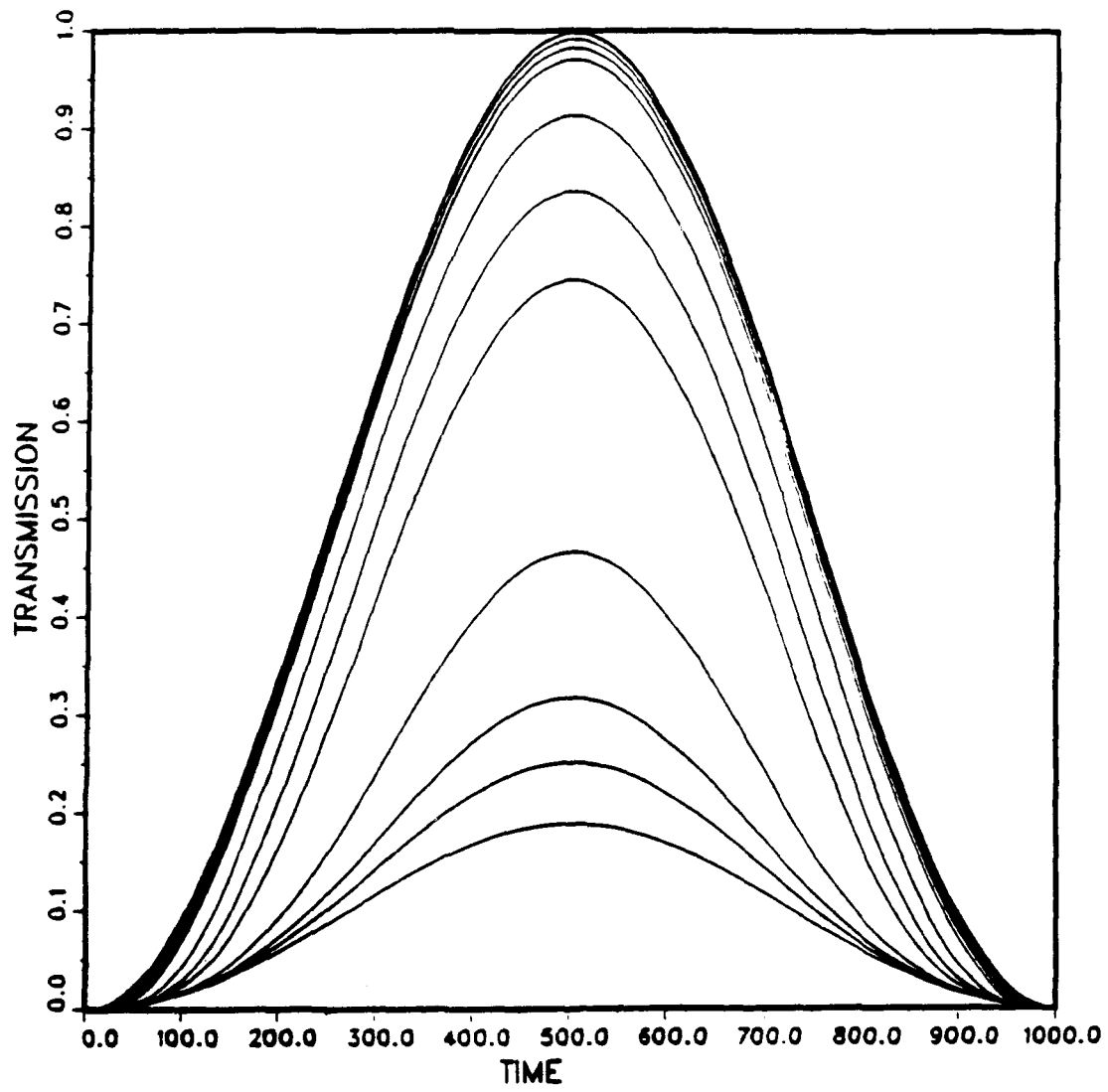
Figure 5.3; Output Pulse Shape for $r = 10^3$
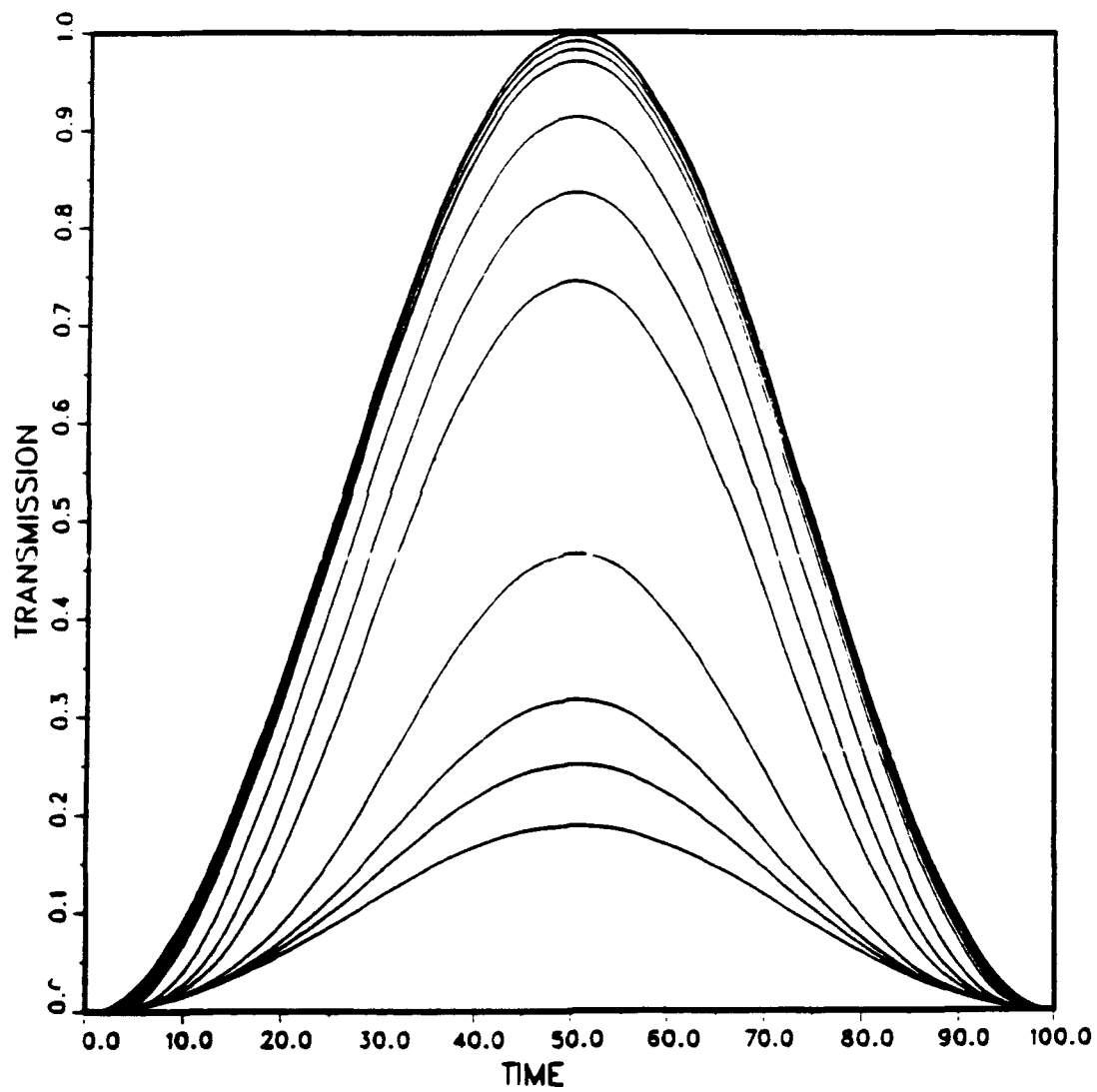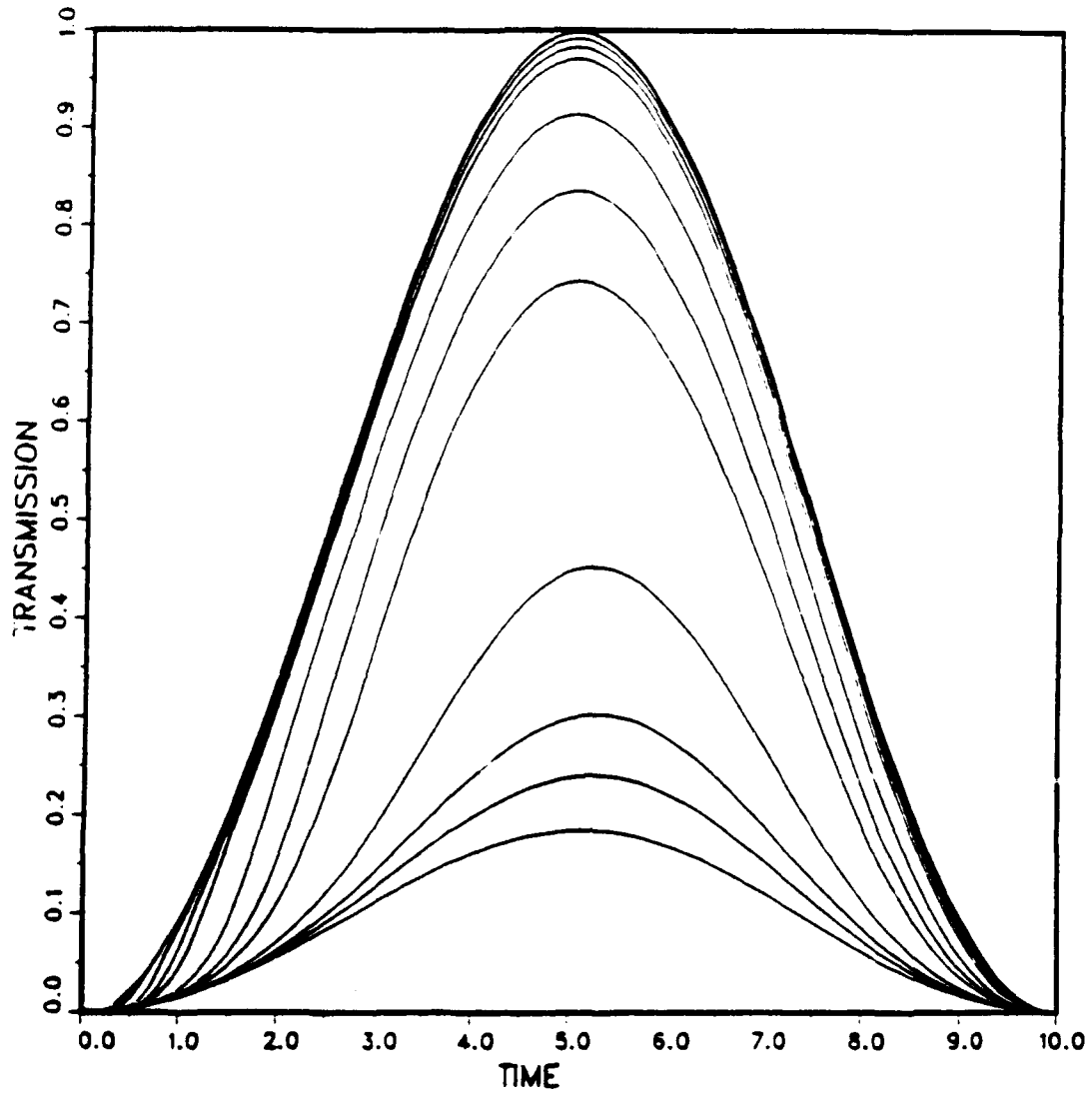
Figure 5.4; Output Pulse Shape for $r = 10^2$

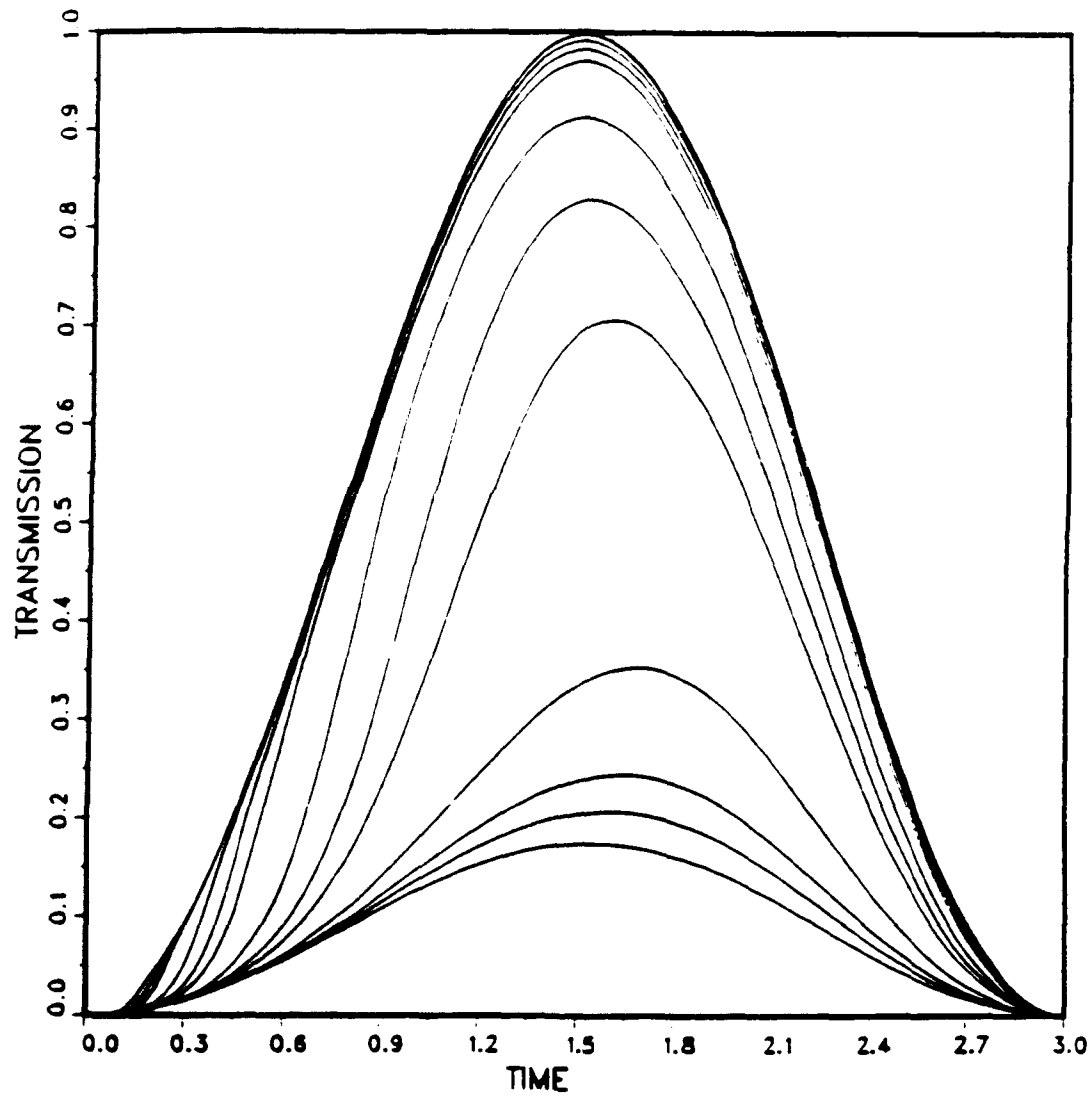Figure 5.5; Output Pulse Shape for $r = 10$
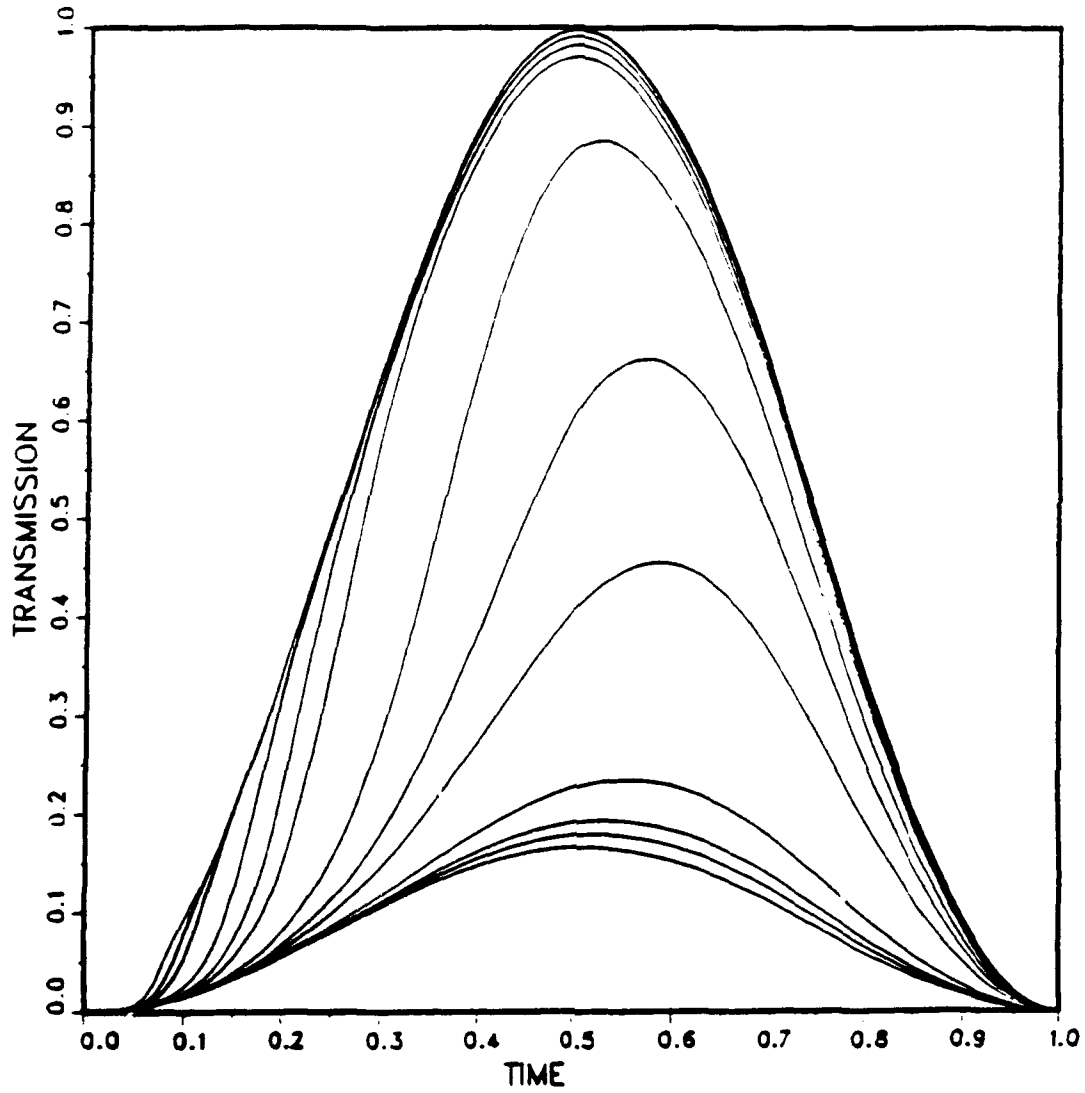
Figure 5.6; Output Pulse Shape for $r = 3.0$

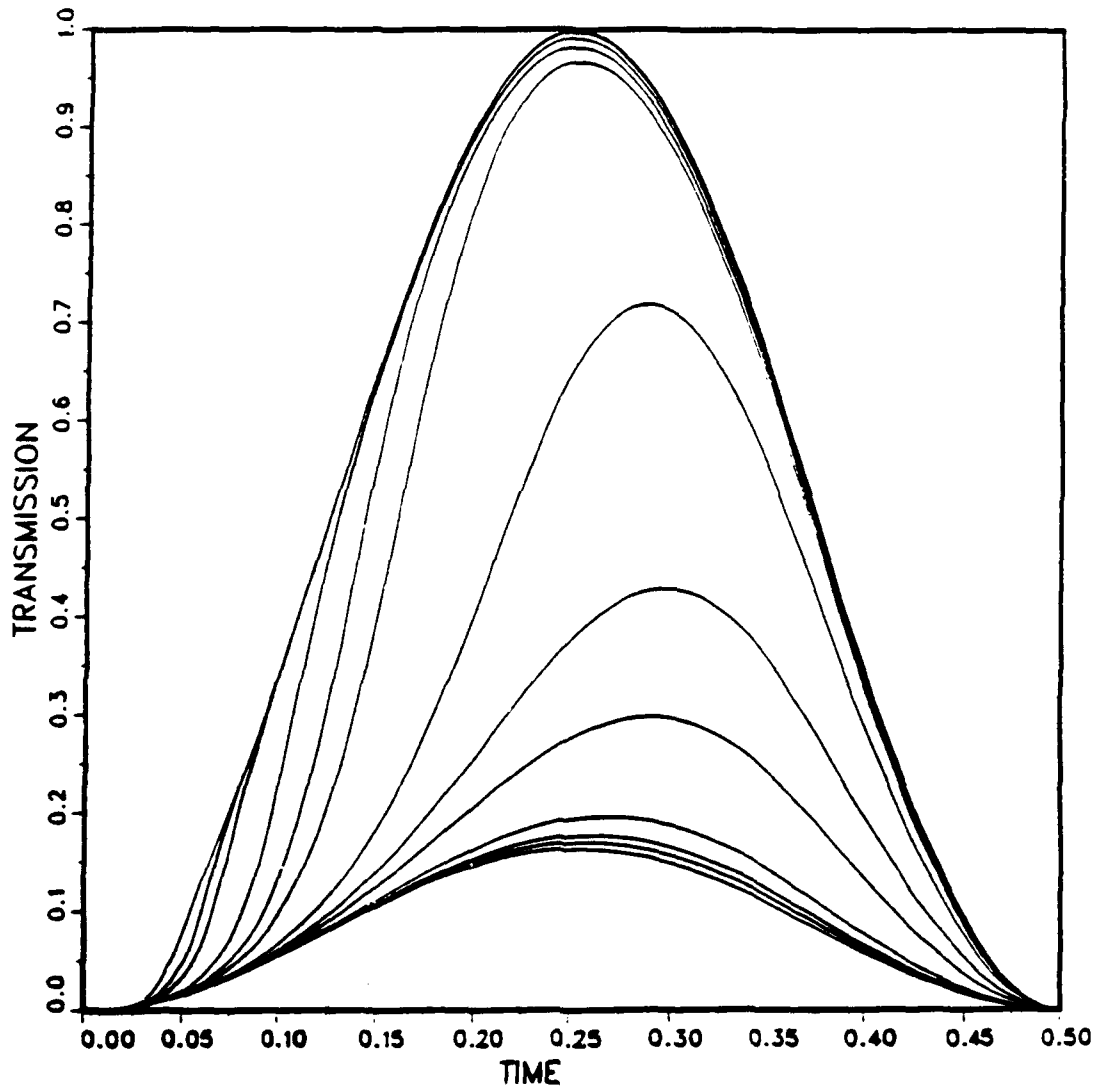Figure 5.7; Output Pulse Shape for $r = 1.0$
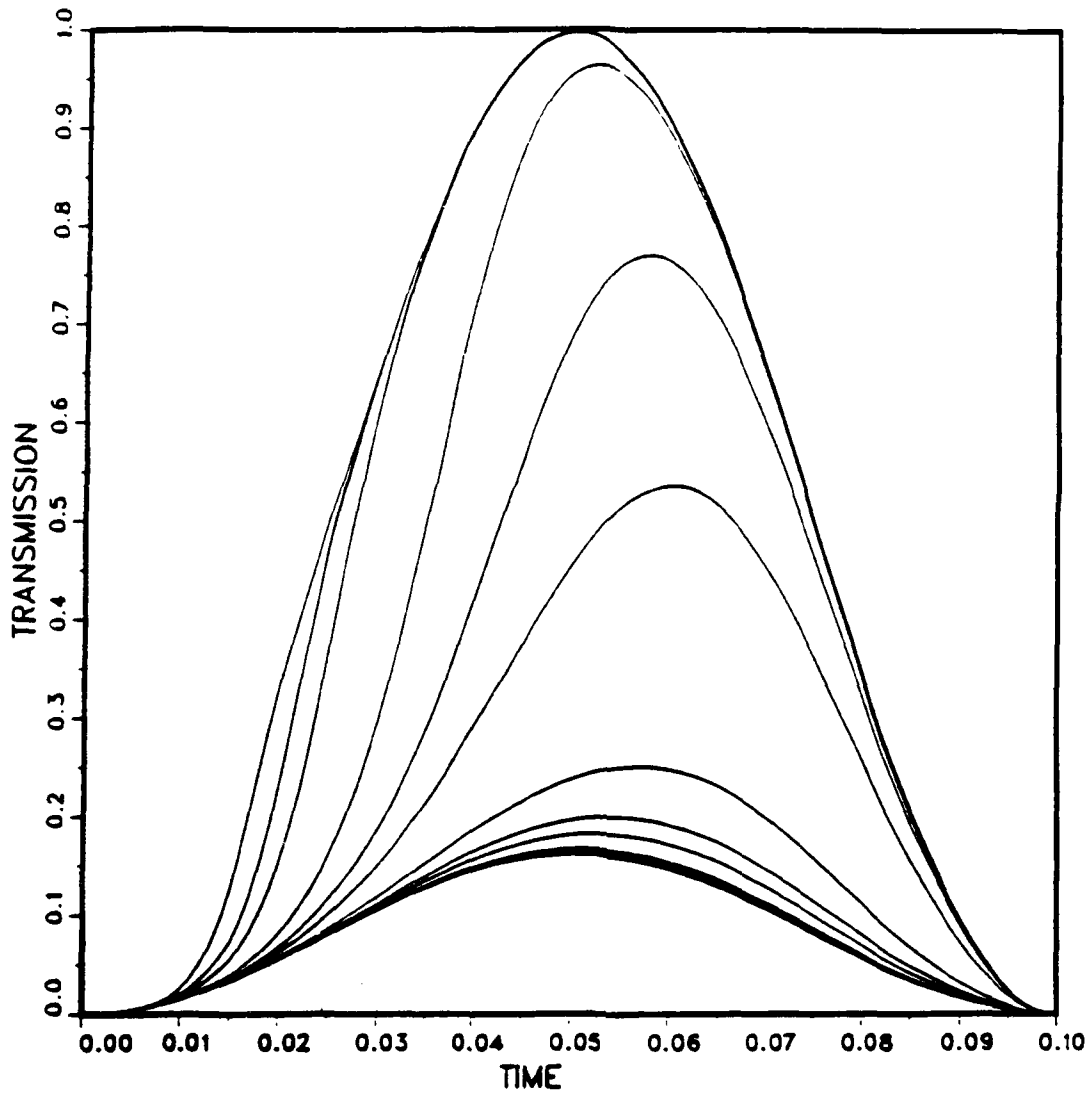
Figure 5.8; Output Pulse Shape for $r = 0.5$

Figure 5.9; Output Pulse Shape for $r = 0.1$

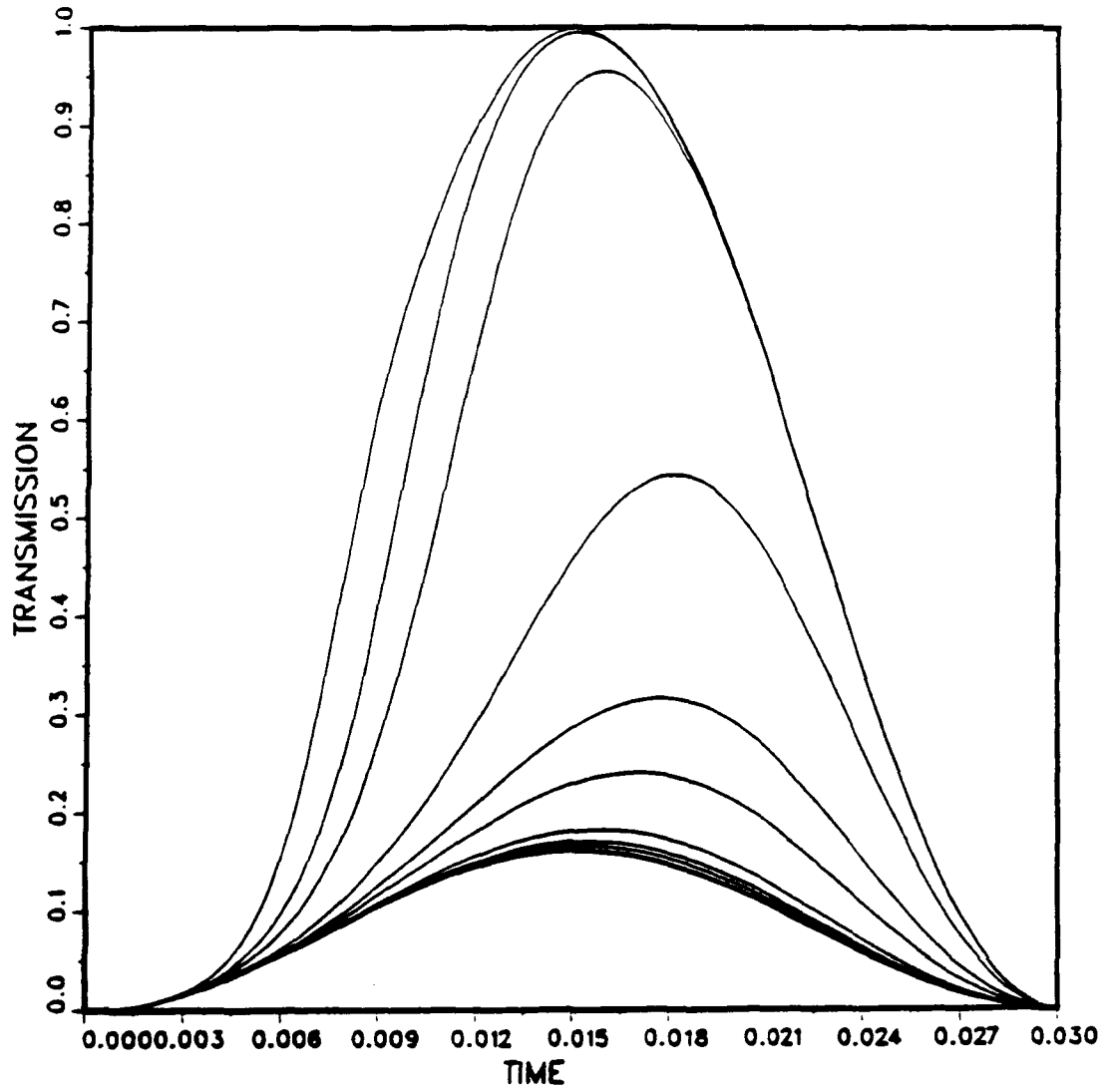Figure 5.10; Output Pulse Shape for $r = 0.03$

Figure 5.11; Output Pulse Shape for $r = 0.01$

Figure 5.12; Output Pulse Shape for $r = 0.001$

Figure 5.13; Numerical Analysis of a Dynamical Transmission

Figure 5.14; Intersystem Crossing

Figure 5.15; Auto-Correlation Measurement of a Raman Output

Figure 5.16; Transmission Spectrum for the 810 nm Spike Filter

Figure 5.17; Acousto-Optic Modulator

Figure 5.18; HP-2-4200-140 Photodiode and Diffuser Box

Figure 5.19; Charge Amplifier Circuit Diagram

Figure 5.20; MRD 510 Photodiode; Negative Polarity

Figure 5.21; MRD 510 Photodiode; Positive Polarity

Figure 5.22; Electrical Signal Splitter for 50 Ohm Cable (I)

Figure 5.23; Electrical Signal Splitter for 50 Ohm Cable (II)

Figure 5.24; Circuit Diagram for Avalanche Photodiode (RCA C30902 E)

Figure 5.25; PMT Voltage Divider Circuit

Figure 5.26; Experimental Layout for Saturable Absorption

Figure 5.27; Transmission Spectrum of Pellicle Beam Splitter

Various Phthalocyanines

Chemical Name		Molecular Weight
Free Base Phthalocyanine	H_2PC	514.55
Cobalt Phthalocyanine	CoPC	571.47
Iron Phthalocyanine	FePC	568.38
Nickel Phthalocyanine	NiPC	571.24
Vanadyl Phthalocyanine	VOPC	579.48
Zinc Phthalocyanine	ZnPC	577.91
Silicon NaPhthalocyanine	SINC	1546
Vanadyl 6-Petra-T-Butyl NaPhthalocyanine	VONC	1004.141

Table 5.1

182

RAMAN LINES

<u>Hydrogen Molecule</u>; H_2

Raman Shift; vibrational $\qquad$ 4155 cm^{-1}

Pumping; Nd:YAG fundamental 1064nm
+2; 565nm
+1; 738 nm
-1; 1.91μm

Pumping; Nd:YAG SHG 532nm
+2; 369nm
+1; 436nm
-1; 683nm

<u>Methane</u>; CH_4

Raman Shift; vibrational $\qquad$ 2916cm^{-1}

Pumping; Nd:YAG fundamental 1064nm
+1;   813 nm
-1;   1.54μm

Pumping; Nd:YAG SHG 532nm
+1;   460nm
-1;   629nm
-2;   770nm

Table 5.2

183

Input Pulse Shape for a Numerical Analysis of Dynamical Transmission
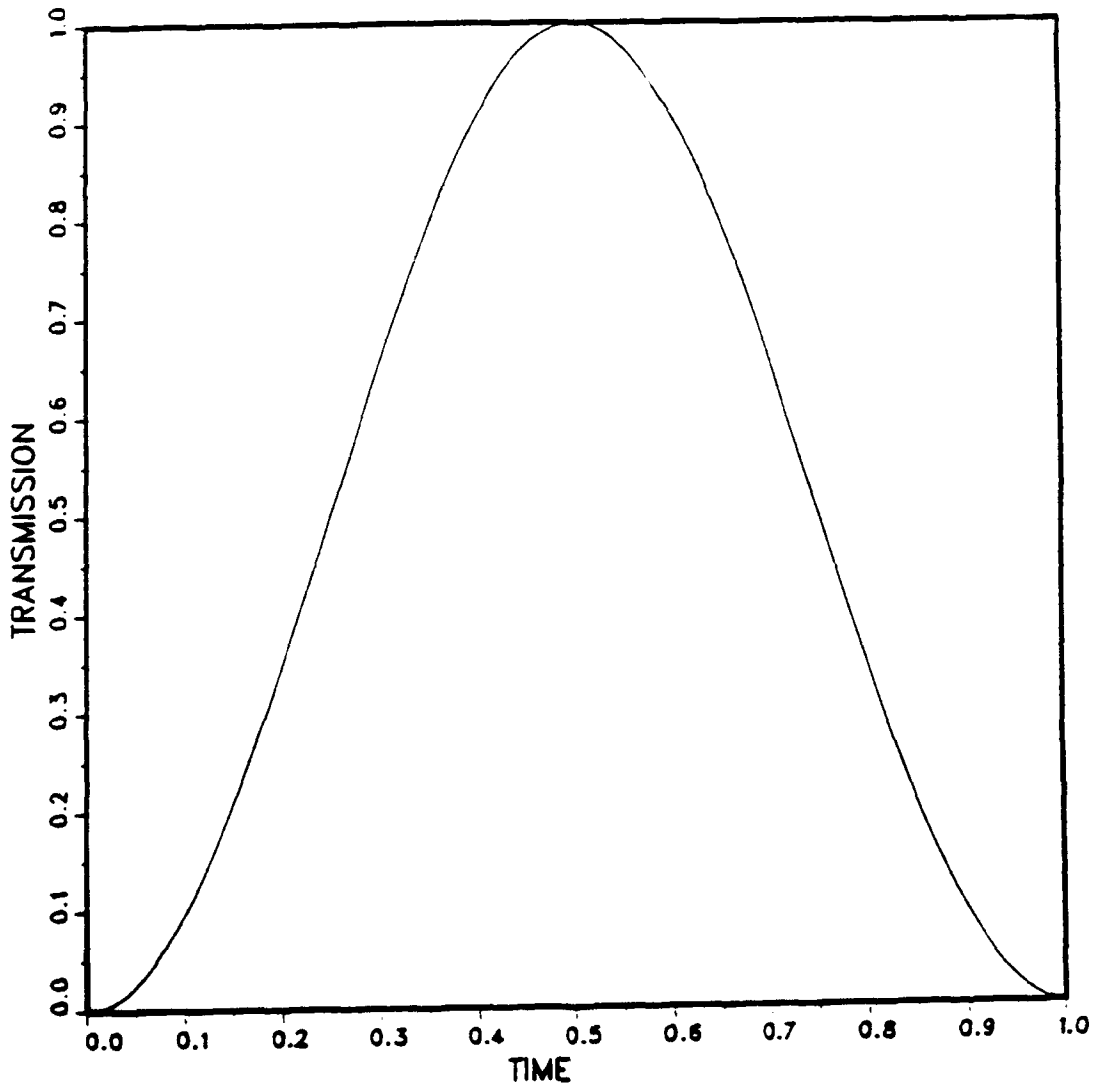
Figure 5.1

Output Pulse Shape for r = 10^4

Figure 5.2

185

Output Pulse Shape for r = 10^3

Figure 5.3

Output Pulse Shape for r = 10^2

Figure 5.4

Output Pulse Shape for r = 10

Figure 5.5

188

Output Pulse Shape for r = 3

Figure 5.6

Output Pulse Shape for r = 1

Figure 5.7

Output Pulse Shape for r = 0.5

Figure 5.8

Output Pulse Shape for r = 0.1

Figure 5.9

Output Pulse Shape for r = 0.03

Figure 5.10

Output Pulse Shape for r = 0.01

Figure 5.11

194
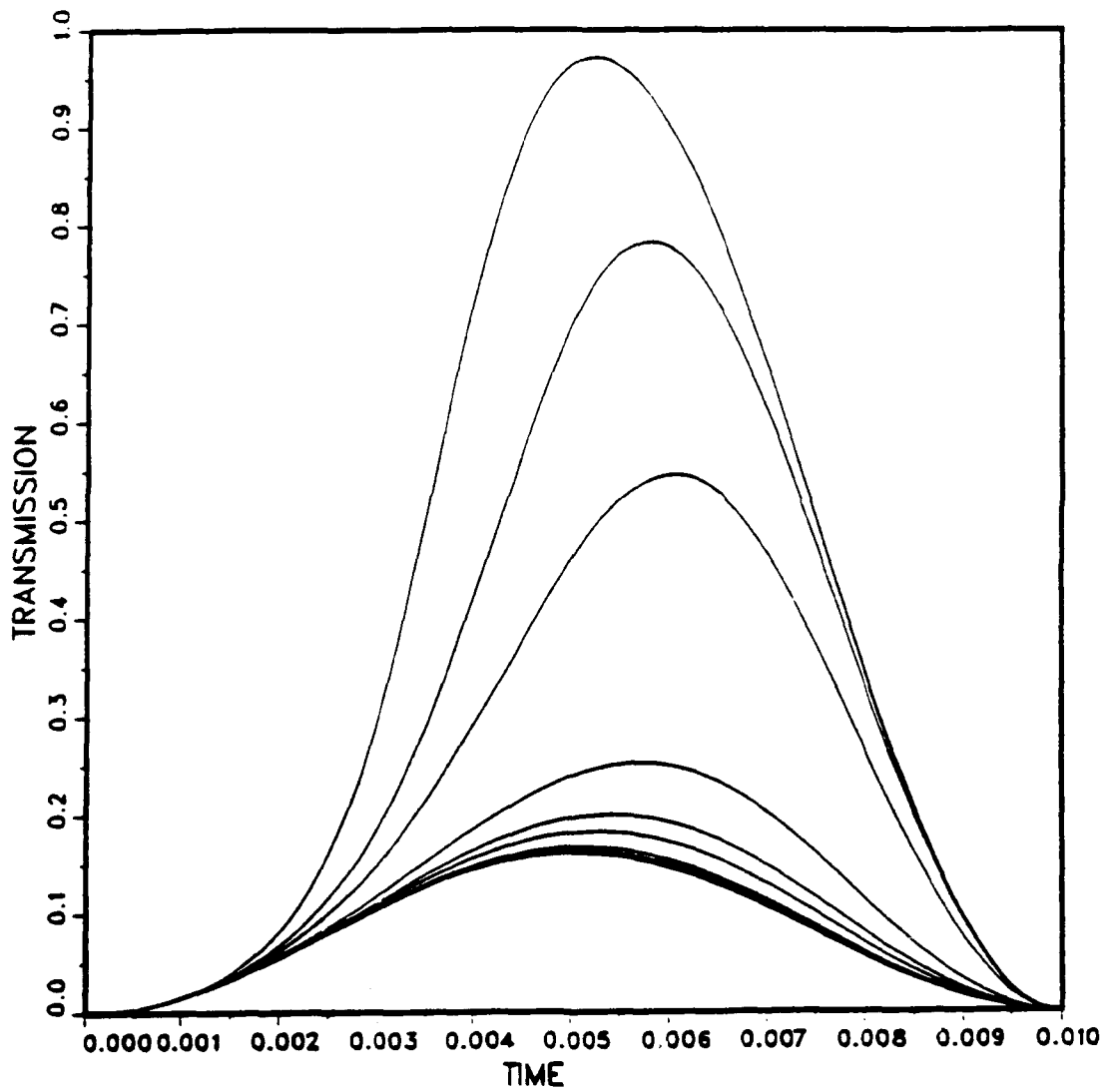
Output Pulse Shape for r = 0.001

Figure 5.12

195
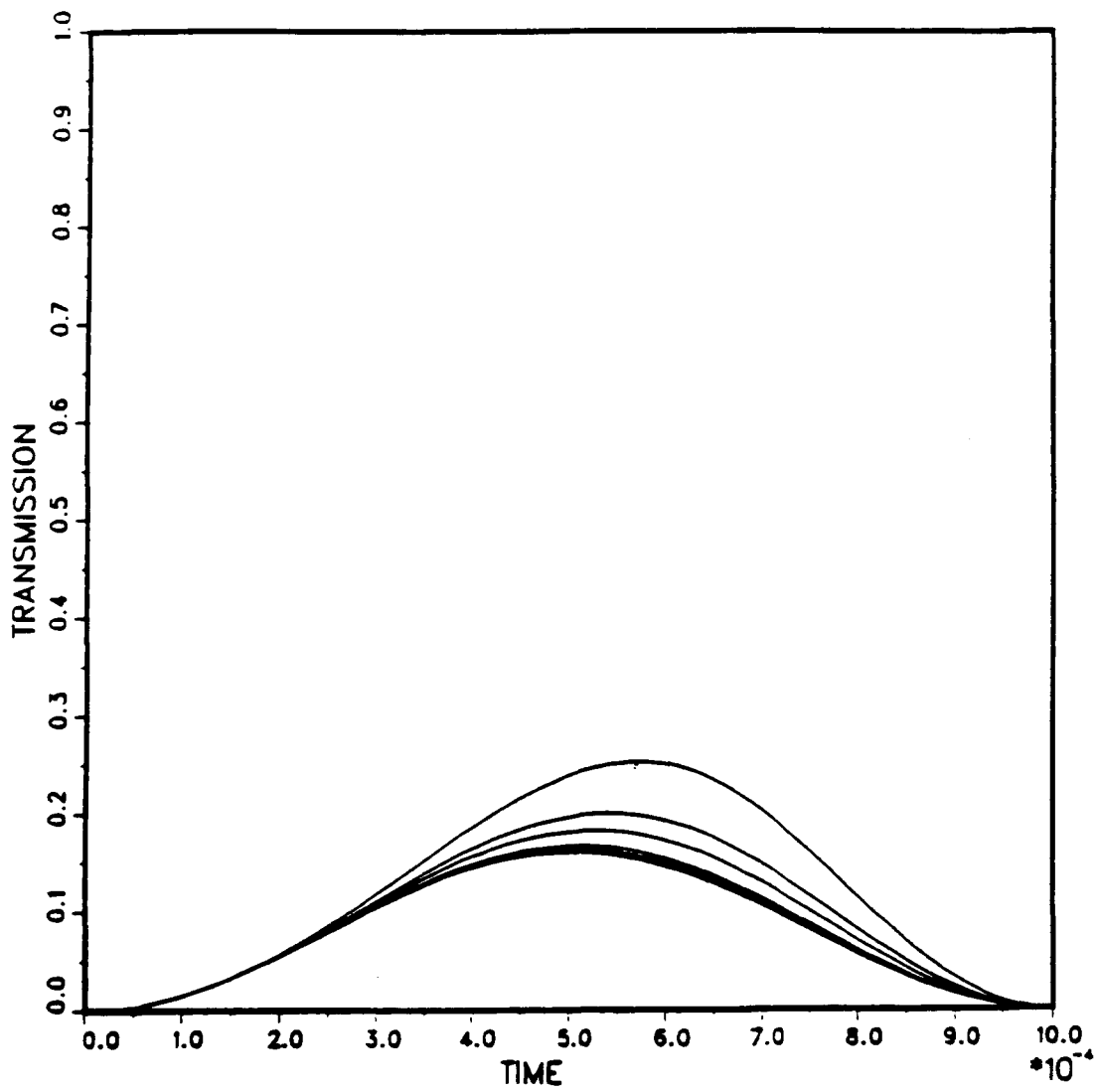
Numerical Analysis of a Dynamical Transmission
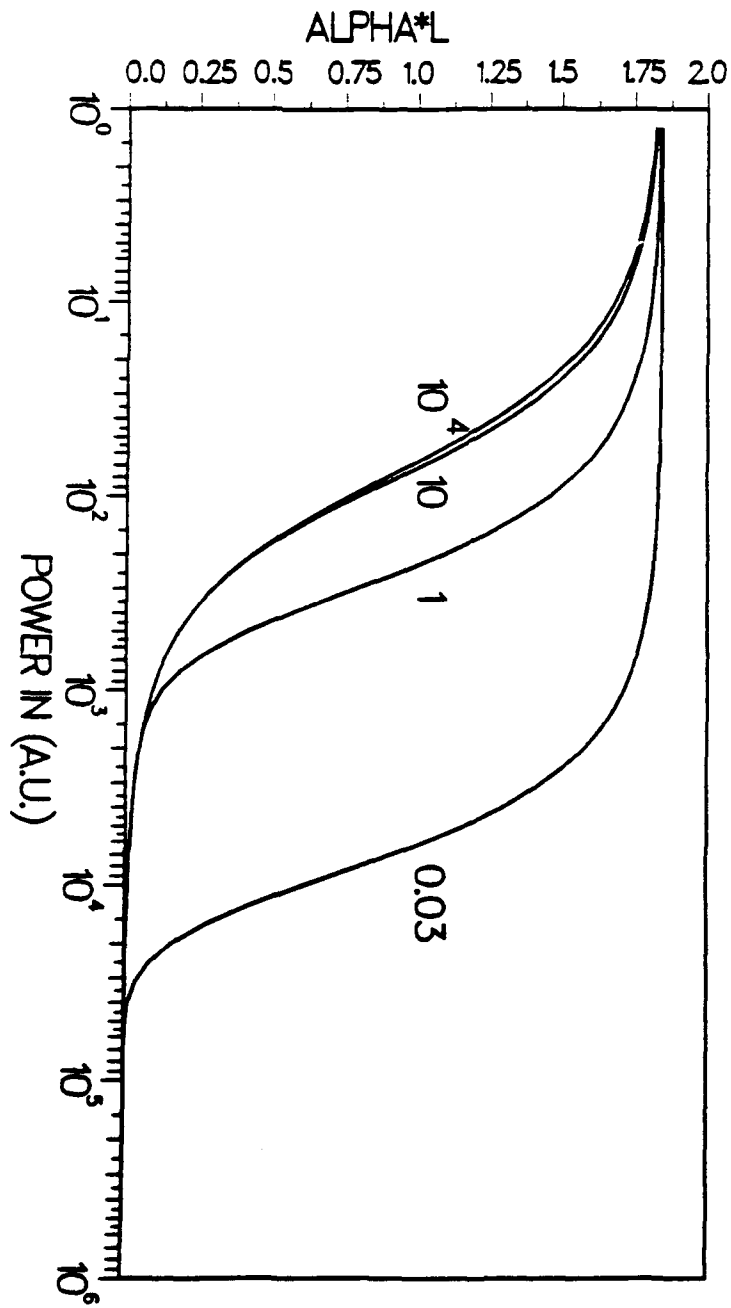
Figure 5.13

Intersystem Crossing

Figure 5.14

197

S.H.G. SIGNAL
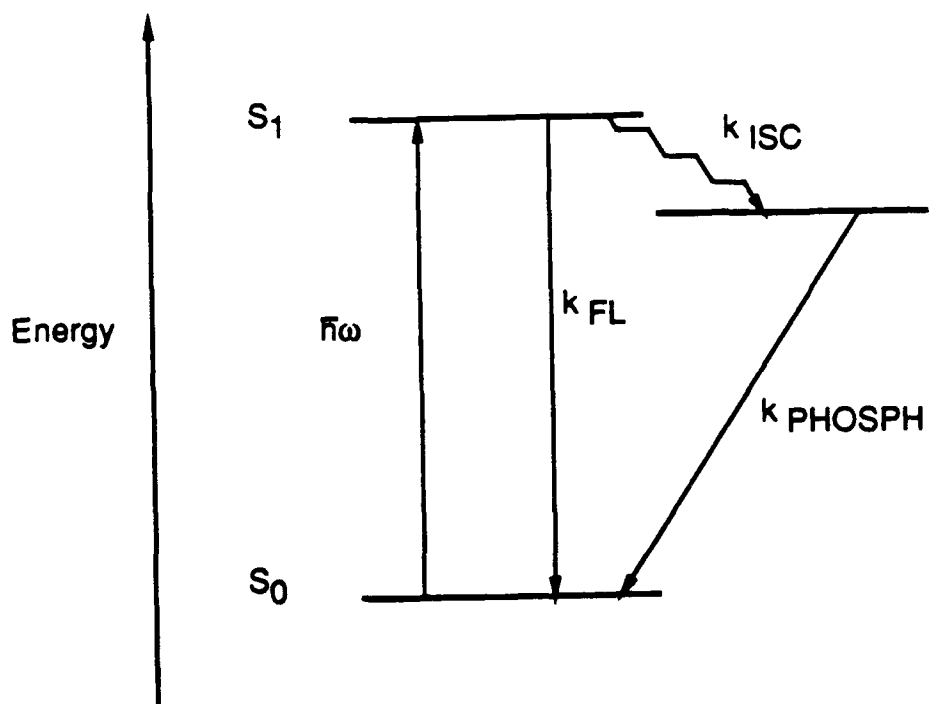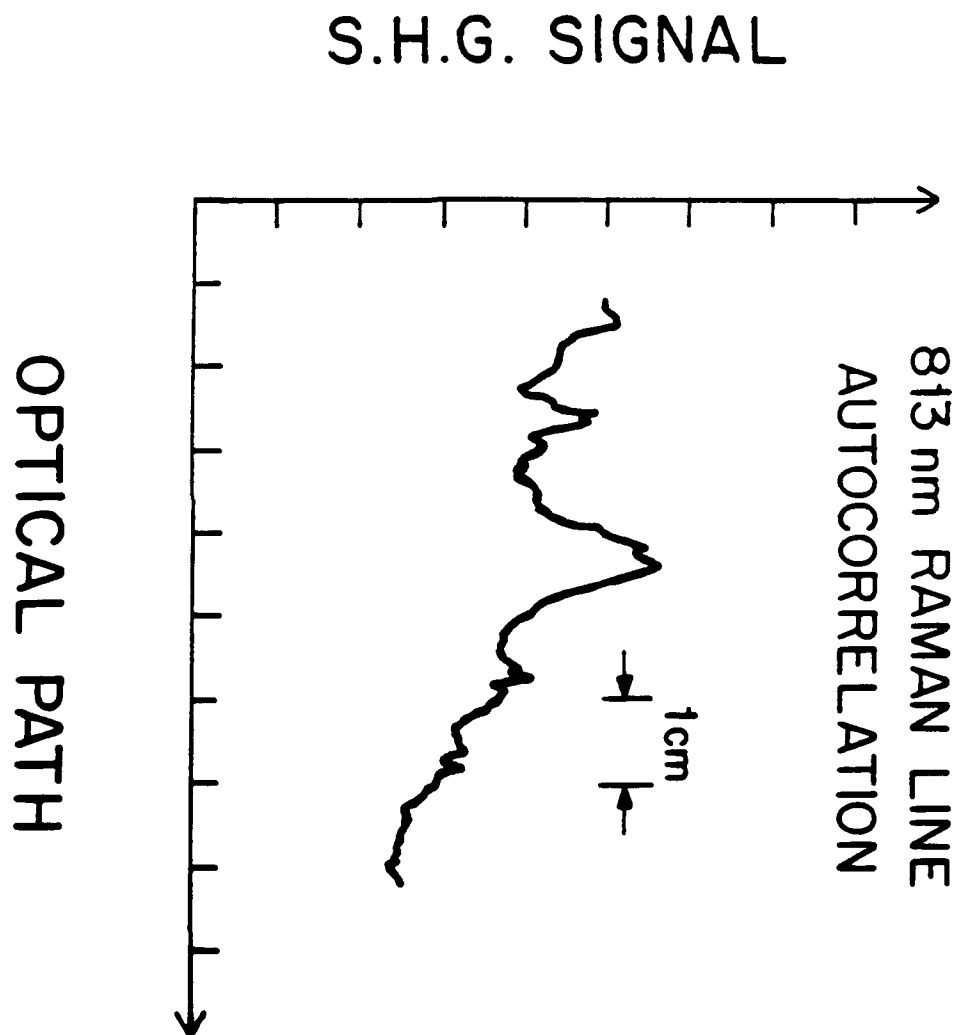
Figure 5.15

Transmission Spectrum for the 810 nm Spike Filter
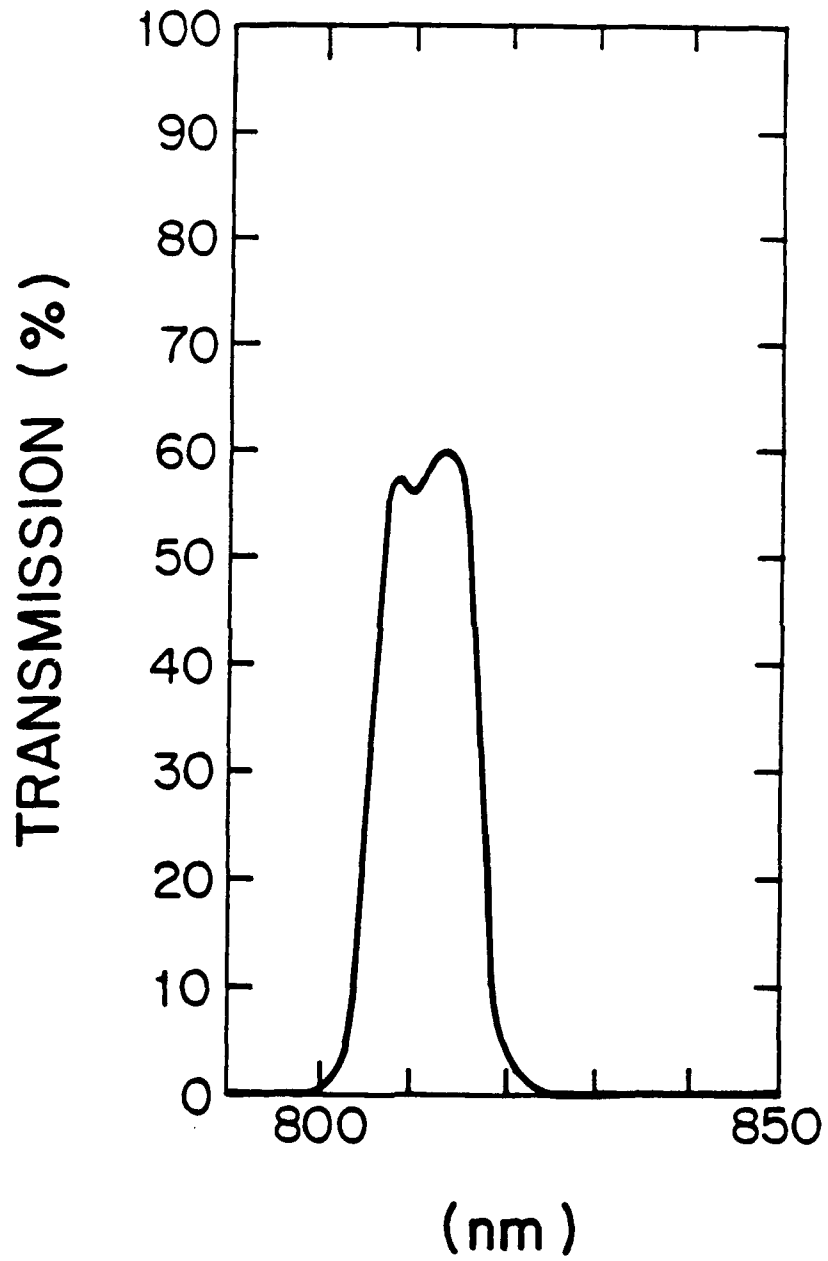
Figure 5.16

ACOUSTO-OPTIC MODULATOR

Incident
Light

Diffracted
Light

Modulated RF
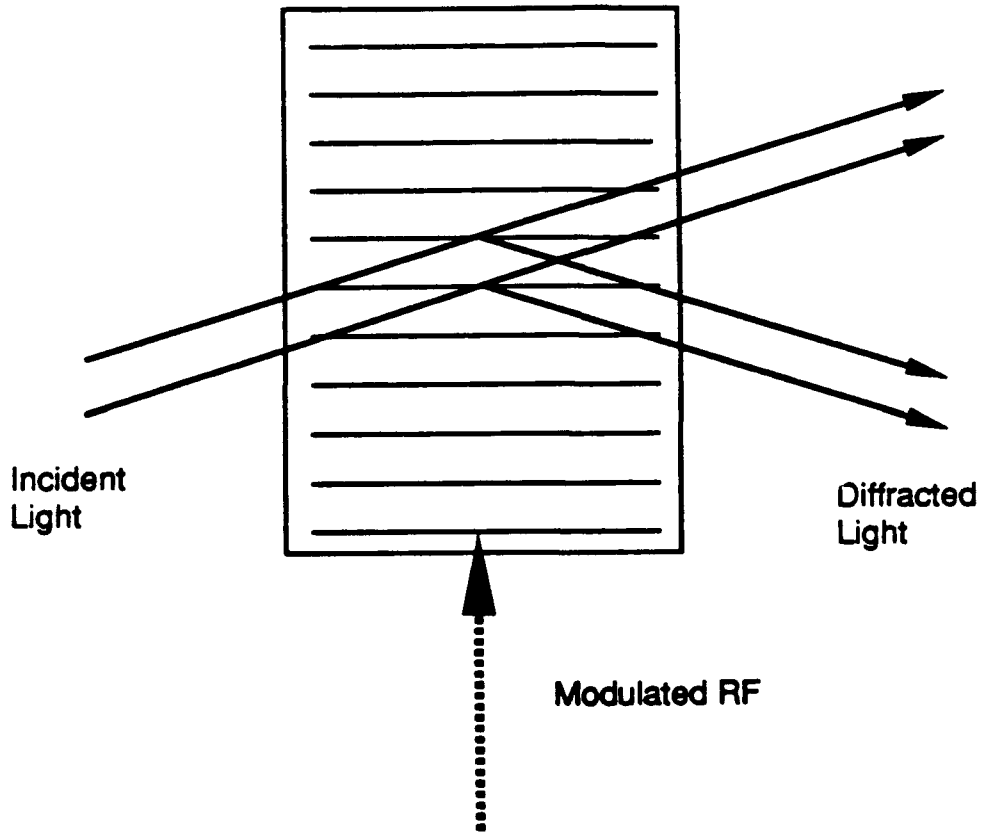
Figure 5.17

HP-2-4200-140 PHOTO-DIODE
& DIFFUSOR BOX
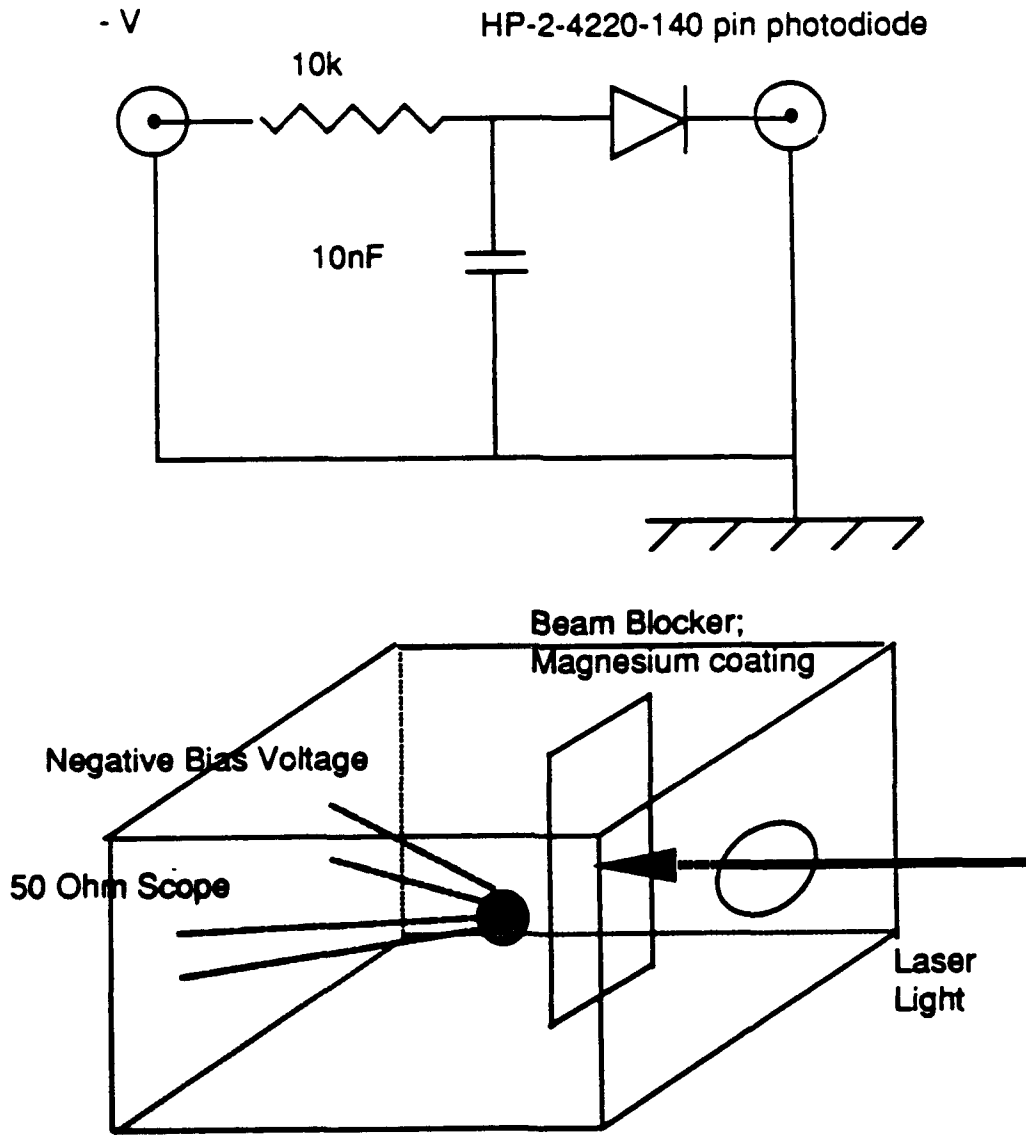
Figure 5.18

Charge Amplifier
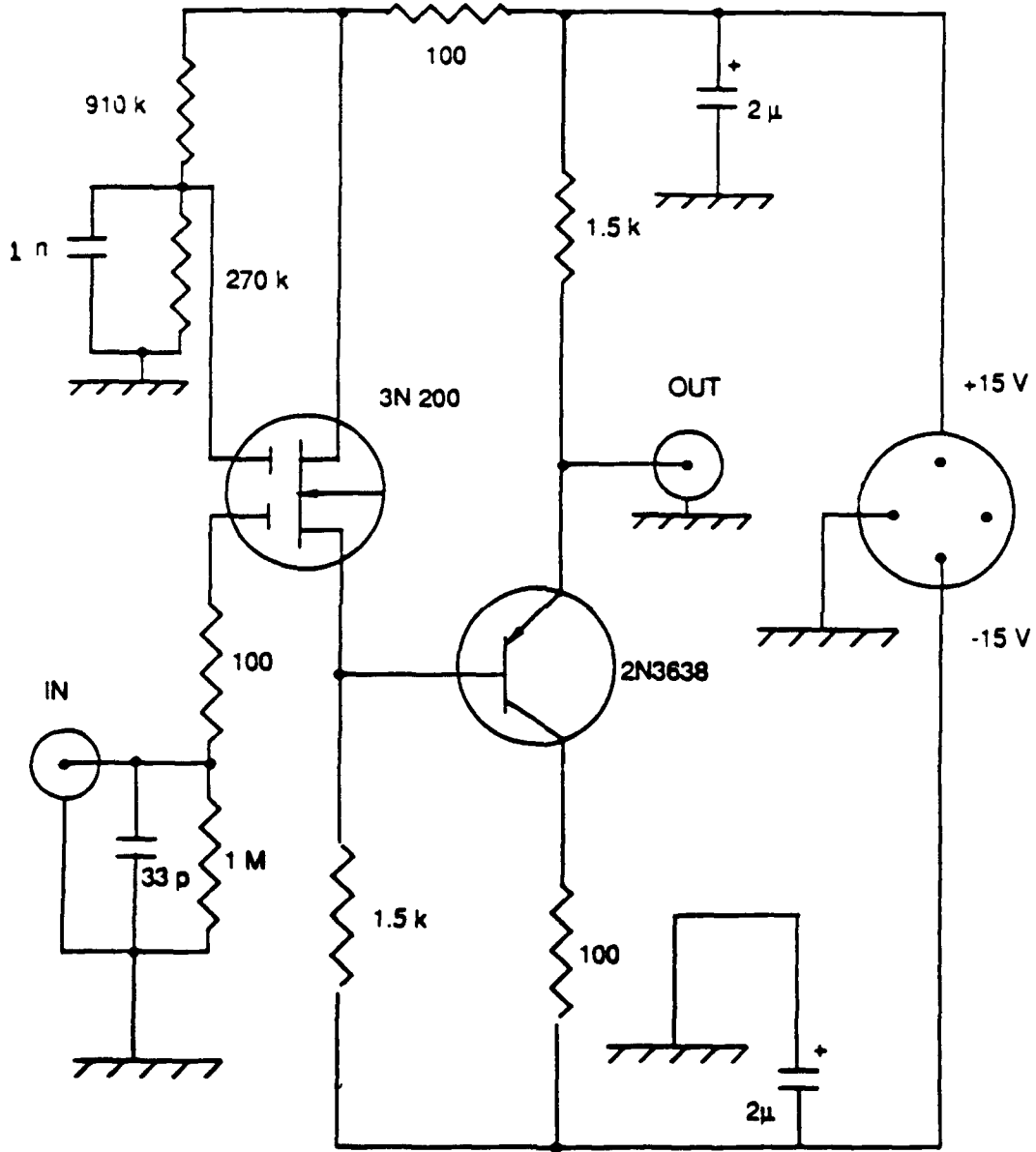
Figure 5.19

MRD 510 PHOTO-DIODE;
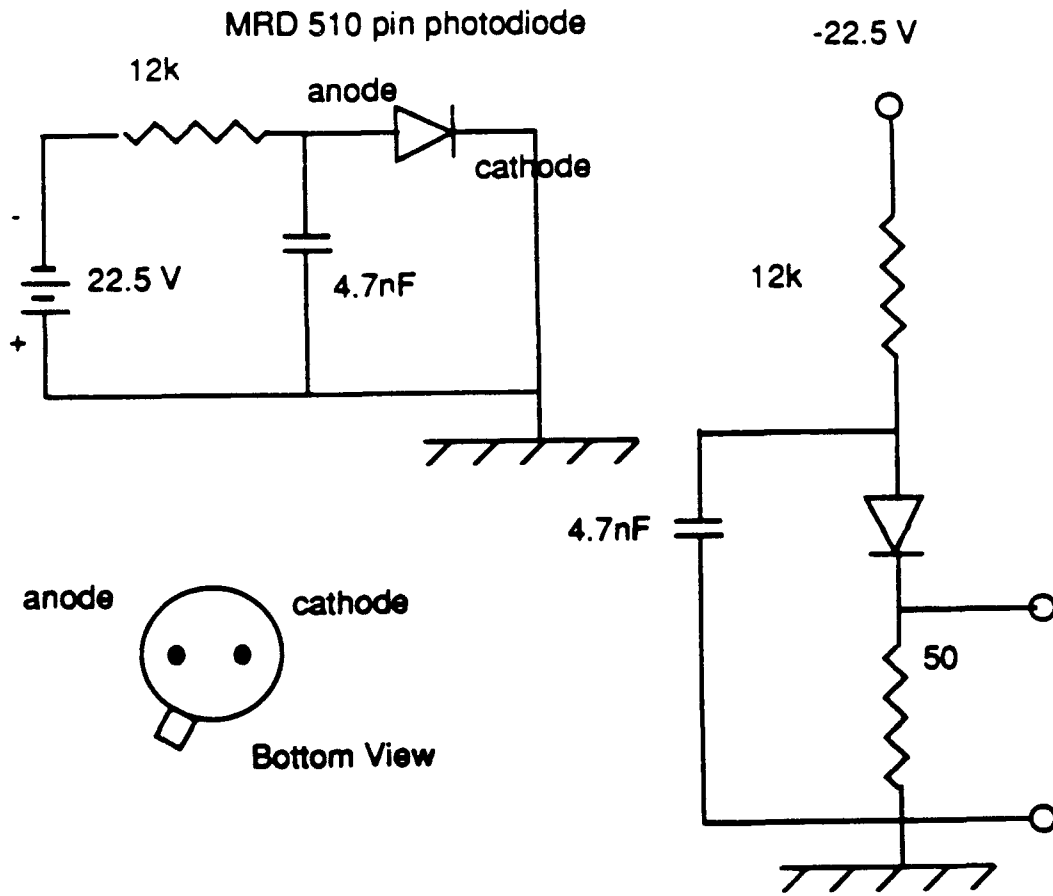## Negative Polarity

MRD 510 pin photodiode

-22.5 V

12k

anode

cathode

22.5 V

4.7nF

12k

4.7nF

50

anode   cathode

Bottom View

Figure 5.20

MRD 510 PHOTO-DIODE;
Positive Polarity

MRD 510 pin photodiode

Bottom View
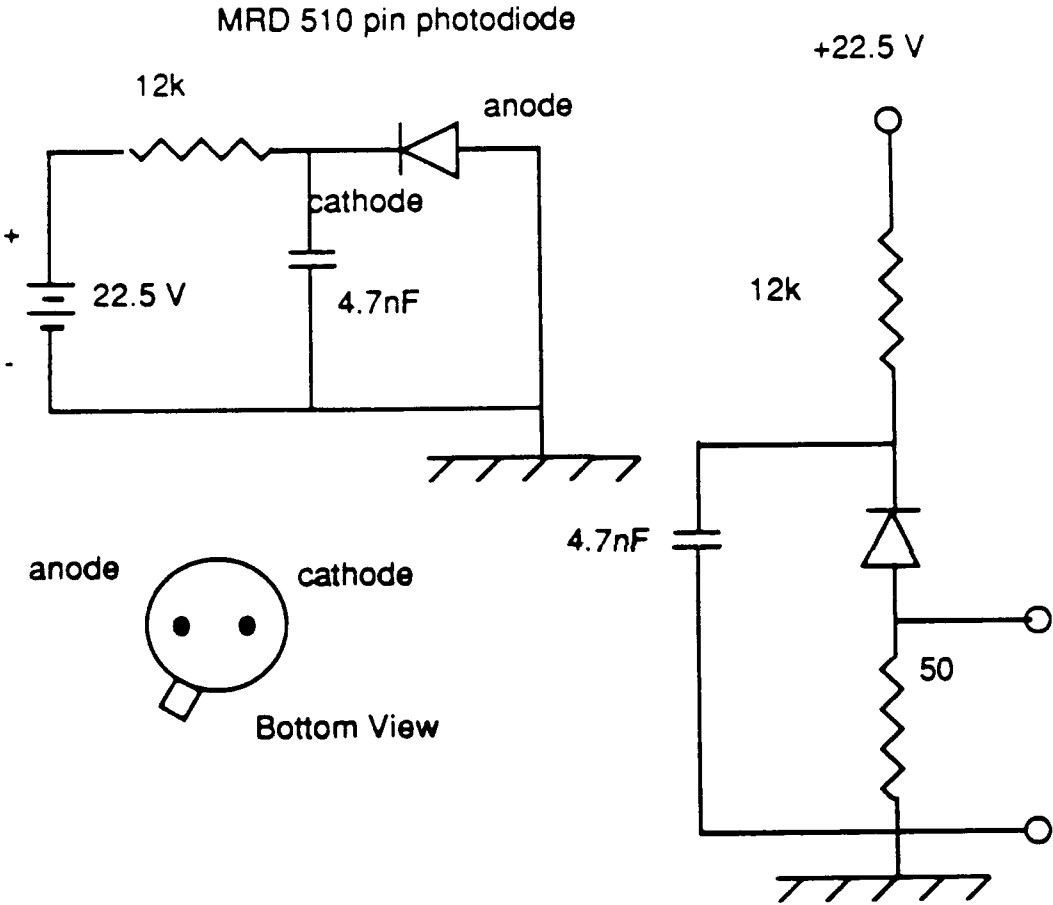
Figure 5.21

**Electrical Signal Splitter
for 50 Ohm Cable**

50 Ohm

16 Ohm

16 Ohm

16 Ohm

50 Ohm

Figure 5.22

Electrical Signal Splitter
for 50 Ohm Cable

50 Ohm

24 Ohm

24 Ohm

24 Ohm

24 Ohm
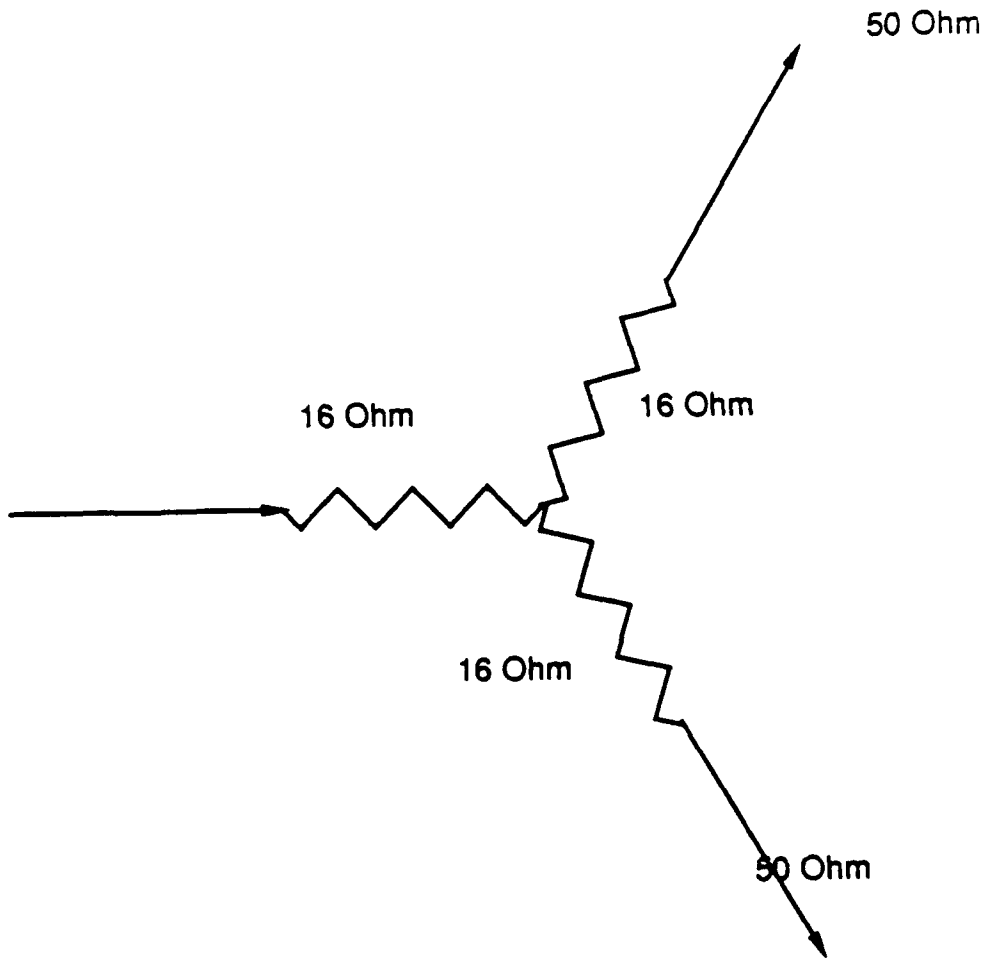
50 Ohm

50 Ohm
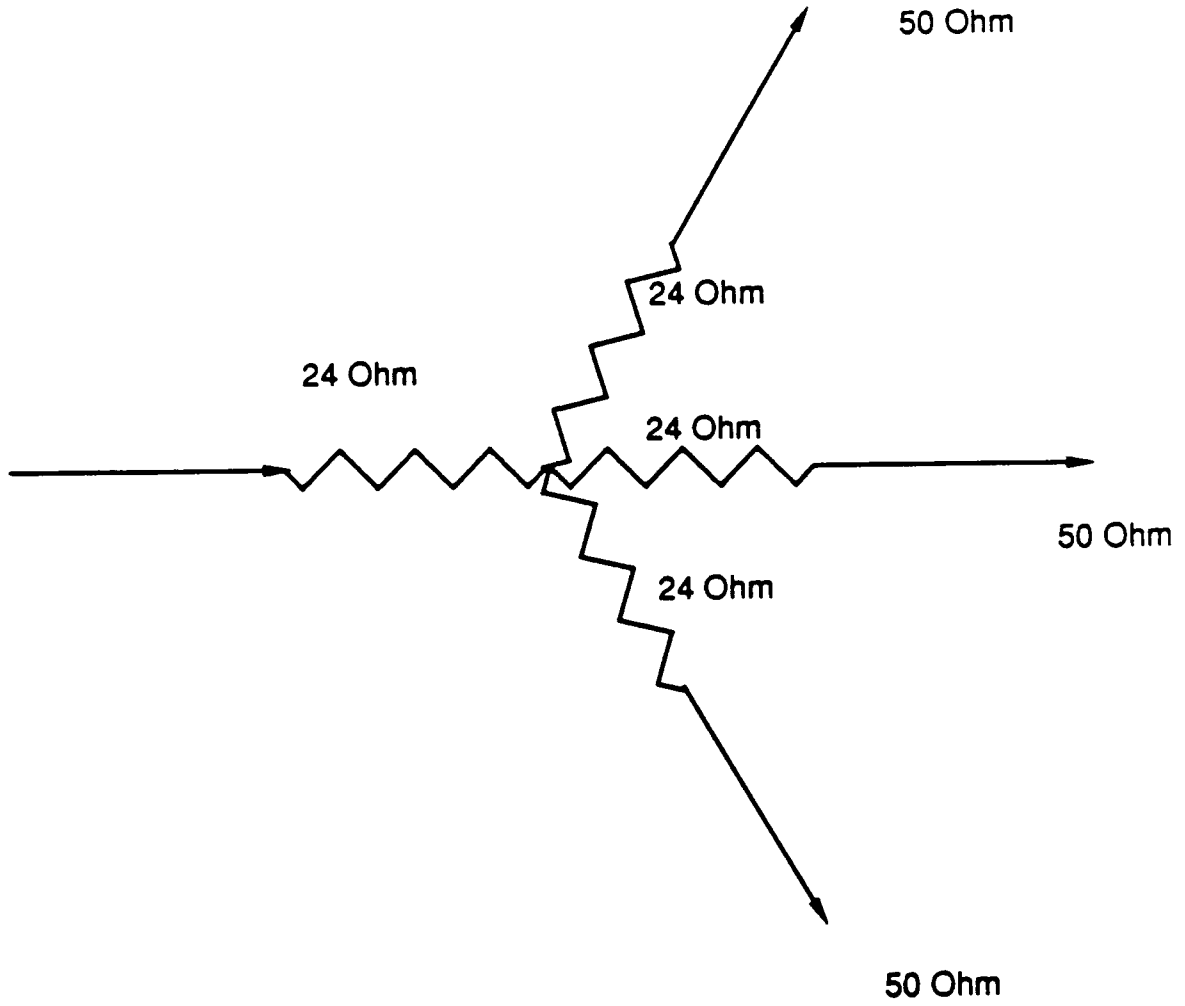
Figure 5.23

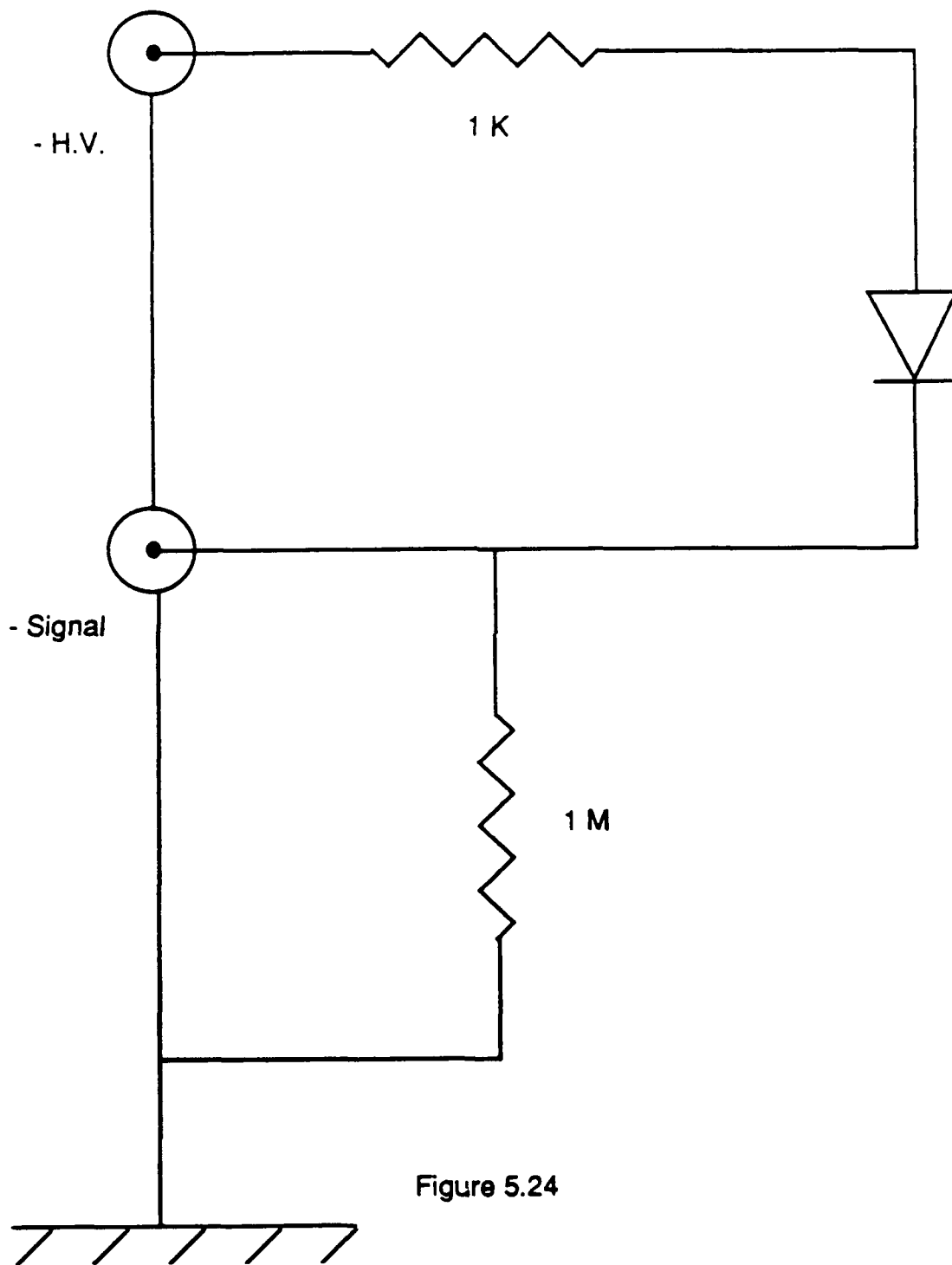**RCA Silicon Avalanche Photodiode; C30902 E**

Figure 5.24

PMT Voltage Divider Circuit

Figure 5.25

208
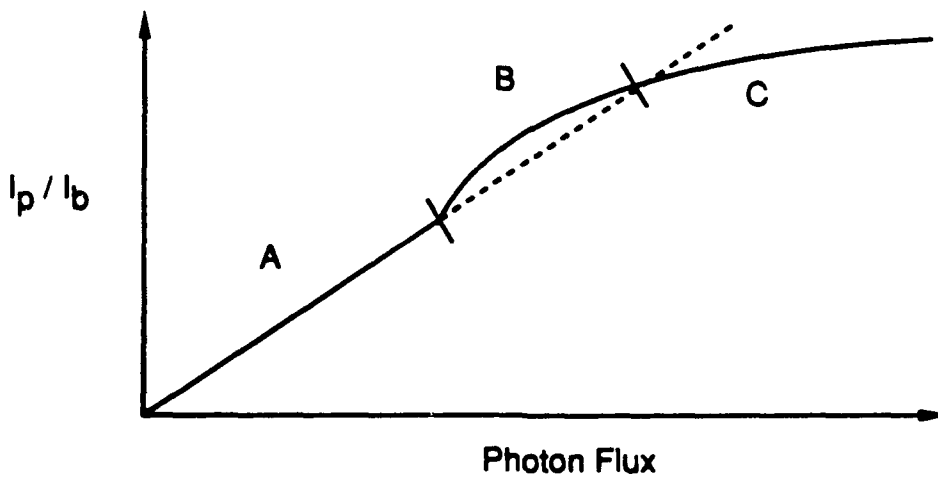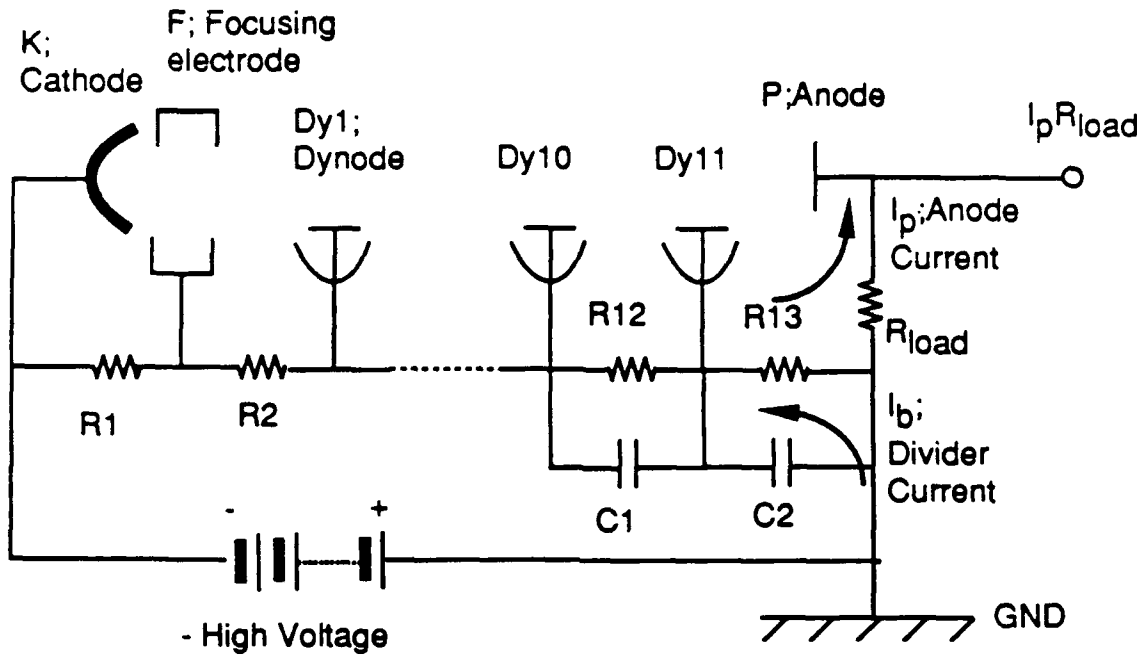
Experimental Layout for Saturable Absorption
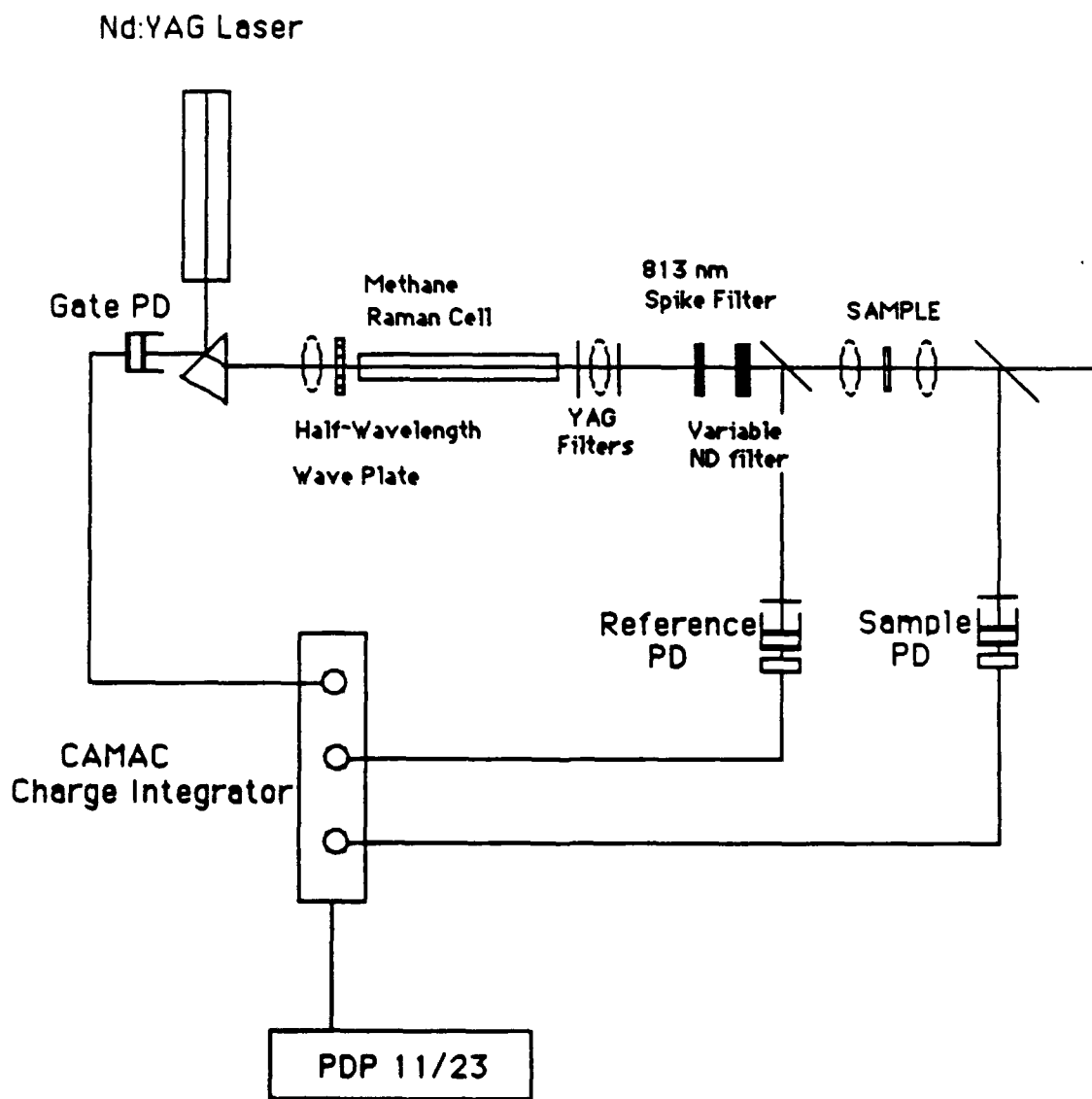

Figure 5.26

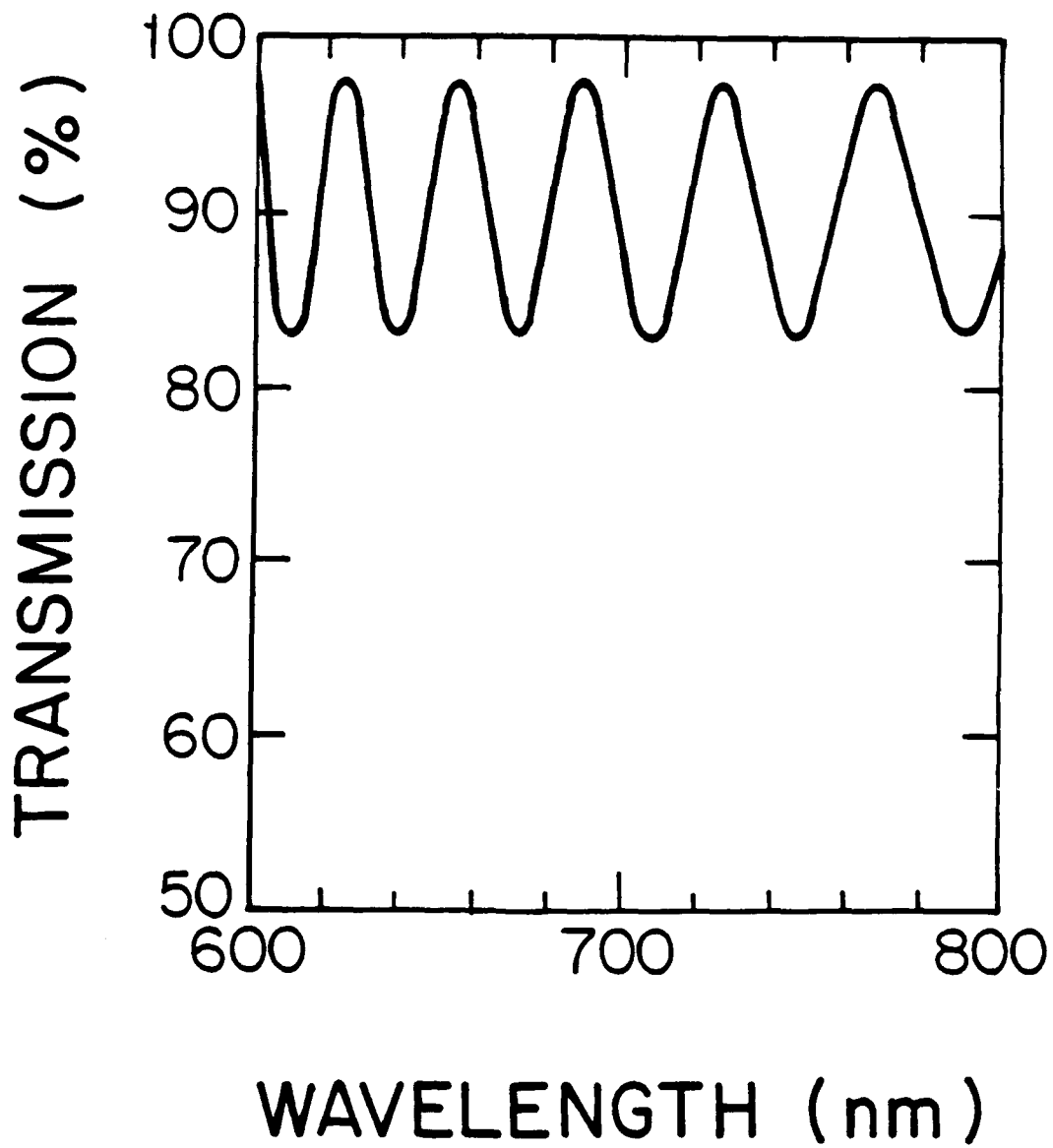**Transmission Spectrum of Pellicle Beam Splitter**
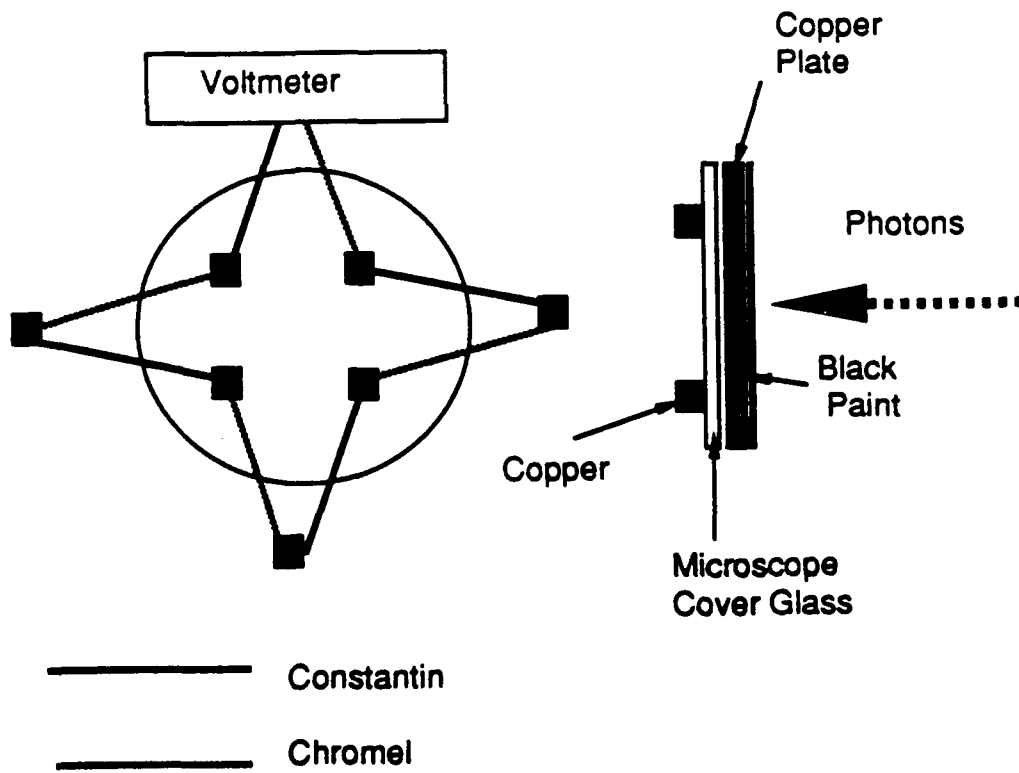

Figure 5.27

Thermocouple Circuit

Figure 5.28

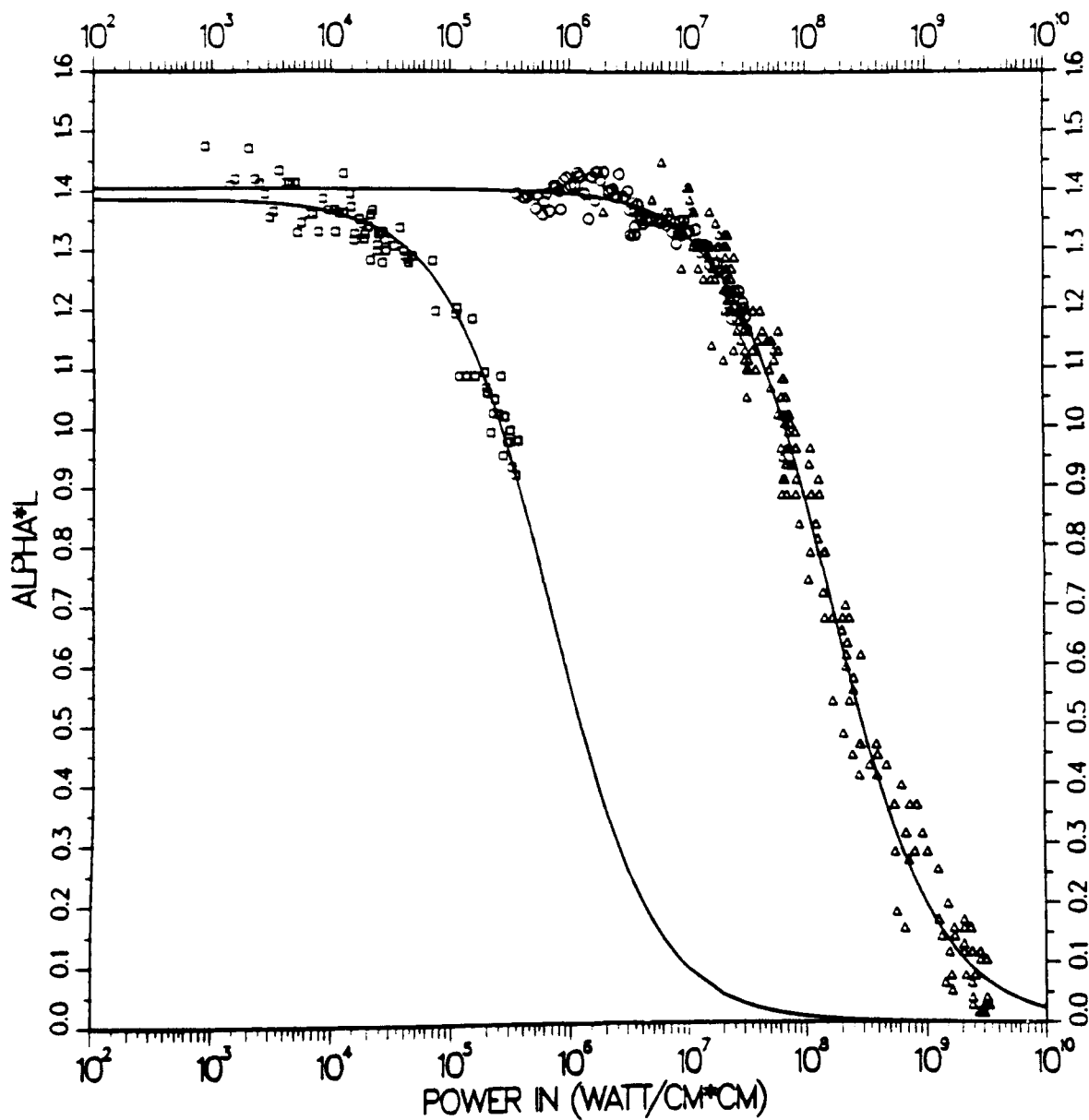## Saturable Absorption Data for Thin Film Sample

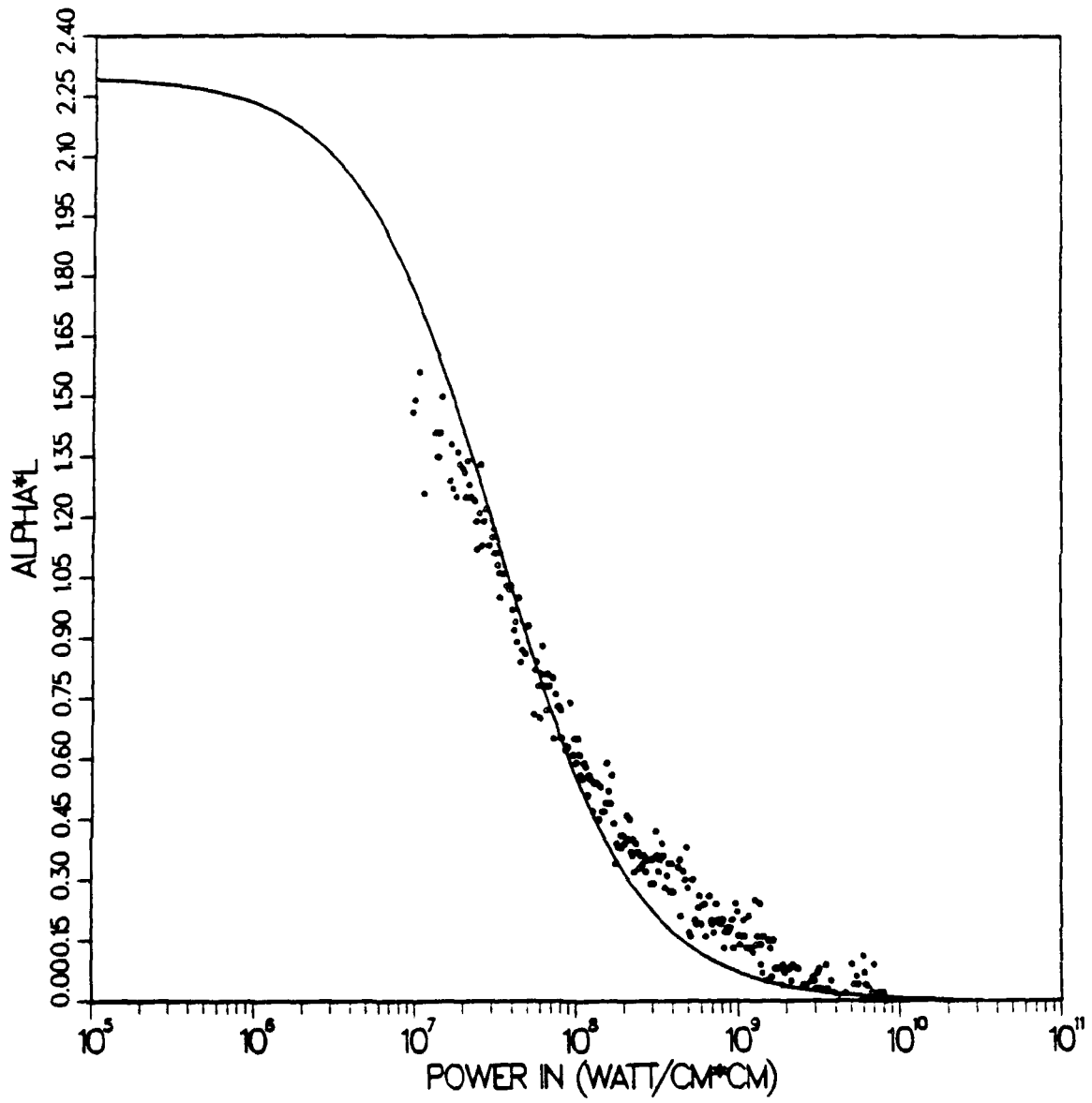
Figure 5.29

Saturable Absorption Data for Liquid Sample

Figure 5.30

Experimental Layout for Dispersion of Saturable Absorption

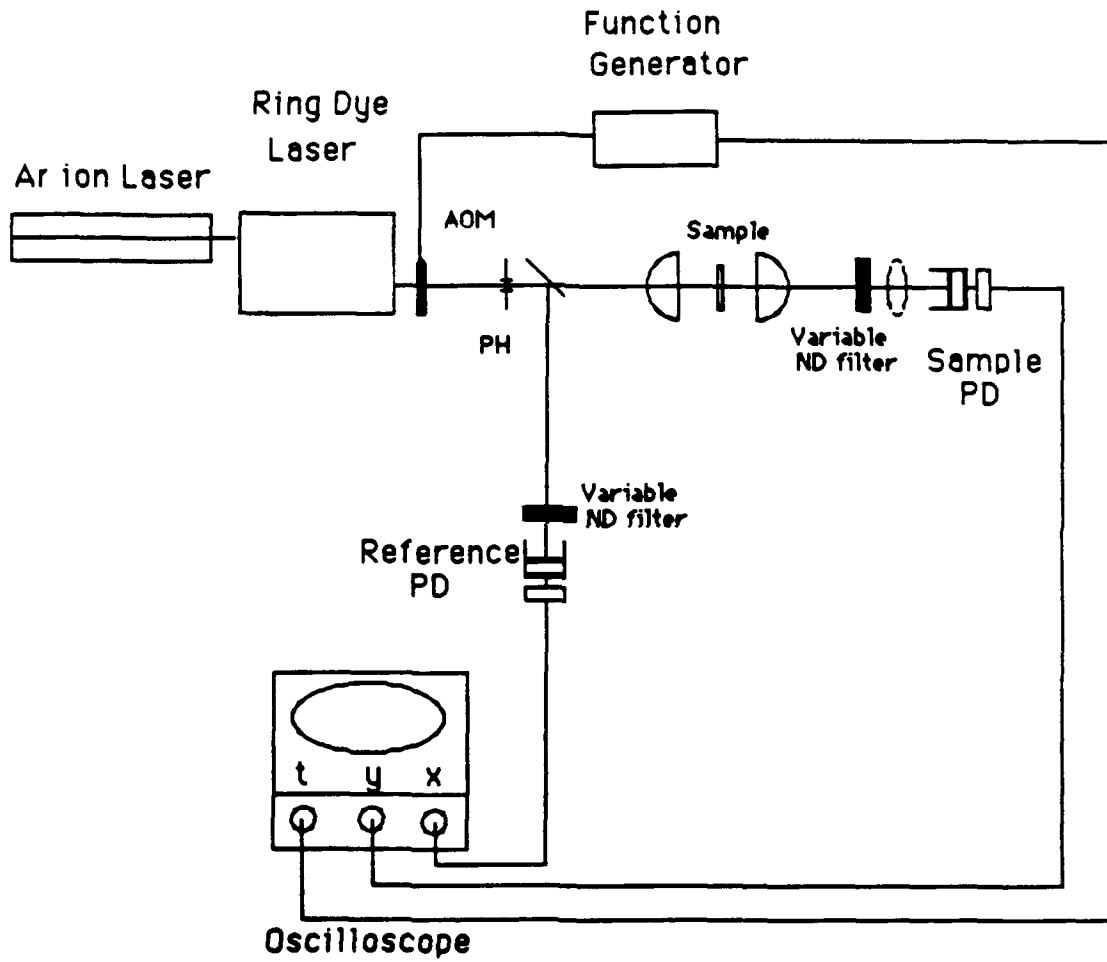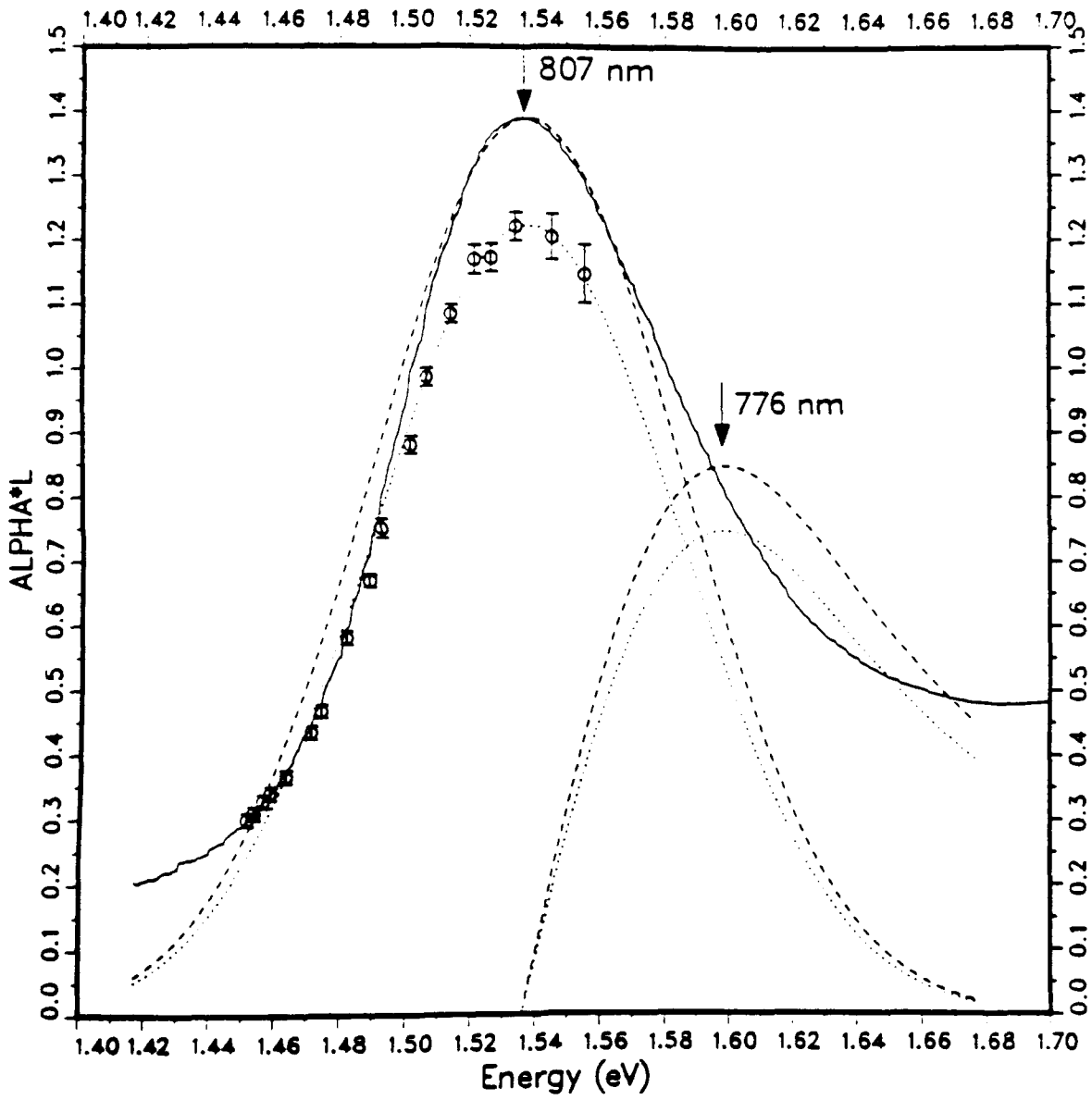

Figure 5.31

Dispersion of Saturable Absorption

Figure 5.32

CHAPTER 6

ABSORPTIVE OPTICAL BISTABILITY

The interpretation of O.B. as a nonequilibrium first order phase transition was obtained from a quantum statistical description of the electric field and microscopic atoms as shown in Chapter 2. The mathematical formulation for the most general case (nonzero detuning of the cavity and the atomic resonance different from the cavity mode) is quite complicated and does not provide a perspective in understanding various kinds of O.B. phenomena. There are different ways to describe O.B. in a steady state in a relatively phenomenological way. One way is to introduce the complex nonlinear eikonal appoximation,[1]−[3] which will not be discussed here. Another simple way to describe a steady state O.B. is that the electric field inside a F-P cavity forms a standing wave satisfying the appropriate boundary conditions, and the average field intensity induces an intensity dependent refractive index change resulting in a nonlinear transmission function for F-P.[4]−[8] The second approach will be adopted here to derive the steady state equation describing the most general case of O.B., allowing the analysis of the transmission function for different initial conditions to classify the different regimes of O.B.. These analyses are based on the steady state behavior of the system corresponding to the case w .en the relevant time scales of nonlinear Fabry-Perot interferometer are much shorter than the light pulse duration.

After the linear response of Fabry-Perot interferometer is briefly reviewed in Sec.6.1, the steady state nonlinear response of an optical Bloch system contained in a Fabry-Perot cavity is discussed in Sec.6.2. In the steady state case, the mathematical analysis allows us to classify O.B. as either dispersive or absorptive, depending upon the major contribution being the real part or imaginary part of the nonlinear susceptibility, respectively. Various regimes of O.B. are, then, discussed in Sec.6.3. Transient behavior of O.B. is briefly discussed in Sec.6.4. In order to describe the

transient response of a nonlinear F-P interferometer, which occurs when the relevant time scales for the interferometer is much shorter than the light pulse width. *the problem of the time evolution of a nonequilibrium phase transition* should be addressed, but unfortunately it is quite formidable. In real experimental situations. a transient thermodynamic instability, such as one that corresponds to tunneling through a Ginzburg-Landau potential well, does not take place, hence, the transient behavior of optical bistability can be accounted for by nonlinear dynamical studies.

In Sec.6.5, the optical bistability experiments perfomed on SINC thin films are presented. After the requirements on the light source and detectors for the measurements of optical bistability are discussed, the observation of electronic absorptive optical bistability at nanosecond time scales is presented, and the results are discussed based on the physical model for optical excitations in a random glassy medium introduced in Chapter 4. Also presented are results in the long pulse regime for thermal effects. which shows a hysteresis behavior completely differnt from electronic, absorptive bistability.

6.1 Fabry-Perot Interferometer

First we review a F-P interferometer.[9]−[10] Let's consider a F-P cavity with two plano-mirrors of reflectivity R as in Figure 6.1. The transmission function of a F-P cavity can be obtained either by considering multiple reflections of the electric field at the cavity mirrors, or by simply solving a boundary value problem with Maxwell equations. We adopt the second approach because it gives a much better physical picture when we consider a nonlinear optical response in the next section. The two mirrors of the F-P cavity provide a boundary condition for the electric fields, and we can solve the the boundary value problem easily. At $z = 0$,

$$\varepsilon_2(0) = \sqrt{1 - R}\varepsilon_1(0) - \sqrt{R}\varepsilon_2'(0) \qquad (6.1.1)$$

$$\varepsilon_1'(0) = \sqrt{R}\varepsilon_1(0) + \sqrt{1 - R}\varepsilon_2'(0) \qquad (6.1.2)$$

at $z = l$,

$$\varepsilon_3(l) = \sqrt{1 - R}\,\varepsilon_2(l) \tag{6.1.3}$$

$$\varepsilon_2'(l) = -\sqrt{R}\,\varepsilon_2(l) \tag{6.1.4}$$

where ε_i are defined in Figure(6.1). From Eq.(6.1.4), the fields at $z = 0$ can be obtained

$$\varepsilon_2'(0)e^{-inkl} = -\sqrt{R}\,\varepsilon_2(0)e^{inkl} \tag{6.1.5}$$

or,

$$\varepsilon_2'(0) = -\sqrt{R}\,\varepsilon_2(0)e^{i\delta} \tag{6.1.6}$$

with

$$\delta = 2nkl \tag{6.1.7}$$

where n is the refractive index, k is wavenumber, and l is cavity length. Substitution of Eq(6.1.6) into Eq(6.1.1) gives the reflected and transmitted fields as well as fields inside the cavity.

$$\varepsilon_2(0) = \frac{\sqrt{1 - R}}{1 - Re^{i\delta}}\varepsilon_1(0) \tag{6.1.7}$$

$$\varepsilon_2'(0) = -\frac{\sqrt{1 - R}\sqrt{R}}{1 - Re^{i\delta}}e^{i\delta}\varepsilon_1(0) \tag{6.1.8}$$

$$\varepsilon_1'(0) = \frac{\sqrt{R}}{1 - Re^{i\delta}}(1 - e^{i\delta})\varepsilon_1(0) \tag{6.1.9}$$

$$\varepsilon_3(l) = \frac{1 - R}{1 - Re^{i\delta}}e^{i\frac{\delta}{2}}\varepsilon_1(0) \tag{6.1.10}$$

Now the ratio $I^{(t)}/I^{(i)}$ of the transmitted intensity to the incident intensity is

$$
\begin{aligned}
\frac{I^{(t)}}{I^{(i)}} &= \frac{|\varepsilon_3(l)|^2}{|\varepsilon_1(0)|^2} = \left|\frac{1 - R}{1 - Re^{i\delta}}e^{i\frac{\delta}{2}}\right|^2 \\
&= \frac{(1 - R)^2}{1 + R^2 - 2R\cos\delta} = \frac{(1 - R)^2}{(1 - R)^2 + 4R\sin^2\frac{\delta}{2}} \\
&= \frac{1}{1 + \dfrac{4R}{(1 - R)^2}\sin^2\frac{\delta}{2}} = \frac{1}{1 + F\sin^2\frac{\theta}{2}}
\end{aligned}
\tag{6.1.11}
$$

218

with

$$\theta = 2M\pi - \delta = 2M\pi - 2nkl$$

$$F = \frac{4R}{(1-R)^2}$$

where θ is the cavity detuning in modulo 2π. The finesse $\mathcal{F}$ is defined by

$$\mathcal{F} = \frac{2\pi}{\varepsilon} = \frac{\pi\sqrt{F}}{2} \tag{6.1.12}$$

where ε is the FWHM of the transmission function. Eq.(6.1.11) describes the transmission function of an empty F-P cavity. First we find that the output intensity is linearly proportional to the input intensity for a given finesse $\mathcal{F}$ and cavity detuning θ. Second, we find that the transmission function has a maximum value of 1 for zero cavity detuning ($\theta = 0$), and that the transmission function depends on the finesse for nonzero cavity detuning, low finesse corresponding to larger leaking of light through F-P as illustrated in Figure 6.2.

6.2 Optical Bistability in Steady State

We now consider the electric field of the light wave propagating through the Fabry-Perot cavity which is filled with the Bloch system resonant with the light frequency. The Maxwell equation for the electromagnetic field inside the nonlinear medium with susceptibility $\chi(\vec{x}, t)$ is readily obtained.

$$\vec{\nabla} \times \vec{E} = -\frac{1}{c}\frac{\partial \vec{B}}{\partial t} \tag{6.2.1}$$

$$\vec{\nabla} \times \vec{H} = \frac{1}{c}\frac{\partial \vec{D}}{\partial t} \tag{6.2.2}$$

The constitutive relation is

$$\vec{D}(\vec{x}, t) = \epsilon(\vec{x}, t)\vec{E}(\vec{x}, t) = (1 + 4\pi\chi(\vec{x}, t))\vec{E}(\vec{x}, t) = \vec{E}(\vec{x}, t) + 4\pi\vec{P}(\vec{x}, t) \tag{6.2.3}$$

From the Eqs.(6.2.1), (6.2.2) and (6.2.3), we get the wave equation for the electric field inside the dielectric medium.

$$(\nabla^2 - \frac{1}{c^2}\frac{\partial^2}{\partial t^2})\vec{E}(\vec{x}, t) = \frac{4\pi}{c^2}\frac{\partial^2}{\partial t^2}\vec{P}(\vec{x}, t) = \frac{1}{c^2}\frac{\partial^2}{\partial t^2}\left(\chi(\vec{x}, t)\vec{E}(\vec{x}, t)\right) \tag{6.2.4}$$

For transverse light with frequency ω, the wave equation can be simplified to the expression

$$\left(\frac{\partial^2}{\partial z^2} + (1 + 4\pi\chi(z))\frac{\omega^2}{c^2}\right)\varepsilon(z) = 0 \tag{6.2.5}$$

For a Bloch system, the susceptibility $\chi(z)$ is a function of the light intensity as well as the coordinate z. From Eq.(3.7.10), the Bloch susceptibility inside the cavity is

$$\chi(z) = \frac{\alpha c}{4\pi\omega}\frac{\Delta + i}{1 + \Delta^2 + |\varepsilon(z)|^2} \tag{6.2.6}$$

The optical bistability phenomena can be explained by solving Eq.(6.2.5) with the Bloch susceptibility Eq.(6.2.6) in the proper boundary conditions determined by the cavity. The field inside the cavity has both a slow variation from the linear absorption and a rapid variation from the interference of the forward and the backward waves, and the Eqs.(6.2.5) and (6.2.6) can be solved numerically for the individual experimental configurations.

An analytical expression is available when a reasonable approximation is made. Because the interference of the forward and the backward waves forms a standing wave in the F-P cavity, we can take a spatial average of the field intensity inside the cavity and get the spatial-averaged nonlinear susceptibility which explains the nonlinear phase shift leading to a nonlinear transmission function of F-P. Taking the spatial average of the field inside the cavity, the nonlinear susceptibility is simply given as

$$\chi(I) = \langle\chi(z, I)\rangle = \frac{\alpha c}{4\pi\omega}\frac{\Delta + i}{1 + \Delta^2 + \langle|\varepsilon(z)|^2\rangle} \tag{6.2.7}$$

To find the electromagnetic field inside the cavity, we note that the forward and the backward waves at the coordinate z are

$$\varepsilon_F(z) = \varepsilon_2(0)e^{inkz} = \frac{\sqrt{1-R}}{1 - Re^{i\delta}}e^{inkz}\varepsilon_1(0) \tag{6.2.8}$$

$$\varepsilon_B(z) = \varepsilon_2'(0)e^{-inkz} = -\frac{\sqrt{1-R}\sqrt{R}}{1 - Re^{i\delta}}e^{i\delta}e^{-inkz}\varepsilon_1(0) \tag{6.2.9}$$

220

where ε_F and ε_B are the forward and backward propagating light wave, respectively. Taking the approximation $R \approx 1$, the field inside the cavity is

$$
\begin{aligned}
\varepsilon(z) &= \varepsilon_F(z) + \varepsilon_B(z) \\
&= \frac{\sqrt{1-R}}{1-Re^{i\delta}} \left(e^{inkz} - e^{i\delta}e^{-inkz} \right) \varepsilon_1(0) \\
&= \frac{e^{-i\frac{\delta}{2}}}{\sqrt{1-R}} \left(e^{inkz} - e^{i\delta}e^{-inkz} \right) \varepsilon_3(l)
\end{aligned}
\tag{6.2.10}
$$

Now taking the spatial average of $|\varepsilon(z)|^2$,

$$
\langle |\varepsilon(z)|^2 \rangle = \frac{1}{1-R} 4 \langle \sin^2 nkz \rangle |\varepsilon_3(l)|^2 = \frac{2}{1-R} |\varepsilon_3(l)|^2
\tag{6.2.11}
$$

Substituting Eq.(6.2.11) into Eq.(6.2.7), the spatially averaged nonlinear susceptibility can be written in terms of the transmitted intensity.

$$
\chi(I) = \langle \chi(z, I) \rangle = \frac{\alpha c}{4\pi\omega} \frac{\Delta + i}{1 + \Delta^2 + \dfrac{2}{1-R}|\varepsilon_3(l)|^2}
\tag{6.2.12}
$$

Now recall that from Eq.(6.1.11) the ratio of the transmitted intensity to the incident intensity is

$$
\frac{|\varepsilon_3(l)|^2}{|\varepsilon_1(0)|^2} = \left| \frac{1-R}{1-Re^{i\delta}} e^{i\frac{\delta}{2}} \right|^2 = \left| \frac{1-R}{1-Re^{i\delta(I)}} \right|^2
\tag{6.2.13}
$$

where $\delta(I)$ is the intensity dependent nonlinear phase shift. The Bloch system inside the cavity has an intensity dependent refractive index, $n(z) = n(z, I)$, and the transmission function of Eq.(6.2.13) has the intensity dependence through $\chi(I)$ as shown in Eq.(6.2.12). More explicitly

$$
\delta = 2nkl = 2(1 + 2\pi\chi)kl = 2kl + 4\pi\chi kl
\tag{6.2.14}
$$

While keeping terms up to first order, we can expand the phase factor $e^{i\delta}$.

$$
e^{i\delta} = e^{-i\theta}e^{i4\pi\chi kl} = 1 + i(4\pi\chi kl - \theta)
\tag{6.2.15}
$$

where $\theta = 2M\pi - 2kl$ is the cavity detuning in the modulo 2π and is assumed to be small relative to 2π. This assumption is reasonable since most of the optical

221

bistability experiments are performed near, or on, the cavity resonance. From Eq.(6.2.13) with Eq.(6.2.15) we can get a nonlinear transmission through the Fabry-Perot cavity containing a Bloch system. Substitution of Eq.(6.2.15) into Eq.(6.2.13) leads to the ratio of the output intensity to the input intensity as

$$\frac{|\varepsilon_3(l)|^2}{|\varepsilon_1(0)|^2} = \left| \frac{1-R}{1-Re^{i\delta(I)}} \right|^2$$

$$\approx \left| \frac{1}{1 - i\dfrac{R}{1-R}(4\pi\chi kl - \theta)} \right|^2$$

$$= \left| \frac{1}{1 - i\dfrac{R}{1-R}\left(\alpha l \dfrac{\Delta + i}{1 + \Delta^2 + \dfrac{2}{1-R}|\varepsilon_3(l)|^2} - \theta\right)} \right|^2 \qquad (6.2.16)$$

Eq.(6.2.16) is the most general expression describing steady state bistable behavior of a nonlinear Fabry-Perot cavity. We find that the transmission through a Fabry-Perot cavity containing an optical Bloch two-level system is a multi-valued function of the output intensity. In another words, the output intensity can assume one or three different values depending on the input light intenisty. In the following section, the various regimes of a steady-state O.B. will be discussed.

6.3 Optical Bistability: Various Regimes

In this section, we discuss different kinds of O.B. by considering various cases of the parameters specifiying the system. The nonlinear transmission function Eq.(6.2.6) describes the steady state O.B. in a general case. Taking the absolute value of the right hand side of Eq.(6.2.6)

$$\frac{|\varepsilon_3(l)|^2}{|\varepsilon_1(0)|^2}$$

$$= \left| \frac{1}{\left(1 + \dfrac{\dfrac{\alpha l R}{1-R}}{1 + \Delta^2 + \dfrac{2}{1-R}|\varepsilon_3(l)|^2}\right) - i\left(\dfrac{\dfrac{\alpha l R}{1-R}\Delta}{1 + \Delta^2 + \dfrac{2}{1-R}|\varepsilon_3(l)|^2} - \dfrac{\theta R}{1-R}\right)} \right|^2$$

$$= \cfrac{1}{\left(1 + \cfrac{\cfrac{\alpha l R}{1 - R}}{1 + \Delta^2 + \cfrac{2}{1 - R}|\varepsilon_3(l)|^2}\right)^2 + \left(\cfrac{\cfrac{\alpha l R}{1 - R}\Delta}{1 + \Delta^2 + \cfrac{2}{1 - R}|\varepsilon_3(l)|^2} - \cfrac{\theta R}{1 - R}\right)^2} \quad (6.3.1)$$

Defining the parameters as follows,

$$X = \sqrt{\frac{2}{1 - R}}\varepsilon_3(l) \qquad (6.3.2)$$

$$Y = \sqrt{\frac{2}{1 - R}}\varepsilon_1(0) \qquad (6.3.3)$$

$$C = \frac{\alpha l R}{2(1 - R)} \qquad (6.3.4)$$

$$\phi = \frac{\theta R}{(1 - R)} \qquad (6.3.5)$$

Eq.(6.3.21 can be rewritten[7]

$$Y^2 = X^2\left((1 + \frac{2C}{1 + \Delta^2 + X^2})^2 + (\frac{2C\Delta}{1 + \Delta^2 + X^2} - \phi)^2\right) \qquad (6.3.6)$$

X and Y are the normalized transmitted and the incident electric amplitudes, respectively. We can define the normalized transmitted and incident light intensity in the same way.

$$I_t = X^2, \quad I_i = Y^2 \qquad (6.3.7)$$

In terms of the intensities Eq.(6.3.6) can be rewritten as

$$I_i = I_t\left((1 + \frac{2C}{1 + \Delta^2 + I_t})^2 + (\frac{2C\Delta}{1 + \Delta^2 + I_t} - \phi)^2\right) \qquad (6.3.8)$$

Eq.(6.3.8) is the steady-state state equation for the nonlinear F-P in a general case. For specific values of the cooperative parameter C and initial cavity detuning ϕ, the state equation can be plotted in terms of the input intensity and the output intensity. The cooperative parameter C is a measure of cooperativity between microscopic dipole moments, already introduced in Chapter 2. Optical bistability

223

cannot be observed for the cooperativite parameter of value less than 4, which is analogous to the absence of ferromagnetism at a temperature above the critical temperature, as discussed in Chapter 2. Let's consider a couple of interesting cases.

First we check the empty cavity case, where C vanishes because there is no absorption inside the cavity. The state equation reduces to

$$I_i = I_t(1 + \phi^2) \tag{6.3.9}$$

which implies that the output intensity is linearly proportional to the input intensity. For comparison, we find the transmission function Eq.(6.1.11) derived for an empty F-P cavity when the detuning θ is to be small. From Eq.(6.1.11)

$$I_i = I_t(1 + F \sin^2 \frac{\theta}{2}) = I_t(1 + \frac{4R}{(1-R)^2} \sin^2 \theta)$$

$$\approx I_t(1 + \frac{4}{(1-R)^2}(\frac{\theta}{2})^2) = I_t(1 + (\frac{\theta}{1-R})^2) = I_t(1 + \phi^2) \tag{6.3.10}$$

We simply reproduce the state equation for the empty case, Eq.(6.3.9).

The next simplest case is when the cavity is tuned on the maximum transmission, $\phi = 0$, and the atomic detuning is zero, $\Delta = 0$. This case is called absorptive O.B.. From Eq.(6.3.8), we get

$$I_i = I_t(1 + \frac{2C}{1 + I_t})^2 \tag{6.3.11}$$

Noting the definition of the normalized amplitudes (Eq.(6.3.7)), we find that the state equation Eq.(6.3.11) is identical to the steady state solution of Fokker-Planck equation shown in Sec.2.2.(Refer to Eq.(2.2.22))

$$Y = X + \frac{2CX}{1 + X^2} \tag{6.3.12}$$

For absorptive O.B. with a detuned cavity in which $\Delta = 0$, $\phi \neq 0$, we find

$$I_i = I_t\{(1 + \frac{2C}{1 + I_t})^2 + \phi^2\}. \tag{6.3.12}$$

224

I_t can be a multiple function of I_i only for the cavity detuning ϕ less than some ϕ_{max} as will be seen shortly.

In a most general case of nonzero Δ and ϕ, a contour diagram can be drawn for a given C where a bistability can take place. This is shown in Figure (6.3).

6.4 Optical Bistability: Transient State

The transient state of O.B. can be properly described by solving the time dependent Fokker-Planck equation introduced in Sec.2.2. Here we have to be careful to distinguish two different kinds of time dependence. The Fokker-Planck equation describes the time evolution of the probability distribution function, and it is useful when we are particularly interested in the stability of the metastable state. According to our assumption of the smallness of q in Eq.(2.2.28), the system in the meatastable state does not decay into the stable state (true minimum) rapidly. The dynamical behvior of O.B. has been studied theoretically by solving the Fokker-Planck equation numerically.[11]-[13] One interesting question is how fast the system decays into the stable state once it is put in the metastable state. This corresponds to the negative slope region in the state diagram. This problem is closely related to the quantum mechanical tunnelling probability of a Brownian particle. According to the numerical calculations, the time required to penetrate the potential well varies for different potential depths and widths, as expected, but is much longer than the other relevant experimental time scales; Hence, in fact the system can be approximated to be in a stationary state. In another words, the relaxation time to the true minimun is much longer than the relevant time scales such as the pulse width of the incident light and the material relaxation time.

The real transient behavior of O.B. should be studied when the external input field changes in time. Now the problem reduces to the calculation of the particle trajectory for the time dependent Ginzburg-Landau potential. Here we can see that the important parameter in the shape of the probability distribution function is the

diffusion constant q, which depends on the spontaneous decay time of the material and the cavity decay time.

The transient behavior can be understood by solving the Newtonian equation of motion describing a particle in the Ginzburg-Landau potential with the time-dependent external field.

$$\frac{d^2\phi}{d\tau^2} = -\frac{\partial F}{\partial \phi} \tag{6.4.1}$$

For the ferromagnets in the magnetic field,

$$\ddot{\phi} = \alpha\phi + \beta\phi^3 + H\sin\omega t \tag{6.4.2}$$

$$\alpha < 0, \quad \beta > 0 \tag{6.4.3}$$

Eq.(6.4.2) is known as Duffing equation, which describes a driven nonlinear oscillator allowing a phase transition. The analytic solution of Eq.(6.4.2) is not available, and the transient behavior can be studied only by numerical method. For O.B., we need to solve the equation

$$\ddot{x} = \frac{2}{q}\{-x - \frac{2Cx}{1+x^2} + y_0\sin\omega t\} \tag{6.4.3}$$

The dynamical behavior for the on-set of O.B. has been studied numerically. [14] A numerical analysis of the dynamical behavior of O.B. shows hysteresis behavior rather than complete switch-on and switch-off. It is important to characterize the dynamical behavior of a first order phase transition far from equilibrium separately from a steady state behavior. One approach in studying the dynamical behavior is to look at a double-well potential, and study the particle motion in a various regimes of the physical parameters.[15]−[19]

6.5 Optical Bistability Experiment

6.5.1 Instrumentations

(A) Ti:Sapphire Laser

We used a single mode pulsed $Ti : Al_2O_3$ laser [20]−[24] pumped by a doubled Nd:YAG laser. The pump laser was a Q-switched nanosecond laser with 10 Hz repetition rate, from which 50 mJ of SHG with 20 ns pulse duration was readily available. In the $Ti : Al_2O_3$ laser cavity, mirrors with reflectivity of 95% and flatness of $\lambda/10$ were used. A typical configuration of $Ti : Al_2O_3$ laser oscillator configuration is shown in Figure(6.4). The SHG power from a Nd:YAG laser is controlled by a thin film polarizer and a half-wave plate assembly. A $Ti : Al_2O_3$ rod has a typical damage threshold of 4 Joule/cm^2. The titanium doped sapphire rod is end-pumped with the pump beam polarization along the optical axis of sapphire rod, and the operating frequency of the laser was selected by a birefringent filter made of quartz plates.[25] A multiple longitudinal mode operation of $Ti : Al_2O_3$ laser is shown in Figure(6.5). The cavity spacing was 36 inches, and it is clearly seen that the separation of each mode is 6 nsec corresponding to the round trip time of the given cavity spacing. When a resonant reflector (etalon) was substituted for the output coupler, we could get a single longitudinal mode output pulse. In single mode $Ti : Al_2O_3$ laser gave a typical energy of $80\mu J$ per pulse with 40 ns pulse width when pumped with 35 mJ of SHG. The band width of single mode $Ti : Al_2O_3$ laser was measured to be less than 1 GHz. The laser frequency of $Ti : Al_2O_3$ laser was tunable between $700nm$ to $1.0\mu m$ by a birefringent filter. In the bistability experiment, a smooth, stable, reproducible temporal shape of the laser pulse is essential to show a direct display of the hysteresis arising from the nonlinear response of polymer dye inside Fabry-Perot cavity, and single mode $Ti : Al_2O_3$ laser gave a satisfactory temporal shape, which is due to the long storage time of fluorescence from Ti^{+3} ion inside sapphire crystal field. A typical temporal shape is shown in Fugure(6.6) Also shown in Figure(6.7) is the temporal pulse shape of SHG of YAG pumping (left) and single mode $Ti : Al_2O_3$ laser output (right).

(B) Laser diode

A laser diode is a convinient light source providing a stable output. [26] In a typical semiconductor laser diode, an active semiconductor layer of thickness of 0.3μm is sandwiched by p and n type semiconductors. The laser operational wavelength depends on the active medium, and can be varied from 800nm to 1.5μm. The most readily available laser diode is a GaAs laser having an operating wavelength near IR, typically 840nm. Since laser operation in a semiconductor occurs upon recombination of electron-hole pairs generated by the injected current, the conversion efficiency is highly dependent on the temperature of the active medium. The natural reflectivity of the semiconductor surface is used as the laser cavity, and a typical size of the laser emitting facet is $0.5\times 2.0\mu$m^2 with cavity length 100μm. Laser light comes out from both facets of the active layer, with one used as the output coupler, the other coupled to a photodiode to monitor the laser power. In an index-guide configuration, the output light has a single transverse mode, while a gain-guided configuration gives multiple transvers modes. The output light is linearly polarized along the facet strip.

Compared to other gas or solid lasers, laser diodes have a rather high laser conversion efficiency, which depends on the laser head temperature. At 25° C, 1.5 mW/facet is easily available with 25 mA operational current in an index-guided configuration. Once the operational current is above the threshold current, the output power is linearly proportional to the operational current up to the breakdown point. In CW operation, the temperature of the laser head and the operational current can be well controlled, giving a very stable output power. A laser diode can also be operated in a pulsed mode, but the varying temperature and current usually cause a much worse operation in the laser spectrum. In fact, even in CW operation the short cavity length (order of 100μm) can support many longitudinal modes, and much technological effort has been focused on reducing the broad line width of output optical spectrum. In a real application of a laser diode as a light source,

good collimation optics is needed to collect large diverging light, which comes from the diffraction of light itself. A typical diverging angle is order of 40°-60°, and a microscopic objective lens can be employed as a collimating optics.

A Mitsubish single mode laser diode (ML 3401) with an operational wavelength of $\lambda=819$ nm was successfully employed at the early stage of the saturable absorption experiments. While a couple of milliwatts is a typical output power available form a single mode laser diode, a couple of hundred milliwatt of laser power can be obtained from a phased-array of diodes, which is commercially available (Spectra Diode Labs; SDL 2422-111 CW laser diode, 200 mW, TO-3 window, SDL 800 laser diode driver, SDL 800-H finned heat-sink, mount for TO-3). One main difficulty in using the phased-array laser diode in the optical bistability experiments has been the light collimation in a long optical path through a Fabry-Perot interferometer.

(C) Light Detectors

In the O.B. experiments, the hysteresis behavior of the transmission from a nonlinear F-P interferometer upon increase and decrease of the incident light intensity is detected by a light detector. In standard nonlinear optical experiments, such as the optical Kerr effect or third harmonic generation, a time-convoluted optical signal is integrated over the entire pulse duration in order to obtain the nonlinear optical response. In O.B. experiments, in contrast, the detailed temporal change experienced by an incident light pulse passing through the nonlinear optical F-P interferometer contains all the information on the dynamical processes resulting from nonlinear optical response. Therefore, it is very important to work in a light intensity range where the light detectors have a completly linear photo response. In order to achieve such a condition, the light intensity impinging on the detector should be quite decreased without introducing any change in beam profile. However, in order to observe O.B., we need to deal with a light intensity strong enough to induce a sufficient nonlinear optical effect. With these considerations, it is found that a pho-

229

tomultiplier tube is not an appropriate detector in an O.B. experiment. A simple Motorola MRD 510 silicon PIN photodiode was employed in O.B. experiments. For a discussion of PIN photodiode circuits, see Sec.5.4.1 (C).

(D) Oscilloscope

In a nonlinear optics experiment where a short optical pulse is used, a large bandwidth oscilloscope is essential to monitor a real time fast signal. Tektronix 7104 1GHz is an adequate oscilloscope for an expeiment involving picosecond and nanosecond pulses. 7104 scope can house 2 amplifier plug-ins and 2 time base plug-ins. With 7B10 time base plug-in, the rising time resolution can be up to 200 ps. This scope can also be operated in X-Y mode, that is one amplifier plug-in at either left or right vertical slot and the other amplifier plug-in at B-horizontal, with a time base at A-horizontal. In option B version of 7104, "a horizontal delay line is attached to the instrument (at B-horizontal) permitting signal phase correction between the vertical and horizontal deflection system", which is important in a nanosecond optical bistability experiment. Tektronix 7A29 amplifier plug-in with option 4 features a variable delay ($\pm$500ps), which is useful in adjusting the synchronization between input and output signals in optical bistability experiment.

(E) Fabry-Perot Interferometer

In the O.B. experiments, a Fabry-Perot interferometer is used with a nonlinear optical material inserted between two mirrors. A standard Fabry-Perot interferometer operation is described here. The Fabry-Perot interferometer[27]−[28] consists of two parallel mirrors mounted on a super-invar bar supported base. The cavity length, or the mirror spacing, is adjustable by moving one mirror along a super-invar bar. The finsesse of the Fabry-Perot interferometer is affected by a couple of instrument parameters. That is, the inverse square of instrumental finesse is given as a sum of inverse squares of the reflection finesse, mirror flatness finesse, and pin hole finesse.

230

The reflectivity of the mirror determines the reflection finesse, $\mathcal{F}_R = 2\pi/\varepsilon = \pi\sqrt{R/(1-R)}$. When absorption occurs inside the cavity, it can be taken into account by redefining an effective reflectivity, $R_\alpha = R \times \exp(-\alpha L)$. The mirror flatness finesse, $\mathcal{F}_F$, is simply $M/2$ for a mirror with the flatness of λ/M. The pin hole finesse, $\mathcal{F}_P$, is determined by the power of the collimating lens and the pin hole diameter; that is, $\mathcal{F}_P = \triangle\lambda\{^\varepsilon/\mathcal{D}^\varepsilon\lceil$, where D is the pin hole diamter, f the focal length of collimating lens, and d the cavity spacing.

For a given fixed cavity length d, the free spectral range (F.S.R.) of a F-P interferometer is given as $c/2nd$, where c is the velocity of light, n the refractive index of material inside the cavity, and d the cavity spacing. The instrumental linewidth (ε) is the ratio of F.S.R. to the finesse. Thus, a large finesse correpsonds to a smaller instrumental linewidth, or higer resolution of the instrument. For a given finesse, the instrumental linewidth can be reduced by reducing the F.S.R., or by simply increasing the cavity spacing, d.

A piezo-electric transducer (PZT) allows a fine control of the mirror position ($2.21\mu/1000$ V). A PZT itself has a hysteresis behavior between the position and the applied high voltage, which has to be taken fully into account when an absolute position of the mirror is measured. By applying a high ramp voltage across PZT, a Fabry-Perot interference pattern can be scanned. A typical interference pattern is shown in Figure(6.8).

A Fabry-Perot interferometer can be used not only for optical bistability experiments, but also for nonlinear optical interferometry experiments[29]-[30] as shown in Figure(6.9). An intense, pulsed, pump beam induces an intensity dependedent refractive index change, resulting in a temporary phase shift. The resulting shift in the Fabry-Perot interference pattern can be.probed by a CW probe light source. Since a transient Fabry-Perot interference pattern is difficult to observe, it is important to employ a pump laser having a pulse duration longer than the cavity round trip time.

231

6.5.2 Experimental Layout

The optical bistability experimental layout (Figure6.10) was basically the same as the arrangement used for measuring the dispersion of saturable absorption. The laser output was partially reflected by a pellicle beam splitter to a reference silicon detector, and the transmitted beam was tightly focused on the thin film which had been spin coated directly onto the front mirror. The output fringes were collimated and passed through a 500 μm pinhole, and a sample silicon detector monitored the intensity at the central part of the Bull's eye interference fringe. Silicon PIN photodiodes were used for reference and sample arms, and the output intensity versus input intensity was directly displayed on a 1 GHz oscilloscope operating in the x-y mode and externally triggered. At nanosecond time scales, initial measurements were attempted at 813 nm using the output from the Nd:YAG pumped methane Raman cell as the laser source, but later, more stable amd smooth pulses at 799 nm from a single-mode pulsed Ti:Al$_2$O$_3$ laser pumped by a frequency doubled Nd:YAG laser were used.

The free spectral range of cavity spacing bewteen two mirrors was set at 2.3 GHz. The 752 nm line of C.W. Kr^+ laser was employed to align Fabry-Perot interferometer. After the alignment of Fabry-Perot is asssured, $Ti : Al_2O_3$ laser output was gradually focused by $f = 2.0m$ lens and passed through the pin holes to follow the same beam path of Kr^+ laser. The maximum incident light intensity at the front mirror of Fabry-Perot was $160kW/cm^2$. The light intensity was controlled by the variable neutral density filter in front of the polarizer. Silicon PIN photodiodes were used for reference arm and sample arm, and the signal, i.e., output intensity versus input intensity, was directly displayed on the 1 GHz oscilloscope in X-Y mode with external triggering.

6.5.3 Measurement and Analysis

The SINC thin films were simply spin coated as a wide area (2 - 5 cm in

diameter) films of approximately 80 nm thickness on the front dielectric mirror of the Fabry-Perot interferometer (Burleigh RC-110). The free spectral range of the cavity was adjustable and set at 12.5 GHz. Initial cavity detuning was adjusted by varying the high voltage applied to PZT annular ring that held the output mirror (the PZT had total motion of 2.21 μm/1000 V), and when this output mirror was scanned, a Fabry-Perot interference pattern with a finesse of 2 was obtained with the sample in the cavity. Refer to Figure(6.11).

Figure(6.12) and (6.13) shows the bistable hysteresis behavior observed when 40 ns pulses with intensity 160 kW/cm^2 at 799 nm were incident on the nonlinear F-P. We found that for zero cavity detuning ($\phi=0.0$) (Figure(6.12)) the bistable behavior was the largest, while when the cavity was detuned ($\phi=\pi$) (Figure(6.13)), the shape of the hysteresis curve changed and the effect became much smaller. In each case, the data were reproducible through many cycles of increased and decreased incident light intensity. Further, the data were also reproducible when focussing at different areas of each film sample. This kind of initial cavity detuning dependence is typical of absorptive OB, which results from saturable absorption and a subsequent change in the loss of the F-P cavity, enabling higher transmission than is possible at low light levels. However, the greatly reduced effects observed for nonzero cavity detuning indicate a very small dispersive contribution.

The incident laser wavelength was moved to 780 nm corresponding to near optimum conditions for possible dispersive contributions to the bistability. The same measurements were repeated, and under all conditions no bistable behavior was observed (Figure(6.14)). The absence of any bistable behavior at 780nm, where a large dispersive effect is expected from the Kramers-Kronig relation analysis, means simply that the relatively broad Q-band is not one single homogeneously broadened line but an inhomogeneously broadened envelope for many homogeneous lines, and supports the microscopic picture of the glassy polymer SINC film introduced in Chapter 4. Thus, near maximum saturable absorption at 810 nm, naphthalocya-

233

nine thin films exhibit primarily absorptive optical bistability at nanosecond time scales. The above analysis is based on steady state conditions for optical bistability because of the relevant time scales (pulse width: 40ns; relaxation time: 5ns; and cavity roundtrip time: 1ns), but transient effects may also play some role in the observed hysteresis behavior, which continues to be examined in on-going studies.

Since purely absorptive optical bistability is rarely observed, a systematic series of studies of possible thermally-induced refractive index changes in the thin films were performed as a function of increased pulse duration from 10^{-6} to 2 seconds. The laser source used in these studies was the AOM chopped, Spectra-Physics CW ring dye laser described above. Refer to Figure(6.15) for the experimental layout. Figure(6.16) shows an example of the optical bistability observed; the pulse width was 2.0 sec and the duty cycle 20%. When the cavity was tuned on resonance with the incident light wavelength (ϕ=0.0, lower right in Figure(6.16)), no hysteresis loop was observed, indicating the lack of an absorptive bistability effect, and this was true even when the dye laser output frequency was resonant with the linear absorption peak of the sample. However, for a negative ϕ (-1.0, left in Figure(6.16)), bistable hysteresis with a counterclockwise circulation was observed, and for positive ϕ (0.75, upper right in Figure(6.16)), the bistable hysteresis had clockwise circulation. With the pulse width and the resonant wavelength near the linear absorption peak of 810 nm, the bistable behavior is due to a thermally-induced dispersive intensity dependent refractive index change. Most importantly, this behavior is distinctly different from the fast pulse bistability observed at nanosecond timescales.

The bistable loops do not show a complete switching on and switching off. The reason for this is that eventhough the resonant n_2 value of the naphthalocyanine oligomer is fairly large, the film thickness (80 nm) is so small that the nonlinear phase shift experienced by the light inside the etalon is not large enough for complete switching to occur. According to the Ginzburg-Landau potential description

234

of O.B.of Chapter 2, the magnitude of hysteresis effect depends on a number of the physical parameters. Among these paramters, the cooperativity C is the most important factor in determining the size of the hyteresis loop. In our experimental conditions, the cooperative value C is approximately 10 corresponding to the conditions shown for Figure (2.16). As can be seen from the figure, these conditions lead to a relatively low contrast loops as observed. Current experiments in our laboratory are focused on this issue and measurements are being performed as a function of film thickness, optical density, cavity length, and pulse width.

References: Chapter 6

[1] Orenstein, M., Katriel, J., and Speiser, S., Phys. Rev. A35, 1192 (1987)

[2] Orenstein, M., Katriel, J., and Speiser, S., Phys. Rev. A35, 2175 (1987)

[3] Speiser, S., and Chisena, F.L., SPIE vol. 824, 144 (1987)

[4] McCall, S.L., Phys. Rev. A9, 1515 (1974)

[5] Felber, F.S. and Marburger, J.H., Appl. Phys. Lett. 28, 731 (1976)

[6] Marburger, J.H. and Felber, F.S., Phys. Rev. A17, 335 (1978)

[7] Agarawal, G.P. and Carmichael H.J., Phys. Rev. A19, 2074 (1979)

[8] Lugiato, L.A., In *Progress in Optics*, ed. E. Wolf, Vol. XXI. North-Holland, Amsterdam (1985)

[9] Born, M. and Wolf, E., *Principles of Optics*, Pergamon, New York, (1970)

[10] Hernandez, G., *Fabry-Perot interferometers*, Cambrige University, New York, (1986)

[11] Schenzle, A. and Brand, H., Opt. Commun. 31, 401 (1979)

[12] Farina, J.D., Narducci, L.M., Yuan, J.M., and Lugiato, L.A., Opt. Eng. 19. 469 (1980)

[13] Lugiato, L.A., Farina, J.D., and Narducci, L.M., Phys. Rev. A22, 253 (1980)

[14] Mandel, P. and Erneux, T., Opt. Commun. 44, 55 (1982)

[15] Stoker, J.J, *Nonlinear Vibrations*, Interscience, New York (1950)

[16] Bray, A.J. and McKane, A.J., Phys. Rev. Lett. 62, 493 (1989)

[17] Tsironis, G.P. and Grigolini, P., Phys. Rev. Lett. 61, 7 (1989)

[18] Jung, P. and Hanggi, P, Phys. Rev. Lett. 61, 11 (1989)

[19] Guckenheimer, J. and Holmes, P., *Nonlinear Oscillations, Dynamical Systems, and Bifurcations of Vector Fields*, Vol. 42 of Applied Mathematical Sciences, Springer, Berlin (1983)

[20] Moulton, P.F., J. Opt. Soc. Am B3, 125 (1986)

[21] Aggarawal, R.L., Sanchez, A., Fahey, R.E., and Strauss, A.J., App. Phys. Lett. 48, 1345 (1986)

[22] Sanchez, A., Fahey, R.E., Strauss, A.J., and Aggarawal, R.L., Optics Lett. **11**, 363 (1986)

[23] Koechner, W., *Solid -State Laser Engineering*, Springer Series in Optical Sciences, Springer-Verlag, New York, (1976)

[24] Kangas, K.W., Lowenthal, D.D., and Muller III, C.H.. Optics Lett. **14**, 21 (1989)

[25] Yariv, A. and Yeh, P., *Optical Waves in Crystals* Wiley, New York, (1984)

[26] Yariv, A., *Quantum Electronics*, 2nd ed., Wiley, New York, (1975)

[27] Gornall, W.S., Lasers & Applications, July, pp 47-52, (1983)

[28] Tech Memo on Fabry-Perot interferometer, Burleigh Instruments, Burleigh Park, Fishers, N.Y. (1986)

[29] Roychoudhuri, C., J. Opt. Soc. Am., **65**, 1418, (1975)

[30] Dangor, A.E. and Fielding, S.T., J. Phy. D: Appl. Phys. **3**, 413, (1970)

Figure Captions; Chapter 6

Figure 6.1; Electromagnetic Wave in Fabry-Perot Interferometer

Figure 6.2; Transmission Function of a Fabry-Perot Interferometer

Figure 6.3; Contour Diagram for Optical Bistability (Δ = atomic detuning, ϕ = initial cavity detuning, C = cooperativity)

Figure 6.4; Ti:Sapphire Laser Oscillator Design

Figure 6.5; Multi Longitudinal Modes from Ti:Sapphire Laser

Figure 6.6; Single Longitudinal Mode from Ti:Sapphire Laser

Figure 6.7; SHG YAG Pumping and Single Mode from Ti:Sapphire Laser

Figure 6.8; Fabry-Perot Interference Pattern for an Empty Cavity

Figure 6.9; Experimental Layout for Nolinear Interferometry

Figure 6.10; Experimental Layout for Optical Bistability Experiment

Figure 6.11; Fabry-Perot Interference Pattern with Sample inside the Cavity

Figure 6.12; Absorptive Optical Bistability with Zero Cavity Detuning

Figure 6.13; Absorptive Optical Bistability at Cavity Detuning

Figure 6.14; No Optical Bistability at Either Cavity Detuning at Maximum Refractive Index Change

Figure 6.15; Experimental Layout for Optical Bistability Experiment; Long Pulse Regime

Figure 6.16; Thermal Dispersive Optical Bistability at with Long Pulse Duration

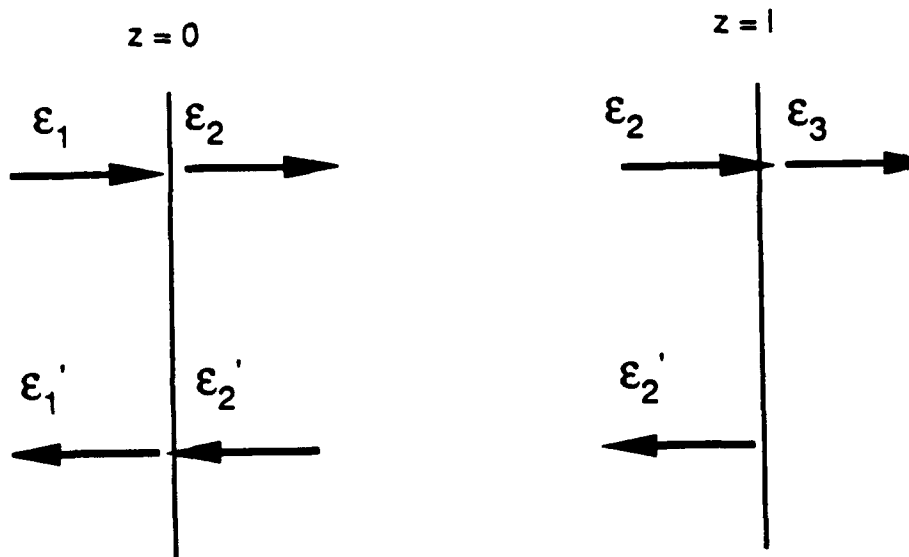# Electromagnetic Wave
In Fabry-Perot Interferometer

Figure 6.1

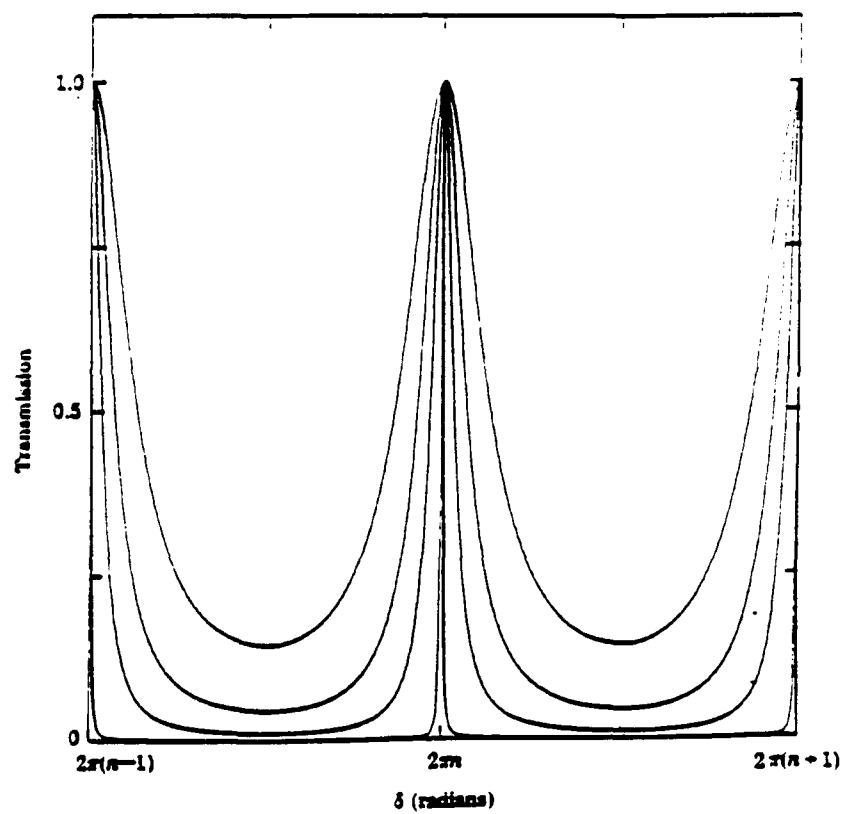# Transmission Function of a Fabry-Perot Interferometer

Figure 6.2

Contour Diagram for Optical Bistability
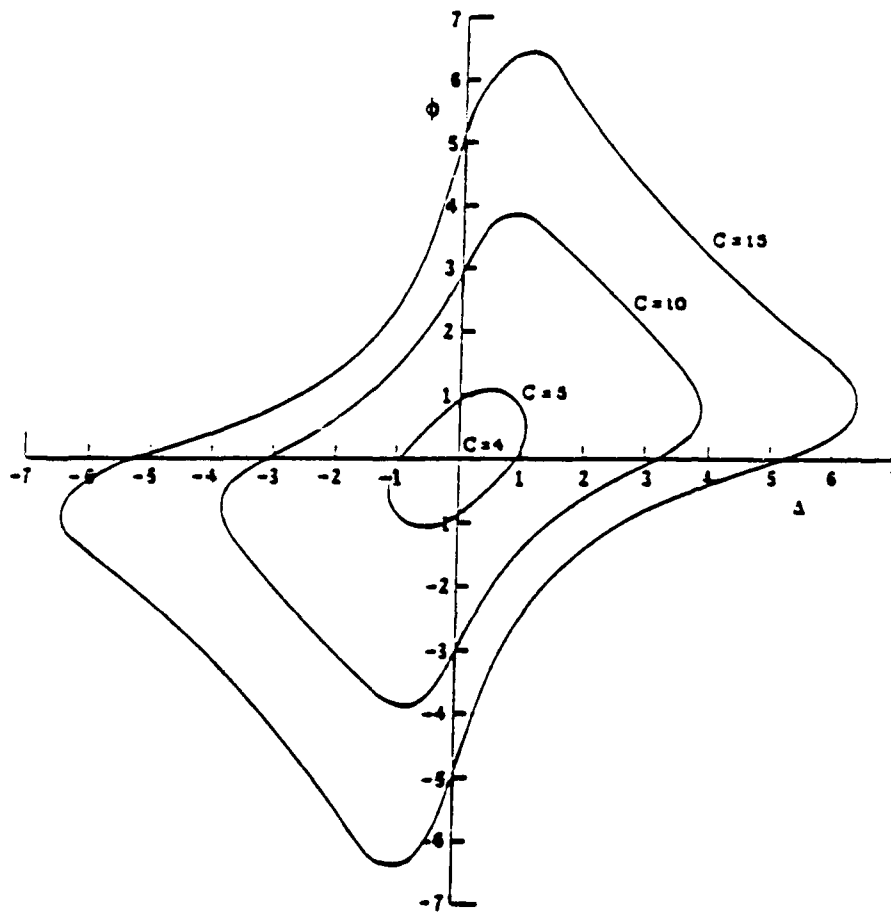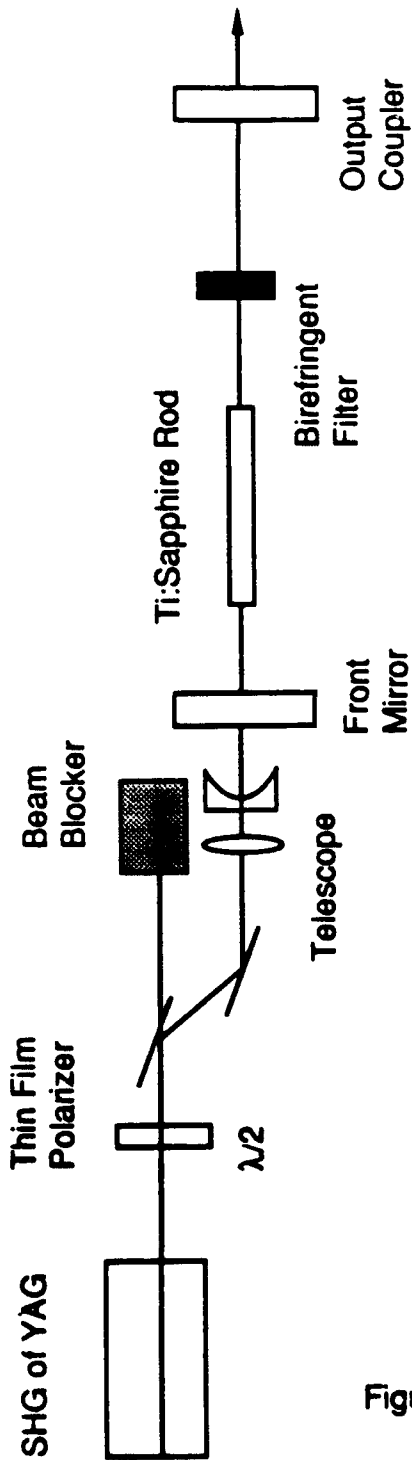**(D= atomic detuning, f, = initial cavity detuning, C = cooperativity)**

Figure 6.3

241

Ti:Sapphire Laser Oscillator Design

Beam Waist; before telescope: 4mm
at Ti:Sapphire rod: 1.5mm

Telescope; f=200mm & f=-100mm

Front mirror; Rmax, Curvature R=5 m

Output Coupler; 98% Reflectivity, t=5mm resonant reflector

Ti:Sapphire Rod; 0.03% Ti, Diameter=0.25", Length= 40mm

Cavity Spacing; Variable, order of 30"

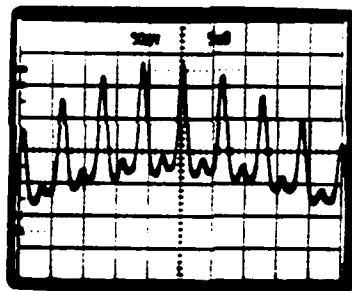Figure 6.4

Multi-Longitudinal Modes from Ti:Sapphire Laser

Figure 6.5

243

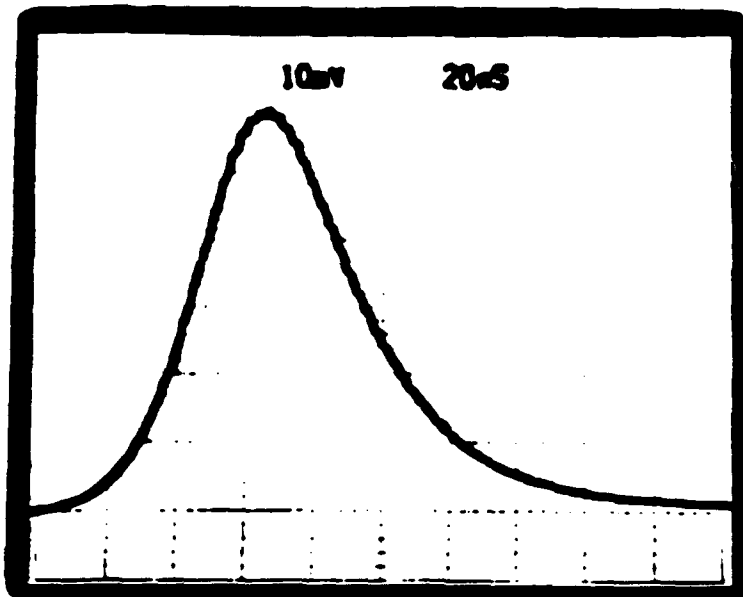# Single Longitudinal Mode from Ti:Sapphire Laser

Figure 6.6

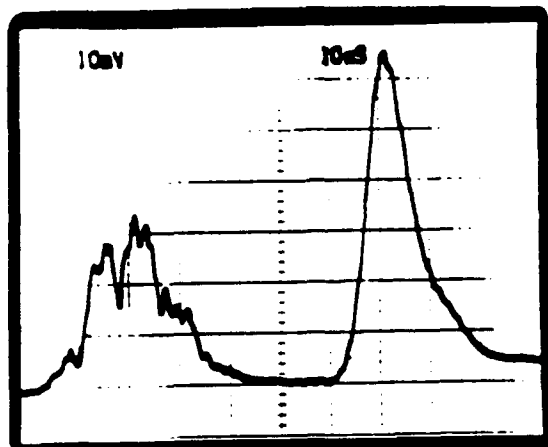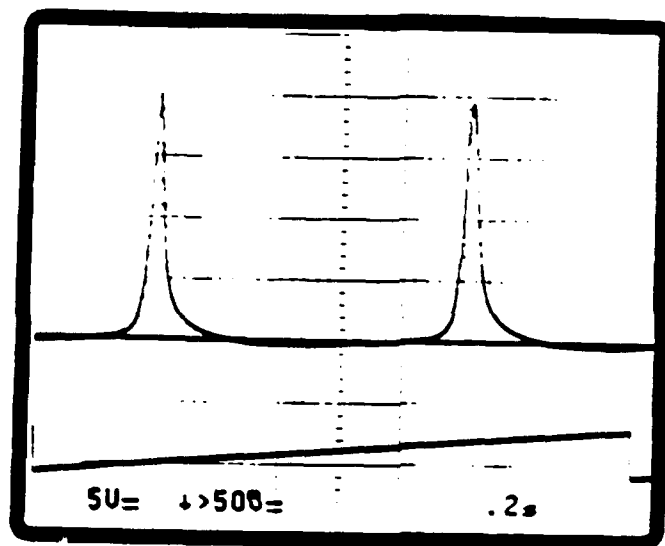# SHG YAG Pumping and Single Mode from Ti:Sapphire Laser

Figure 6.7

Fabry-Perot Interference Pattern for an Empty Cavity

Figure 6.8

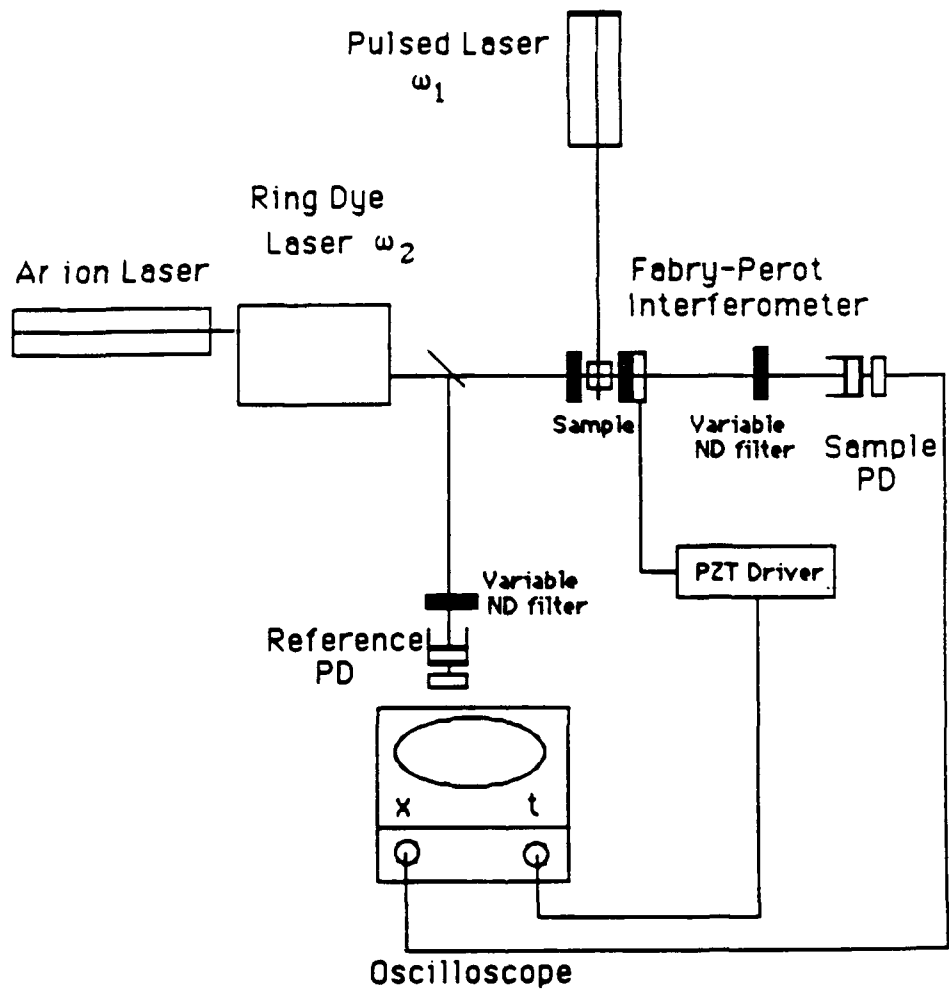**Experimental Layout for Nonlinear Interferometry**

Figure 6.9

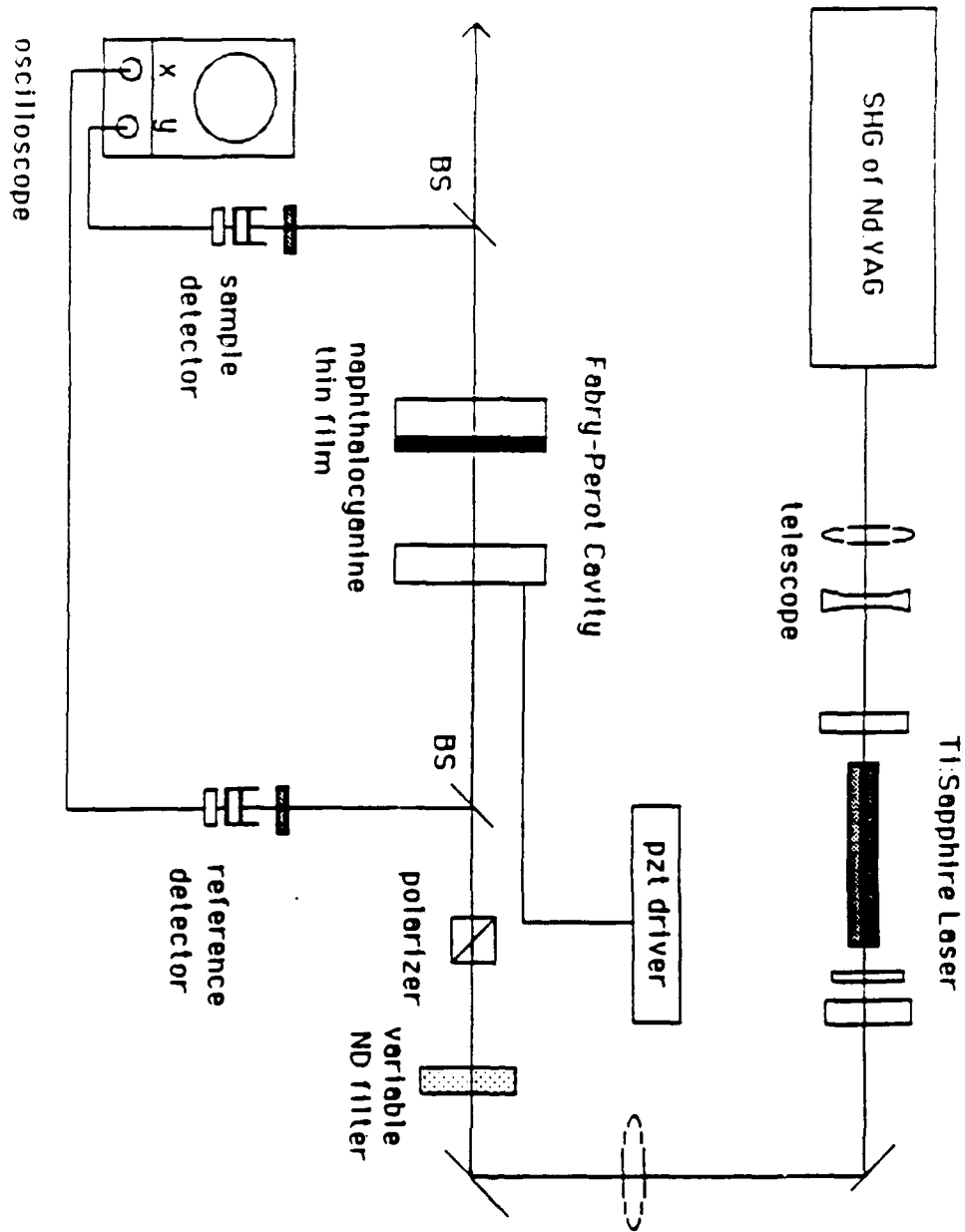# Experimental Layout for Optical Bistability Experiment

Figure 6.10

Fabry-Perot Interference Pattern with a Sample inside the Cavity
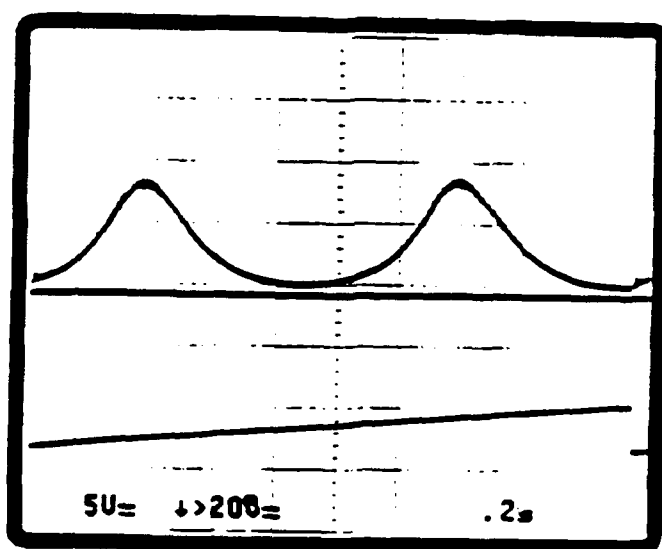
Figure 6.11

Absorptive Optical Bistability with Zero Cavity Detuning

Output Power

Figure 6.12

Absorptive Optical Bistability at Cavity Detuning

Output Power

Input Power

Figure 6.13

**No Optical Bistability with Either Cavity Detuning
at Maximum Refractive Index Change**

Figure 6.14

252

Experimental Layout for Optical Bistability Experiment; Long Pulse Regime

Figure 6.15

Output Power

Figure 6.16

CHAPTER 7

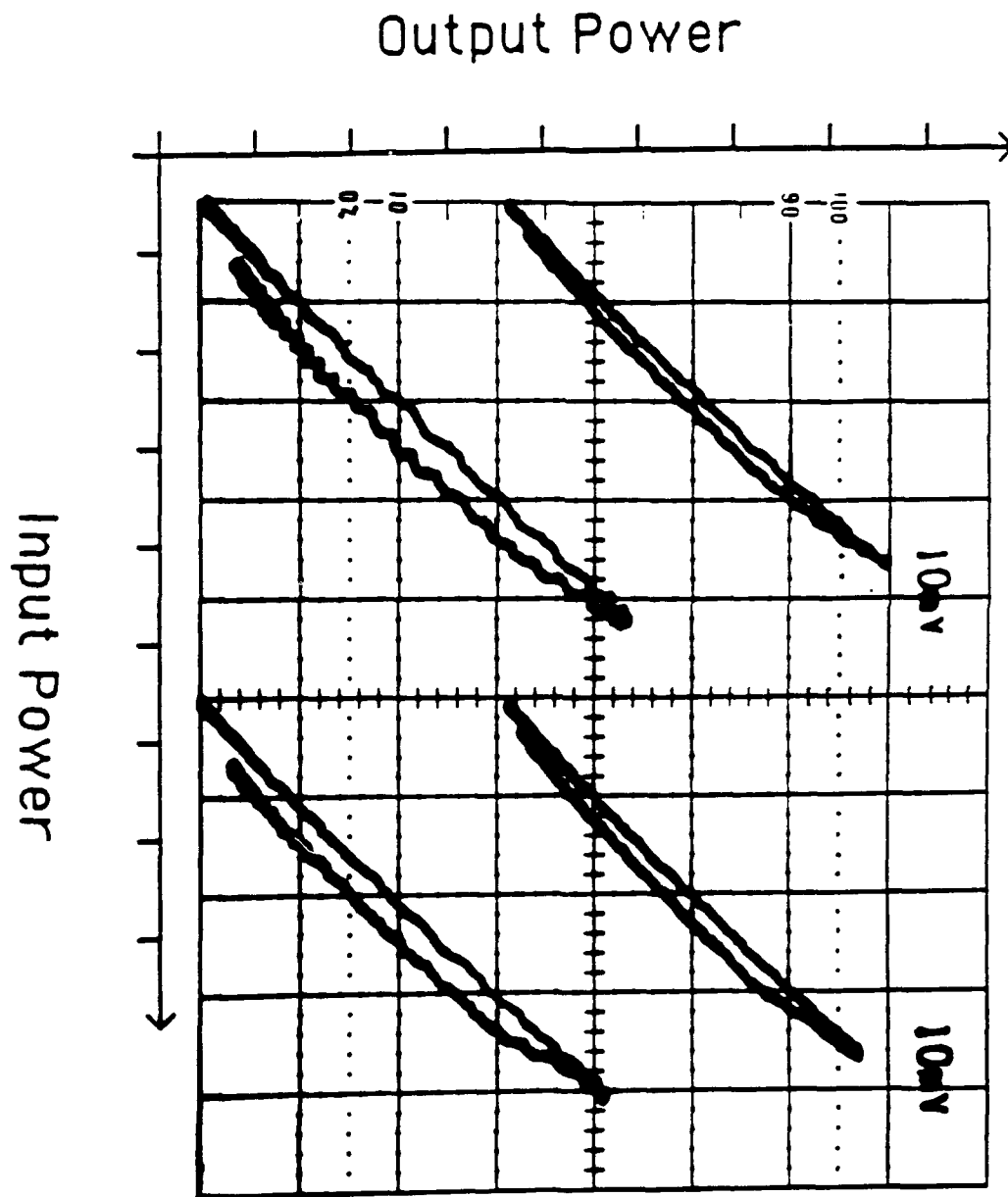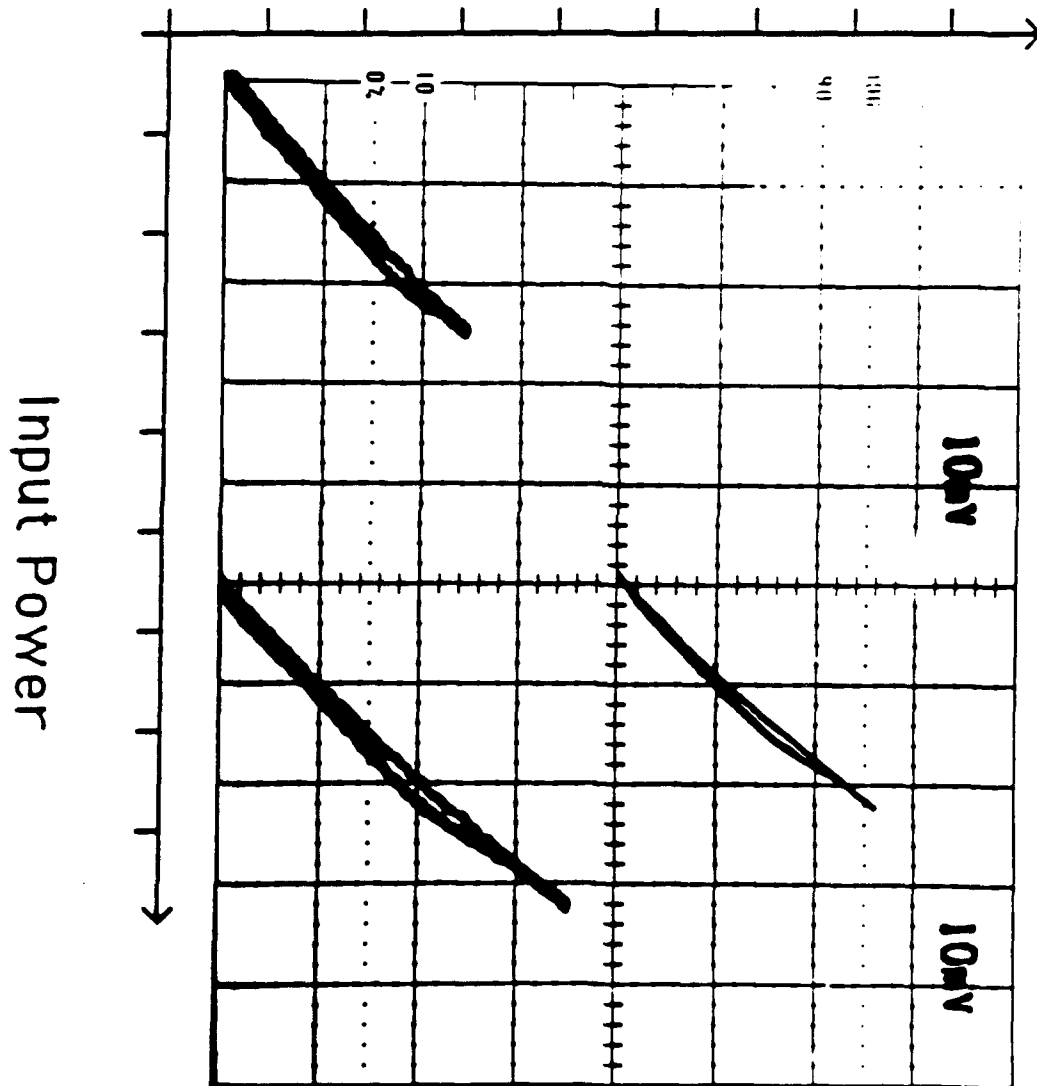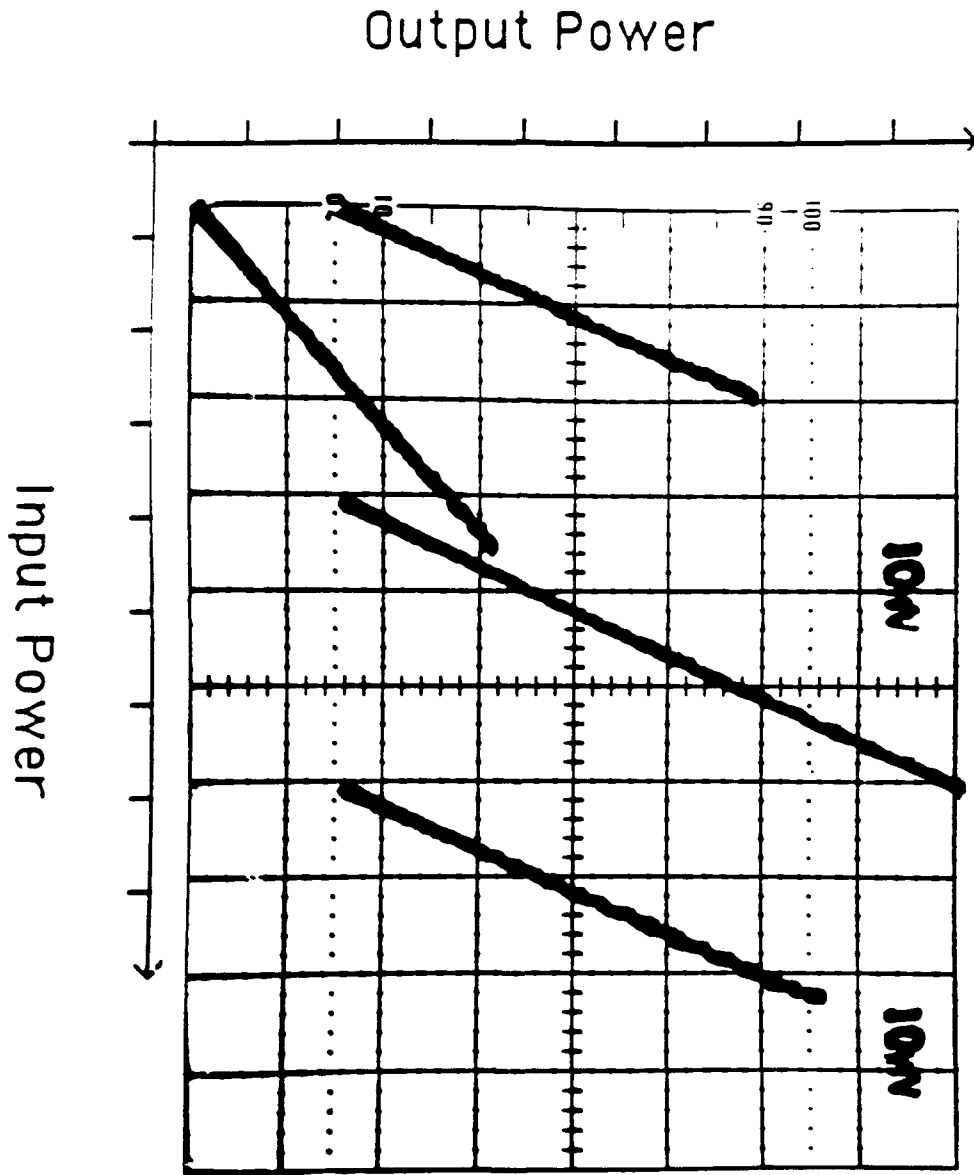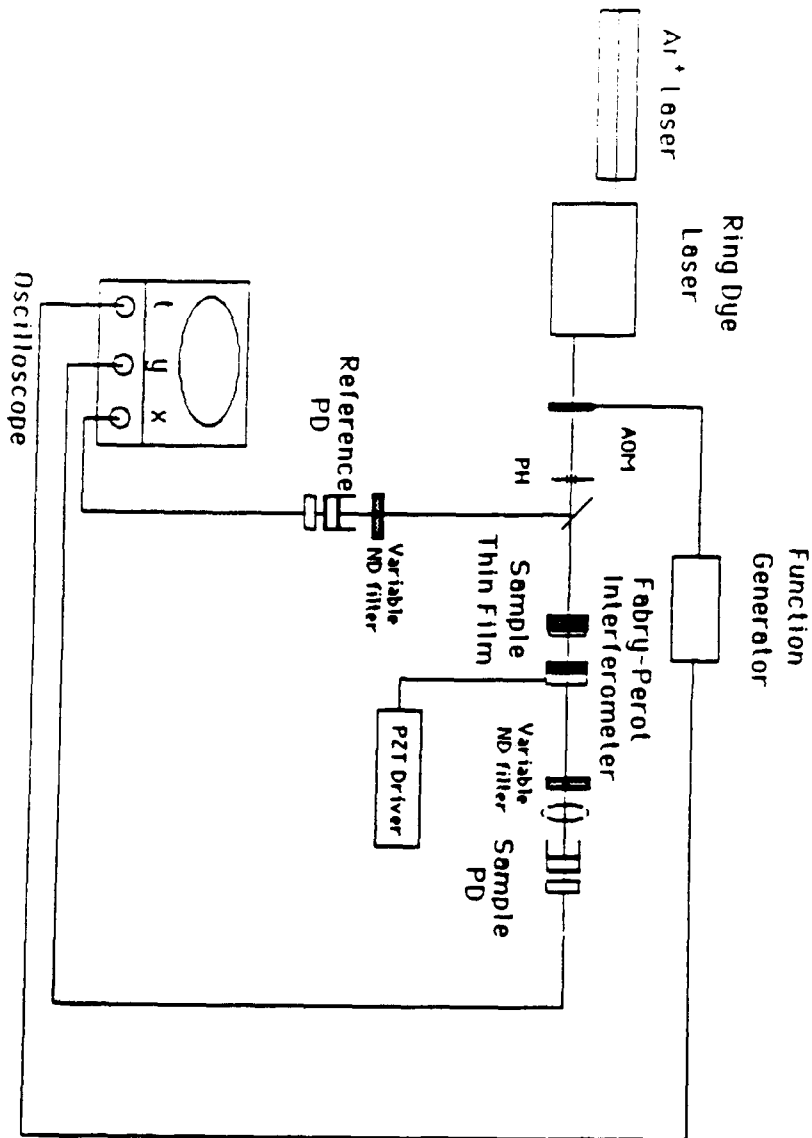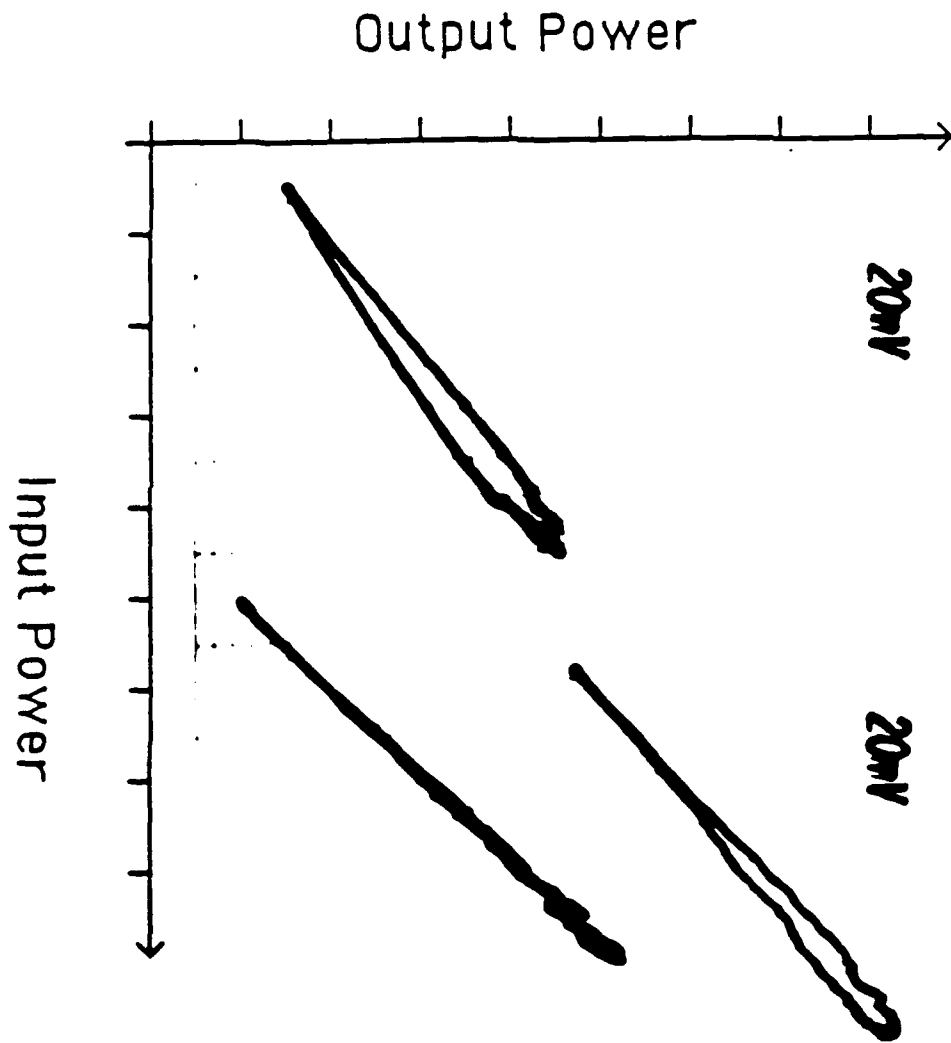## CONCLUSION

The presence of large oscillator strength π-electron bands in the visible and near ultraviolet characteristic of conjugated quasi two dimensional structure provides attractive conditions for studying resonant $\chi^{(3)}$ processes, especially in phthalocyanine related structures. A physical model for the thin film that a microscopic composites system of molecular optical sites distributed in a TLS glass random medium is presented. The resonant nonlinear optical properties of homogeneously broadened lines contained in the inhomogeneously broadened Gaussian envelope were directly investigated by a standard saturable absorption measurements. These results showed for the SINC films that saturable absorption occurs at the peak maximum of the low-frequency Q band near 810 nm with essentailly zero unsaturable background absorption and that on-site π-electron excitations of the Q band in individual molecular sites are responsible for the large resonant nonlinear optical response n_2 of 1×10^{-4} cm^2/kW at 810 nm.

Optical bistability is a quantum optical example of a first order nonequilibrium phase transition. A nonlinear optical material contained in an optical cavity driven resonantly by an external coherent optical field undergoes a first order phase transition to a new nonequilibrium stationary state of broken symmetry. A careful experimetal study of optical bistability in thin film etalon demonstrated that near the peak maximum of the saturable Q band centered at 810 nm. SINC thin films exhibit primarily electronic absorptive optical bistability at fast time scales (nanoseconds). At long time scales (seconds), thermally induced dispersive bistability occurs. which is entirely different and distinct from the observed fast time behavior.

Appendix 1. Second Quantization Expression of Maxwell-Bloch Equation

The vector potential for a electromagnetic field is expressed in a second quantization form as follows.

$$\vec{A}(x,t) = \sum_{\lambda} \sqrt{\frac{2\pi\hbar}{V\omega_{\lambda}}} c(b_{\lambda}^{\dagger} \vec{e}_{\lambda} e^{i(\omega t - kz)} + b_{\lambda} \vec{e}_{\lambda}^{*} e^{i(\omega t - kz)}) \qquad (A1.1)$$

The atoms are described by the wavefunction $|\psi_1\rangle$ and $|\psi_2\rangle$ when in the excited and the ground state respectively. In the second quantization the atomic state at postion x_{μ} is described by $a_{\mu}^{\dagger}$ and a_{μ},

$$|\psi_1\rangle = a_{\mu}^{\dagger}|\psi_2\rangle, \quad |\psi_2\rangle = a_{\mu}|\psi_1\rangle \qquad (A1.2)$$

According to the minimal coupling

$$H_{int} = -\frac{e}{mc}\vec{p} \bullet \vec{A} = -\hbar\frac{e}{m}\sqrt{\frac{2\pi}{\hbar\omega_{\lambda}V}}\langle\psi_1|\vec{e}_{\lambda} \bullet \vec{p}|\psi_2\rangle \qquad (A1.3)$$

The Hamiltonian of the system composed of a field and a matter in the dipole approxiamtion is

$$H = \sum_{\lambda} \hbar\omega_{\lambda} b_{\lambda}^{\dagger} b_{\lambda} + \sum_{\mu} \hbar\varepsilon\, a_{\mu}^{\dagger} a_{\mu} + \hbar \sum_{\mu\lambda}(h_{\mu\nu}^{*} a_{\mu}^{\dagger} b_{\nu} + h.c.) \qquad (A1.4)$$

where

$$h_{\mu\nu} = -\frac{e}{m}\sqrt{\frac{2\pi}{\hbar\omega_{\lambda}V}}\langle\psi_1|\vec{e}_{\lambda} \bullet \vec{p}|\psi_2\rangle \qquad (.A1.5)$$

According to the Heisenberg equation of motion

$$\frac{db_{\lambda}^{\dagger}}{dt} = i\omega_{\lambda}b_{\lambda}^{\dagger} + i\sum_{\mu} h_{\mu\nu}^{*} a_{\mu}^{\dagger} \qquad (A1.6)$$

$$\frac{da_{\mu}^{\dagger}}{dt} = i\varepsilon a_{\mu}^{\dagger} - i\sum_{\lambda} h_{\mu\nu} b_{\lambda}^{\dagger} \sigma_{\mu} \qquad (A1.7)$$

256

$$\sigma_\mu = a_\mu^\dagger a_\mu - a_\mu a_\mu^\dagger \qquad (A1.8)$$

The above equations are true when there is no optical pumping. If the external driving field is present, the population inversion σ_μ is not a constant but time-dependent.

$$\frac{d\sigma_\mu}{dt} = -\frac{1}{T}(\sigma_\mu - \sigma_0) + 2i(a_\mu \sum_\lambda h_{\mu\lambda} b_\lambda^\dagger - h.c.) \qquad (A1.9)$$

For simplicity we assume that the F-P cavity support only one single mode resonant with the atomic frequency.

$$\omega_\lambda = \omega = \varepsilon \qquad (A1.10)$$

Introducing the harmonic time-dependence, the Maxwell-Bloch equation reduces to

$$\frac{db^\dagger}{dt} = -\kappa b^\dagger + i \sum_\mu h_\mu^* a_\mu^\dagger \qquad (A1.11)$$

$$\frac{da_\mu^\dagger}{dt} = -\frac{1}{T_2} a_\mu^\dagger - i h_\mu b^\dagger \sigma_\mu \qquad (A1.12)$$

$$\frac{d\sigma_\mu}{dt} = -\frac{1}{T_1}(\sigma_\mu - \sigma_0) + 2i(h_\mu a_\mu b^\dagger - h.c.) \qquad (A1.13)$$

Reference

Haken, H. and Sauermann, H., Z. Physik **173**, 261 (1963)

Appendix 2. Nonlinear Optical Response

Now the interaction Hamitonian is known as Eq(A1.1). Adopting the convention for the electric field as follows,

$$\vec{E}(t) = Re\{\hat{e}\varepsilon e^{-i\omega t}\} = \frac{1}{2}\hat{e}(\varepsilon e^{-i\omega t} - \varepsilon^* e^{+i\omega t}) \qquad (A2.1)$$

The dipole moment induced by the external field is

$$
\begin{aligned}
P_i(t) = &\int_0^\infty \chi_{ij}^{(1)}(\tau)E_j(t-\tau)d\tau \\
&+ \int_0^\infty \chi_{ijk}^{(2)}(\tau,\tau')E_j(t-\tau)E_k(t-\tau')d\tau d\tau' \\
&+ \int_0^\infty \chi_{ijkl}^{(3)}(\tau,\tau',\tau'')E_j(t-\tau)E_k(t-\tau')E_l(t-\tau'')d\tau d\tau' d\tau'' \\
&+ \dots \qquad\qquad\qquad\qquad\qquad\qquad\qquad\qquad (A2.2)
\end{aligned}
$$

Here the induced dipole moment is a real quantity and the external field is real, hence, the response function $\chi^{(1)}(t)$ is a real quantity. First we consider the linear response. Define the Fourier component of the polarizability.

$$\chi_{ij}^{(1)}(\omega) = \int_0^\infty \chi_{ij}^{(1)}(t)e^{+i\omega t}dt \qquad (A2.3)$$

From the definition itself it follows one important property of the polarizability.

$$\chi_{ij}^{(1)*}(\omega) = \chi_{ij}^{(1)}(-\omega) \qquad (A2.4)$$

In the physical process we are intersted in the light frequency of the dipole radiation from the induced dipole moment. We need to calculate the Fourier components of the induced dipole moments.

$$
\begin{aligned}
P_i^{(1)}(t) &= \int_0^\infty \chi_{ij}^{(1)}(\tau)E_j(t-\tau)d\tau \\
&= \int_0^\infty \chi_{ij}^{(1)}(\tau)Re\{\varepsilon_j e^{-i\omega(t-\tau)}\}d\tau
\end{aligned}
$$

$$= \frac{1}{2} \int_0^\infty \chi_{ij}^{(1)}(\tau)(\varepsilon_j e^{-i\omega(t-\tau)} + \varepsilon_j^* e^{+i\omega(t-\tau)}) d\tau$$

$$= \frac{1}{2} \frac{1}{2\pi} \int_0^\infty \chi_{ij}^{(1)}(\omega') e^{-i\omega'\tau} d\omega' (\varepsilon_j e^{-i\omega(t-\tau)} + \varepsilon_j^* e^{+i\omega(t-\tau)}) d\tau$$

$$= \frac{1}{2} \int_0^\infty d\omega' [\chi_{ij}^{(1)}(\omega')\varepsilon_j e^{-i\omega t}\delta(\omega' - \omega) + \chi_{ij}^{(1)}(\omega')\varepsilon_j^* e^{+i\omega t}\delta(\omega' + \omega)]$$

$$= \frac{1}{2}[\chi_{ij}^{(1)}(\omega)\varepsilon_j e^{-i\omega t} + \chi_{ij}^{(1)}(-\omega)\varepsilon_j^* e^{+i\omega t}]$$

$$= Re\{\chi_{ij}^{(1)}(\omega)\varepsilon_j e^{-i\omega t}\} \tag{A2.5}$$

That is,

$$P_i^{(1)}(\omega) = \chi_{ij}^{(1)}(-\omega;\omega)\varepsilon_j^\omega \tag{A2.6}$$

This relation describes most of the linear optics phenomena. Now the problem has been reduced to calculating the microscopic susceptibility $\chi_{ij}^{(1)}(-\omega;\omega)$ from the microscopic description of the system.

Let's go to the second order processes. We follow the identical steps allowing upto the 2nd orders. The Fourier components are

$$\chi_{ijk}^{(2)}(\omega_1,\omega_2) = \int_0^\infty \chi_{ijk}^{(2)}(t_1,t_2)e^{i\omega_1 t_1}e^{i\omega_2 t_2} dt_1 dt_2 \tag{A2.7}$$

$$P_i^{(2)}(t) = \int_0^\infty \chi_{ijk}^{(2)}(\tau,\tau')E_j(t-\tau)E_k(t-\tau') d\tau d\tau'$$

$$= (\frac{1}{2})^2 (\frac{1}{2\pi})^2 \int_0^\infty \chi_{ijk}^{(2)}(\omega_1',\omega_2')e^{-i\omega_1'\tau}e^{-i\omega_1'\tau'} d\omega_1' d\omega_2'$$

$$(\varepsilon_j e^{-i\omega_1(t-\tau)} + \varepsilon_j^* e^{+i\omega_1(t-\tau)})(\varepsilon_k e^{-i\omega_2(t-\tau')} + \varepsilon_k^* e^{+i\omega_2(t-\tau')}) d\tau d\tau'$$

$$= (\frac{1}{2})^2 [\chi_{ijk}^{(2)}(\omega_1,\omega_2)\varepsilon_j\varepsilon_k e^{-i(\omega_1+\omega_2)t}$$

$$+ \chi_{ijk}^{(2)}(-\omega_1,\omega_2)\varepsilon_j^*\varepsilon_k e^{-i(-\omega_1+\omega_2)t}$$

$$+ \chi_{ijk}^{(2)}(\omega_1,-\omega_2)\varepsilon_j\varepsilon_k^* e^{+i(-\omega_1+\omega_2)t}$$

$$+ \chi_{ijk}^{(2)}(-\omega_1,-\omega_2)\varepsilon_j^*\varepsilon_k^* e^{+i(\omega_1+\omega_2)t}]$$

$$= \frac{1}{2}Re\{\chi_{ijk}^{(2)}(-\omega_1-\omega_2;\omega_1,\omega_2)\varepsilon_j(\omega_1)\varepsilon_k(\omega_2)e^{-i(\omega_1+\omega_2)t}$$

$$+ \chi_{ijk}^{(2)}(\omega_1-\omega_2;-\omega_1,\omega_2)\varepsilon_j^*(\omega_1)\varepsilon_k(\omega_2)e^{-i(-\omega_1+\omega_2)t}\} \tag{A2.8}$$

Eq(A2.8) describes the 2nd order nonlinear optical processes. For the degenerate photons, it represents the second harmonic generation and the optical rectification, and for the non-degenerate photons, the sum frequency generation and the difference frequency generations are possible. Similarly, in a 3rd order process, the Fourier components are

$$\chi^{(3)}_{ijkl}(\omega_1,\omega_2,\omega_3) = \int_0^\infty \chi^{(3)}_{ijkl}(t_1,t_2,t_3)e^{i\omega_1 t_1}e^{i\omega_2 t_2}e^{i\omega_3 t_3}dt_1 dt_2 dt_3 \qquad (A2.9)$$

$$
\begin{aligned}
P_i^{(3)}(t) =& (\frac{1}{2})^2 Re\{\chi^{(3)}_{ijkl}(-\omega_1-\omega_2-\omega_3;\omega_1,\omega_2,\omega_3)\varepsilon_j(\omega_1)\varepsilon_k(\omega_2)\varepsilon_l(\omega_3)e^{-i(\omega_1+\omega_2+\omega_3)t} \\
&+\chi^{(3)}_{ijkl}(\omega_1-\omega_2-\omega_3;-\omega_1,\omega_2,\omega_3)\varepsilon_j^*(\omega_1)\varepsilon_k(\omega_2)\varepsilon_l(\omega_3)e^{-i(-\omega_1+\omega_2+\omega_3)t} \\
&+\chi^{(3)}_{ijkl}(-\omega_1+\omega_2-\omega_3;\omega_1,-\omega_2,\omega_3)\varepsilon_j(\omega_1)\varepsilon_k^*(\omega_2)\varepsilon_l(\omega_3)e^{-i(\omega_1-\omega_2+\omega_3)t} \\
&+\chi^{(3)}_{ijkl}(-\omega_1-\omega_2+\omega_3;\omega_1,\omega_2,-\omega_3)\varepsilon_j(\omega_1)\varepsilon_k(\omega_2)\varepsilon_l^*(\omega_3)e^{-i(\omega_1+\omega_2-\omega_3)t}\}
\end{aligned}
$$

$$(A2.10)$$

The 3rd order processes are very interesting, and we can have nonlinear phenomena that are not realizable in the 2nd order processes. Before we discuss the individual nonlinear processes, we consider the symmetrical porperties of the nonlinear susceptibility tensors.

First, for a non-dissipative system the susceptibilities are symmetric under the permutation of the tensor indices with the tensor arguments permuted similarly. For example,

$$
\begin{aligned}
\chi^{(2)}_{ijk}(-\omega_3;\omega_1,\omega_2) &= \chi^{(2)}_{ikj}(-\omega_3;\omega_2,\omega_1) \\
\chi^{(3)}_{ijkl}(-\omega_4;\omega_1,\omega_2,\omega_3) &= \chi^{(3)}_{ikjl}(-\omega_4;\omega_2,\omega_1,\omega_3) \\
= \chi^{(3)}_{ilkj}(-\omega_4;\omega_3,\omega_2,\omega_1) &= \chi^{(3)}_{ijlk}(-\omega_4;\omega_1,\omega_3,\omega_2) \\
= \chi^{(3)}_{iljk}(-\omega_4;\omega_3,\omega_1,\omega_2) &= \chi^{(3)}_{iklj}(-\omega_4;\omega_2,\omega_3,\omega_1)
\end{aligned}
\qquad (A2.11)
$$

The above symmetry can be seen easily from the symmetric property of $\chi^{(2)}_{ijk}(\tau,\tau')$ and $\chi^{(3)}_{ijkl}(\tau,\tau',\tau'')$ in Eq.(A2.2). The symmetric property can be extended to the

index i, which is an important property of the nonlinear susceptibility tensor and can be proven by the energy conservation consideration in a non-trivial way.

$$\chi_{ijk}^{(2)}(-\omega_3;\omega_1,\omega_2) = \chi_{jik}^{(2)}(\omega_1;-\omega_3,\omega_2)$$

$$\chi_{ijkl}^{(3)}(-\omega_4;\omega_1,\omega_2,\omega_3) = \chi_{jikl}^{(3)}(\omega_1;-\omega_4,\omega_2,\omega_3) \qquad (A2.12)$$

Eq.(A2.11) and (A2.12) lists most of the intrinsic symmetry properties of the nonlinear susceptibility tensors, and the independent number of the tensor components in a particular nonlinear process can be reduced by imposing this symmetry rules.

Secondly there is another symmetry relation called the Kleinman conjecture, which says that in the far off-resonance regime, the nonlinear suceptibility tensors are completely symmetric, i.e., symmetric under the permutation of the tensor indices with the tensor arguments fixed. This is a very strong symmetry rule, and can be seen from the static limit of the nonlinear optical response, where the distiction between different frequencies, $\omega_1,\omega_2,\omega_3,\omega_4$, vanishes. But in real systems, there exists a slight dispersion even at the far off-resonant regime; therefore, the Kleinman symmetry does not hold rigorously.

Thirdly, we can list the symmetry property of the nonlinear susceptibility tensors under the point group. Physical systems, in general, possess a spatial symmtry which can be expressed in terms of a point group, and the nonlinear optical response of the system should obey the same symmetry governed by the point group. From the tensorial transformation property under a particular point group operation, a relation between the tensor components can be obtained, and the independent components can be found for a general nonlinear optical processes. For example, in an isotropic medium,

$$\chi_{1111}^{(3)}(-\omega_4;\omega_1,\omega_2,\omega_3) = \chi_{iiii}^{(3)}(-\omega_4;\omega_1,\omega_2,\omega_3)$$

$$\chi_{1122}^{(3)}(-\omega_4;\omega_1,\omega_2,\omega_3) = \chi_{iijj}^{(3)}(-\omega_4;\omega_1,\omega_2,\omega_3)$$

$$\chi_{1212}^{(3)}(-\omega_4;\omega_1,\omega_2,\omega_3) = \chi_{ijij}^{(3)}(-\omega_4;\omega_1,\omega_2,\omega_3)$$

$$\chi_{1221}^{(3)}(-\omega_4;\omega_1,\omega_2,\omega_3) = \chi_{ijji}^{(3)}(-\omega_4;\omega_1,\omega_2,\omega_3)$$

$$\chi_{1111}^{(3)}(-\omega_4;\omega_1,\omega_2,\omega_3) = \chi_{1212}^{(3)}(-\omega_4;\omega_1,\omega_2,\omega_3)$$

$$+ \chi_{1221}^{(3)}(-\omega_4;\omega_1,\omega_2,\omega_3)$$

$$+ \chi_{1122}^{(3)}(-\omega_4;\omega_1,\omega_2,\omega_3) \qquad (A2.13)$$

Now let's consider an individual 3rd order process. For example, if there is only one frequency of photons, i.e. $\omega_1 = \omega_2 = \omega_3 = \omega$, we have the third harmonic generation and the self-focusing processes as examples. For self-focusing we have

$$
\begin{aligned}
P_i^{(\omega)} = \frac{1}{4}\{ & \chi_{ijkl}^{(3)}(-\omega;-\omega,\omega,\omega)\varepsilon_j^*(\omega)\varepsilon_k(\omega)\varepsilon_l(\omega) \\
& + \chi_{ijkl}^{(3)}(-\omega;\omega,-\omega,\omega)\varepsilon_j(\omega)\varepsilon_k^*(\omega)\varepsilon_l(\omega) \\
& + \chi_{ijkl}^{(3)}(-\omega;\omega,\omega,-\omega)\varepsilon_j(\omega)\varepsilon_k(\omega)\varepsilon_l^*(\omega)\} e^{-i\omega t} \qquad (A2.14)
\end{aligned}
$$

In another example of the optical Kerr effect, we have $\omega_1 = \omega_3 = \omega$, $\omega_2 = \omega'$,

$$
\begin{aligned}
P_i^{(\omega')} = \frac{1}{4}\{ & \chi_{ijkl}^{(3)}(-\omega';-\omega,\omega',\omega)\varepsilon_j^*(\omega)\varepsilon_k(\omega')\varepsilon_l(\omega) \\
& + \chi_{ijkl}^{(3)}(-\omega';\omega,\omega',-\omega)\varepsilon_j(\omega)\varepsilon_k^*(\omega')\varepsilon_l(\omega)\} e^{-i\omega' t} \qquad (A2.15)
\end{aligned}
$$

Appendix 3. Canonical Transformation of Interaction Hamiltonian

Here we show the equivalence of the minimal coupling formed by replacing the momentum $\vec{p}$ with $\vec{p} - \frac{e}{c}\vec{A}$ to the dipole interaction Hamiltonian defined by $-\vec{\mu} \cdot \vec{E}$.

$$
\begin{aligned}
H &= \frac{1}{2m}(\vec{p} - \frac{e}{c}\vec{A})^2 + V(x) \\
&= \frac{\vec{p}^2}{2m} + V(x) - \frac{e}{mc}\vec{A} \cdot \vec{p} + \frac{e^2}{2mc^2}\vec{A} \cdot \vec{A}
\end{aligned}
\qquad (A3.1)
$$

Hamilton's equation of motion for the Hamiltonian is

$$
\frac{d\vec{x}}{dt} = \dot{\vec{x}} = \frac{\partial H}{\partial \vec{p}} = \frac{\vec{p}}{m} - \frac{e}{mc}\vec{A}
\qquad (A3.2)
$$

Now the corresponding Lagrangian can be obtained by the Legendre transformation.

$$
\begin{aligned}
L(\dot{\vec{x}}, \vec{x}) &= \dot{\vec{x}} \cdot \vec{p} - H \\
&= \dot{\vec{x}} \cdot (m\dot{\vec{x}} + \frac{e}{c}\vec{A}) - \frac{1}{2m}(m\dot{\vec{x}} + \frac{e}{c}\vec{A})^2 - V(x) \\
&\quad + \frac{e}{mc}\vec{A} \cdot (m\dot{\vec{x}} + \frac{e}{c}\vec{A}) - \frac{e^2}{2mc^2}\vec{A} \cdot \vec{A} \\
&= \frac{1}{2}m\dot{\vec{x}}^2 - V(x) + \frac{e}{c}\dot{\vec{x}} \cdot \vec{A}
\end{aligned}
\qquad (A3.3)
$$

Since the equation of motion is invariant evenif the Lagrangian is changed upto a total derivative of an arbitrary function, we transform the Lagrangian by adding $-\frac{d}{dt}(\frac{e}{c}\vec{x} \cdot \vec{A})$.

$$
\begin{aligned}
\bar{L}(\dot{\vec{x}}, \vec{x}) &= L(\dot{\vec{x}}, \vec{x}) - \frac{d}{dt}(\frac{e}{c}\vec{x} \cdot \vec{A}) \\
&= \frac{1}{2}m\dot{\vec{x}}^2 - V(x) - \frac{e}{c}(\vec{x} \cdot \frac{d\vec{A}}{dt})
\end{aligned}
\qquad (A3.4)
$$

Now we make the Legendre transformation back to get the Hamiltonian. The canonical momentum $\bar{p}$ conjugate to $\dot{\vec{x}}$ is

$$
\bar{p} = \frac{\partial \bar{L}}{\partial \dot{\vec{x}}} = m\dot{\vec{x}}
\qquad (A3.5)
$$

The new Hamiltonian is

$$\bar{H}(\vec{x}, \vec{p}) = \dot{\vec{x}} \bullet \vec{p} - \bar{L}$$

$$= \vec{p} \bullet \frac{\vec{p}}{m} - \frac{m}{2} (\frac{\vec{p}}{m})^2 + V(x) + \frac{e}{c} (\vec{x} \bullet \frac{d\vec{A}}{dt})$$

$$= \frac{\vec{p}^2}{2m} + V(\vec{x}) + \frac{e}{c} \vec{x} \bullet \frac{d\vec{A}}{dt} \qquad (A3.6)$$

The vector potential A is a fuction of time and space, and the total time derivative is given as

$$\frac{d\vec{A}}{dt} = \frac{\partial \vec{A}}{\partial t} + (\vec{v} \bullet \vec{\nabla})\vec{A} \qquad (A3.7)$$

The electric field can be expressed in terms of the vector potential.

$$\vec{E} = -\frac{1}{c} \frac{\partial A}{\partial t} \qquad (A3.8)$$

In the dipole approximation the vector potential has no spatial dependence, i.e., Eq.(A3.7) is related to the electric field.

$$\frac{d\vec{A}}{dt} = \frac{\partial \vec{A}}{\partial t} = -c\vec{E} \qquad (A3.9)$$

Plugging Eq(A3.9) into Eq(A3.6), the total Hamiltonian in Eq(A3.6) is

$$\bar{H}(\vec{x}, \vec{p}) = \frac{\vec{p}^2}{2m} + V(x) - e\vec{x} \bullet \vec{E} = H_0 + H_1(t) \qquad (A3.10)$$

Therefore the interaction Hamilitonian is

$$H_1(t) = -e\vec{x} \bullet \vec{E}(t) = -\vec{\mu} \bullet \vec{E} \qquad (A3.11)$$

264

Appendix 4. Orthogonal Transformation of Bloch Equation

Here we present another way to transform to the rotating frame. In the rotating frame of reference where $\vec{\Omega}^F$ is stationary.

$$\frac{d}{dt} \Rightarrow \frac{d}{dt} + \vec{\omega} \times \tag{A4.1}$$

$$H \Rightarrow OHO^{-1}$$

$$= \exp(i\frac{\sigma_z}{2}\theta)\frac{1}{2}(I + \hbar\vec{\Omega}^F \bullet \sigma)\exp(-i\frac{\sigma_z}{2}\theta)$$

$$= \frac{1}{2}I + \hbar\exp(i\frac{\sigma_z}{2}\theta)(\Omega^{+F}\sigma^+ + \Omega^{-F}\sigma^- + \Omega^{0F}\sigma_z)\exp(-i\frac{\sigma_z}{2}\theta)$$

$$= \frac{1}{2}I + \hbar(\Omega^{+F}e^{i\theta}\sigma^+ + \Omega^{-F}e^{-i\theta}\sigma^- + \Omega^{0F}\sigma_z) \tag{A4.2}$$

where the Pauli matrices are defined as follows;

$$\sigma_x = \begin{pmatrix} 0 & 1 \\ 1 & 0 \end{pmatrix}, \qquad \sigma_y = \begin{pmatrix} 0 & -i \\ i & 0 \end{pmatrix}, \qquad \sigma_z = \begin{pmatrix} 1 & 0 \\ 0 & -1 \end{pmatrix} \tag{A4.3}$$

$$\sigma^+ = \frac{1}{2}(\sigma_x + i\sigma_y) = \begin{pmatrix} 0 & 1 \\ 0 & 0 \end{pmatrix}, \qquad \sigma^- = \frac{1}{2}(\sigma_x - i\sigma_y) = \begin{pmatrix} 0 & 0 \\ 1 & 0 \end{pmatrix} \tag{A4.4}$$

The last step in Eq(A4.2) follows from the transformation properties of σ^+ and σ^- under the rotation along the 3-axis.

$$O\sigma^+O^{-1} = \exp(i\frac{\sigma_z}{2}\theta)\sigma^+\exp(-i\frac{\sigma_z}{2}\theta)$$

$$= (\cos\frac{\theta}{2} + i\sigma_z\sin\frac{\theta}{2})\sigma^+(\cos\frac{\theta}{2} - i\sigma_z\sin\frac{\theta}{2})$$

$$= \sigma^+e^{i\theta} \tag{A4.5}$$

$$O\sigma^-O^{-1} = \sigma^-e^{-i\theta} \tag{A4.6}$$

$$\text{since} \quad \sigma^+\sigma_z = -\sigma^+, \qquad \sigma_z\sigma^+ = \sigma^+$$

$$\sigma^-\sigma_z = \sigma^-, \qquad \sigma_z\sigma^- = -\sigma^- \tag{A4.7}$$

Noting

$$\vec{\Omega} \bullet \vec{\sigma}$$

$$= \Omega_x \sigma_x + \Omega_y \sigma_y + \Omega_z \sigma_z$$

$$= \Omega_x (\sigma^+ + \sigma^-) + (-i)\Omega_y (\sigma^+ - \sigma^-) + \Omega_z \sigma_z$$

$$= (\Omega_x - i\Omega_y)\sigma^+ + (\Omega_x + i\Omega_y)\sigma^- + \Omega_z \sigma_z \qquad (A4.8)$$

$$\Omega^{+F} = \Omega_x - i\Omega_y = -\kappa\varepsilon\cos\omega t - i\kappa\varepsilon\sin\omega t = -\kappa\varepsilon e^{-i\omega t} \qquad (A4.9)$$

$$\Omega^{-F} = \Omega_x + i\Omega_y = -\kappa\varepsilon\cos\omega t - i\kappa\varepsilon\sin\omega t = -\kappa\varepsilon e^{+i\omega t}, \qquad (A4.10)$$

and substituting Eq.(A4.9) and (A4.10) into Eq.(A4.2) leads to the same result as Eq.(3.5.23).

266

Appendix 5. Linear Response Theory

We review the linear response theory. The total Hamiltonian is

$$H = H_0 - \mu E(t) \tag{A5.1}$$

The eqution of motion for the densty matrix is

$$i\hbar \frac{\partial \rho(t)}{\partial t} = [H, \rho(t)] \tag{A5.2}$$

Now we suppose that the interaction is much smaller than the unperturbed Hamiltonian H_0, and we expand the density matrix in the small quantity.

$$\rho(t) = \rho_0 + \delta\rho(t) \tag{A5.3}$$

Then the equation of motion for the change in the density matrix is

$$i\hbar \frac{\partial \delta\rho(t)}{\partial t} = [H_0, \delta\rho(t)] - E(t)[\mu, \rho_0] \tag{A5.4}$$

To make the calculation easier, we introduce a Liouville operator L.

$$LA = [H, A] \tag{A5.5}$$

In terms of the Liouville operator the equation of motion for the density matrix is

$$i\hbar \frac{\partial \rho(t)}{\partial t} = L\rho(t) \tag{A5.6}$$

$$i\hbar \frac{\partial \delta\rho(t)}{\partial t} = (L_0 + L_a)(\rho_0 + \delta\rho(t)) = L_0\delta\rho(t) + L_a\rho_0 \tag{A5.7}$$

With the initial condition that

$$\rho(t = -\infty) = \rho_0 \tag{A5.8}$$

267

Eq.(A5.7) can be solved in a straightforward way.

$$\delta\rho(t) = e^{-iL_0(t-t(-\infty))/\hbar}\delta\rho(-\infty) + \int_{-\infty}^{t} dt' e^{-iL_0(t-t')/\hbar}(-i\frac{L_a}{\hbar})\rho_0$$

$$= \int_{-\infty}^{t} dt' e^{-iL_0(t-t')/\hbar}(-\frac{i}{\hbar})[-\mu E(t'), \rho_0]$$

$$= \frac{i}{\hbar}\int_{-\infty}^{t} dt' [-\mu(t-t'), \rho_0] E(t') \qquad (A5.9)$$

Now let's consider the change in the dipole moment due to the interaction. The change in the dipole moment can be accounted for by the change in the densty matrix.

$$\delta p(t) = Tr\{\delta\rho(t)\mu\}$$

$$= \frac{i}{\hbar}\int_{-\infty}^{t} dt' Tr\{[\mu(t-t'), \rho_0]\mu\} E(t')$$

$$= \frac{i}{\hbar}\int_{-\infty}^{t} dt' Tr\{\rho[\mu, \mu(t-t')]\} E(t') \qquad (A5.10)$$

The susceptibility is defined

$$\delta p(t) = \int_{-\infty}^{t} dt' \chi(t-t') E(t') \qquad (A5.11)$$

We find that

$$\chi(t) = \frac{i}{\hbar} = Tr\{\rho_0[\mu, \mu(t)]\} \qquad (A5.12)$$

The Fourier transform of the susceptibility gives the information on the spectral structure.

$$\chi(\omega) = \int_0^\infty \chi(t) e^{i\omega t} dt \qquad (A5.13)$$

Let's look at the imaginary part of the susceptibility which is related to the dissipation of the system.

$$\chi''(\omega) = \int_0^\infty dt \sin(\omega t)\chi(t)$$

$$= \frac{i}{\hbar}\int_0^\infty dt \sin(\omega t) Tr\{\rho[\mu, \mu(t)]\}$$

268

$$= \frac{i}{\hbar} \int_0^\infty dt \, \sin(\omega t) Tr\{\rho\mu\mu(t)\} - \int_0^\infty dt \, \sin(\omega t) Tr\{\rho\mu(t)\mu\}$$

$$= \frac{i}{\hbar} \int_0^\infty dt \, \sin(\omega t) Tr\{\rho\mu\mu(t)\} + \int_{-\infty}^0 dt \, \sin(\omega t) Tr\{\rho\mu(-t)\mu\}$$

$$= \frac{i}{\hbar} \int_{-\infty}^\infty dt \, \sin(\omega t) Tr\{\rho\mu\mu(t)\}$$

$$= \frac{i}{\hbar} Im \int_{-\infty}^\infty dt e^{i\omega t} Tr\{\rho\mu\mu(t)\} \qquad (A5.14)$$

where the following identity has been used.

$$Tr\{\rho\mu(-t)\mu\} = Tr\{\rho e^{-iH_0 t/\hbar}\mu e^{+iH_0 t/\hbar}\mu\}$$

$$= Tr\{\mu e^{+iH_0 t/\hbar}\mu\rho_0 e^{-iH_0 t/\hbar}\} = Tr\{\rho\mu\mu(t)\} \qquad (A5.15)$$

Appendix 6. Formal Solution for the Line Shape Function

We find a formal solution for the line shape function.

$$
\begin{aligned}
F(\omega) &= \frac{1}{\pi} Re \int_0^\infty dt e^{i\omega t} C_{xx}(t) \\
&= \frac{1}{\pi} Re \int_0^\infty dt e^{i\omega t} Tr\{x^s e^{-iLt}\rho x^s\} \\
&= \frac{1}{\pi} Re Tr\{x^s i \frac{1}{\omega - L}\rho x^s\} \\
&= -\frac{1}{\pi} Im Tr\{x^s \frac{1}{\omega - L_0}(1 + M(\omega)\frac{1}{\omega - L_0})\rho x^s\}
\end{aligned}
\qquad (A6.1)
$$

where the identity of operator has been used.

$$
\frac{1}{\omega - L} = \frac{1}{\omega - L_0}(1 + M(\omega)\frac{1}{\omega - L_0})
\qquad (A6.2)
$$

with

$$
M(\omega) = L_1 + L_1 \frac{1}{\omega - L_0} M(\omega)
\qquad (A6.3)
$$

From the initial conditions Eq.(4.3.25) the densty matrix of the bath appears only in the inteaction Hamiltonian, and the Liouville operator for the unperturbed Hamiltonian changes to the Liouvilles operator for the system only.

$$
F(\omega) = -\frac{1}{\pi} Im Tr^s\{x^s \frac{1}{\omega - L_0^s}(1 + \langle M(\omega)\rangle \frac{1}{\omega - L_0^s})\rho^s x^s\}
\qquad (A6.4)
$$

where the operator $M(\omega)$ containing the interaction Hamiltonian appears as an average value over the bath variables.

$$
\langle M(\omega)\rangle = Tr^b\{M(\omega)\rho^b\}
\qquad (A6.5)
$$

270

Appendix 7. Intersystem Crossing in a Many-electron System

Now let's look at the selection rule more carefully. In a polyatomic molecule we have more than one center ion, therefore we have to consider the interaction of each electrons with all the different centers.

$$
\begin{aligned}
H' &= \frac{1}{2m^2c^2} \sum_{k=1}^{N} \sum_{i=1}^{n} \frac{1}{r_{ik}} \frac{\partial V(r_{ik})}{\partial r_{ik}} \vec{l}_{ik} \bullet \vec{s}_{ik} \\
&= \sum_{i=1}^{n} A_i \vec{l}_i \bullet \vec{s}_i = \sum_{i=1}^{n} H'_i
\end{aligned}
\qquad (A7.1)
$$

For a multi-electron molecule the wavefunction should be properly antisymmetrized. For example the singlet state is expressed in Slater determinant.

$$
S_k = \frac{1}{\sqrt{2}} \bigg(|(filledMO)a\alpha_1 b\beta_2| - |(filledMO)a\beta_1 b\alpha_2| \bigg)
\qquad (A7.2)
$$

and the triplet states are

$$
\begin{aligned}
T_j^{+1} &= |(filledMO)a\alpha_1 c\alpha_2| \\
T_j^0 &= \frac{1}{\sqrt{2}} \bigg(|(filledMO)a\alpha_1 c\beta_2| + |(filledMO)a\beta_1 c\alpha_2| \bigg) \\
T_j^{-1} &= |(filledMO)a\beta_1 c\beta_2|
\end{aligned}
\qquad (A7.3)
$$

Let's look at the matrix element between S_k and T_j^{+1}.

$$
\begin{aligned}
&\langle S_k | H' | T_j^{+1} \rangle \\
&= \frac{1}{\sqrt{2}} \langle |a\alpha_1 b\beta_2| - |a\beta_1 b\alpha_2| | H' | (a\alpha_1 c\alpha_2) \rangle \\
&= \frac{1}{\sqrt{2}} \bigg(\langle a\alpha_1 b\beta_2 | (H'_1 + H'_2) | (a\alpha_1 c\alpha_2) \rangle - \langle a\alpha_2 b\beta_1 | (H'_1 + H'_2) | (a\alpha_1 c\alpha_2) \rangle \\
&\quad - \langle a\beta_1 b\alpha_2 | (H'_1 + H'_2) | (a\alpha_1 c\alpha_2) \rangle + \langle a\beta_2 b\alpha_1 | (H'_1 + H'_2) | (a\alpha_1 c\alpha_2) \rangle \bigg) \\
&= \frac{1}{\sqrt{2}} \bigg(\langle a\alpha_1 | a\alpha_1 \rangle \langle b\beta_2 | H'_2 | c\alpha_2 \rangle - \langle b\beta_1 | H'_1 | a\alpha_1 \rangle \langle a\alpha_2 | c\alpha_2 \rangle
\end{aligned}
$$

$$- \langle a\beta_1 | H'_1 | a\alpha_1 \rangle \langle b\alpha_2 | c\alpha_2 \rangle + \langle b\alpha_1 | a\alpha_1 \rangle \langle a\beta_2 | H'_2 | c\alpha_2 \rangle \Big)$$

$$= \frac{1}{\sqrt{2}} \langle b\beta_2 | H'_{x_2} + H'_{y_2} + H'_{z_2} | c\alpha_2 \rangle$$

$$= \frac{1}{\sqrt{2}} \left(\langle b | A_2 l_{z_2} | c \rangle \frac{\hbar}{2} + \langle b | A_2 l_{y_2} | c \rangle \frac{i\hbar}{2} \right)$$

$$= \frac{1}{\sqrt{2}} \left(\langle b | H'_{l_x} | c \rangle + i \langle b | H'_{l_y} | c \rangle \right) \tag{A7.4}$$

In the same way,

$$\langle S_k | H' | T_j^0 \rangle$$

$$= - \langle b | A_2 l_{z_2} | c \rangle \frac{\hbar}{2}$$

$$= - \langle b | H'_{l_z} | c \rangle \tag{A7.5}$$

$$\langle S_k | H' | T_j^{-1} \rangle$$

$$= \frac{1}{\sqrt{2}} \left(- \langle b | A_2 l_{x_2} | c \rangle \frac{\hbar}{2} + \langle b | A_2 l_{y_2} | c \rangle \frac{i\hbar}{2} \right)$$

$$= \frac{1}{\sqrt{2}} \left(- \langle b | H'_{l_x} | c \rangle + i \langle b | H'_{l_y} | c \rangle \right) \tag{A7.6}$$

Appendix 8. Kramers-Kronig Relation

From causality and the linear response theoy we can get the Kramers-Kronig (K-K) relations. The relation between the real part and imaginary part of the dielectric constant $\epsilon(\omega)$ satisfies the following Kramers-Kronig relation.

$$\epsilon(\omega) = \epsilon'(\omega) + i\epsilon''(\omega) \tag{A8.1}$$

$$\epsilon'(\omega) - 1 = \frac{1}{\pi}P\int_{-\infty}^{\infty}\frac{\epsilon''(x)}{x-\omega}dx \tag{A8.2}$$

$$\epsilon''(\omega) = -\frac{1}{\pi}P\int_{-\infty}^{\infty}\frac{\epsilon'(x)-1}{x-\omega}dx \tag{A8.3}$$

Or, in terms of the susceptibility

$$\epsilon(\omega) = 1 + 4\pi\chi(\omega) \tag{A8.4}$$

$$\chi'(\omega) = \frac{1}{\pi}P\int_{-\infty}^{\infty}\frac{\chi''(x)}{x-\omega}dx \tag{A8.5}$$

$$\chi''(\omega) = -\frac{1}{\pi}P\int_{-\infty}^{\infty}\frac{\chi'(x)}{x-\omega}dx \tag{A8.6}$$

Now in order to change the integration intervals we make use of the symmetric properties of the dielectric constant in frequency domain.

$$D(\omega) = \epsilon(\omega)E(\omega) \tag{A8.7}$$

Taking a Fourier transformation to the time domain,

$$D(t) = \int_{-\infty}^{\infty}D(\omega)e^{-i\omega t}d\omega \tag{A8.8}$$

$$E(t) = \int_{-\infty}^{\infty}E(\omega)e^{-i\omega t}d\omega \tag{A8.9}$$

Since $D(t)$ is a real function,

$$D^*(t) = \int_{-\infty}^{\infty} D^*(\omega)e^{i\omega t} d\omega$$

$$= -\int_{\infty}^{-\infty} D^*(-\omega)e^{-i\omega t} d\omega$$

$$= \int_{-\infty}^{\infty} D^*(-\omega)e^{-i\omega t} d\omega$$

$$= D(t) \tag{A8.10}$$

Therefore

$$\epsilon^*(-\omega) = \epsilon(\omega) \tag{A8.11}$$

$$\epsilon'(\omega) - i\epsilon''(\omega) = \epsilon'(-\omega) - i\epsilon''(-\omega) \tag{A8.12}$$

Or,

$$\epsilon'(\omega) = \epsilon'(-\omega), \quad \epsilon''(\omega) = -\epsilon''(-\omega) \tag{A8.13}$$

$$\chi'(\omega) = \chi'(-\omega), \quad \chi''(\omega) = -\chi''(-\omega) \tag{A8.14}$$

In conclusion ϵ' is an even function of ω, while ϵ'' is an odd function of ω.

Now using Eq.(A8.14) we can get another form of Kramers-Kronig relation.

$$\chi'(\omega) = \frac{1}{\pi} P \int_{-\infty}^{\infty} \frac{\chi''(x)}{x - \omega} dx$$

$$= \frac{1}{\pi} P \int_{-\infty}^{\infty} \frac{\chi''(x)}{x - \omega} \frac{x + \omega}{x + \omega} dx$$

$$= \frac{1}{\pi} P \left(\int_{-\infty}^{\infty} \frac{x\chi''(x)}{x - \omega} dx + \int_{-\infty}^{\infty} \frac{\omega\chi''(x)}{x - \omega} dx \right)$$

$$= \frac{2}{\pi} P \int_{0}^{\infty} \frac{x\chi''(x)}{x^2 - \omega^2} dx \tag{A8.15}$$

and,

$$\chi''(\omega) = -\frac{2}{\pi} P \int_{0}^{\infty} \frac{\omega\chi'(x)}{x^2 - \omega^2} dx \tag{A8.16}$$

Eq.(A8.2) and (A8.3) are a pair of K-K relation, and Eq.(A8.5) and (A8.6) are another pair. The integration interval can be changed to $(0, \infty)$ leading to a

274

K-K relation Eq.(A8.15) and (A8.16). There exist another form of K-K relation between the imaginary and the real part of the linear refractive index. This is the most useful relation enabling one to get the frequency dependent refractive index from the linear absorption curve. We make use of a linear relationship between the magnetic field and the electric field.

$$|\vec{H}| = \sqrt{\epsilon}|\vec{E}| = n|\vec{E}| = (\eta + i\kappa)|\vec{E}| \tag{A8.17}$$

Let

$$n(\omega) = \eta(\omega) + i\kappa(\omega) = \sqrt{\epsilon(\omega)} = \sqrt{\epsilon' + i\epsilon''} \tag{A8.18}$$

$$\epsilon' = \eta^2 - \kappa^2, \quad \epsilon'' = 2\eta\kappa \tag{A8.19}$$

$$\eta(\omega) - 1 = \frac{2}{\pi} \int_0^\infty \frac{x\kappa(x)}{x^2 - \omega^2} dx \tag{A8.20}$$

Now the absorption coefficient $\alpha(\omega)$ is related to the imaginary part of the refractive index $\kappa(\omega)$.

$$\alpha(\omega) = 2\kappa(\omega)\frac{\omega}{c} \tag{A8.21}$$

Substituting Eq.(A8.21) into Eq.(A8.20) leads to

$$\eta(\omega) - 1 = \frac{c}{\pi} \int_0^\infty \frac{\alpha(x)}{x^2 - \omega^2} dx \tag{A8.22}$$

Now we look at the qualitative behavior of susceptibilities from the K-K relation. From Eqs.(A8.15),(A8.16) we can get a qualitative properties of the Kramers-Kronig relation. Integrating Eq.(A8.15) (A8.16) by parts,

$$\int_0^\infty \frac{2x}{x^2 - \omega^2} \chi''(x) dx = \ln|x^2 - \omega^2|\chi''(x)\Big]_0^\infty - \int_0^\infty \ln|x^2 - \omega^2|\frac{d\chi''(x)}{dx} dx$$

$$= +\int_0^\infty \ln\frac{1}{|x^2 - \omega^2|}\frac{d\chi''(x)}{dx} dx \tag{A8.23}$$

$$\int_0^\infty \frac{-2\omega}{x^2 - \omega^2} \chi'(x) dx = \ln|\frac{x + \omega}{x - \omega}|\chi'(x)\Big]_0^\infty - \int_0^\infty \ln|\frac{x + \omega}{x - \omega}|\frac{d\chi'(x)}{dx} dx$$

$$= -\int_0^\infty \ln|\frac{x + \omega}{x - \omega}|\frac{d\chi'(x)}{dx} dx \tag{A8.24}$$

275

where the first term vanishes from the boundness of physical fields.

$$\chi'(\omega) = \frac{1}{\pi} \int_0^\infty \frac{d\chi''(x)}{dx} \ln \frac{1}{(x^2 - \omega^2)} dx \qquad (A8.25)$$

$$\chi''(\omega) = -\frac{1}{\pi} \int_0^\infty \frac{d\chi'(x)}{dx} \ln |\frac{x + \omega}{x - \omega}| dx \qquad (A8.26)$$

Since both the logarithmic function in the integrand have peaks at $x = \omega$, which means that the derivatives of susceptibilities at $x = \omega$ have the most of the contribution to the integrals. Or in another words $\chi'(\omega)$ peaks at the frequency where $\chi''(\omega)$ has the largest positive slope, and $\chi''(\omega)$ peaks at the frequency where $\chi'(\omega)$ has the largest negative slope.

For example, for the Lorentzian absorption curve,

$$\chi''(\omega) = \frac{\lambda}{(\omega - \omega_0)^2 + (\frac{\Gamma}{2})^2} \qquad (A8.27)$$

the real part of susceptibility peaks at

$$\omega = \omega_0 \pm \frac{1}{\sqrt{3}} \frac{\Gamma}{2} \qquad (A8.28)$$

For a Gaussian absorption curve

$$\chi''(\omega) = \chi_0 e^{-\frac{x^2}{\sigma^2}} \qquad (A8.29)$$

the real part of susceptibility peaks at

$$\omega = \omega_0 \pm \frac{\sigma}{\sqrt{2}} \qquad (A8.30)$$

For a Lorentzian absorption line shape the Kramers-Kronig relation is trivial and the real part and imaginary part of the complex refractive index satisfies the K-K relation trivially. But for the Gaussian absorption line shape it is not trivial to find the real part of the complex refractive index. The Gaussian lineshape has been studied long ago in the development of NMR.

$$\chi''(\omega) = \chi_0 \omega_0 T_2 e^{-T_2^2(\omega_0 - \omega)^2/\pi} \qquad (A8.31)$$

276

then

$$\chi'(\omega) = \chi_0\omega_0 T_2 \frac{2}{\sqrt{\pi}} F\Big(\frac{T_2(\omega_0 - \omega)}{\sqrt{\pi}}\Big) \qquad (A8.32)$$

where

$$F(x) = e^{-x^2} \int\limits_0^x e^{y^2}\, dy \qquad (A8.33)$$